# TCDD-ELICITED METABOLIC REPROGRAMMING IN THE PROGRESSION OF NON-ALCOHOLIC FATTY LIVER DISEASE

**By**

**Rance Nault**

**A DISSERTATION**

**Submitted to**
**Michigan State University**
**in partial fulfillment of the requirements**
**for the degree of**

**Biochemistry and Molecular Biology-Environmental Toxicology - Doctor of Philosophy**

**2016**

## ABSTRACT

### TCDD-ELICITED METABOLIC REPROGRAMMING IN THE PROGRESSION OF NON-ALCOHOLIC FATTY LIVER DISEASE

**By**

**Rance Nault**

The prevalence of metabolic disorders such as cardiovascular disease, type II diabetes, and non-alcoholic fatty liver disease (NAFLD) is reaching epidemic proportions in Western societies. Several factors are implicated in the development of these diseases including age, sex, genetics, diet, and lifestyle. In recent years exposure to environmental contaminants has also been linked to the development of metabolic diseases. Notably, 2,3,7,8-tetrachlorodibenzo-*p*-dioxin (TCDD) has been associated with NAFLD development in epidemiological and rodent studies. TCDD is the prototypical ligand for the aryl hydrocarbon receptor (AhR) which is activated by structurally diverse environmental contaminants, natural products, and endogenous metabolites. In mice, exposure results in the development of hepatic steatosis (fat accumulation) via an AhR dependent mechanism, which is reversed upon cessation of exposure. Continuous TCDD exposure on the other hand leads to collagen deposition indicating progression through the NAFLD disease spectrum (e.g., simple steatosis - steatohepatitis (steatosis with inflammation) – fibrosis/cirrhosis). However, little is known about the mechanism through which AhR activation contributes to NAFLD disease etiology.

The advent of high-throughput and data rich ‘omics’ technologies have facilitated the large-scale assessment of molecular responses and mechanisms of action through the integration of disparate datasets and use of enrichment and systems biology approaches. The present report evaluates the time- and dose-dependent progression of TCDD-elicited NAFLD pathology in mice gavaged with TCDD every 4 days for 28 or 92 days. ‘Layers’ of biological organization are interrogated through the computational identification of genome-wide dioxin response elements (DREs), chromatin immunoprecipitation sequencing (ChIP-Seq), total RNA sequencing (RNA-

Seq), targeted metabolomics, and quantitative evaluation of histological features using the in-house developed Quantitative Histological Analysis Tool (QuHAnT). Systems biology based approaches were used to integrate these disparate datasets to elucidate a mode of action underlying TCDD-elicited disease progression revealing a coordinated reorganization of hepatic gene expression and metabolism characterized by 1) a Warburg effect-like reprogramming of carbohydrate metabolism in an AhR-dependent manner, 2) amino acid metabolism redirection, and 3) widespread inflammatory and matrisomal gene expression changes. These metabolic changes underlie the time- and dose-dependent progression of hepatic steatosis to steatohepatitis, and collagen deposition (fibrosis) providing evidence that persistent AhR activation can promote NAFLD pathology progression. Ultimately, these studies indicate complex reprogramming of hepatic metabolism resulting from AhR activation that include not only the promotion of disease progression, but also novel defensive counter measures in an attempt to reduce TCDD-elicited hepatotoxicity.

## ACKNOWLEDGEMENTS

I had never expected to find myself in Graduate school at Michigan State University, but my experience here has been one of tremendous learning opportunities, and personal and professional development for which I am extremely grateful. My success at MSU, however, would not have been possible without the many people who have supported and guided me throughout this experience.

First and foremost I thank my advisor, Dr. Tim Zacharewski, for giving me the opportunity to join and work in his lab. I am grateful to the numerous opportunities and advice he has provided me throughout my time at MSU which has significantly contributed to my professional and personal development, and becoming a good scientist. I am also thankful for his encouragement to develop essential skills that will of enormous benefit in the future.

I would also like to thank my Graduate Dissertation Committee members; Drs. Christina Chan, Bill Henry, Dan Jones, and Norb Kaminski who have provided valuable guidance for dissertation project. Moreover, I thank them for the interesting discussions about science whether related or not to my own research.

Much of the work I've done throughout my graduate career at MSU would not have been possible without the many colleagues, collaborators, and friends who have shared their expertise. I thank Drs. Dirk Colbry and Sophia Lunt for their valuable advice, help, and training throughout the years. Thanks as well as past and current lab members; Drs. Michelle Angrish, Agnes Forgacs, Anna Kopec, Suntae Kim, as well as Kelly Fader and the many undergraduate students who have assisted along the way; Dustin Ammendolia, Mathew Kirby, and Daria Tarasova.

I must also express my gratitude to Dr. Thomas Moon at the University of Ottawa with whom I completed my Master's degree. In addition to initiating my interest in scientific research in the fields of biochemistry and toxicology, he has provided valuable advice which has led to my graduate career at MSU.

Finally, there have been several people in my life who have been extremely supportive without whom none of this would have been possible, family and friends. My mother Sylvie, father Emile, sister Adina, nephews Thomas and Noah, niece Stacy and great friend Pamela. Thank you all for your love and support throughout my graduate career and as I continue to pursue a career no matter how far or close to home I am.

**TABLE OF CONTENTS**

## LIST OF TABLES

## LIST OF FIGURES

## KEY TO ABBREVIATIONS

| | |
|---|---|
| AFLD | alcoholic fatty liver disease |
| AhR | aryl hydrocarbon receptor |
| ARNT | aryl hydrocarbon receptor nuclear translocator |
| bHLH-PAS | basic helix-loop-helix per-arnt-sim |
| CVD | cardiovascular disease |
| ChIP-Seq | Chromatin immunoprecipitation sequencing |
| DLC | dioxin like compound |
| DRE | dioxin response element |
| EMT | epithelial to mesenchymal transition |
| FFA | free fatty acid |
| H&E | hematoxylin & eosin |
| HCC | hepatocellular carcinoma |
| HDL | high density lipoprotein |
| HSV | hue, saturation, value |
| LDL | low density lipoprotein |
| NAFLD | nonalcoholic fatty liver disease |
| NAS | nonalcoholic fatty liver disease activity score |
| NASH | nonalcoholic steatohepatitis |
| NC-XRE | non-consensus xenobiotic response element |
| NLS | nuclear localization signal |
| ORO | oil red o |
| PCB | polychlorinated biphenyl |
| PCDD | polychlorinated dibenzodioxin |
| PCDF | polychlorinated dibenzofuran |

| | |
|---|---|
| PND | post-natal day |
| POP | persistent organic pollutant |
| PSR | picrosirius red |
| PWM | position weight matrix |
| QuHAnT | quantitative histological analysis tool |
| RfD | reference dose |
| RNA-Seq | RNA sequencing |
| ROS | reactive oxygen species |
| T2D | type 2 diabetes |
| TAG | triglyceride |
| TCA | tricarboxylic acid cycle |
| TCDD | 2,3,7,8-tetrachlorodibenzo-p-dioxin |
| VLDL | very low density lipoprotein |
| VV | volume density |
| WSI | whole slide imaging |
| XRE | xenobiotic response element |

# CHAPTER 1. LITERATURE REVIEW: ARYL-HYDROCARBON RECEPTOR SIGNALING AND HEPATIC METABOLISM

## INTRODUCTION

The incidence of non-alcoholic fatty liver disease (NAFLD) and related metabolic disorders such as type II diabetes (T2D) and cardiovascular disease (CVD) has reached epidemiological proportions in the United States and other western countries [1-3]. Several factors have been implicated in the development of NAFLD including diet, age, sex, lifestyle, and genetics [4-6]. In recent years epidemiological studies have also implicated exposure to environmental contaminants in the disruption of liver metabolism, including chlorinated compounds such as 2,3,7,8-tetrachlorodibenzo-*p*-dioxin (TCDD) [3, 7, 8]. In rodent models, features of NAFLD have been reported following TCDD exposure from simple hepatic lipid accumulation (steatosis), inflammation (hepatitis), and collagen deposition (fibrosis), all of which are believed to occur in an aryl hydrocarbon receptor (AhR) dependent manner [9-13]. Nevertheless, little is known about the mechanism through which AhR activation contributes to disease etiology. Novel technologies and tools such as transcriptomic evaluation by RNA-Sequencing, profiling of metabolites using metabolomic approaches, computational and systems biology approaches to integrate disparate data types, and the numerous biological databases provide a unique opportunity to further elucidate the etiology of diseases associated with AhR activation. Ultimately, examining large, high-throughput datasets within their biological context will address knowledge gaps regarding the toxicity of TCDD and related compounds and elicited disease processes.

## TCDD, DIOXINS, AND DIOXIN-LIKE CHEMICALS

2,3,7,8-Tetrachlorodibenzo-*p*-dioxin (TCDD) is a member of a class of chemicals named dioxins which are derivatives of dibenzo-*p*-dioxin and is composed of several other polychlorinated dibenzo-*p*-dioxins (PCDDs). These chemicals are considered persistent environmental contaminants due to their long half-lives in the environment ranging from 10 – 12 years [14]. These compounds also share the ability to bind and activate the AhR, for which TCDD is the prototypical ligand [14-17]. Other polychlorinated compounds such as polychlorinated

dibenzofurans (PCDFs) and polychlorinated biphenyls (PCBs) share characteristics with dioxins including the ability to activate the AhR and are therefore commonly referred to as dioxin-like compounds (DLC; Figure 1) [14-17]. For PCBs this represents 12 congeners (unique arrangements of chlorines around the phenyl rings) which are able to adopt a co-planar conformation due to the absence of chlorine substitutions in the *ortho* position, while 10 PCDF and 7 PCDD congeners are considered to be DLCs [14, 18-20]. Furthermore, several natural and endogenous compounds have shown AhR activation capabilities including tryptophan metabolites, heme degradation products, and arachidonic acid metabolites [16, 21, 22].

Anthropogenic sources have largely contributed to the environmental dispersion of dioxins and DLCs including TCDD, although some natural sources also exist [23-25]. Amounts produced through natural sources, however, are much less of a concern than those produced by human activity. TCDD, for example, was largely released as a by-product of industrial processes such as pulp & paper mill bleaching, incineration of waste, incomplete combustion of organic matter, and production of organochlorine pesticides and herbicides [23, 24, 26]. Consequently, use of the herbicide Agent Orange during the Vietnam War in the 1960's represents one of the largest sources of TCDD contamination, and several human epidemiological studies regarding TCDD exposure were performed on Operation Ranch Hand servicemen who were involved in the dispersion of this herbicide, as well as the exposed Vietnamese population [27-32]. Conversely, PCBs were intentionally produced for use as heat transfer fluids in transformers [33]. In Michigan, historical industrial activity along the Great Lakes, as well as the Saginaw and Tittabawasee rivers has led to contamination by dioxins and DLCs where consumption of fish from these areas have been linked to high serum and milk levels [34-38]. Acknowledgement of their persistence and toxicity eventually led to cessation of production. Other persistent organic pollutants (POPs), along with dioxins and DLCs, famously known as the 'dirty dozen' or 'legacy chemicals', ceased production under the Stockholm convention which was ratified in 2004 by 131 countries [19, 39, 40].

Today, dioxins and DLCs continue to be a concern due to their persistence in the environment. Their chemical properties make them difficult to degrade through natural processes, and their lipophilic nature results in bioaccumulation in organisms, and biomagnification in the food chain [14, 15, 20, 35, 36, 41, 42]. Due to bioaccumulation and biomagnification, diet represents the primary source of exposure in humans through consumption of contaminated fish, meat, and dairy products [15, 36, 38, 41, 42]. However, air and soil represent additional sources of exposure, and 'backyard burning' of household wastes is rapidly becoming the primary source of human dioxin exposure in the U.S [23]. Further impacting human exposure, the half-life of DLCs in humans is estimated at 7 – 12 years [27-29, 43] and consequently, lifetime exposure could contribute to dioxin and DLC toxicities in humans. In the most recent report on TCDD released by the US EPA, the oral reference dose (RfD) was established at 0.7 pg/kg/day in order to protect human health [44]. Current estimates place human exposure below these levels in normal populations [45], however historical exposures continue to be of concern [36, 38] as well as the plethora of other natural and anthropogenic AhR ligands.

Toxicity of dioxins and DLCs has largely been characterized following accidental or occupational exposures. For example, the herbicide Agent Orange used during the Vietnam War was contaminated by TCDD and consequently, over 360 kg of TCDD was released in Vietnam covering over 2.6 million acres and affecting ~4.8 million residents and war veterans [46, 47]. Today, studies continue to monitor elevated levels of TCDD levels in Vietnam residents [32]. In Seveso, Italy, a chemical plant accidently released 1 kg of TCDD within tetrachloroethylene in the surrounding community [26, 48]. Three zones of contamination were established to monitor the exposed population for dose-dependent health effects [26, 48]. Moreover, in a rare instance of intentional exposure, Ukrainian presidential candidate Victor Yushchenko was poisoned with TCDD in 2004 resulting in blood concentrations 50,000-fold larger than the general population [49]. These events, and others, have demonstrated that TCDD exposure leads to chloracne, hepatic toxicity, impaired immune function, impaired nervous system, impaired development, and

metabolic disorders such as dyslipidemia, T2D, CVD, and NAFLD [27-31, 48-50]. Studies on these effects in animal models have subsequently revealed that most, if not all, toxic effects by dioxin and DLCs are mediated through activation of the AhR [11].

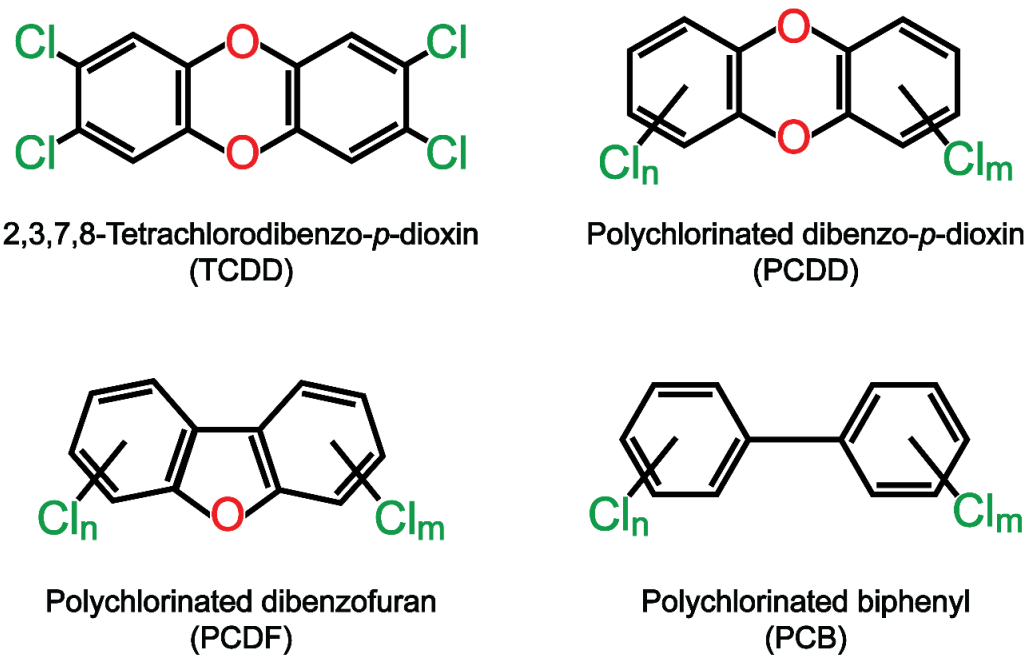


**FIGURE 1. CHEMICAL STRUCTURES OF DIOXINS AND DIOXIN-LIKE CHEMICALS**

## ARYL HYDROCARBON RECEPTOR SIGNALING

The aryl hydrocarbon receptor (AhR) is a ligand-dependent basic helix-loop-helix PER-ARNT-SIM (bHLH-PAS) transcription factor which is well conserved among mammals with ~87% amino acid sequence similarity between mouse, rat, and human PAS domain [51]. Interestingly, homologs of the AhR with similar functionality have been identified in several species ranging from fish to birds, reptiles, amphibians, and mammals [52]. Similarly, homologs have been identified in invertebrates such as the nematode (*C. elegans*), the fruit fly (*D. melanogaster*), and molluscs, although these do not respond to xenobiotics such as DLCs [52]. Despite being a well-known target of dioxins and DLCs, the true physiological ligand of the vertebrate AhR is unknown, although indoles or other tryptophan catabolites, heme degradation products such as bilirubin,

and/or arachidonic acid metabolites have been shown to bind and activate the AhR [16, 21, 22]. Being so well conserved across species, it is unlikely that the role of AhR in response to dioxin and DLCs has arisen in response to anthropogenic chemicals despite TCDD exhibiting much higher binding affinity than any other natural or man-made compound. The absence of any identified natural ligand which exhibits such binding affinity contributes the poorly understood physiological role of the AhR [16, 18, 53].

Over the years several AhR knock-out models have been developed which provided insight on its putative physiological role, and have demonstrated the requirement of the receptor for dioxin and DLC mediated toxicities [11, 54]. Whole-body knock-out mice ($Ahr^{-/-}$) caused a 50 – 60% death rate within 4 days following parturition, reduced growth rates, and lymphocyte infiltration in the gut, urinary tract, and lung [54]. Moreover, livers were smaller in $Ahr^{-/-}$ mice characterized by spontaneous fibrosis, inflammatory changes in the bile ducts, centrilobular hypercellularity, and glycogen depletion [54, 55]. Mutation in the DNA-binding domain of the AhR results in similar hepatic impairments [56]. Collectively, these and other studies examining keratinocytes [57], dendritic cells [58], and the intestinal epithelia [59] support the conclusion that the AhR serves a physiological role and possesses a natural ligand. More recently, a hepatocyte-specific AhR knock-out model has also been developed [60] as well as a tamoxifen inducible hepatocyte specific model which has been shown to impact energy metabolism in the liver and adipose tissue [61]. Future studies in these models will aid in understanding AhR-mediated toxicity following exposure to dioxin and DLCs.

The AhR shares many characteristics of ligand activated nuclear receptors such as ligand binding with subsequent conformational changes, and the ability to regulate gene expression. However, unlike nuclear receptors, the AhR is located in the cytosol and translocates to the nucleus only following ligand activation (Figure 2) [62]. In its unliganded state the AhR is bound by chaperone proteins including a heat shock protein 90 (HSP90) dimer [16, 63-66], p23, and AhR interacting protein (AIP, also known as ARA9 or XAP-2) [16, 67]. Following ligand binding, a

conformational change exposes the nuclear localization signal (NLS) leading to dissociation of HSP90, p23, and AIP followed by translocation to the nucleus [16, 65-67]. The ligand bound AhR then dimerizes with the AhR nuclear translocator (ARNT) and the heterodimer subsequently acts as a transcription factor, binding to dioxin response elements (DRE, also known as xenobiotic response elements; XRE) composed of the core sequence 5'-GCGTG-3', and leading to transcriptional regulation [16, 65, 66]. DRE independent mechanisms of AhR mediated gene regulation have also been demonstrated such as non-consensus binding sites (NC-XRE) [68-70] or tethering to other transcription factors [71]. Negative regulation of this signaling cascade can be achieved through a variety of mechanisms including (i) degradation of ligand by xenobiotic metabolizing enzymes, (ii) AhR degradation, or (iii) the AhR repressor (AHRR) or TCDD induced poly(ADP-ribose) polymerase (TiPARP) through a negative auto-regulatory feedback loop [72, 73].

Members of the bHLH-PAS protein family largely consist of transcription factors which are signal activated, and differ from other bHLH containing proteins by their ability to recognize different DNA response elements [74]. They can be further categorized in classes; class I proteins neither homodimerize or dimerize with other class I proteins while class II can dimerize with itself and most other dimerization partners [74]. The mammalian AhR is an example of class I bHLH-PAS protein, dimerizing with the class II protein ARNT. The AhR protein in addition to the bHLH domain, possesses two PAS domains (A and B) and a transactivation domain. The bHLH domain regulate DNA binding as well as heterodimerization in concert with the PAS domains. Unliganded, the AhR bHLH and PAS B domains, which form the ligand binding region, are associated with HSP90 which is believe to result in masking of its NLS [74, 75]. The PAS A domain, conversely, is believed to play an important role in determining dimerization specificity of the AhR [76].

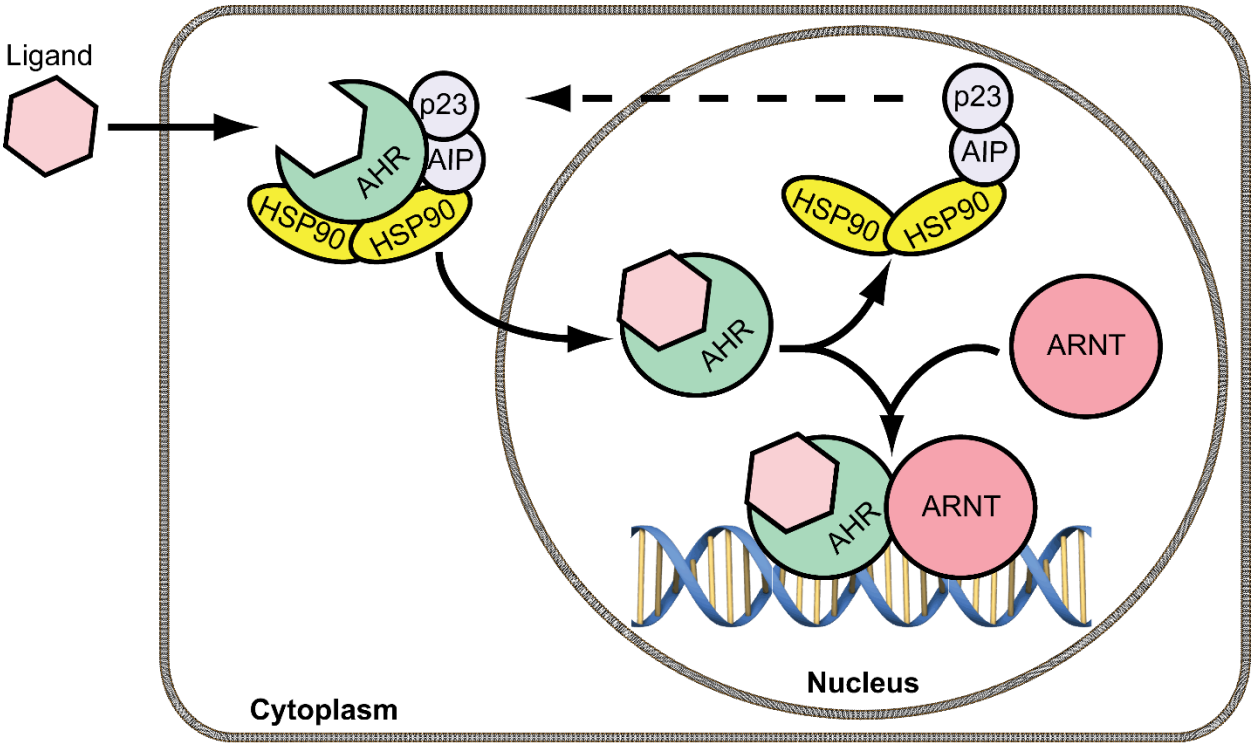


**FIGURE 2. ARYL HYDROCARBON SIGNALING PATHWAY**

AhR-mediated gene expression changes are numerous and often species-, tissue-, context-, and ligand-dependent [51, 77-84]. Sensitivity to AhR-mediated toxicities, for example, show a 10-, and 1,000-fold difference within mouse and rat strains, respectively, and 1,000-fold difference between the Guinea pig and hamster described as the most sensitive and resistant species, respectively [85]. In rats, point mutations in the transactivation domain play critical roles in sensitivity differences [86] while point mutations in the ligand binding domain of the mouse AhR may also contribute to strain sensitivity differences [87] Interestingly, the human AhR is reported to be most similar to the Guinea pig AhR yet absence of lethality in accidental exposures reveals additional factors affecting sensitivity which are unknown at the moment [85]. Nevertheless, differential expression of the 'AhR gene battery' is typically observed following exposure to an exogenous ligand, including phase I and II xenobiotic metabolizing enzymes (*Cyp1a1*, *Cyp1a2*, *Nqo1*, *Aldh3a1*, *Ugt1a6*). Studies in Nrf2-null mice have also implicated *Nrf2* as a key player in

the induction of some “AhR battery” genes, particularly, *Nqo1*, *Ugt1a6*, and several glutathione synthesis genes [88]. Moreover, in *Cyp1a1*-null mice, TCDD-elicited toxicity is attenuated with reduced lethality and hepatic fat accumulation [89] indicating the importance of the AhR gene battery in TCDD-elicited toxicities. The importance of these genes in the production and response to oxidative stress certainly points to a role of reactive oxygen species (ROS) in TCDD-elicited toxicity [12, 90-92].

## ROLE OF TCDD IN FATTY LIVER DISEASE

Fatty liver disease typically describes a spectrum of liver pathologies ranging from the simple, reversible, and benign lipid accumulation (hepatic steatosis), steatosis with inflammation (steatohepatitis), and collagen deposition (fibrosis/cirrhosis) (Figure 3) [93, 94]. Fatty liver disease is commonly classified by its etiology as either alcoholic fatty liver disease (AFLD) when linked to excessive alcohol consumption, or non-alcoholic fatty liver disease (NAFLD) when occurring without alcohol consumption. In the U.S population, the incidence of NAFLD is estimated at 18 – 35%, and is increasing in the U.S. and worldwide [94-97]. Moreover, NAFLD is an important risk factor for more complex metabolic diseases including CVD, T2D, hepatocellular carcinoma (HCC), and liver failure [4-6]. Consequently, understanding the mechanism of NAFLD pathogenesis is of utmost importance for human health.

Several groups have attempted to describe the mechanism of fatty liver disease pathogenesis in a simplified manner. For example, the ‘two-hit hypothesis’ describes an initial lipid accumulation (first ‘hit’) which predisposes the liver to lipid peroxidation (second ‘hit’) and subsequent progression towards NAFLD pathologies [93, 98]. Since then, the complexity of NAFLD pathogenesis has led to ‘three-hit’, ‘four-hit’, and finally ‘multiple-hit’ hypotheses [99-101]. Indeed, development of NAFLD involves numerous factors including lipid accumulation, cytokines, hormones, nutrition, lifestyle, genetics, and even changes in the intestinal microbiome [101]. Additionally, epidemiological data and rodent studies have implicated xenobiotics such as

TCDD, dioxins, and DLCs in the perturbation of hepatic lipid metabolism and NAFLD etiology [3, 9-11, 13, 102]. For example, mice gavaged with a single bolus dose of TCDD have increased lipid accumulation as early as 24 hours following exposure [9] which, in the absence of additional exposure, is completely reversed by 4 weeks [102] similarly to human hepatic steatosis [94].

In NAFLD the liver accumulates fats in the form of triglycerides (TAGs) produced through the esterification of glycerol and free fatty acids (FFAs) obtained either through *de novo* synthesis in the liver, or from peripheral sources such as the adipose tissue or diet [101, 103]. Hepatic lipid accumulation of TAGs, however, is not inherently adverse as it may protect the liver from lipotoxicity which is clearly demonstrated in mice unable to synthesize TAGs [101, 104, 105]. Free fatty acids in the liver promote lipid peroxides and reactive oxygen species (ROS) production which contribute to hepatic damage, as well as promote the development of more severe features of NAFLD [93, 98, 105]. In agreement with the role of oxidative stress in NAFLD, mice lacking the "AhR battery" gene *Nrf2* which regulates antioxidant responses exposed to TCDD show progression of hepatic steatosis to steatohepatitis [91]. Indeed, AhR activation is known to increase ROS production which contributes to the development of AhR-mediated NAFLD progression [106, 107]. However, protection from TCDD-induced steatosis in glutathione-deficient mice [12] highlights the complexity of AhR-mediated NAFLD development.

A variety of other factors are implicated in the progression of NAFLD pathologies such as proinflammatory and profibrotic cytokines. For example, increased levels of interleukin-6 (IL-6) and tumor necrosis factor α (TNFα) promotes inflammatory cell recruitment and extracellular matrix remodeling in NAFLD [108]. TCDD represses hepatic carboxylesterase (CES3) resulting in the accumulation of substrates possessing proinflammatory signaling functions implicating the AhR in inflammation [109]. Recently, Pierre *et al.* [10] demonstrated that weekly TCDD dosing also activated profibrotic pathways leading to excessive collagen production by myofibroblasts and hepatic collagen deposition. These studies illustrate the potential of TCDD and DLCs to promote the progression of simple steatosis to more severe NAFLD pathologies. However, none

report the time- or dose-dependent occurrence of these pathologies, or their progression from steatosis to fibrosis.

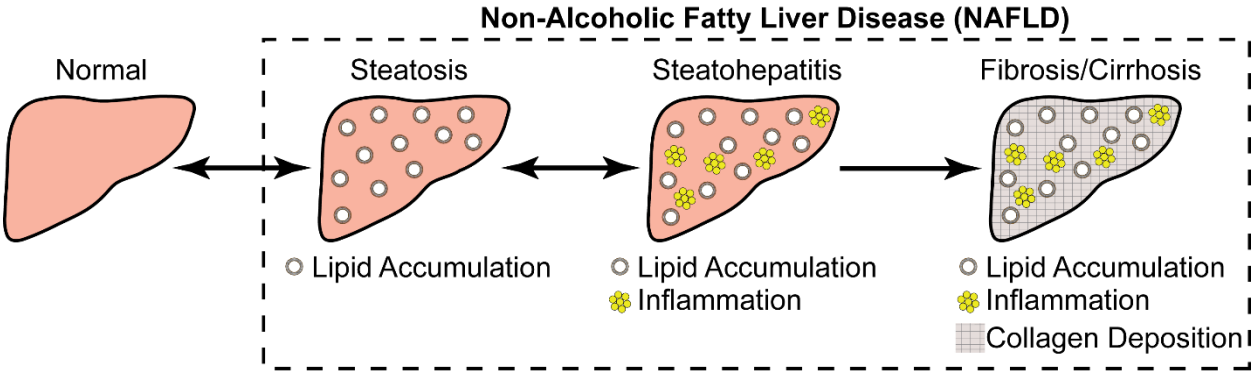


**FIGURE 3. SPECTRUM OF NON-ALCOHOLIC FATTY LIVER DISEASE**

## LIVER ENERGY METABOLISM AND TCDD EXPOSURE

The liver performs essential physiological functions including (i) processing of nutrients absorbed from the diet, (ii) storing and/or production of vitamins, minerals, and sugars, (iii) biosynthesis of bile for digestion and fat absorption, (iv) production of factors for clotting and nutrient absorption, and (v) metabolism and elimination of endogenous and exogenous compounds. The liver receives nutrients and toxicants directly from the diet via the portal vein which connects the gastrointestinal tract to the liver, making it one of the first responders to nutritional signals. Consequently, the liver is an important metabolic organ playing a key role in energy homeostasis (Figure 4) [110]. Not surprisingly, disruption of hepatic glucose and lipid metabolism is involved in the development of metabolic diseases such as T2D and CVD.

Maintenance of blood glucose homeostasis is essential as is illustrated in diabetes which is characterized by the inability to maintain a proper glycemic level. The liver plays a critical role in regulating blood glucose levels [110, 111]. In a postprandial state, excess glucose is converted to glycogen, fatty acid, or amino acids as a form of storage or used in other metabolic pathways [110]. Upon uptake, glucose is converted to glucose-6-phosphate (G6P) with serves as substrate glycogen synthesis, the pentose phosphate pathway to produce NADPH, or for the production of

pyruvate through the glycolysis pathway. Pyruvate is subsequently directed into the tricarboxylic acid (TCA) cycle where it is used to produce ATP via oxidative phosphorylation in the mitochondria. Conversely, in a fasted state or other periods of low carbohydrate availability (e.g. starvation and exercise) hepatic glycolysis is reversed to produce and export glucose for use by other tissues which is derived from lactate, pyruvate, amino acids, and glycerol obtained by lipolysis [110]. The enzyme phosphoenolpyruvate carboxylase (PEPCK-C) plays a critical role in gluconeogenesis from lactate and amino acids [110, 112-114]. Following TCDD exposure, repression of gluconeogenesis is observed in mice and rats and is believed to be partly mediated by the "AhR battery" gene TiPARP which mono-ADP-ribosylates PEPCK-C [115-119]. Few studies, however, have reported disruption of glycolysis or oxidative phosphorylation, although reduced ATP production by mitochondria is reported in mice [120] and several studies have shown impaired mitochondrial function associated with increased production of reactive oxygen species (ROS) [120-122].

Of particular importance in dioxin and DLC disruption of hepatic metabolism is the impact on lipid metabolism. Fatty acids can either be obtained through dietary consumption, redistribution by lipoproteins, or through *de novo* synthesis. They are stored and used largely by; adipose tissue, liver, and skeletal muscle [123]. Adipose tissue serves as the major site of fatty acid storage which are stored as triglycerides (TAGs) while the liver is the major tissue for *de novo* fatty acid synthesis [110, 123]. Skeletal muscle also has the capacity to perform de *novo* lipogenesis [124]. The liver and muscle, however, largely use free fatty acids obtained from TAGs as an energy substrate through β-oxidation due to their high energy density [110, 123]. Lipids obtained from diet are taken up by the liver which repackages them for systemic distribution via lipoproteins, particles consisting of a core of non-polar lipids and membrane of polar lipids and apolipoproteins [123, 125]. Consequently, the liver is the principal producer of apolipoproteins which are recognized by specific lipoprotein receptors [125]. The protein CD36 has been implicated as a key player in the uptake of fat by the liver [126, 127] and is induced by TCDD via the AhR [13]. Similarly, serum

apolipoprotein B (Apob100 and Apob48) found in chylomicrons and very low density lipoprotein (VLDL), as well as low density (LDL) and high density (HDL) lipoproteins, are reduced by TCDD in mice indicating reduced efflux of hepatic lipids [128]. Moreover, TCDD also represses hepatic β-oxidation of lipids [13]. These studies suggest TCDD (i) increases hepatic lipid uptake, (ii) reduces lipid export, and (iii) inhibits lipid catabolism resulting in steatosis, although the mechanism underlying these changes in hepatic lipid metabolism remain unresolved.

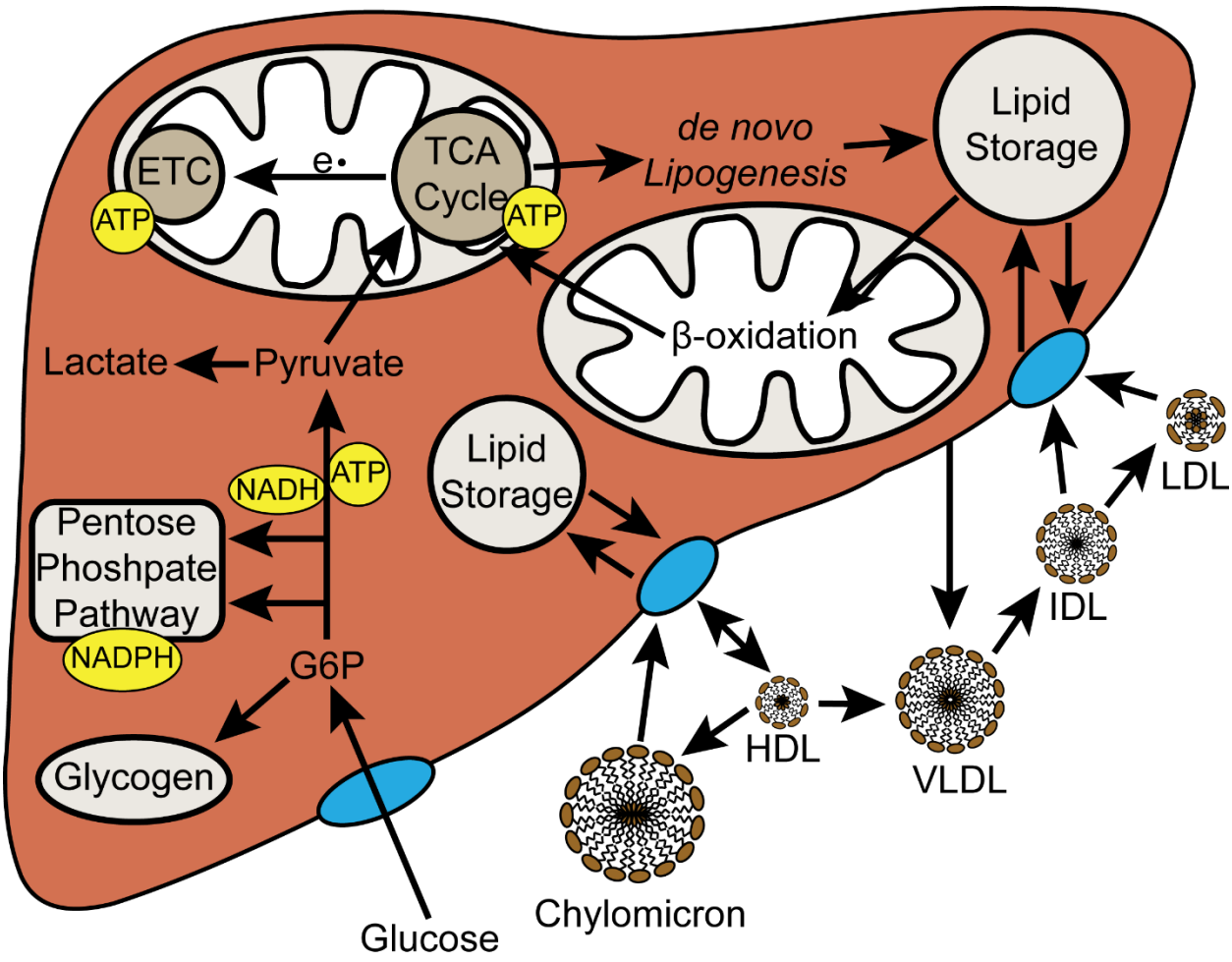


**FIGURE 4. OVERVIEW OF HEPATIC METABOLISM**

Hepatic metabolism of carbohydrates and lipids is regulated by a variety of nutrient signals. Insulin, a peptide hormone produced by beta cells in the pancreas, for example, is

induced upon dietary signals promoting the storage of glucose in the liver. Conversely, glucagon promotes the induction of gluconeogenesis in the liver. Exposure to dioxin and DLCs has been associated with impaired insulin signaling in human populations [3, 7, 8], however studies in mice have been inconclusive demonstrating both increased insulin sensitivity and reduced insulin secretion [129], and reduced sensitivity in a circadian rhythm dependent manner [130]. Recently, fibroblast growth factor 21 (FGF21) was demonstrated as a direct AhR target with increased levels detected in the serum [131]. FGF21 improves insulin sensitivity and glucose uptake, although this is dependent on adiponectin [132], illustrating the complexity of hepatic metabolism regulation. Understanding how TCDD alters hepatic metabolism and its regulation is just beginning to inform on the possible role in development of AhR-mediated NAFLD.

## QUANTITATIVE SYSTEMS APPROACHES TO ELUCIDATE MECHANISM

Technological advances have dramatically altered how scientific research can be performed, leading to the advent of new areas of research such as systems biology or more globally as hypothesis generating research. “Omics” approaches including transcriptomic, metabolomic, proteomic, and phenomic evaluations allows researchers to profile biological responses in an untargeted and largely unbiased approach, facilitating the identification of novel or unexpected information to guide future research. Furthermore, continuous improvements in methodology and technology have increased throughput and data density. Transcriptomics alone, for example, has witnessed the use of probe-based microarray technology becoming rapidly outdated and replaced by sequencing technology which is independent of pre-determined probes, and more quantitative in nature [133-136]. Similarly, as molecular approaches have aimed to increase throughput, information density, and improve the quantitative nature of measurements, many have also aimed to develop high-throughput quantitative techniques to evaluate phenotypic responses which have largely been qualitative in nature [137-139]. In biomedical research,

development of high-quality whole slide imaging have significantly facilitated the development of quantitative phenotypic evaluations.

"Omics" approaches interrogate almost every layer of biology from identification of transcription factor binding sites (i.e. identification of response elements and/or chromatin immunoprecipitation sequencing; ChIP-Seq) to metabolite profiling [71, 140]. Concomitantly, numerous tools and databases have permitted the evaluation of these datasets using enrichment analyses or the integration of these various datasets to examine responses within biological networks (i.e. as connected components of a metabolic pathway). While enrichment and overrepresentation approaches provide valuable information, systems approaches which describe observed responses within their biological contexts will undoubtedly become an important approach for the identification and description of mechanisms by outlining biologically relevant models which can be tested computationally, and experimentally (Figure 5).

## CONCLUSIONS

The pathogenesis of NAFLD is complex and involves the interaction of several factors including lifestyle, diet, genetics, and exposure to environmental contaminants. Dioxin and DLCs have been linked to NAFLD and metabolic disease in humans [3, 7, 8], and rodent studies have clearly demonstrated that the activation of the AhR can induce NAFLD pathologies [9-11, 13, 77, 91, 102, 128]. Although recent studies have demonstrated that TCDD can lead to development of more severe NAFLD pathologies such as steatohepatitis and fibrosis, there is little known about the progression of the disease following AhR activation, or the mechanism through which these features progress. In humans, steatosis is considered reversible, as was demonstrated in TCDD exposed mice [102], but steatohepatitis and fibrosis are much less so or not at all [94]. Collectively, NAFLD represents a key risk factor for development of more severe disease including T2D, CVD, and HCC. Therefore, examining the mechanism through which the AhR mediates development

and progression of NAFLD pathologies plays an important role in understanding of this disease which is reaching epidemic proportions in the U.S. and worldwide.

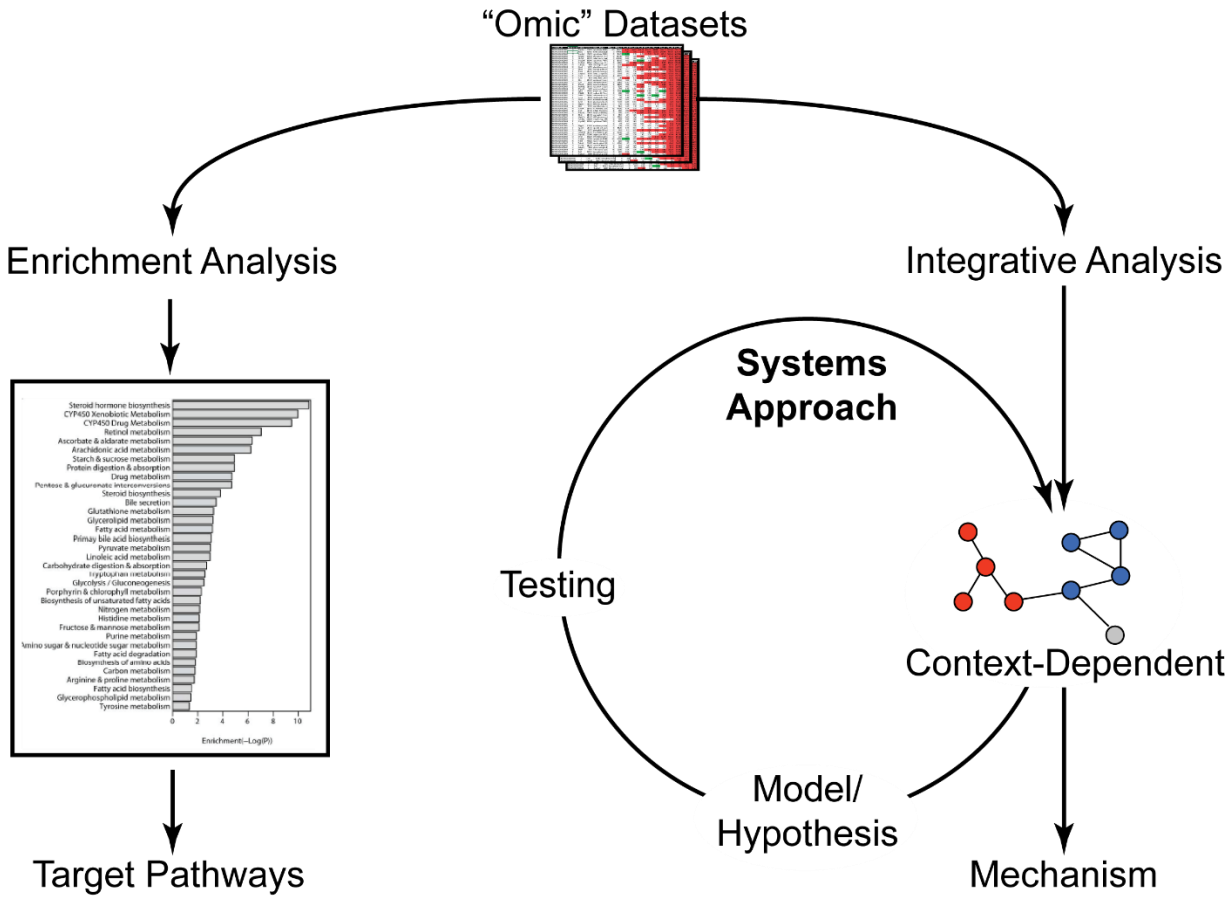


**FIGURE 5. ENRICHMENT AND SYSTEMS APPROACHES FOR THE ANALYSIS OF OMICS DATA**

## REFERENCES

## REFERENCES


1. Ford, E.S., C. Li, and G. Zhao, *Prevalence and correlates of metabolic syndrome based on a harmonious definition among adults in the US.* J Diabetes, 2010. 2(3): p. 180-93.

2. Vanni, E., E. Bugianesi, A. Kotronen, S. De Minicis, H. Yki-Jarvinen, and G. Svegliati-Baroni, *From the metabolic syndrome to NAFLD or vice versa?* Dig Liver Dis, 2010. 42(5): p. 320-30.

3. Neel, B.A. and R.M. Sargis, *The paradox of progress: environmental disruption of metabolism and the diabetes epidemic.* Diabetes, 2011. 60(7): p. 1838-48.

4. Unger, R.H. and P.E. Scherer, *Gluttony, sloth and the metabolic syndrome: a roadmap to lipotoxicity.* Trends Endocrinol Metab, 2010. 21(6): p. 345-52.

5. Unger, R.H., G.O. Clark, P.E. Scherer, and L. Orci, *Lipid homeostasis, lipotoxicity and the metabolic syndrome.* Biochim Biophys Acta, 2010. 1801(3): p. 209-14.

6. Pitsavos, C., D. Panagiotakos, M. Weinem, and C. Stefanadis, *Diet, exercise and the metabolic syndrome.* Rev Diabet Stud, 2006. 3(3): p. 118-26.

7. Taylor, K.W., R.F. Novak, H.A. Anderson, L.S. Birnbaum, C. Blystone, M. Devito, D. Jacobs, J. Kohrle, D.H. Lee, L. Rylander, A. Rignell-Hydbom, R. Tornero-Velez, M.E. Turyk, A.L. Boyles, K.A. Thayer, and L. Lind, *Evaluation of the association between persistent organic pollutants (POPs) and diabetes in epidemiological studies: a national toxicology program workshop review.* Environ Health Perspect, 2013. 121(7): p. 774-83.

8. Lee, D.H., I.K. Lee, M. Porta, M. Steffes, and D.R. Jacobs, Jr., *Relationship between serum concentrations of persistent organic pollutants and the prevalence of metabolic syndrome among non-diabetic adults: results from the National Health and Nutrition Examination Survey 1999-2002.* Diabetologia, 2007. 50(9): p. 1841-51.

9. Boverhof, D.R., L.D. Burgoon, C. Tashiro, B. Chittim, J.R. Harkema, D.B. Jump, and T.R. Zacharewski, *Temporal and dose-dependent hepatic gene expression patterns in mice provide new insights into TCDD-Mediated hepatotoxicity.* Toxicol Sci, 2005. 85(2): p. 1048-63.

10. Pierre, S., A. Chevallier, F. Teixeira-Clerc, A. Ambolet-Camoit, L.C. Bui, A.S. Bats, J.C. Fournet, P. Fernandez-Salguero, M. Aggerbeck, S. Lotersztajn, R. Barouki, and X. Coumoul, *Aryl hydrocarbon receptor-dependent induction of liver fibrosis by dioxin.* Toxicol Sci, 2014. 137(1): p. 114-24.

11. Fernandez-Salguero, P.M., D.M. Hilbert, S. Rudikoff, J.M. Ward, and F.J. Gonzalez, *Aryl-hydrocarbon receptor-deficient mice are resistant to 2,3,7,8-tetrachlorodibenzo-p-dioxin-induced toxicity.* Toxicol Appl Pharmacol, 1996. 140(1): p. 173-9.

12. Chen, Y., M. Krishan, D.W. Nebert, and H.G. Shertzer, *Glutathione-deficient mice are susceptible to TCDD-Induced hepatocellular toxicity but resistant to steatosis.* Chem Res Toxicol, 2012. 25(1): p. 94-100.

13. Lee, J.H., T. Wada, M. Febbraio, J. He, T. Matsubara, M.J. Lee, F.J. Gonzalez, and W. Xie, *A novel role for the dioxin receptor in fatty acid metabolism and hepatic steatosis.* Gastroenterology, 2010. 139(2): p. 653-63.

14. Birnbaum, L.S. and M.J. DeVito, *Use of toxic equivalency factors for risk assessment for dioxins and related compounds.* Toxicology, 1995. 105(2-3): p. 391-401.

15. Van den Berg, M., L.S. Birnbaum, M. Denison, M. De Vito, W. Farland, M. Feeley, H. Fiedler, H. Hakansson, A. Hanberg, L. Haws, M. Rose, S. Safe, D. Schrenk, C. Tohyama, A. Tritscher, J. Tuomisto, M. Tysklind, N. Walker, and R.E. Peterson, *The 2005 World Health Organization reevaluation of human and Mammalian toxic equivalency factors for dioxins and dioxin-like compounds.* Toxicol Sci, 2006. 93(2): p. 223-41.

16. Denison, M.S. and S.R. Nagy, *Activation of the aryl hydrocarbon receptor by structurally diverse exogenous and endogenous chemicals.* Annu Rev Pharmacol Toxicol, 2003. 43: p. 309-34.

17. Denison, M.S., A.A. Soshilov, G. He, D.E. DeGroot, and B. Zhao, *Exactly the same but different: promiscuity and diversity in the molecular mechanisms of action of the aryl hydrocarbon (dioxin) receptor.* Toxicol Sci, 2011. 124(1): p. 1-22.

18. Denison, M.S. and S. Heath-Pagliuso, *The Ah receptor: a regulator of the biochemical and toxicological actions of structurally diverse chemicals.* Bull Environ Contam Toxicol, 1998. 61(5): p. 557-68.

19. Hestermann, E.V., J.J. Stegeman, and M.E. Hahn, *Relative contributions of affinity and intrinsic efficacy to aryl hydrocarbon receptor ligand potency.* Toxicol Appl Pharmacol, 2000. 168(2): p. 160-72.

20. Tavakoly Sany, S.B., R. Hashim, A. Salleh, M. Rezayi, D.J. Karlen, B.B. Razavizadeh, and E. Abouzari-Lotf, *Dioxin risk assessment: mechanisms of action and possible toxicity in human health.* Environ Sci Pollut Res Int, 2015. 22(24): p. 19434-50.

21. Wei, Y.D., H. Helleberg, U. Rannug, and A. Rannug, *Rapid and transient induction of CYP1A1 gene expression in human cells by the tryptophan photoproduct 6-formylindolo[3,2-b]carbazole.* Chem Biol Interact, 1998. 110(1-2): p. 39-55.

22. Rannug, U., A. Rannug, U. Sjoberg, H. Li, R. Westerholm, and J. Bergman, *Structure elucidation of two tryptophan-derived, high affinity Ah receptor ligands.* Chem Biol, 1995. 2(12): p. 841-5.

23. *An Inventory of Sources and Environmental Releases of Dioxin-Like Compounds on the United States for the Years 1987, 1985, and 2000.* 2006.

24. Travis, C.C. and H.A. Hattemer-Frey, *Human exposure to dioxin.* Sci Total Environ, 1991. 104(1-2): p. 97-127.

25. Ferrario, J.B., C.J. Byrne, and D.H. Cleverly, *2,3,7,8-Dibenzo-p-dioxins in Mined Clay Products from the United States: Evidence for Possible Natural Origin.* Environmental Science & Technology, 2000. 34(21): p. 4524-4532.

26. Boffetta, P., K.A. Mundt, H.O. Adami, P. Cole, and J.S. Mandel, *TCDD and cancer: a critical review of epidemiologic studies.* Crit Rev Toxicol, 2011. 41(7): p. 622-36.

27. Wolfe, W.H., J.E. Michalek, J.C. Miner, J.L. Pirkle, S.P. Caudill, D.G. Patterson, Jr., and L.L. Needham, *Determinants of TCDD half-life in veterans of operation ranch hand.* J Toxicol Environ Health, 1994. 41(4): p. 481-8.

28. Pirkle, J.L., W.H. Wolfe, D.G. Patterson, L.L. Needham, J.E. Michalek, J.C. Miner, M.R. Peterson, and D.L. Phillips, *Estimates of the half-life of 2,3,7,8-tetrachlorodibenzo-p-dioxin in Vietnam Veterans of Operation Ranch Hand.* J Toxicol Environ Health, 1989. 27(2): p. 165-71.

29. Michalek, J.E., R.C. Tripathi, S.P. Caudill, and J.L. Pirkle, *Investigation of TCDD half-life heterogeneity in veterans of Operation Ranch Hand.* J Toxicol Environ Health, 1992. 35(1): p. 29-38.

30. Steenland, K., G. Calvert, N. Ketchum, and J. Michalek, *Dioxin and diabetes mellitus: an analysis of the combined NIOSH and Ranch Hand data.* Occup Environ Med, 2001. 58(10): p. 641-8.

31. Henriksen, G.L., N.S. Ketchum, J.E. Michalek, and J.A. Swaby, *Serum Dioxin and Diabetes Mellitus in Veterans of Operation Ranch Hand.* Epidemiology, 1997. 8(3): p. 252-258.

32. Manh, H.D., T. Kido, P.T. Tai, R. Okamoto, S. Honma, S.X. Liang, T. Anh le, S. Maruzeni, T.N. Nghi, M. Nishijo, H. Nakagawa, D.D. Nhu, D. Van Tung, N.N. Hung, and K. Son le, *Levels of polychlorinated dibenzodioxins and polychlorinated dibenzofurans in breast milk samples from three dioxin-contaminated hotspots of Vietnam.* Sci Total Environ, 2015. 511: p. 416-22.

33. National Toxicology, P., *NTP toxicology and carcinogenesis studies of 3,3',4,4',5-pentachlorobiphenyl (PCB 126) (CAS No. 57465-28-8) in female Harlan Sprague-Dawley rats (Gavage Studies).* Natl Toxicol Program Tech Rep Ser, 2006(520): p. 4-246.

34. Wan, Y., P.D. Jones, R.R. Holem, J.S. Khim, H. Chang, D.P. Kay, S.A. Roark, J.L. Newsted, W.P. Patterson, and J.P. Giesy, *Bioaccumulation of polychlorinated dibenzo-p-dioxins, dibenzofurans, and dioxin-like polychlorinated biphenyls in fishes from the Tittabawassee and Saginaw Rivers, Michigan, USA.* Sci Total Environ, 2010. 408(11): p. 2394-401.

35. Tryphonas, H., *Immunotoxicity of PCBs (Aroclors) in relation to Great Lakes.* Environ Health Perspect, 1995. 103 Suppl 9: p. 35-46.

36. Turyk, M., G. Fantuzzi, V. Persky, S. Freels, A. Lambertino, M. Pini, D.H. Rhodes, and H.A. Anderson, *Persistent organic pollutants and biomarkers of diabetes risk in a cohort of Great Lakes sport caught fish consumers.* Environ Res, 2015. 140: p. 335-44.

37. Humphrey, H.E., J.C. Gardiner, J.R. Pandya, A.M. Sweeney, D.M. Gasior, R.J. McCaffrey, and S.L. Schantz, *PCB congener profile in the serum of humans consuming Great Lakes fish.* Environ Health Perspect, 2000. 108(2): p. 167-72.

38. Garabrant, D.H., A. Franzblau, J. Lepkowski, B.W. Gillespie, P. Adriaens, A. Demond, E. Hedgeman, K. Knutson, L. Zwica, K. Olson, T. Towey, Q. Chen, B. Hong, C.W. Chang, S.Y. Lee, B. Ward, K. Ladronka, W. Luksemburg, and M. Maier, *The University of Michigan Dioxin Exposure Study: predictors of human serum dioxin concentrations in Midland and Saginaw, Michigan.* Environ Health Perspect, 2009. 117(5): p. 818-24.

39. Weber, R., A. Watson, M. Forter, and F. Oliaei, *Review Article: Persistent organic pollutants and landfills - a review of past experiences and future challenges.* Waste Manag Res, 2011. 29(1): p. 107-21.

40. Kelly, B.C., M.G. Ikonomou, J.D. Blair, A.E. Morin, and F.A. Gobas, *Food web-specific biomagnification of persistent organic pollutants.* Science, 2007. 317(5835): p. 236-9.

41. Larsen, J.C., *Risk assessments of polychlorinated dibenzo- p-dioxins, polychlorinated dibenzofurans, and dioxin-like polychlorinated biphenyls in food.* Mol Nutr Food Res, 2006. 50(10): p. 885-96.

42. Liem, A.K., P. Furst, and C. Rappe, *Exposure of populations to dioxins and related compounds.* Food Addit Contam, 2000. 17(4): p. 241-59.

43. DeVito, M.J., L.S. Birnbaum, W.H. Farland, and T.A. Gasiewicz, *Comparisons of estimated human body burdens of dioxinlike chemicals and TCDD body burdens in experimentally exposed animals.* Environ Health Perspect, 1995. 103(9): p. 820-31.

44. Dourson, M.L., B. Gadagbui, S. Griffin, D.H. Garabrant, L.C. Haws, C. Kirman, and C. Tohyama, *The importance of problem formulations in risk assessment: a case study involving dioxin-contaminated soil.* Regul Toxicol Pharmacol, 2013. 66(2): p. 208-16.

45. Aylward, L.L. and S.M. Hays, *Temporal trends in human TCDD body burden: decreases over three decades and implications for exposure levels.* J Expo Anal Environ Epidemiol, 2002. 12(5): p. 319-28.

46. Dwernychuk, L.W., H.D. Cau, C.T. Hatfield, T.G. Boivin, T.M. Hung, P.T. Dung, and N.D. Thai, *Dioxin reservoirs in southern Viet Nam--a legacy of Agent Orange.* Chemosphere, 2002. 47(2): p. 117-37.

47. Stellman, J.M., S.D. Stellman, R. Christian, T. Weber, and C. Tomasallo, *The extent and patterns of usage of Agent Orange and other herbicides in Vietnam.* Nature, 2003. 422(6933): p. 681-7.

48. Signorini, S., P.M. Gerthoux, C. Dassi, M. Cazzaniga, P. Brambilla, N. Vincoli, and P. Mocarelli, *Environmental exposure to dioxin: the Seveso experience.* Andrologia, 2000. 32(4-5): p. 263-70.

49. Sorg, O., M. Zennegg, P. Schmid, R. Fedosyuk, R. Valikhnovskyi, O. Gaide, V. Kniazevych, and J.H. Saurat, *2,3,7,8-tetrachlorodibenzo-p-dioxin (TCDD) poisoning in Victor Yushchenko: identification and measurement of TCDD metabolites.* Lancet, 2009. 374(9696): p. 1179-85.

50. Eskenazi, B., P. Mocarelli, M. Warner, S. Samuels, P. Vercellini, D. Olive, L.L. Needham, D.G. Patterson, Jr., P. Brambilla, N. Gavoni, S. Casalini, S. Panazza, W. Turner, and P.M.

Gerthoux, *Serum dioxin concentrations and endometriosis: a cohort study in Seveso, Italy.* Environ Health Perspect, 2002. 110(7): p. 629-34.

51. Tian, J., Y. Feng, H. Fu, H.Q. Xie, J.X. Jiang, and B. Zhao, *The Aryl Hydrocarbon Receptor: A Key Bridging Molecule of External and Internal Chemical Signals.* Environ Sci Technol, 2015. 49(16): p. 9518-31.

52. Hahn, M.E., *Aryl hydrocarbon receptors: diversity and evolution.* Chem Biol Interact, 2002. 141(1-2): p. 131-60.

53. Jeuken, A., B.J. Keser, E. Khan, A. Brouwer, J. Koeman, and M.S. Denison, *Activation of the Ah receptor by extracts of dietary herbal supplements, vegetables, and fruits.* J Agric Food Chem, 2003. 51(18): p. 5478-87.

54. Fernandez-Salguero, P., T. Pineau, D.M. Hilbert, T. Mcphail, S.S.T. Lee, S. Kimura, D.W. Nebert, S. Rudikoff, J.M. Ward, and F.J. Gonzalez, *Immune-System Impairment and Hepatic-Fibrosis in Mice Lacking the Dioxin-Binding Ah Receptor.* Science, 1995. 268(5211): p. 722-726.

55. Schmidt, J.V., G.H. Su, J.K. Reddy, M.C. Simon, and C.A. Bradfield, *Characterization of a murine Ahr null allele: involvement of the Ah receptor in hepatic growth and development.* Proc Natl Acad Sci U S A, 1996. 93(13): p. 6731-6.

56. Bunger, M.K., E. Glover, S.M. Moran, J.A. Walisser, G.P. Lahvis, E.L. Hsu, and C.A. Bradfield, *Abnormal liver development and resistance to 2,3,7,8-tetrachlorodibenzo-p-dioxin toxicity in mice carrying a mutation in the DNA-binding domain of the aryl hydrocarbon receptor.* Toxicol Sci, 2008. 106(1): p. 83-92.

57. van den Bogaard, E.H., M.A. Podolsky, J.P. Smits, X. Cui, C. John, K. Gowda, D. Desai, S.G. Amin, J. Schalkwijk, G.H. Perdew, and A.B. Glick, *Genetic and pharmacological analysis identifies a physiological role for the AHR in epidermal differentiation.* J Invest Dermatol, 2015. 135(5): p. 1320-8.

58. Vogel, C.F., E.M. Kahn, P.S. Leung, M.E. Gershwin, W.L. Chang, D. Wu, T. Haarmann-Stemmann, A. Hoffmann, and M.S. Denison, *Cross-talk between Aryl Hydrocarbon Receptor and the inflammatory response: a Role for NF-kappaB.* J Biol Chem, 2013.

59. Jin, U.H., S.O. Lee, G. Sridharan, K. Lee, L.A. Davidson, A. Jayaraman, R.S. Chapkin, R. Alaniz, and S. Safe, *Microbiome-derived tryptophan metabolites and their aryl hydrocarbon receptor-dependent agonist and antagonist activities.* Mol Pharmacol, 2014. 85(5): p. 777-88.

60. Walisser, J.A., E. Glover, K. Pande, A.L. Liss, and C.A. Bradfield, *Aryl hydrocarbon receptor-dependent liver development and hepatotoxicity are mediated by different cell types.* Proc Natl Acad Sci U S A, 2005. 102(49): p. 17858-63.

61. Carter, D.E., C. Porter, and C. Elferink, *Loss of Hepatic Aryl Hydrocarbon Receptor Alters the Thermogenic Properties of White Fat and Protects Against Diet-Induced Obesity.* Society of Toxicology Annual Meeting, 2016. March 13-17, New Orleans, LA.

62. Kronenberg, S., C. Esser, and C. Carlberg, *An aryl hydrocarbon receptor conformation acts as the functional core of nuclear dioxin signaling.* Nucleic Acids Res, 2000. 28(12): p. 2286-91.

63. Denis, M., S. Cuthill, A.C. Wikstrom, L. Poellinger, and J.A. Gustafsson, *Association of the dioxin receptor with the Mr 90,000 heat shock protein: a structural kinship with the glucocorticoid receptor.* Biochem Biophys Res Commun, 1988. 155(2): p. 801-7.

64. Perdew, G.H., *Association of the Ah receptor with the 90-kDa heat shock protein.* J Biol Chem, 1988. 263(27): p. 13802-5.

65. Hankinson, O., *The aryl hydrocarbon receptor complex.* Annu Rev Pharmacol Toxicol, 1995. 35: p. 307-40.

66. Hankinson, O., *Role of coactivators in transcriptional activation by the aryl hydrocarbon receptor.* Archives of Biochemistry and Biophysics, 2005. 433(2): p. 379-386.

67. Kekatpure, V.D., A.J. Dannenberg, and K. Subbaramaiah, *HDAC6 Modulates Hsp90 Chaperone Activity and Regulates Activation of Aryl Hydrocarbon Receptor Signaling.* Journal of Biological Chemistry, 2009. 284(12): p. 7436-7445.

68. Jackson, D.P., H. Li, K.A. Mitchell, A.D. Joshi, and C.J. Elferink, *Ah receptor-mediated suppression of liver regeneration through NC-XRE-driven p21Cip1 expression.* Mol Pharmacol, 2014. 85(4): p. 533-41.

69. Wilson, S.R., A.D. Joshi, and C.J. Elferink, *The tumor suppressor Kruppel-like factor 6 is a novel aryl hydrocarbon receptor DNA binding partner.* J Pharmacol Exp Ther, 2013. 345(3): p. 419-29.

70. Huang, G. and C.J. Elferink, *A novel nonconsensus xenobiotic response element capable of mediating aryl hydrocarbon receptor-dependent gene expression.* Mol Pharmacol, 2012. 81(3): p. 338-47.

71. Dere, E., R. Lo, T. Celius, J. Matthews, and T.R. Zacharewski, *Integration of genome-wide computation DRE search, AhR ChIP-chip and gene expression analyses of TCDD-elicited responses in the mouse liver.* BMC Genomics, 2011. 12: p. 365.

72. Pollenz, R.S., *The mechanism of AH receptor protein down-regulation (degradation) and its impact on AH receptor-mediated gene regulation.* Chem Biol Interact, 2002. 141(1-2): p. 41-61.

73. Macpherson, L., S. Ahmed, L. Tamblyn, J. Krutmann, I. Forster, H. Weighardt, and J. Matthews, *Aryl Hydrocarbon Receptor Repressor and TiPARP (ARTD14) Use Similar, but also Distinct Mechanisms to Repress Aryl Hydrocarbon Receptor Signaling.* Int J Mol Sci, 2014. 15(5): p. 7939-7957.

74. Kewley, R.J., M.L. Whitelaw, and A. Chapman-Smith, *The mammalian basic helix-loop-helix/PAS family of transcriptional regulators.* Int J Biochem Cell Biol, 2004. 36(2): p. 189-204.

75. Ikuta, T., H. Eguchi, T. Tachibana, Y. Yoneda, and K. Kawajiri, *Nuclear localization and export signals of the human aryl hydrocarbon receptor.* J Biol Chem, 1998. 273(5): p. 2895-904.

76. Pongratz, I., C. Antonsson, M.L. Whitelaw, and L. Poellinger, *Role of the PAS domain in regulation of dimerization and DNA binding specificity of the dioxin receptor.* Mol Cell Biol, 1998. 18(7): p. 4079-88.

77. Boverhof, D.R., L.D. Burgoon, C. Tashiro, B. Sharratt, B. Chittim, J.R. Harkema, D.L. Mendrick, and T.R. Zacharewski, *Comparative toxicogenomic analysis of the hepatotoxic effects of TCDD in Sprague Dawley rats and C57BL/6 mice.* Toxicol Sci, 2006. 94(2): p. 398-416.

78. Forgacs, A.L., E. Dere, M.M. Angrish, and T.R. Zacharewski, *Comparative Analysis of Temporal and Dose-Dependent TCDD-Elicited Gene Expression in Human, Mouse, and Rat Primary Hepatocytes.* Toxicological Sciences, 2013. 133(1): p. 54-66.

79. Dere, E., A.W. Lee, L.D. Burgoon, and T.R. Zacharewski, *Differences in TCDD-elicited gene expression profiles in human HepG2, mouse Hepa1c1c7 and rat H4IIE hepatoma cells.* BMC Genomics, 2011. 12: p. 193.

80. Nault, R., A.L. Forgacs, E. Dere, and T.R. Zacharewski, *Comparisons of differential gene expression elicited by TCDD, PCB126, betaNF, or ICZ in mouse hepatoma Hepa1c1c7 cells and C57BL/6 mouse liver.* Toxicol Lett, 2013. 223(1): p. 52-59.

81. De Vito, M.J., W.E. Maier, J.J. Diliberto, and L.S. Birnbaum, *Comparative Ability of Various PCBs, PCDFs, and TCDD to Induce Cytochrome P450 1A1 and 1A2 Activity Following 4 Weeks of Treatment.* Toxicological Sciences, 1993. 20(1): p. 125-130.

82. Boutros, P.C., K.A. Bielefeld, R. Pohjanvirta, and P.A. Harper, *Dioxin-dependent and dioxin-independent gene batteries: comparison of liver and kidney in AHR-null mice.* Toxicol Sci, 2009. 112(1): p. 245-56.

83. Prokopec, S.D., J.D. Watson, J. Lee, R. Pohjanvirta, and P.C. Boutros, *Sex-related differences in murine hepatic transcriptional and proteomic responses to TCDD.* Toxicol Appl Pharmacol, 2015. 284(2): p. 188-96.

84. Boutros, P.C., R. Yan, I.D. Moffat, R. Pohjanvirta, and A.B. Okey, *Transcriptomic responses to 2,3,7,8-tetrachlorodibenzo-p-dioxin (TCDD) in liver: comparison of rat and mouse.* BMC Genomics, 2008. 9: p. 419.

85. Korkalainen, M., J. Tuomisto, and R. Pohjanvirta, *The AH receptor of the most dioxin-sensitive species, guinea pig, is highly homologous to the human AH receptor.* Biochem Biophys Res Commun, 2001. 285(5): p. 1121-9.

86. Pohjanvirta, R., J.M. Wong, W. Li, P.A. Harper, J. Tuomisto, and A.B. Okey, *Point mutation in intron sequence causes altered carboxyl-terminal structure in the aryl hydrocarbon receptor of the most 2,3,7,8-tetrachlorodibenzo-p-dioxin-resistant rat strain.* Mol Pharmacol, 1998. 54(1): p. 86-93.

87. Poland, A., D. Palen, and E. Glover, *Analysis of the four alleles of the murine aryl hydrocarbon receptor.* Mol Pharmacol, 1994. 46(5): p. 915-21.

88. Yeager, R.L., S.A. Reisman, L.M. Aleksunes, and C.D. Klaassen, *Introducing the "TCDD-inducible AhR-Nrf2 gene battery".* Toxicol Sci, 2009. 111(2): p. 238-46.

89. Uno, S., T.P. Dalton, P.R. Sinclair, N. Gorman, B. Wang, A.G. Smith, M.L. Miller, H.G. Shertzer, and D.W. Nebert, *Cyp1a1(-/-) male mice: protection against high-dose TCDD-induced lethality and wasting syndrome, and resistance to intrahepatocyte lipid accumulation and uroporphyria.* Toxicol Appl Pharmacol, 2004. 196(3): p. 410-21.

90. Shertzer, H.G., D.W. Nebert, A. Puga, M. Ary, D. Sonntag, K. Dixon, L.J. Robinson, E. Cianciolo, and T.P. Dalton, *Dioxin causes a sustained oxidative stress response in the mouse.* Biochem Biophys Res Commun, 1998. 253(1): p. 44-8.

91. Lu, H., W. Cui, and C.D. Klaassen, *Nrf2 protects against 2,3,7,8-tetrachlorodibenzo-p-dioxin (TCDD)-induced oxidative injury and steatohepatitis.* Toxicol Appl Pharmacol, 2011. 256(2): p. 122-35.

92. Nebert, D.W., A.L. Roe, M.Z. Dieter, W.A. Solis, Y. Yang, and T.P. Dalton, *Role of the aromatic hydrocarbon receptor and [Ah] gene battery in the oxidative stress response, cell cycle control, and apoptosis.* Biochem Pharmacol, 2000. 59(1): p. 65-85.

93. Najjar, S.M., *Non-Alcoholic Fatty Liver Disease and the Metabolic Syndrome*, in *Metabolic Basis of Obesity*, R.S. Ahima, Editor. 2011, Springer New York. p. 219-227.

94. Moore, J.B., *Non-alcoholic fatty liver disease: the hepatic consequence of obesity and the metabolic syndrome.* Proc Nutr Soc, 2010. 69(2): p. 211-20.

95. Ford, E.S., *Prevalence of the metabolic syndrome defined by the International Diabetes Federation among adults in the U.S.* Diabetes Care, 2005. 28(11): p. 2745-9.

96. Younossi, Z.M., M. Stepanova, F. Negro, S. Hallaji, Y. Younossi, B. Lam, and M. Srishord, *Nonalcoholic fatty liver disease in lean individuals in the United States.* Medicine (Baltimore), 2012. 91(6): p. 319-27.

97. Fazel, Y., A.B. Koenig, M. Sayiner, Z.D. Goodman, and Z.M. Younossi, *Epidemiology and natural history of non-alcoholic fatty liver disease.* Metabolism, 2016.

98. Day, C.P. and O.F.W. James, *Steatohepatitis: A tale of two "hits"?* Gastroenterology, 1998. 114(4): p. 842-845.

99. Wanless, I.R. and K. Shiota, *The pathogenesis of nonalcoholic steatohepatitis and other fatty liver diseases: a four-step model including the role of lipid release and hepatic venular obstruction in the progression to cirrhosis.* Semin Liver Dis, 2004. 24(1): p. 99-106.

100. Charlton, M., *Noninvasive indices of fibrosis in NAFLD: starting to think about a three-hit (at least) phenomenon.* Am J Gastroenterol, 2007. 102(2): p. 409-11.

101. Buzzetti, E., M. Pinzani, and E.A. Tsochatzis, *The multiple-hit pathogenesis of non-alcoholic fatty liver disease (NAFLD).* Metabolism, 2016.

102. Kopec, A.K., D.R. Boverhof, R. Nault, J.R. Harkema, C. Tashiro, D. Potter, B. Sharratt, B. Chittim, and T.R. Zacharewski, *Toxicogenomic Evaluation of Long-term Hepatic Effects of TCDD in Immature, Ovariectomized C57BL/6 Mice.* Toxicol Sci, 2013. 135(2): p. 465-75.

103. Jacome-Sosa, M.M. and E.J. Parks, *Fatty acid sources and their fluxes as they contribute to plasma triglyceride concentrations and fatty liver in humans.* Curr Opin Lipidol, 2014. 25(3): p. 213-20.

104. Koliwad, S.K., R.S. Streeper, M. Monetti, I. Cornelissen, L. Chan, K. Terayama, S. Naylor, M. Rao, B. Hubbard, and R.V. Farese, Jr., *DGAT1-dependent triacylglycerol storage by macrophages protects mice from diet-induced insulin resistance and inflammation.* J Clin Invest, 2010. 120(3): p. 756-67.

105. Yamaguchi, K., L. Yang, S. McCall, J. Huang, X.X. Yu, S.K. Pandey, S. Bhanot, B.P. Monia, Y.X. Li, and A.M. Diehl, *Inhibiting triglyceride synthesis improves hepatic steatosis but exacerbates liver damage and fibrosis in obese mice with nonalcoholic steatohepatitis.* Hepatology, 2007. 45(6): p. 1366-74.

106. He, J., B. Hu, X. Shi, E.R. Weidert, P. Lu, M. Xu, M. Huang, E.E. Kelley, and W. Xie, *Activation of the aryl hydrocarbon receptor sensitizes mice to nonalcoholic steatohepatitis by deactivating mitochondrial sirtuin deacetylase Sirt3.* Mol Cell Biol, 2013. 33(10): p. 2047-55.

107. Dalton, T.P., A. Puga, and H.G. Shertzer, *Induction of cellular oxidative stress by aryl hydrocarbon receptor activation.* Chem Biol Interact, 2002. 141(1-2): p. 77-95.

108. Tilg, H. and G.S. Hotamisligil, *Nonalcoholic fatty liver disease: Cytokine-adipokine interplay and regulation of insulin resistance.* Gastroenterology, 2006. 131(3): p. 934-45.

109. Matsubara, T., N. Tanaka, K.W. Krausz, S.K. Manna, D.W. Kang, E.R. Anderson, H. Luecke, A.D. Patterson, Y.M. Shah, and F.J. Gonzalez, *Metabolomics identifies an inflammatory cascade involved in dioxin- and diet-induced steatohepatitis.* Cell Metab, 2012. 16(5): p. 634-44.

110. Rui, L., *Energy metabolism in the liver.* Compr Physiol, 2014. 4(1): p. 177-97.

111. Moore, M.C., K.C. Coate, J.J. Winnick, Z. An, and A.D. Cherrington, *Regulation of hepatic glucose uptake and storage in vivo.* Adv Nutr, 2012. 3(3): p. 286-94.

112. Burgess, S.C., N. Hausler, M. Merritt, F.M. Jeffrey, C. Storey, A. Milde, S. Koshy, J. Lindner, M.A. Magnuson, C.R. Malloy, and A.D. Sherry, *Impaired tricarboxylic acid cycle activity in mouse livers lacking cytosolic phosphoenolpyruvate carboxykinase.* J Biol Chem, 2004. 279(47): p. 48941-9.

113. She, P., M. Shiota, K.D. Shelton, R. Chalkley, C. Postic, and M.A. Magnuson, *Phosphoenolpyruvate carboxykinase is necessary for the integration of hepatic energy metabolism.* Mol Cell Biol, 2000. 20(17): p. 6508-17.

114. Weber, L.W., M. Lebofsky, H. Greim, and K. Rozman, *Key enzymes of gluconeogenesis are dose-dependently reduced in 2,3,7,8-tetrachlorodibenzo-p-dioxin (TCDD)-treated rats.* Arch Toxicol, 1991. 65(2): p. 119-23.

115. Ahmed, S., D. Bott, A. Gomez, L. Tamblyn, A. Rasheed, T. Cho, L. MacPherson, K.S. Sugamori, Y. Yang, D.M. Grant, C.L. Cummins, and J. Matthews, *Loss of the Mono-ADP-ribosyltransferase, Tiparp, Increases Sensitivity to Dioxin-induced Steatohepatitis and Lethality.* J Biol Chem, 2015. 290(27): p. 16824-40.

116. Diani-Moore, S., P. Ram, X. Li, P. Mondal, D.Y. Youn, A.A. Sauve, and A.B. Rifkind, *Identification of the aryl hydrocarbon receptor target gene TiPARP as a mediator of suppression of hepatic gluconeogenesis by 2,3,7,8-tetrachlorodibenzo-p-dioxin and of nicotinamide as a corrective agent for this effect.* J Biol Chem, 2010. 285(50): p. 38801-10.

117. Diani-Moore, S., S. Zhang, P. Ram, and A.B. Rifkind, *Aryl hydrocarbon receptor activation by dioxin targets phosphoenolpyruvate carboxykinase (PEPCK) for ADP-ribosylation via 2,3,7,8-tetrachlorodibenzo-p-dioxin (TCDD)-inducible poly(ADP-ribose) polymerase (TiPARP).* J Biol Chem, 2013. 288(30): p. 21514-25.

118. Viluksela, M., M. Unkila, R. Pohjanvirta, J.T. Tuomisto, B.U. Stahl, K.K. Rozman, and J. Tuomisto, *Effects of 2,3,7,8-tetrachlorodibenzo-p-dioxin (TCDD) on liver phosphoenolpyruvate carboxykinase (PEPCK) activity, glucose homeostasis and plasma amino acid concentrations in the most TCDD-susceptible and the most TCDD-resistant rat strains.* Arch Toxicol, 1999. 73(6): p. 323-36.

119. Zhang, W., R.M. Sargis, P.A. Volden, C.M. Carmean, X.J. Sun, and M.J. Brady, *PCB 126 and Other Dioxin-Like PCBs Specifically Suppress Hepatic PEPCK Expression via the Aryl Hydrocarbon Receptor.* PLoS One, 2012. 7(5): p. e37103.

120. Shertzer, H.G., M.B. Genter, D. Shen, D.W. Nebert, Y. Chen, and T.P. Dalton, *TCDD decreases ATP levels and increases reactive oxygen production through changes in mitochondrial F(0)F(1)-ATP synthase and ubiquinone.* Toxicol Appl Pharmacol, 2006. 217(3): p. 363-74.

121. Nohl, H., D. de Silva, and K.H. Summer, *2,3,7,8, tetrachlorodibenzo-p-dioxin induces oxygen activation associated with cell respiration.* Free Radic Biol Med, 1989. 6(4): p. 369-74.

122. Senft, A.P., T.P. Dalton, D.W. Nebert, M.B. Genter, A. Puga, R.J. Hutchinson, J.K. Kerzee, S. Uno, and H.G. Shertzer, *Mitochondrial reactive oxygen production is dependent on the aromatic hydrocarbon receptor.* Free Radic Biol Med, 2002. 33(9): p. 1268-78.

123. Frayn, K.N., P. Arner, and H. Yki-Jarvinen, *Fatty acid metabolism in adipose tissue, muscle and liver in health and disease.* Essays Biochem, 2006. 42: p. 89-103.

124. Funai, K., H. Song, L. Yin, I.J. Lodhi, X. Wei, J. Yoshino, T. Coleman, and C.F. Semenkovich, *Muscle lipogenesis balances insulin sensitivity and strength through calcium signaling.* J Clin Invest, 2013. 123(3): p. 1229-40.

125. Feingold, K.R. and C. Grunfeld, *Introduction to Lipids and Lipoproteins*, in *Endotext*, L.J. De Groot, P. Beck-Peccoz, G. Chrousos, K. Dungan, A. Grossman, J.M. Hershman, C. Koch, R. McLachlan, M. New, R. Rebar, F. Singer, A. Vinik, and M.O. Weickert, Editors. 2000: South Dartmouth (MA).

126. Schneider, H., S. Staudacher, M. Poppelreuther, W. Stremmel, R. Ehehalt, and J. Fullekrug, *Protein mediated fatty acid uptake: synergy between CD36/FAT-facilitated transport and acyl-CoA synthetase-driven metabolism.* Arch Biochem Biophys, 2014. 546: p. 8-18.

127. Xu, S., A. Jay, K. Brunaldi, N. Huang, and J.A. Hamilton, *CD36 enhances fatty acid uptake by increasing the rate of intracellular esterification but not transport across the plasma membrane.* Biochemistry, 2013. 52(41): p. 7254-61.

128. Angrish, M.M., C.Y. Dominici, and T.R. Zacharewski, *TCDD-elicited effects on liver, serum, and adipose lipid composition in C57BL/6 mice.* Toxicol Sci, 2013. 131(1): p. 108-15.

129. Kurita, H., W. Yoshioka, N. Nishimura, N. Kubota, T. Kadowaki, and C. Tohyama, *Aryl hydrocarbon receptor-mediated effects of 2,3,7,8-tetrachlorodibenzo-p-dioxin on glucose-stimulated insulin secretion in mice.* J Appl Toxicol, 2009. 29(8): p. 689-94.

130. Takuma, M., K. Ushijima, M. Kumazaki, H. Ando, and A. Fujimura, *Influence of dioxin on the daily variation of insulin sensitivity in mice.* Environ Toxicol Pharmacol, 2015. 40(2): p. 349-351.

131. Cheng, X., S.G. Vispute, J. Liu, C. Cheng, A. Kharitonenkov, and C.D. Klaassen, *Fibroblast growth factor (Fgf) 21 is a novel target gene of the aryl hydrocarbon receptor (AhR).* Toxicol Appl Pharmacol, 2014.

132. Lin, Z., H. Tian, K.S. Lam, S. Lin, R.C. Hoo, M. Konishi, N. Itoh, Y. Wang, S.R. Bornstein, A. Xu, and X. Li, *Adiponectin mediates the metabolic effects of FGF21 on glucose homeostasis and insulin sensitivity in mice.* Cell Metab, 2013. 17(5): p. 779-89.

133. Nault, R., K.A. Fader, and T. Zacharewski, *RNA-Seq versus oligonucleotide array assessment of dose-dependent TCDD-elicited hepatic gene expression in mice.* BMC Genomics, 2015. 16(1): p. 373.

134. Wang, C., B. Gong, P.R. Bushel, J. Thierry-Mieg, D. Thierry-Mieg, J. Xu, H. Fang, H. Hong, J. Shen, Z. Su, J. Meehan, X. Li, L. Yang, H. Li, P.P. Labaj, D.P. Kreil, D. Megherbi, S. Gaj, F. Caiment, J. van Delft, J. Kleinjans, A. Scherer, V. Devanarayan, J. Wang, Y. Yang, H.R. Qian, L.J. Lancashire, M. Bessarabova, Y. Nikolsky, C. Furlanello, M. Chierici, D. Albanese, G. Jurman, S. Riccadonna, M. Filosi, R. Visintainer, K.K. Zhang, J. Li, J.H. Hsieh, D.L. Svoboda, J.C. Fuscoe, Y. Deng, L. Shi, R.S. Paules, S.S. Auerbach, and W. Tong, *The concordance between RNA-seq and microarray data depends on chemical treatment and transcript abundance.* Nat Biotechnol, 2014. 32(9): p. 926-32.

135. Su, Z., Z. Li, T. Chen, Q.Z. Li, H. Fang, D. Ding, W. Ge, B. Ning, H. Hong, R.G. Perkins, W. Tong, and L. Shi, *Comparing next-generation sequencing and microarray technologies in a toxicological study of the effects of aristolochic acid on rat kidneys.* Chem Res Toxicol, 2011. 24(9): p. 1486-93.

136. Zhao, S., W.P. Fung-Leung, A. Bittner, K. Ngo, and X. Liu, *Comparison of RNA-Seq and microarray in transcriptome profiling of activated T cells.* PLoS One, 2014. 9(1): p. e78644.

137. Pantanowitz, L., J.H. Sinard, W.H. Henricks, L.A. Fatheree, A.B. Carter, L. Contis, B.A. Beckwith, A.J. Evans, A. Lal, and A.V. Parwani, *Validating whole slide imaging for diagnostic purposes in pathology: guideline from the College of American Pathologists Pathology and Laboratory Quality Center.* Arch Pathol Lab Med, 2013. 137(12): p. 1710-22.

138. Long, R.E., A. Smith, S.V. Machotka, E. Chlipala, J. Cann, B. Knight, Y. Kawano, J. Ellin, and A. Lowe, *Scientific and Regulatory Policy Committee (SRPC) paper: validation of digital pathology systems in the regulated nonclinical environment.* Toxicol Pathol, 2013. 41(1): p. 115-24.

139. Al-Janabi, S., A. Huisman, and P.J. Van Diest, *Digital pathology: current status and future perspectives.* Histopathology, 2012. 61(1): p. 1-9.

140. Dere, E., A.L. Forgacs, T.R. Zacharewski, and L.D. Burgoon, *Genome-wide computational analysis of dioxin response element location and distribution in the human, mouse, and rat genomes.* Chem Res Toxicol, 2011. 24(4): p. 494-504.

# CHAPTER 2. RATIONALE, HYPOTHESIS AND SPECIFIC AIMS

## RATIONALE

The ubiquitous environmental contaminant TCDD is the prototypical ligand representing the structurally diverse environmental contaminants, natural products, and endogenous metabolites that bind and activate the AhR. Studies in Ahr-null mice have demonstrated that most, if not all, TCDD-elicited toxic responses are mediated by the AhR [1-4]. Recent studies have implicated TCDD and related compounds in the disruption of hepatic metabolism, leading to development of NAFLD which includes reversible hepatic steatosis, steatohepatitis, and fibrosis [2, 5, 6], as well as development of hepatocellular carcinoma and other complex metabolic diseases such as type 2 diabetes (T2D) in humans [7, 8]. Nevertheless, little is known about the pathogenesis of AhR-mediated NAFLD. These studies will examine NAFLD pathology progression following repeated TCDD dosing that more closely mimics human exposure to TCDD and related compounds, using an integrated 'omics' approach. These studies will not only provide valuable insight in the pathogenesis of NAFLD but may also identify novel intervention targets for associated metabolic diseases

## HYPOTHESIS

Repeated TCDD exposure will promote the progression of NAFLD pathologies and reprogram hepatic metabolism.

## SPECIFIC AIMS

**Specific Aim 1:** Test the sub-hypothesis that repeated oral TCDD gavage promotes the dose-dependent progression of NAFLD pathologies in mice.

**Specific Aim 2:** Test the sub-hypothesis that TCDD-elicited progression of NAFLD pathologies is associated with systemic metabolic reprogramming.

**Specific Aim 3:** Test the sub-hypothesis that repeated TCDD exposure alters the hepatic transcriptome and hepatic, urinary, and serum metabolome, consistent with the reprogramming of lipid and glucose metabolism.

**Specific Aim 4:** Use computational approaches to integrate dose-dependent transcriptomic, metabolomic, and phenotypic data to develop mechanistic models describing the development of TCDD-elicited NAFLD pathologies.

# REFERENCES

## REFERENCES


1. Fernandez-Salguero, P.M., D.M. Hilbert, S. Rudikoff, J.M. Ward, and F.J. Gonzalez, *Aryl-hydrocarbon receptor-deficient mice are resistant to 2,3,7,8-tetrachlorodibenzo-p-dioxin-induced toxicity.* Toxicol Appl Pharmacol, 1996. 140(1): p. 173-9.

2. Pierre, S., A. Chevallier, F. Teixeira-Clerc, A. Ambolet-Camoit, L.C. Bui, A.S. Bats, J.C. Fournet, P. Fernandez-Salguero, M. Aggerbeck, S. Lotersztajn, R. Barouki, and X. Coumoul, *Aryl hydrocarbon receptor-dependent induction of liver fibrosis by dioxin.* Toxicol Sci, 2014. 137(1): p. 114-24.

3. Matsubara, T., N. Tanaka, K.W. Krausz, S.K. Manna, D.W. Kang, E.R. Anderson, H. Luecke, A.D. Patterson, Y.M. Shah, and F.J. Gonzalez, *Metabolomics identifies an inflammatory cascade involved in dioxin- and diet-induced steatohepatitis.* Cell Metab, 2012. 16(5): p. 634-44.

4. Tanos, R., R.D. Patel, I.A. Murray, P.B. Smith, A.D. Patterson, and G.H. Perdew, *Aryl hydrocarbon receptor regulates the cholesterol biosynthetic pathway in a dioxin response element-independent manner.* Hepatology, 2012. 55(6): p. 1994-2004.

5. Kopec, A.K., D.R. Boverhof, R. Nault, J.R. Harkema, C. Tashiro, D. Potter, B. Sharratt, B. Chittim, and T.R. Zacharewski, *Toxicogenomic Evaluation of Long-term Hepatic Effects of TCDD in Immature, Ovariectomized C57BL/6 Mice.* Toxicol Sci, 2013. 135(2): p. 465-75.

6. Fader, K.A., R. Nault, D.A. Ammendolia, J.R. Harkema, K.J. Williams, R.B. Crawford, N.E. Kaminski, D. Potter, B. Sharratt, and T.R. Zacharewski, *2,3,7,8-Tetrachlorodibenzo-p-Dioxin Alters Lipid Metabolism and Depletes Immune Cell Populations in the Jejunum of C57BL/6 Mice.* Toxicol Sci, 2015. 148(2): p. 567-80.

7. Taylor, K.W., R.F. Novak, H.A. Anderson, L.S. Birnbaum, C. Blystone, M. Devito, D. Jacobs, J. Kohrle, D.H. Lee, L. Rylander, A. Rignell-Hydbom, R. Tornero-Velez, M.E. Turyk, A.L. Boyles, K.A. Thayer, and L. Lind, *Evaluation of the association between persistent organic pollutants (POPs) and diabetes in epidemiological studies: a national toxicology program workshop review.* Environ Health Perspect, 2013. 121(7): p. 774-83.

8. Lee, D.H., I.K. Lee, M. Porta, M. Steffes, and D.R. Jacobs, Jr., *Relationship between serum concentrations of persistent organic pollutants and the prevalence of metabolic syndrome among non-diabetic adults: results from the National Health and Nutrition Examination Survey 1999-2002.* Diabetologia, 2007. 50(9): p. 1841-51.

# CHAPTER 3. DEVELOPMENT OF A COMPUTATIONAL HIGH-THROUGHPUT TOOL FOR THE QUANTITATIVE EXAMINATION OF DOSE-DEPENDENT HISTOLOGICAL FEATURES.

**ABSTRACT**

High resolution digitalizing of histology slides facilitates the development of computational alternatives to manual quantitation of features of interest. We developed a MATLAB based high-throughput quantitative histological analysis tool (QuHAnT) for the high-throughput quantitative histological feature assessment. QuHAnT validation was demonstrated by comparison to manual quantitation using liver sections from mice orally gavaged with sesame oil vehicle or 2,3,7,8-tetrachlorodibenzo-*p*-dioxin (TCDD; 0.001- 30 μg/kg) every 4 days for 28 days which elicits hepatic steatosis and fibrosis. A quality control module of QuHAnT reduced the number of quantifiable Oil Red O (ORO) stained images from 3,123 to 2,756. Increased ORO staining was measured at 10 and 30 μg/kg TCDD with a high correlation between manual and computational volume densities ($V_v$), although the dynamic range of QuHAnT was 10-fold greater. Additionally, QuHAnT determined the size of each ORO vacuole which could not be accurately quantified by visual examination or manual point counting. PicroSirius Red (PSR) quantitation demonstrated superior collagen deposition detection due to the ability to consider all images within each section. QuHAnT dramatically reduced analysis time and facilitated the comprehensive assessment of features improving accuracy and sensitivity, and represents a complementary tool for tissue/cellular features which are difficult to assess via subjective or semi-quantitative methods.

**INTRODUCTION**

Digital pathology and whole slide imaging (WSI) are becoming increasingly popular in research, clinical, and toxicological settings [1-4]. Digitized images from tissue sections facilitate storage and sharing of histological slides, and allow quantitative analyses in a rapid and unbiased manner [1-4]. Furthermore, sharing of WSI is an effective strategy to minimize inter-laboratory variation in histological assessments influenced by tissue quality and internal immunohistochemical protocols [5, 6], by reducing inter- and intraobserver variation in the quantitation of histological features [5-8].

Quantitation of features of interest in clinical and toxicological studies largely consist of subjective or semi-quantitative scoring systems used by trained pathologists [9, 10]. For example, the NASH (non-alcoholic steatohepatitis) Clinical Research Network developed the NAFLD (non-alcoholic fatty liver disease) Activity Score (NAS) to standardize NAFLD severity assessments using H&E stained tissue sections based on a scale of 0–8 that considers lipid accumulation, inflammation, and hepatocellular ballooning [11, 12]. Similarly, the Ishak system assesses liver fibrosis on a 0-6 scale based on observed characteristics [13, 14]. In toxicology, scoring systems are commonly used for toxicity and/or carcinogenicity, and to determine exposure limits [15, 16]. However, these systems can be onerous and involve several pathologists or working groups for large studies [16] that may not be entirely free of bias and subjectivity.

Alternatively, digital image analyses provide ratio scale (e.g. 0 – 100%) as opposed to ordinal scale measurements (e.g. severity scale of 0 – 8), thus improving the quantitative characterization of the histopathological response [3, 8]. Manual point counting and computational feature extraction have been used to analyze digital images. Morphometry is commonly used for quantitation of histological features [17, 18] aided by programs such as STEPanizer and Image-Pro Plus [17-19]. Although visual-based assessment is the current standard for quantitation of histological features, it is time-consuming and potentially subject to inter- and intra-observer variability. To address these limitations, automated feature extraction approaches have been developed [9, 20]. Commercial tools are available for automated detection and quantitation of features of interest, but typically require purchasing a license and rarely take advantage of advanced computing resources such as high performance or cloud computing that facilitate high-throughput analysis and the storage of memory intensive digital data. In-house developed tools have also been created to examine specific histological features of interest. For example, a MATLAB algorithm was developed for the quantitation of estrogen and progesterone receptor staining in breast cancer tumor sections [20] but is not extendible to other types of features.

The present study describes the development of the Quantitative Histological Analysis Tool (QuHAnT), a MATLAB based automated image analysis tool developed for the high-throughput quantitative assessment of pathologist identified and characterized histopathological features of interest. Unlike other approaches, QuHAnT uses a modular framework for (1) threshold determination, (2) quality control, (3) feature extraction and quantitation, and (4) result output. Comparison to manual point counting using the dose-dependent increase in Oil Red O (ORO) and PicroSirius Red (PSR) staining in livers of mice following treatment with TCDD [21-24] demonstrated that QuHAnT outperforms manual point counting, and provides additional complementary quantitative data. In summary, QuHAnT is an accurate and extendible high-throughput tool that can be used to quantitate histological features which are difficult to assess using subjective or semi-quantitative methods such as the modest increase in collagen deposition induced by TCDD, and the dose-dependent increase in micro and macrovesicular steatosis.

## MATERIALS AND METHODS

### ANIMAL HUSBANDRY AND TREATMENT

Female C57BL/6 mice received on postnatal day 25 (PND25) were obtained from Charles Rivers Laboratories (Portage, MI). Mice were housed in polycarbonate cages with cellulose fiber chips (Aspen Chip Laboratory Bedding, Northeastern Products, Warrensberg, NY) and maintained at 30-40% humidity and a 12 h light/dark cycle. Mice were fed *ad libitum* with Harlan Teklad 22/5 Rodent Diet 8940 (Madison, WI) and had free access to deionized water. On PND 28 (day 0) and every following 4$^{th}$ day (days 4, 8, 12, 16, 20, and 24) animals were orally gavaged with 0.1 mL sesame oil vehicle control or 0.001, 0.01, 0.03, 0.1, 0.3, 1, 3, 10, or 30 µg/kg of TCDD (Dow Chemical Company, Midland, MI) for a total of 7 exposures over 28 days. On day 28 mice were sacrificed and the right liver lobe was fixed in 10% neutral buffered formalin (Sigma-Aldrich, MO) for collagen staining or frozen in Tissue-Tek O.C.T. compound (Sakura, CA) for lipid staining.

All animal procedures were approved by the Michigan State University Institutional Animal Care and Use Committee.

## HISTOLOGICAL PROCESSING AND WHOLE SLIDE IMAGING

All histological processing was performed at the Michigan State University Investigative HistoPathology Laboratory (humanpathology.msu.edu/histology). Staining of frozen liver sections for lipids using Oil Red O (ORO, Sigma-Aldrich) was performed as previously described [25]. Briefly, livers were sectioned at 6 µm, stained with an ORO solution, and counterstained with Gill 2 hematoxylin. For collagen staining by PicroSirius Red (PSR), paraffin embedded livers were sectioned at 4–5 µm and stained with Hematoxylin & Eosin (H&E) and 0.1% PSR. Slides were digitized using the Olympus Virtual Slide System VS110 (Olympus, PA) at 20x magnification (0.32 µm/pixel). For quantitative analyses of ORO and PSR staining, images were randomly sampled using Visiomorph Microimager (Visiopharm, Denmark) across two adjacent sections on the same slide (N= 6 individual livers) in each treatment group.

## QUANTITATIVE ANALYSES

Manual point counting was performed using STEPanizer [19]. Briefly, a 4x4 or 16x16 test system grid was superimposed on each image and the number of points overlapping a feature of interest (e.g., ORO, PSR) were counted. Volume density was calculated as the sum of positive hits ($P_{positive\ staining}$) divided by the total number of tissue hits ($P_{tissue}$) for each section ($V_v = (P_{positive\ staining}/P_{tissue}) \times 100$).

For QuHAnT analysis Hue, Saturation, and Value (HSV) thresholds were determined using the ImageJ color threshold tool (http://rsb.info.nih.gov/ij/). Prior to quantitation using QuHAnT, visual quality control was performed using the incorporated quality control module to remove images containing false positives or debris. Volume density was estimated as the sum of the area of positive staining ($A_{positive\ staining}$) divided by the sum of tissue area ($A_{tissue}$) for each liver

section ($V_v$ = ($A_{positive\ staining}/A_{tissue}$) x 100). Only features larger than 6.3 $\mu m^2$ (4 pixels) were considered to minimize noise. For the assessment of the variability associated with slide coverage, 100% of slides from 3 animals (vehicle, 0.01, and 30 µg/kg) were sampled and quantitated and randomly selected *a posteriori* using an in-house written python script (www.python.org). QuHAnT analyses were performed using the Michigan State University High Performance Computing Center. Statistical analyses were performed using SAS 9.2 (SAS Institute Inc., NC).

## RESULTS

### IMPLEMENTATION OF QUHANT

Figure 6 provides an overview of the implementation of QuHAnT compared to manual point counting using the dose-dependent increase in ORO staining of hepatic vacuoles in mice following oral gavage with TCDD [21-24]. For the assessment of QuHAnT performance, 42-55 images were randomly sampled using Visiomorph Microimager across two adjacent sections on the same slide for each animal in sesame oil vehicle control, 0.001, 0.01, 0.03, 0.1, 0.3, 1, 3, 10, or 30 µg/kg TCDD treatment groups (n=6 animals) resulting in a total of 3,123 images across all the treatment groups.

For QuHAnT analysis, Hue, Saturation, and Value (HSV) thresholds used for image segmentation (herein referred to as feature extraction) were determined using ImageJ (http://rsb.info.nih.gov/ij/) from a random subset of images (~1% of images) containing positive staining, background tissue, and/or blank background. For ORO, optimal HSV thresholds used for feature extraction were determined to be 0 – 50 and 225 – 255 (hue), 125 – 255 (saturation), and 0 – 255 (value) while optimal total tissue feature extraction thresholds were 0 – 255 (hue), 20 – 255 (saturation), and 0 – 255 (value). Of the 3,123 captured images 367 were eliminated from further analysis due to the absence of any tissue or the presence of false positives (e.g., ORO

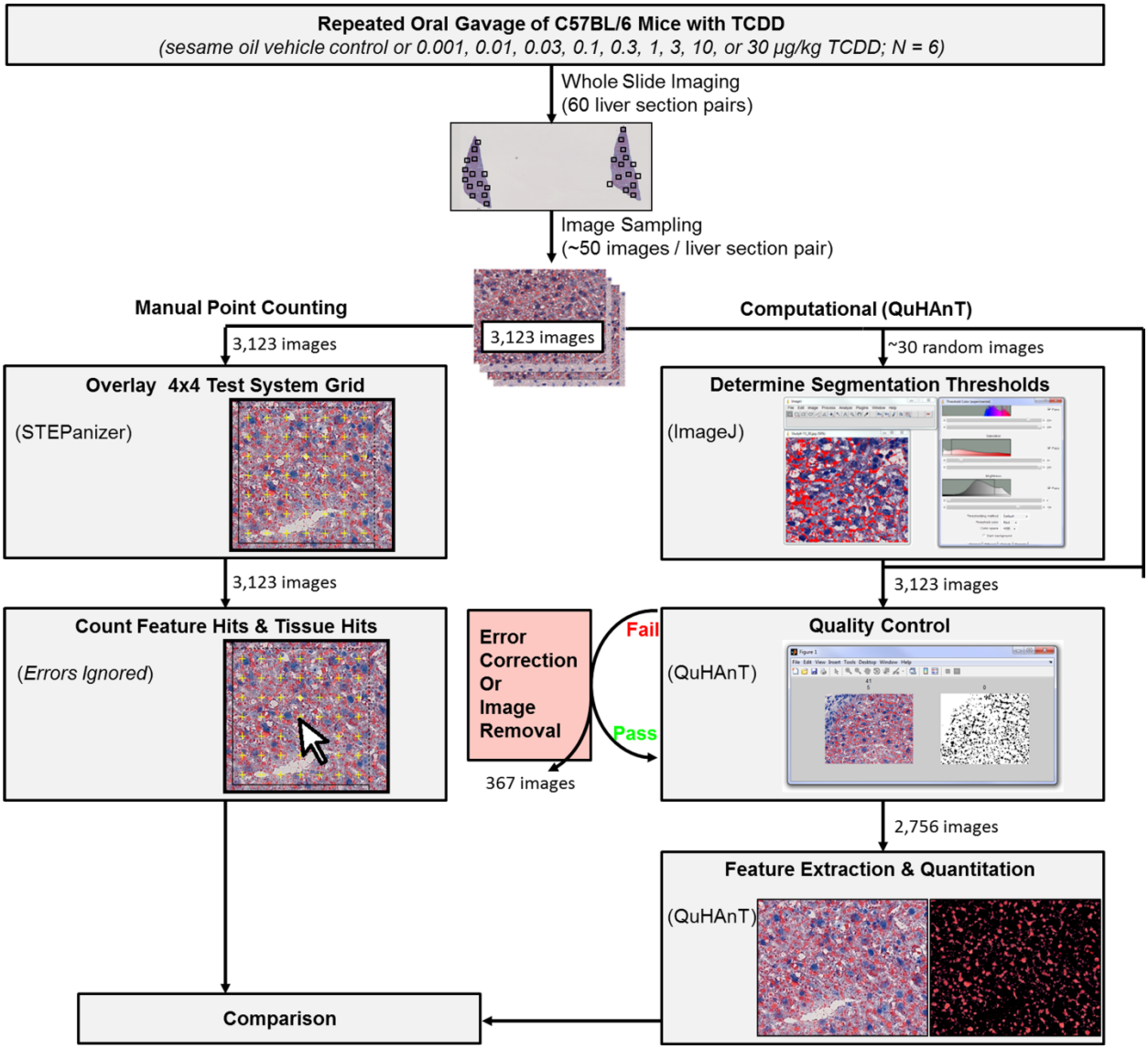


**FIGURE 6. MANUAL AND AUTOMATED MORPHOMETRY METHODS**

Overview of comparative histological feature quantitation analysis approaches for dose-dependent TCDD elicited steatosis by manual point counting using STEPanizer [19] and the developed Quantitative Histological Analysis Tool (QuHAnT).

droplets present in absence of tissue) or the presence of debris (e.g., bubbles) as identified using the quality control module within QuHAnT. Although the tool provides the option to perform image correction using external editors, this was not performed due to the availability of additional images to compensate for eliminated images. QuHAnT quantified the remaining 2,756 images in less than 1 h using the High Performance Computing Center (HPCC) at Michigan State University.

Data output consisted of three tab-delimited files containing information of each individual feature within an image and background tissue area. The output summary provided feature count, mean size, and total area as well as background tissue information for each image. The data can then be imported into any common analysis software including SAS (SAS institute inc.) and R (http://www.r-project.org/).

For validation, the same initial 3,123 images were also assessed using manual point counting. A 4x4 grid was superimposed on each image by STEPanizer [19], and the number of points overlapping an ORO stained feature or unstained area were manually counted. In cases where errors were observed, overlapping points were ignored (not counted) as no initial quality screening was performed for manual point counting. Elimination of the same 367 images omitted from QuHAnT analysis for manual point counting did not result in any significant difference in final $V_v$ estimates.

**COMPARING QUHANT TO MANUAL POINT COUNTING $V_V$ ESTIMATES**

Both manual point counting and QuHAnT analyses identified a dose-dependent ~5% and ~15% increase in hepatic ORO $V_v$ estimates at 10 and 30 µg/kg TCDD, respectively (Table 1). Although high dose $V_v$ estimates were similar across both methods, those using manual point counting ranged from 0.4 – 14.6% while QuHAnT estimates ranged from 0.04 – 14% representing a 10-fold increase in the dynamic range. Dose-dependent manual point counting and QuHAnT $V_v$ estimates were consistent with visual assessment by a pathologist of whole liver slides which reported mild to moderate hepatic lipid accumulation at 10 µg/kg TCDD and widespread microvesicular and macrovesicular lipid accumulation in the centriacinar, mid-zonal, and periportal regions of the liver at 30 µg/kg TCDD. Correlation analysis between manual point counting and QuHAnT $V_v$ estimates revealed a high concordance between both measures

**TABLE 1. COMPARISON OF MANUAL POINT COUNTING AND QUHANT ANALYSIS OF OIL RED O AND PICROSIRIUS RED VOLUME DENSITY ($V_V$) ESTIMATES IN TCDD TREATED MOUSE LIVER SECTIONS.**

| Dose (µg/kg TCDD) | $V_v$ (% Tissue Area) Manual Point Counting | QuHAnT |
|---|---|---|
| **Oil Red O** | | |
| 0 | 0.36 ± 0.13 | 0.11 ± 0.03 |
| 0.001 | 0.60 ± 0.25 | 0.05 ± 0.01 |
| 0.01 | 0.48 ± 0.19 | 0.07 ± 0.03 |
| 0.03 | 0.65 ± 0.22 | 0.20 ± 0.10 |
| 0.1 | 0.41 ± 0.14 | 0.08 ± 0.04 |
| 0.3 | 0.85 ± 0.10 | 0.1 ± 0.04 |
| 1 | 2.43 ± 0.68 | 0.17 ± 0.06 |
| 3 | 3.28 ± 1.72 | 0.48 ± 0.17 |
| 10 | 5.63 ± 1.85[a] | 4.07 ± 1.26[a] |
| 30 | 14.61 ± 1.94[a] | 13.99 ± 3.56[a] |
| **PicroSirius Red** | | |
| 0 | 0.96 ± 0.26[b] | 0.80 ± 0.10 |
| 30 | 1.60 ± 0.43[b] | 1.34 ± 0.20[a] |

[a]Indicates significant differences ($P \leq 0.05$) compared to vehicle control determined by ANOVA followed by Dunnett's *post-hoc* test.

[b]Manual point counting estimates for PSR was performed on a feasible ~50 images per slide and compared to 100% sampling for QuHAnT analysis.

(Pearson correlation coefficient (PCC) of 0.82) (Figure 7). QuHAnT estimates, although highly correlated to manual estimates overall, are ~10-fold lower than the corresponding manual point counting estimates at low $V_v$ values while high $V_v$ values are comparable (slope > 1). Similar high concordance between manual point counting and QuHAnT $V_v$ estimates were found in ORO stained liver sections processed and quantitated in an independent study using the same feature extraction HSV threshold values (data not shown).

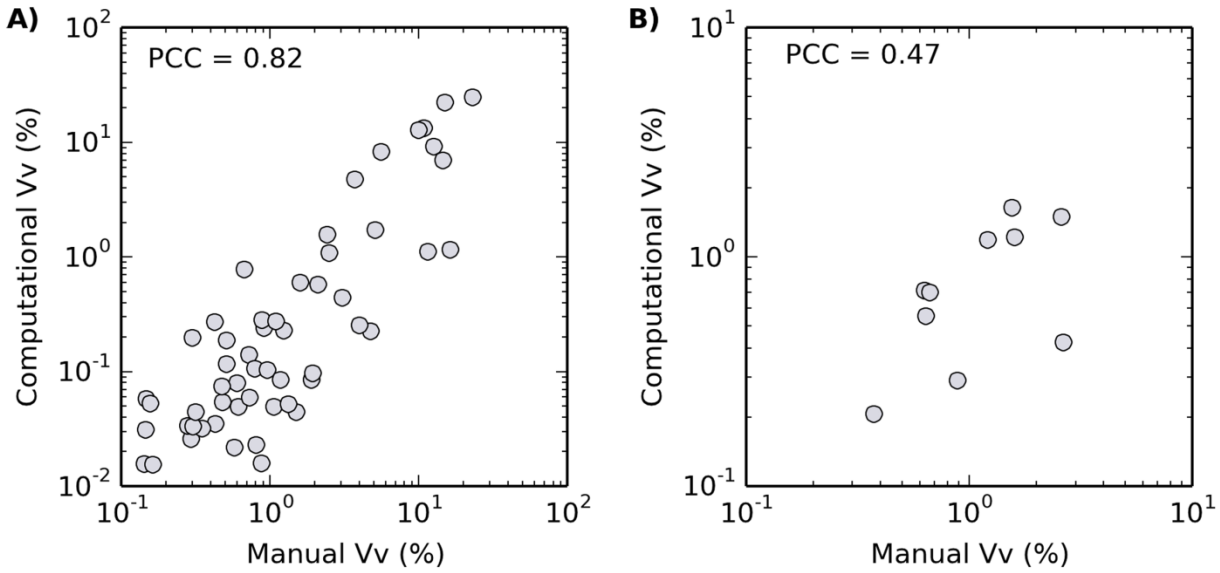


**FIGURE 7. COMPARISON OF MANUAL AND AUTOMATED $V_V$ ESTIMATES**

Correlation analysis of manual point counting and QuHAnT estimated (A) Oil Red O and (B) PicroSirius Red volume densities ($V_v$). Data points represent the mean $V_v$ (% tissue area) estimated for each liver section using 42 – 55 images at 20x magnification per liver section. A Pearson correlation coefficient (PCC) of 0.82 ($P \leq 0.05$) was calculated for Oil Red O $V_v$ estimates. No significant correlation was observed for PicroSirius Red manual point counting and QuHAnT $V_v$ estimates.

**SUPERIOR QUHANT PERFORMANCE**

Manual point counting estimates improve with increased grid density (i.e., 16x16) since more points are counted at the expense of analysis time. A sample image was quantitated using 4x4 and 16x16 grid densities in order to determine the trade-off between accuracy and quantitation time, and for accuracy comparison to QuHAnT which represents a theoretical ~1.3 million points (each pixel represents one point) per image (Table 2). The QuHAnT $V_v$ estimate of 28% was found to be much closer to the 33% manual point counting estimate determined using a 16x16 grid compared to the 6% estimate on the 4x4 grid. $V_v$ estimates of 28 – 33% for the sample image is also more consistent with visual assessment of the images. However, improved accuracy with increased grid density in manual point counting came a ≥5 fold increase in

assessment time while QuHAnT analysis was ~5% of the time required for manual point counting using a 4x4 grid while simultaneously providing a more comprehensive assessment (i.e., considered each pixel).

**TABLE 2. ACCURACY AND ANALYSIS TIME COMPARISON OF MANUAL AND QUHANT QUANTITATION**

| Quantitation Method | Grid Density[a] (W x H) | Volume Density | Analysis Time (image$^{-1}$) | Study Analysis (hrs)[b] |
|---|---|---|---|---|
| Point Counting | 4 x 4 | 6% | 1-2 min | 45 |
| | 16 x 16 | 33% | 5 -6 min | 225 |
| QuHAnT | 1280 x 1024 | 28% | 1 sec[b] | 1[c] |

[a]Image used for comparison across grid sizes is shown in Figure 9 (top).

[b]Manual point counting was performed on 3,123 images and QuHAnT analysis was performed on 2,756 images.

[c]Analysis time was determined based on the use of the Intel Xeon E5620 2.4 GHz core processor with TurboBoost within the High Performance Computing Center at Michigan State University.

Unlike manual point counting, computational approaches can also provide estimates for the number of individual features per tissue area, and the size distribution of features of interest at little to no cost in accuracy, effort, or time. Testing of this advantage was demonstrated using a previously established 15 μM diameter (~176 μM$^2$ area) threshold to distinguish microvesicular from macrovesicular lipid droplets [26]. Applying this threshold, QuHAnT not only identified independent dose-dependent increases in microvesicular and macrovesicular lipid droplets, but also distinguished the emergence of macrovesicular lipid droplets at lower doses (10 μg/kg TCDD, Table 3) compared to visual assessment by a pathologist which only reported macrovesicular lipid droplets at 30 μg/kg TCDD. However, it should be noted that this approach assumes each distinct feature represents a single spherical droplet which, by visual assessment, appears to be largely true (droplets appear as circles in the images and are not expected to have any specific orientation).

**TABLE 3. TOTAL COUNT OF LIPID VACUOLES REPRESENTING MICROVESICULAR OR MACROVESICULAR STEATOSIS DETERMINED USING QUHANT.**

| Dose | Vacuolization type ((Count / Tissue Area)$_x10^{-6}$) | |
|---|---|---|
| (µg/kg TCDD) | Microvesicular ( ≤ 176 µm$^2$)[a] | Macrovesicular ( ≥ 176 µm$^2$)[a] |
| 0 | 28.7 ± 8.6 | 1.4 ± 0.3 |
| 0.001 | 12.4 ± 3.3 | 0.6 ± 0.1 |
| 0.01 | 19.0 ± 11.2 | 0.8 ± 0.2 |
| 0.03 | 70.3 ± 38.6 | 1.1 ± 0.4 |
| 0.1 | 22.1 ± 12.2 | 1.1 ± 0.4 |
| 0.3 | 28.2 ± 12.8 | 1.0 ± 0.2 |
| 1 | 100.1 ± 71.6 | 3.4 ± 2.6 |
| 3 | 117.3 ± 41.4 | 6.5 ± 2.4 |
| 10 | 437.4 ± 71.3[b] | 97.3 ± 35.1[b] |
| 30 | 555.1 ± 65.2[b] | 251.5 ± 56.0[b] |

[a]Area of 176 µm$^2$ was estimated based on a diameter of 15 µm previously reported to distinguish between microvesicular steatosis from macrovesicular steatosis [26].

[b]Indicates significant differences ($P \leq 0.05$) compared to vehicle control determined by ANOVA followed by Dunnett's *post-hoc* test.

**INFLUENCE OF RANDOM TISSUE SAMPLING ON $V_V$ ESTIMATES**

To quantify a feasible number of images by manual point counting in a reasonable amount of time, ~50 images were randomly sampled for each pair of liver sections per slide representing only ~40% of the tissue section. However, the high throughput capability of QuHAnT allows whole slide analysis (quantitation of the whole liver section) with little additional effort and time. To investigate optimal sampling coverage, images from three liver sections were randomly sampled from ~1% to 100% a total of 50 times at each percentage (e.g. 20 images were randomly sampled 50 times) and the standard error of the mean (SEM) was calculated to determine the variability in $V_v$ estimates (Figure 8). Random sampling was associated with large variability when

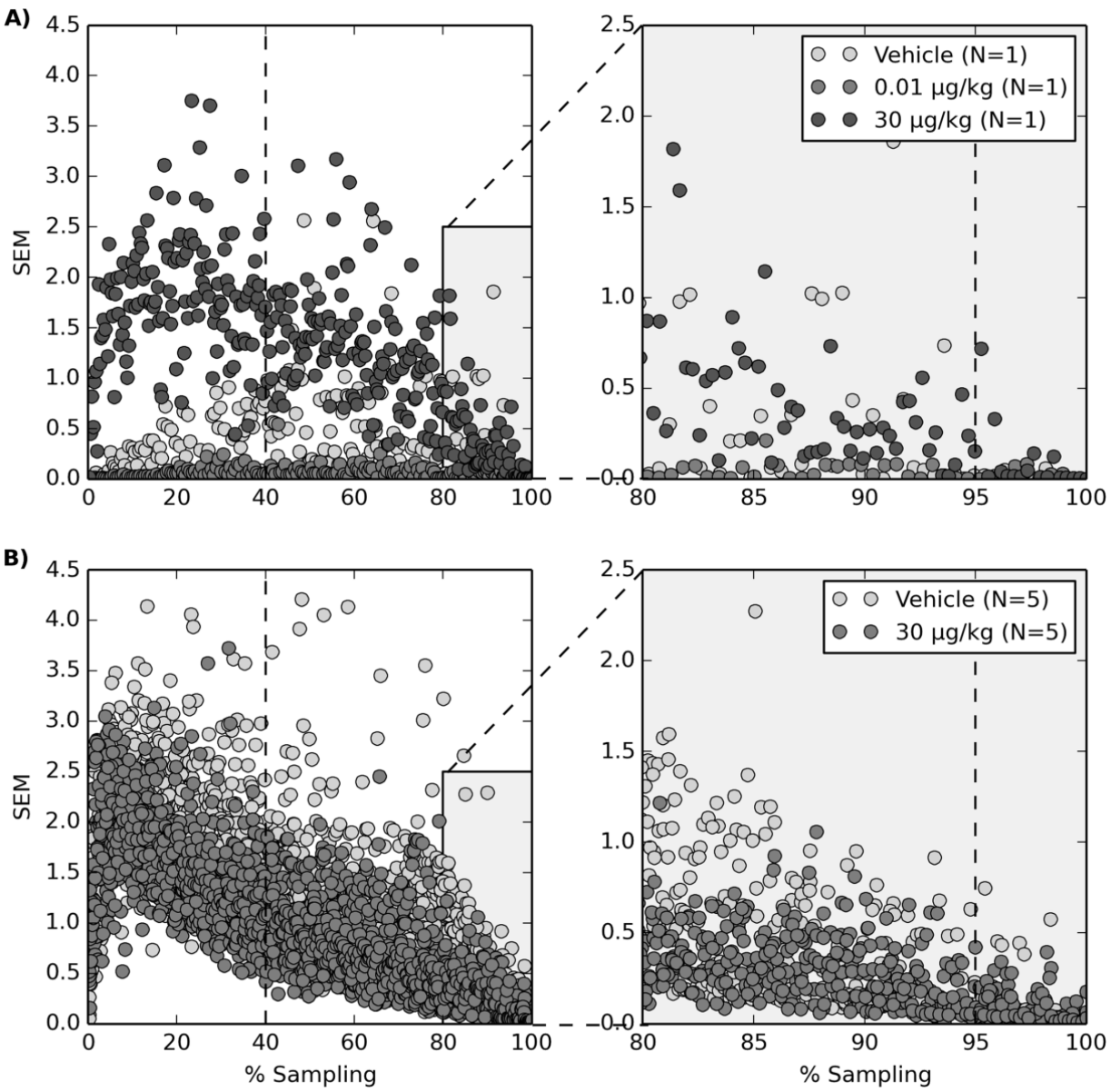


**FIGURE 8. IMPACT OF TISSUE COVERAGE ON $V_V$ ESTIMATES**

Variability of (A) Oil Red O and (B) PicroSirius Red volume density ($V_v$) estimates using QuHAnT with increasing slide coverage and random sampling of liver sections. Data points represent standard error of the mean (SEM) for 50 individual randomly selected images of liver sections from mice dosed every 4 days for 28 days with sesame oil vehicle, 0.01 µg/kg TCDD (Oil Red O only), or 30 µg/kg TCDD. 40% slide coverage representing the coverage used for quantitation approach comparisons is represented by a dashed vertical line (left panel). The right panel (expanded inset from left panel (grey background)) represents 95% slide coverage where variability is minimized.

considering only 40% of the tissue section particularly for sections with a large $V_v$ (30 µg/kg TCDD sample) or features with non-homogenous distribution (e.g. periportal fibrosis). In general, $V_v$ estimates exhibited higher variability when <95% of the tissue section was considered. The effect of sampling coverage on $V_v$ estimate variability was less in vehicle and in liver sections for lower TCDD doses with much lower ORO $V_v$ estimates.

**EXTENSIBILITY OF QUHANT**

In addition to hepatic fat accumulation, TCDD also induces immune cell infiltration and collagen deposition in mice [21-23]. The extensibility of QuHAnT was investigated by examining PSR (Table 1, Figures 7-8) stained liver sections from the same animals. No significant increase in PSR staining was detected by manual point counting or QuHAnt when only ~40% of the images were randomly sampled and analyzed. In contrast, a significant increase in PSR staining was detected at 30 µg/kg TCDD when 100% of the stained liver sections were sampled and quantified using QuHAnT. Although $V_v$ values for PSR staining were similar for both approaches, there was no correlation between QuHAnT and manual point counting (Figure 7B). QuHAnT was able to detect periportal and sinusoidal fibrosis missed by manual point counting at higher % sampling of liver sections. Large variability in $V_v$ estimates were found at low % tissue sampling levels while very little variation was observed at ≥95% tissue sampling, similar to ORO estimates (Figure 9, right panel). These results suggest manual counting could be improved by increasing the percentage of tissue sampling or the use of a mixed size point count grid with a coarse and fine mesh for the reference area and the structure on interest area, respectively, but will likely be associated with increased time, effort and labor. Unlike lipid vacuoles which can be assumed to be spherical with no specific orientation, collagen deposition form continuous fibers confound accurate counting of individual features or determination of feature size. Therefore, these parameters were not assessed for PSR staining, although QuHAnT could be used to calculate these values using standard morphometric concepts.

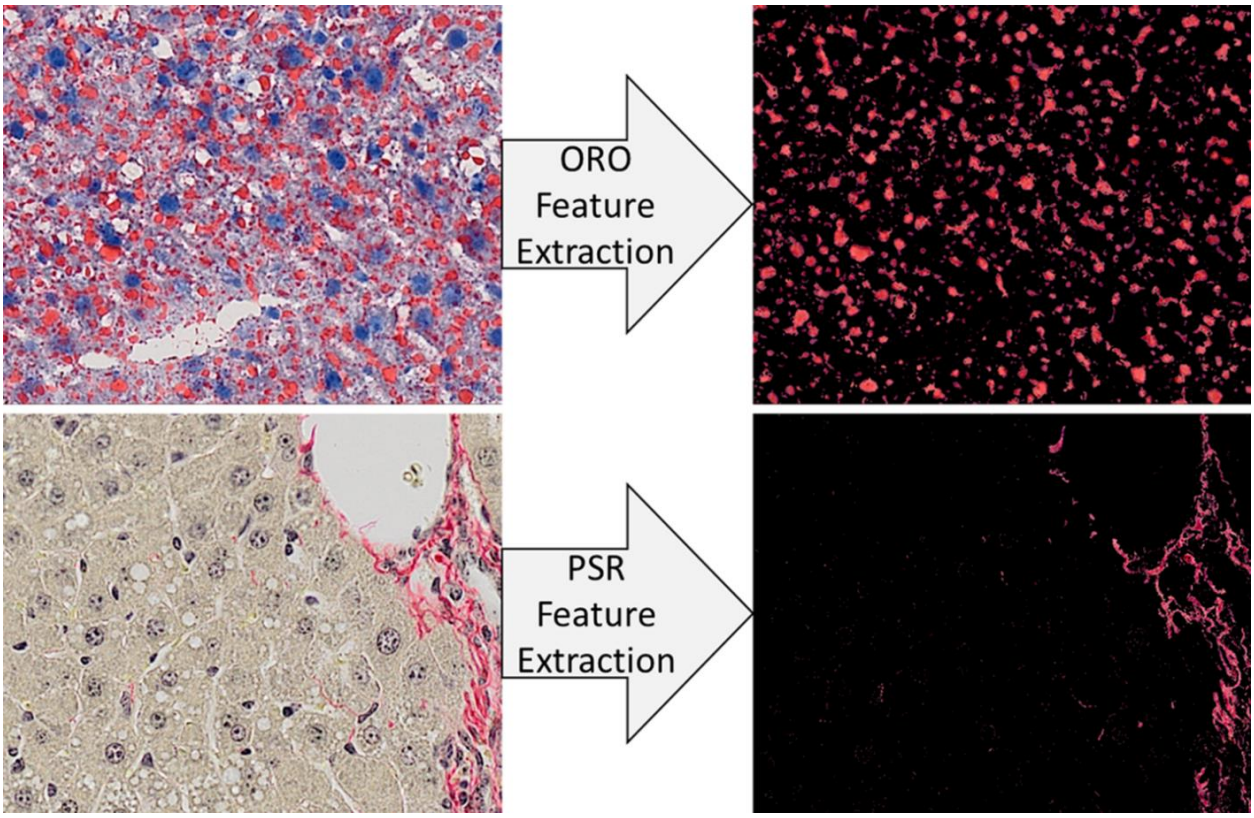


**FIGURE 9. SAMPLE THRESHOLDED IMAGES FOR AUTOMATED QUANTITATION**

Examples of Oil Red O (top) and PicroSirius Red (bottom) images (left) and extracted features (right). Images represent a 20x liver section from mice dosed every 4 days for 28 days with 30 µg/kg TCDD. ImageJ was used to establish independent Hue, Saturation, and Value (HSV) thresholds. In addition to quantitation of features of interest by QuHAnT, the digital images also provide a digital copy that can be shared upon request for further quality control or independent visual assessment.

## DISCUSSION

Complex diseases and adverse effects induced by chemical or biological agents are rarely the result of disruption of a single gene or pathway. Histopathology can be used to identify apical responses and/or key events within a mode of action. It also places complex biological responses and potential interactions reflected in transcriptomic, proteomic and metabolomic studies into cellular and morphological as well as spatial and temporal context within a tissue or specimen. Histopathology has historically been a qualitative technique with lesion severity scoring largely

based on visual assessment, semi-quantitative scoring, and/or manual quantitation [9, 10, 15, 16, 27]. Whole slide digital imaging represents an emerging approach that facilitates automated quantitative measures of histopathological features in a rapid and repeatable manner reducing human workload and minimizing inter- and intraobserver biases and variability [1-4]. Interoperability and standards for image data collection, reporting and analysis are in development to ensure rigorous and reproducible quantitative results between independent laboratories [28, 29]. In this study we describe the development and testing of QuHAnT, a flexible high-throughput computational tool that reduces inter- and intraobserver/laboratory biases and variability for the quantitation of pathologist characterized features while dramatically reducing human workload.

ORO and PSR stained liver sections from mice dosed every 4 days for 28 days with TCDD were used to compare QuHAnT with manual point counting. TCDD elicits dose-dependent hepatic lipid accumulation and collagen deposition [21-24], and provides a relevant model for QuHAnT performance testing. Comparative analysis indicates QuHAnT accurately quantitated increases in lipid vacuolization compared to manual point counting as demonstrated by the high $V_v$ value concordance between these approaches. These results confirm that QuHAnT is a valuable tool to complement the assessment of pathologists and suggest that it is a more appropriate approach for the quantitation of histological features compared to manual point-counting [3, 11, 27].

Unlike ORO, increases in PSR staining were only detectable using QuHAnT due to the ability to consider all of the images comprising the section. PSR staining of collagen deposition was dispersed throughout the section as marbled veins highly localized to portal areas. Consequently, the detection and quantitation of collagen deposition would require a more comprehensive and labor intensive assessment. For example, PSR quantitation is highly correlated to automated analysis when using a 200 point grid for manual quantitation [27]. However, using a 200-point grid density or alternative manual approach is not practical when

examining thousands of images further emphasizing the value of a high-throughput image analysis tool.

In addition to showing high concordance with point counting, QuHAnT also provided feature size characteristics that cannot be easily acquired using manual approaches [30, 31]. More specifically, QuHAnT was used to count the profile number of vacuoles and determine the size distribution, another challenging manual quantitation task. This data was used to identify the dose-dependent transition from microvesicular to macrovesicular steatosis which is associated with increasing disease severity [30, 31].

The greatest advantage is QuHAnT's ability to comprehensively assess feature characteristics, such as profile counts, area, length and size, for thousands of images in a fraction of the time compared to manual morphometry. This high-throughput capability and the use of the High Performance Computing Center at Michigan State University reduced analysis time to the extent that entire tissue sections could be quantitated rapidly and consistently. This refinement was particularly evident for features that exhibit random localization such as hepatic lipid accumulation or collagen deposition. Furthermore, our studies show that minimal variability in $V_v$ estimates was achieved when ≥95% of the images for the entire specimen were considered for both high TCDD dose ORO and PSR staining. These results provide compelling evidence that whole slide analysis improves detection and quantitation of histological features compared to random sampling of images. Although high performance computing was a significant factor in reducing analysis time, QuHAnT can also be implemented on any personal computer with high-throughput assessments in a fraction of the time compared to manual point counting.

Although our study was limited to ORO and PSR, QuHAnT is extensible to a variety of features of interest. It provides a framework that includes quality control, feature extraction, quantitation, and result output that simplifies the extension of QuHAnT to other features of interest. In theory, QuHAnT could be used for any *in-situ* hybridization and/or immunocytochemically distinguishable feature either by finding appropriate thresholds for feature

extraction or creating custom modules. Image analysis data has also been used to investigate associations between feature staining and related quantitative data such hepatocellular hypertrophy, circulating hormone levels, and differential gene expression [3, 32]. Moreover, QuHAnT data obtained using standard morphometry concepts, facilitates quantitative dose-response modeling to estimate points of departure (POD) to determine acceptable levels of exposure [33, 34]. In contrast, semi-quantitative scoring of histological features by manual morphometry is sub-optimal for modeling, limiting the quantitative potential of large scale toxicological studies such as those submitted to, or contracted by, regulatory agencies.

Imaging technologies have been incorporated into various drug discovery stages including target discovery, candidate screening and early safety evaluation (Lang et al, 2006). QuHAnT, as well as other similar approaches, extend image analysis into preclinical development [3] and risk assessment. QuHAnT is a high-throughput image analysis tool that aids with subjective or semi-quantitative feature analysis by maximizing the extraction of quantitative information from data rich histopathology images while minimizing bias by reducing inter-observer variability. Particularly important for the reduction of inter-observer reliability is the transparency in setting feature detection thresholds which is not typically reported. This study has shown that QuHAnT outperforms manual morphometry in accuracy, reproducibility, and analysis time as well as providing additional complementary information not easily obtained using manual approaches. It is also easily extensible to other distinguishable histological features of interest. The ability to phenotypically anchor transcriptomic, proteomic and metabolomic responses to quantitated key histopathological effects facilitates a more statistically robust interpretation of the data and facilitates the differentiation of adverse effects from adaptive responses. QuHAnT also supports the identification and refinement of mechanistically-based biomarkers of adverse reactions, and advances the assessment of the potential toxicological relevance of the mode of action to humans.

# REFERENCES

## REFERENCES


1. Pantanowitz, L., P.N. Valenstein, A.J. Evans, K.J. Kaplan, J.D. Pfeifer, D.C. Wilbur, L.C. Collins, and T.J. Colgan, *Review of the current state of whole slide imaging in pathology.* J Pathol Inform, 2011. 2: p. 36.

2. Romero Lauro, G., W. Cable, A. Lesniak, E. Tseytlin, J. McHugh, A. Parwani, and L. Pantanowitz, *Digital pathology consultations-a new era in digital imaging, challenges and practical applications.* J Digit Imaging, 2013. 26(4): p. 668-77.

3. Garrido, R., T.S. Zabka, J. Tao, M. Fielden, A. Fretland, and M. Albassam, *Quantitative histological assessment of xenobiotic-induced liver enzyme induction and pituitary-thyroid axis stimulation in rats using whole-slide automated image analysis.* J Histochem Cytochem, 2013. 61(5): p. 362-71.

4. Ying, X. and T.M. Monticello, *Modern imaging technologies in toxicologic pathology: An overview.* Toxicol Pathol, 2006. 34(7): p. 815-26.

5. Mengel, M., R. von Wasielewski, B. Wiese, T. Rudiger, H.K. Muller-Hermelink, and H. Kreipe, *Inter-laboratory and inter-observer reproducibility of immunohistochemical assessment of the Ki-67 labelling index in a large multi-centre trial.* J Pathol, 2002. 198(3): p. 292-9.

6. Oyama, T., Y. Ishikawa, M. Hayashi, K. Arihiro, and J. Horiguchi, *The effects of fixation, processing and evaluation criteria on immunohistochemical detection of hormone receptors in breast cancer.* Breast Cancer, 2007. 14(2): p. 182-8.

7. Lawrie, C.H., E. Ballabio, E. Soilleux, J. Sington, C.S. Hatton, S. Dirnhofer, and A. Tzankov, *Inter- and intra-observational variability in immunohistochemistry: a multicentre analysis of diffuse large B-cell lymphoma staining.* Histopathology, 2012. 61(1): p. 18-25.

8. Huang, Y., W.B. de Boer, L.A. Adams, G. MacQuillan, E. Rossi, P. Rigby, S.C. Raftopoulos, M. Bulsara, and G.P. Jeffrey, *Image analysis of liver collagen using sirius red is more accurate and correlates better with serum fibrosis markers than trichrome.* Liver Int, 2013. 33(8): p. 1249-56.

9. Ge, F., H.t. Lobdell, S. Zhou, C. Hu, and P.D. Berk, *Digital analysis of hepatic sections in mice accurately quantitates triglycerides and selected properties of lipid droplets.* Exp Biol Med (Maywood), 2010. 235(11): p. 1282-6.

10. Gurcan, M.N., L.E. Boucheron, A. Can, A. Madabhushi, N.M. Rajpoot, and B. Yener, *Histopathological image analysis: a review.* IEEE Rev Biomed Eng, 2009. 2: p. 147-71.

11. Levene, A.P., H. Kudo, M.J. Armstrong, M.R. Thursz, W.M. Gedroyc, Q.M. Anstee, and R.D. Goldin, *Quantifying hepatic steatosis - more than meets the eye.* Histopathology, 2012. 60(6): p. 971-81.

12. Nishida, T., K. Tsuneyama, M. Fujimoto, K. Nomoto, S. Hayashi, S. Miwa, T. Nakajima, Y. Nakanishi, Y. Sasaki, W. Suzuki, S. Iizuka, M. Nagata, T. Shimada, M. Aburada, Y. Shimada, and J. Imura, *Spontaneous onset of nonalcoholic steatohepatitis and*

*hepatocellular carcinoma in a mouse model of metabolic syndrome.* Lab Invest, 2013. 93(2): p. 230-41.

13. Standish, R.A., E. Cholongitas, A. Dhillon, A.K. Burroughs, and A.P. Dhillon, *An appraisal of the histopathological assessment of liver fibrosis.* Gut, 2006. 55(4): p. 569-78.

14. Ishak, K., A. Baptista, L. Bianchi, F. Callea, J. De Groote, F. Gudat, H. Denk, V. Desmet, G. Korb, R.N. MacSween, and et al., *Histological grading and staging of chronic hepatitis.* J Hepatol, 1995. 22(6): p. 696-9.

15. Crissman, J.W., D.G. Goodman, P.K. Hildebrandt, R.R. Maronpot, D.A. Prater, J.H. Riley, W.J. Seaman, and D.C. Thake, *Best practices guideline: toxicologic histopathology.* Toxicol Pathol, 2004. 32(1): p. 126-31.

16. Boorman, G.A., J.K. Haseman, M.D. Waters, J.F. Hardisty, and R.C. Sills, *Quality review procedures necessary for rodent pathology databases and toxicogenomic studies: the National Toxicology Program experience.* Toxicol Pathol, 2002. 30(1): p. 88-92.

17. Bringhenti, I., J.A. Moraes-Teixeira, M.R. Cunha, F. Ornellas, C.A. Mandarim-de-Lacerda, and M.B. Aguila, *Maternal obesity during the preconception and early life periods alters pancreatic development in early and adult life in male mouse offspring.* Plos One, 2013. 8(1): p. e55711.

18. Frantz, E.D., C. Crespo-Mascarenhas, A.R. Barreto-Vianna, M.B. Aguila, and C.A. Mandarim-de-Lacerda, *Renin-angiotensin system blockers protect pancreatic islets against diet-induced obesity and insulin resistance in mice.* Plos One, 2013. 8(7): p. e67192.

19. Tschanz, S.A., P.H. Burri, and E.R. Weibel, *A simple tool for stereological assessment of digital images: the STEPanizer.* J Microsc, 2011. 243(1): p. 47-59.

20. Rexhepaj, E., D.J. Brennan, P. Holloway, E.W. Kay, A.H. McCann, G. Landberg, M.J. Duffy, K. Jirstrom, and W.M. Gallagher, *Novel image analysis approach for quantifying expression of nuclear proteins assessed by immunohistochemistry: application to measurement of oestrogen and progesterone receptor levels in breast cancer.* Breast Cancer Res, 2008. 10(5): p. R89.

21. Boverhof, D.R., L.D. Burgoon, C. Tashiro, B. Chittim, J.R. Harkema, D.B. Jump, and T.R. Zacharewski, *Temporal and dose-dependent hepatic gene expression patterns in mice provide new insights into TCDD-Mediated hepatotoxicity.* Toxicol Sci, 2005. 85(2): p. 1048-63.

22. Pierre, S., A. Chevallier, F. Teixeira-Clerc, A. Ambolet-Camoit, L.C. Bui, A.S. Bats, J.C. Fournet, P. Fernandez-Salguero, M. Aggerbeck, S. Lotersztajn, R. Barouki, and X. Coumoul, *Aryl Hydrocarbon Receptor-Dependent Induction of Liver Fibrosis by Dioxin.* Toxicol Sci, 2013.

23. Lu, H., W. Cui, and C.D. Klaassen, *Nrf2 protects against 2,3,7,8-tetrachlorodibenzo-p-dioxin (TCDD)-induced oxidative injury and steatohepatitis.* Toxicol Appl Pharmacol, 2011. 256(2): p. 122-35.

24. Kopec, A.K., L.D. Burgoon, D. Ibrahim-Aibo, B.D. Mets, C. Tashiro, D. Potter, B. Sharratt, J.R. Harkema, and T.R. Zacharewski, *PCB153-elicited hepatic responses in the immature, ovariectomized C57BL/6 mice: comparative toxicogenomic effects of dioxin and non-dioxin-like ligands.* Toxicol Appl Pharmacol, 2010. 243(3): p. 359-71.

25. Kopec, A.K., M.L. D'Souza, B.D. Mets, L.D. Burgoon, S.E. Reese, K.J. Archer, D. Potter, C. Tashiro, B. Sharratt, J.R. Harkema, and T.R. Zacharewski, *Non-additive hepatic gene expression elicited by 2,3,7,8-tetrachlorodibenzo-p-dioxin (TCDD) and 2,2',4,4',5,5'-hexachlorobiphenyl (PCB153) co-treatment in C57BL/6 mice.* Toxicol Appl Pharmacol, 2011. 256(2): p. 154-67.

26. Zaitoun, A.M., H. Al Mardini, S. Awad, S. Ukabam, S. Makadisi, and C.O. Record, *Quantitative assessment of fibrosis and steatosis in liver biopsies from patients with chronic hepatitis C.* J Clin Pathol, 2001. 54(6): p. 461-5.

27. Hadi, A.M., K.T. Mouchaers, I. Schalij, K. Grunberg, G.A. Meijer, A. Vonk-Noordegraaf, W.J. van der Laarse, and J.A. Belien, *Rapid quantification of myocardial fibrosis: A new macro-based automated analysis.* Anal Cell Pathol (Amst), 2010. 33(5): p. 257-69.

28. Chieco, P., A. Jonker, B.A. De Boer, J.M. Ruijter, and C.J. Van Noorden, *Image cytometry: protocols for 2D and 3D quantification in microscopic images.* Prog Histochem Cytochem, 2013. 47(4): p. 211-333.

29. Eliceiri, K.W., M.R. Berthold, I.G. Goldberg, L. Ibanez, B.S. Manjunath, M.E. Martone, R.F. Murphy, H. Peng, A.L. Plant, B. Roysam, N. Stuurman, J.R. Swedlow, P. Tomancak, and A.E. Carpenter, *Biological imaging software tools.* Nat Methods, 2012. 9(7): p. 697-710.

30. Day, C.P. and O.F. James, *Hepatic steatosis: innocent bystander or guilty party?* Hepatology, 1998. 27(6): p. 1463-6.

31. Deutsch, M.J., S.C. Schriever, A.A. Roscher, and R. Ensenauer, *Digital image analysis approach for lipid droplet size quantitation of Oil Red O-stained cultured cells.* Anal Biochem, 2014. 445: p. 87-9.

32. Kind, C.N., *The application of in-situ hybridisation and immuno-cytochemistry to problem resolution in drug development.* Toxicol Lett, 2000. 112-113: p. 487-92.

33. *Benchmark Dose Technical Guidance.* 2012.

34. Davis, J.A., J.S. Gift, and Q.J. Zhao, *Introduction to benchmark dose methods and U.S. EPA's benchmark dose software (BMDS) version 2.1.1.* Toxicol Appl Pharmacol, 2011. 254(2): p. 181-91.

# CHAPTER 4. PYRUVATE KINASE ISOFORM SWITCHING AND HEPATIC METABOLIC REPROGRAMMING BY THE ENVIRONMENTAL CONTAMINANT 2,3,7,8-TETRACHLORODIBENZO-P-DIOXIN.

**ABSTRACT**

The environmental contaminant 2,3,7,8-tetrachlorodibenzo-*p*-dioxin (TCDD) elicits various hepatic effects including fat accumulation, inflammation, and fibrosis that can progress to hepatocellular carcinoma. To further investigate the effects of TCDD on hepatic metabolism, female C57BL/6 mice were gavaged every 4 days for 28 days with sesame oil vehicle, 0.01, 0.03, 0.1, 0.3, 1, 3, 10, or 30 µg/kg TCDD. RNA-Seq data, revealing differential expression of 3,406 genes (|fold-change| ≥ 1.5, P1(*t*) ≥ 0.8), was integrated with complementary targeted metabolomics of the liver and serum, dioxin response element (DRE) location, and aryl hydrocarbon receptor (AhR) ChIP-Seq data. Our integrative analysis identified altered hepatic levels of pentose phosphate pathway (PPP) metabolites (1.5-fold increase in ribulose-5-phosphate levels, 2-5-fold decrease in 6-phosphogluconic acid, erythrose-4-phosphate, fructose-6-phosphate, ribose-5-phosphate and glucose-6-phosphate) consistent with increased PPP flux. A concomitant 40-fold increase in expression of pyruvate kinase isoform M2 (*Pkm2*) was observed, as well as a 2.4-fold increase at the protein level, revealing a response similar to the Warburg effect observed in cancer cells. Consequently, we examined protein levels of glutaminase (GLS1) GAC and KGA isoforms, another feature of cancer cells, demonstrating a 1.7-fold increase in the GAC:KGA ratio consistent with cancer. Collectively, this integrative analysis provides evidence that PKM isoform switching by TCDD redirects glycolytic intermediates towards the PPP and serine biosynthesis, and that glutaminolysis may be serving an anaplerotic role in the TCA cycle. We propose that these responses represent AhR-mediated hepatic metabolic reprogramming in order to increase NADPH production and support glutathione metabolism, as an oxidative stress counter-measure.

**INTRODUCTION**

2,3,7,8-Tetrachlorodibenzo-p-dioxin (TCDD) is the prototypical ligand for a series of structurally diverse environmental contaminants, natural products, and endogenous metabolites

that bind and activate the aryl hydrocarbon receptor (AhR), a basic helix-loop-helix ligand activated transcription factor [1]. Binding of TCDD and related compounds to the cytosolic AhR causes chaperone protein dissociation, followed by nuclear translocation and heterodimerization with the AhR nuclear translocator (ARNT). The TCDD-AhR-ARNT complex binds dioxin response elements (DRE; also known as AHRE and XRE) consisting of the invariant core sequence 5'-GCGTG-3', eliciting changes in gene expression, although DRE-independent interactions have also been described [2-4].

TCDD and related compounds elicit a variety of adverse effects including teratogenesis, immunosuppression, and tumor promotion [5], and have also been implicated in the development of non-alcoholic fatty liver disease (NAFLD) and type II diabetes (T2D)[6]. In mice, a single bolus dose of TCDD results in hepatic fat accumulation with reduced *de novo* fatty acid synthesis and β-oxidation [7, 8]. Conversely, repeated treatment sustains lipid accumulation with progression to steatohepatitis and fibrosis [9, 10]. TCDD-elicited metabolic disruption is not limited to lipid metabolism, but also disrupts glycolysis, the TCA cycle, and nucleoside metabolism [11-13]. However, these were short term exposure studies involving a single bolus dose, or did not include complementary 'omic' data.

The objective of this study was to further investigate TCDD-elicited metabolic disruption by integrating AhR ChIP-Seq, hepatic RNA-Seq, and hepatic and serum metabolomic data to understand the impact on the metabolic pathways. Changes in central carbon and amino acid metabolism were reminiscent of the Warburg effect, including pyruvate kinase isoform switching [14], enhanced glutaminolysis [15], and increased serine (Ser) metabolism [16, 17] were observed. We propose that this reprogramming of metabolism may represent a more general response to support cell survival in normal tissue following toxic insult.

## MATERIALS AND METHODS

### ANIMAL TREATMENT

Postnatal day 25 (PND25) female C57BL/6 mice (Charles River Laboratories, Portage, MI), housed in polycarbonate cages with cellulose fiber chips (Aspen Chip Laboratory Bedding, Warrensberg, NY) at 30-40% humidity and a 12h light/dark cycle and acclimatized for 4d, were fed *ad libitum* (Harlan Teklad 22/5 Rodent Diet 8940, Madison, WI) with free access to deionized water. On PND 28 and every following 4th day animals (N = 5) were orally gavaged with 0.1 mL sesame oil or 0.01, 0.03, 0.1, 0.3, 1, 3, 10 and 30 µg/kg TCDD (Dow Chemical Company, Midland, MI) for a total of 28d. Blood was collected by submandibular vein puncture into BD microtainer tubes with serum separator and centrifuged at 10,000xg for 5 min and stored at -80ºC. Liver samples were frozen in liquid nitrogen, and stored at -80$^0$C. Only 30 µg/kg samples were analyzed by ChIP-Seq at 2 hrs. Livers from 92d treated mice were collected using the same treatment and collection methods. Hepatic samples from female C57BL/6 mice treated with 100 µg/kg β-naphthoflavone (βNF) were collected following daily gavage for 28d. TCDD time course, 3,3',4,4',5-pentachlorobiphenyl (PCB126), 2,3,7,8-tetrachlorodibenzofuran (TCDF), 2,2',4,4',5,5'-hexachlorobiphenyl (PCB153) were collected as described [7, 18, 19]. All procedures were approved by the All-University Committee on Animal Use and Care.

### IDENTIFICATION OF BONA FIDE DRES AND CALCULATION OF MS SCORES

*Bona fide* DREs were identified DREs from previous computational analysis of genome wide DREs [20, 21] and through literature searching. Newly identified DREs were considered *bona fide* if (1) Direct AhR binding was confirmed, (2) AhR binding to the DRE was shown to elicit changes in gene expression (e.g. reporter assay), and (3) removal of the DRE ablated the transcriptional response. Consequently, four new functional DREs reported for human *Bach2* [22] and *Cyp1b1* [23] were added. *Bona fide* DRE sequences are provided in Table 4. The new position weight matrix (PWM) was calculated as previously described [20]. To update matrix

similarity scores, the mouse genome (mm10; GRCm38) was downloaded from the UCSC genome database and the UCSC tool findMotif was used to extract all DREs. The UCSC tool twoBitToFA was used to extract DRE sequences and 5' and 3' flanking regions. Matrix similarity scores (MSS) were calculated for the 19bp sequences as previously described [20]

**TABLE 4. BONA FIDE DRE SEQUENCES USED TO CONSTRUCT POSITION WEIGHT MATRIX (PWM)**

| Specie | Gene Symbol | *bona fide* DRE sequence (5'->3') | matrix similarity score (MSS) | Reference |
|---|---|---|---|---|
| Mouse | *Cyp1a1* | CAAGCTCGCGTGAGAAGCG | 0.954 | [1] |
| | *Cyp1a1* | CCTGTGTGCGTGCCAAGCA | 0.919 | [1] |
| | *Cyp1a1* | CGGAGTTGCGTGAGAAGAG | 0.964 | [1] |
| | *Cyp1a1* | CCAGCTAGCGTGACAGCAC | 0.910 | [1] |
| | *Cyp1a1* | CGGGTTTGCGTGCGATGCT | 0.979 | [1] |
| | *Cyp1b1* | CCCCCTTGCGTGCGGAGCT | 0.971 | [1] |
| Rat | *Cyp1a1* | CGGAGTTGCGTGAGAAGAG | 0.964 | [1] |
| | *Cyp1a1* | CCAGCTAGCGTGACAGCAC | 0.910 | [1] |
| | *Aldh3a1* | TGCCCTGGCGTGACTTTGT | 0.856 | [1] |
| | *Nqo1* | TCCCCTTGCGTGCAAAGGC | 0.926 | [1] |
| | *Sod1* | GAGGCCTGCGTGCGCGCCT | 0.870 | [1] |
| | *Gsta2*[a] | GCATGTTGCGTGCATCCCT | | [1] |
| | *Ugt1a6* | AGAATGTGCGTGACAAGGT | 0.907 | [1] |
| Human | *Cyp1b1* | CGCCTCCGCGTGTCAGGTG | 0.881 | [23] |
| | *Cyp1b1* | CCCCTTTGCGTGCGGAGCT | 0.968 | [23] |
| | *Cyp1b1* | GGGCTTTGCGTGCGCCGCT | 0.939 | [23] |
| | *Bach2* | TAACACAGCGTGAGCCCTT | 0.833 | [22] |

[a]Not present in Rn5 genome build

**HEPATIC AHR CHIP-SEQ**

Cross-linked DNA was immunoprecipitated with either rabbit IgG or rabbit IgG and anti-AhR as previously described [3, 24]. Libraries prepared using the MicroPlex kit (Diagenode, Denville, NJ) were pooled and sequenced at a depth of ~30M on an Illumina HiSeq 2500 at the MSU Research and Technology Support Facility Core. Read processing and analysis was performed using the MSU High Performance Computing Center. Quality was determined using FASTQC v0.11.2 and adaptor sequences removed using Cutadapt v1.4.1 while low-complexity reads were cleaned using FASTX v0.0.14. Reads were mapped to the mouse reference genome (GRCm38 release 76) using Bowtie 2.0.0 and alignments were converted to SAM format using SAMTools v0.1.19. Normalization and peak calling was performed using CisGenome [25] determined by comparison of IgG control and AhR enriched samples (n=5) using a bin size (-b) of 25 and boundary refinement resolution (-bw) of 1 with default parameters.

**METABOLITE EXTRACTION**

Liver (~100 mg) and serum (30 µL) metabolites were extracted using chloroform:water:methanol. Briefly, frozen liver samples were homogenized (Polytron PT2100, Kinematica) or vortexed (serum) in HPLC grade methanol:water (5:3, 4.63 mL, -20°C) in Pyrex glass tubes. HPLC-grade chloroform was added following homogenization (methanol:water:chloroform, 5:3:5), vortexed, shaken on ice for 10 min, and centrifuged at 3,000xg. The transferred aqueous phase was dried under nitrogen gas at room temperature and resuspended in HPLC-grade water prior to analysis. Hepatic extract protein layers were dried and a bicinchoninic acid assay (Sigma-Aldrich) on a Tecan Infinite 200 microplate reader (Männedorf, Switzerland) was used to normalize signal in liver.

Amino acids were carbobenzyloxy (cbz) derivatized for analysis. Redissolved solutions (20 µl) were added to 80 µl of HPLC-grade methanol, and 2.5 µl of triethylamine. 0.5 µl

benzylchloroformate was added and samples were vortexed then centrifuged, and the supernatant was transferred to HPLC vials for analysis.

**TARGETED METABOLOMIC ANALYSIS**

Hepatic extracts were first loaded onto a trapping column (C18, 4 mm×2 mm, Phenomenex) and washed for 30s with HPLC grade water containing 10 mM tributylamine and 15 mM acetic acid for desalting. Hepatic extracts were examined by liquid chromatography (LC) and tandem mass spectrometry (MS/MS) using a Paradigm MS4 HPLC (Michrom Bioresources, Auburn, CA), and a Synergi Hydro column (4 µm particle size, 80 Å, 150 mm×2 mm, from Phenomenex) [26]. HPLC was coupled with negative-mode electrospray ionization (ESI) to a TSQ Vantage Triple Stage Quadrupole Mass Spectrometer (Thermo Scientific) operating in multiple reaction monitoring (MRM) mode. Serum extracts were analyzed using an Acquity UPLC system (Waters), Ascentis Express column (C18, 5 cm x 2.1 mm, 2.7 µm, Sigma-Aldrich) while MRM was performed using a Xevo TQ-S triple quadrupole mass spectrometer (Waters).

For the analysis of hepatic extracts, the LC parameters were as follows: autosampler temperature, 10 ºC; injection volume, 10 µl; column temperature, room temperature; and flow rate, 200 µl·min$^{-1}$. The LC solvents were Solvent A: 10 mM tributylamine and 15 mM acetic acid in 97:3 water:methanol (pH 4.95); and Solvent B: methanol. Elution from the column was performed over 50 min with the following gradient: t = 0, 0% B; t = 5, 0% B; t = 10, 20% B; t = 20, 20% B; t = 35, 65% B; t = 38, 95% B; t = 42, 95% B, t = 43, 0% B; t = 50, 0% B. ESI spray voltage was 3,000 V. Nitrogen was used as the sheath gas at 30 psi and as the auxiliary gas at 10 psi, and argon as the collision gas at 1.5 mTorr, with the capillary temperature at 325 ºC. Scan time for each MRM transition was 0.1 s with a scan width of 1 m/z. The LC runs were divided into time segments, with the MRM scans within each time segment containing compounds eluting during that time interval. For compounds eluting near boundaries between time segments, the MRM scan corresponding to the compound was conducted in both time segments. Instrument control,

chromatographic control, and data acquisition were performed by the Xcalibur software (Thermo Scientific).

For analysis of serum extracts, the LC parameters were as follows: autosampler temperature, 10 ºC; injection volume, 10 µl; column temperature, 50ºC and flow rate, 150 µl·min$^{-1}$. The LC solvents were Solvent A: 10 mM tributylamine and 15 mM acetic acid in 97:3 water:methanol (pH 4.95); and Solvent B: methanol. Elution from the column was performed over 11 min with the following gradient: t = 0, 0% B; t = 3, 20% B; t = 7.5, 55% B; t = 9, 95% B; t = 10, 95% B; t = 10.5, 0% B. The LC runs were divided into time segments, with the MRM scans within each time segment containing compounds eluting during that time interval. For compounds eluting near boundaries between time segments, the MRM scan corresponding to the compound was conducted in both time segments. Instrument control, chromatographic control, and data acquisition were performed by the MassLynx software (Waters).

Data analysis, including peak integration was performed using MAVEN [27, 28]. Waters raw data were converted to mzxml format using msconvert in the ProteoWizard Tools [29] prior to analysis by MAVEN. One-way ANOVA was performed in SAS 9.3 (SAS Institute, Inc., Cary, NC). Raw data and MRM parameters are deposited in www.ebi.ac.uk/metabolights (MTBLS225).

**HEPATIC GLUTATHIONE LEVELS**

Total hepatic glutathione levels were determined according to manufacturer's instructions (Sigma-Aldrich) using a Tecan Infinite 200 microplate reader (Männedorf, Switzerland).

**HEPATIC GENE EXPRESSION**

Published RNA-Seq data (GSE62902) were used for the integrative analysis [30]. Filtering criteria of |fold-change| ≥ 1.5 and P1(*t*) ≥ 0.8 were used for all data analysis. UCSC Genome browser tracks combine all reads from vehicle or 30 µg/kg doses (http://dbzach.fst.msu.edu/index.php/supplementarydata.html). Quantitative real-time PCR

(QRTPCR) was performed as previously described [7]. Relative expression was determined using the $2^{-\Delta\Delta CT}$ method and the geometric mean of reference genes *ActB*, *Gapdh*, and *Hprt*. Statistical analyses of QRTPCR data were performed using a one-way ANOVA for dose-response study designs followed by Dunnett's *post-hoc* test. For time-course designs a two-way ANOVA with dose and time as factors was used followed by Tukey's *post-hoc* test. For chemical treatment, each study was considered independently and analyzed by Student's t-test. Statistical analyses were performed using SAS 9.3 (SAS Institute Inc.).

**PROTEIN MEASUREMENTS**

Liver samples (~25 mg, n=5) were ground by mortar and pestle in radioimmunoprecipitation (RIPA) buffer supplemented with protease inhibitor cocktail (Sigma-Aldrich), sonicated on ice, and centrifuged. Total protein in the supernatant was quantitated by bicinchoninic acid assay (Sigma-Aldrich). Protein levels were determined using the Wes (ProteinSimple, San Jose, CA) system. PKM1 (Sigma-Aldrich; 1:400), PKM2 (Cell Signaling, Danvers, MA; 1:65), PKM1/2 (Cell Signaling; 1:65), and GLS1 (ProteinTech, Chicago, IL; 1:30) antibodies were duplexed with β-actin (Cell Signaling; 1:65) as loading control and detected by goat anti-rabbit secondary antibody. Chemiluminescence signals were exported from Compass software (ProteinSimple) and used to calculate fold-change. Statistical analyses were performed using Student's t-test in SAS 9.3.

**ENRICHMENT ANALYSES AND KEGG PATHWAY INTEGRATION**

Over-represented metabolites within a pathway, as well as impact scores representing the connectivity to other metabolites or clusters was determined using MetPA [31]. Over-represented differentially expressed genes compared to all mouse KEGG pathway genes was assessed using ClusterProfiler in R 3.2.0 [32]. Pathways were manually curated to include only normal

metabolism pathways which were considered relevant to the expression dataset (e.g. signaling, tissue specific, and cancer pathways were removed).

The CytoKegg 0.0.5 plugin (Cytoscape 3.2.0) was used to generate pathway templates. Through manual curation for completeness, and refinement, pathways were streamlined by combining reactions with the same compounds as a single node. pDRE, AhR enrichment, differential gene expression, and altered metabolite level data represent the most significant change for each node (e.g. highest MSS score or largest |fold-change|). An expandable interactive versions can be viewed at http://dbzach.fst.msu.edu/index.php/supplementarydata.html.

## RESULTS

### ALTERATIONS IN CENTRAL CARBON, AMINO ACID AND LIPID METABOLISM

TCDD elicits significant lipidomic changes consistent with the development of fatty liver and steatohepatitis in mice [7, 33]. In this study, complementary targeted metabolomics was used to examine metabolite changes in hepatic extracts and serum from mice treated with 3, 10 and 30 µg/kg TCDD every 4d for 28d. Of the ~190 metabolites examined, only 124 and 84 were detected in hepatic and serum samples, respectively, with 48 hepatic and 41 serum metabolites altered ($P \leq 0.05$) by treatment. This included an 11-fold increase in hepatic oxaloacetate (OAA) and >1,000-fold decrease in serum xanthine. Altered metabolite levels were analyzed for pathway over-representation (enrichment) and connectivity within related metabolites (impact) using MetPA [31]. Central carbon (glycolysis/gluconeogenesis, the TCA cycle, and the pentose phosphate pathway (PPP)), and amino acid metabolism consistently exhibited higher enrichment (-log($p$)) and/or impact scores (Figure 10).

RNA-Seq [30] and metabolomic data were integrated using KEGG metabolic pathways. Analysis of 3,406 differentially expressed genes (DEGs) (|fold-change| ≥ 1.5 and P1($t$) ≥ 0.8) using clusterProfiler [32] identified over-represented ($P \leq 0.05$) pathways associated with altered

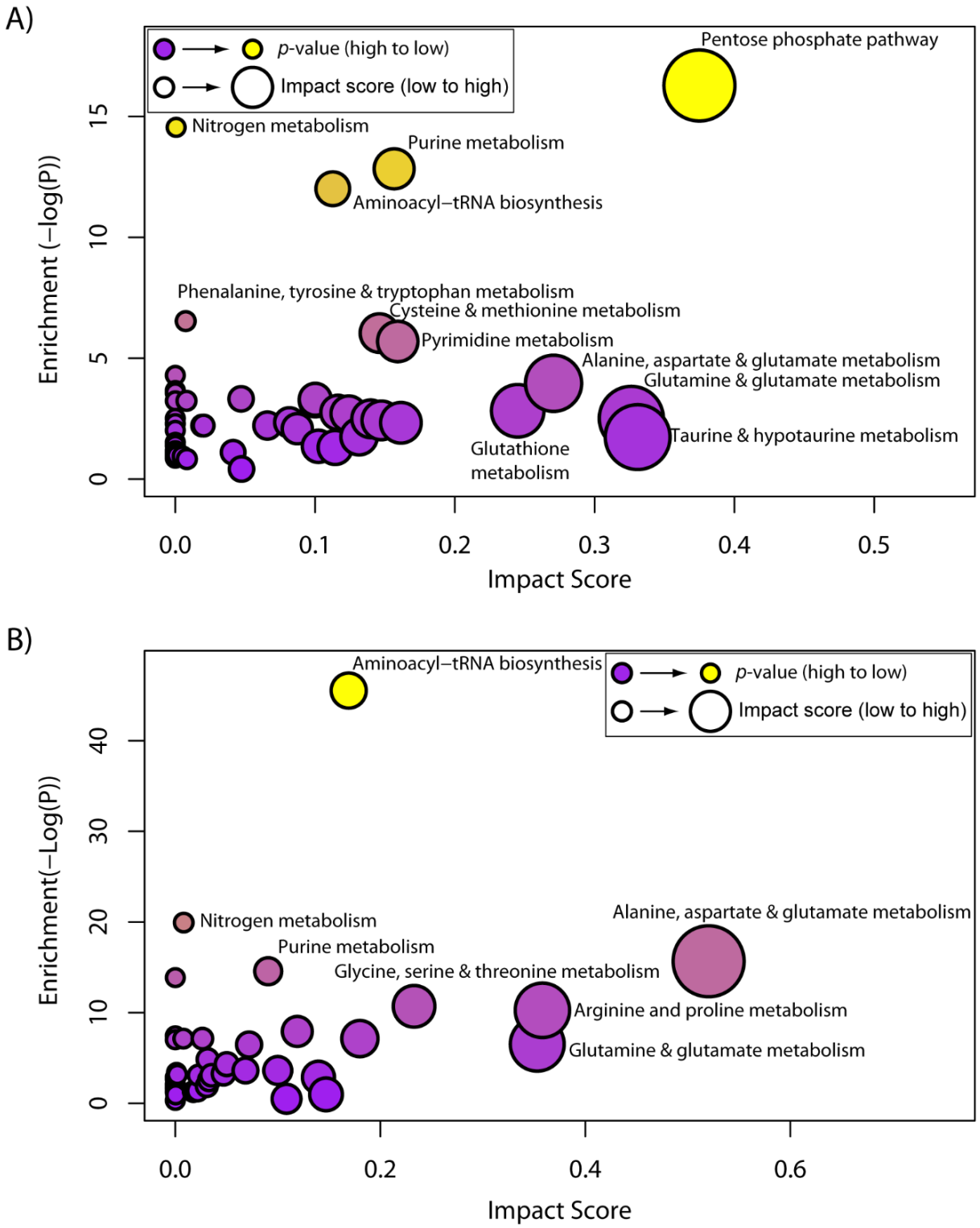


**FIGURE 10. METABOLIC PATHWAY ENRICHMENT OF TCDD ALTERED METABOLITES**

Metabolic pathway enrichment analysis (MetPA) of altered metabolites ($P \leq 0.05$) in (A) hepatic and (B) serum extracts. Enrichment values ≥ 4.0 were considered significant and impact scores were used to rank pathways.

glucose, amino acid, and fatty acid metabolism (Figure 11). KEGG enrichment also identified drug, starch and sucrose, and pyruvate metabolism enrichment. Overall, metabolite changes were consistent with the DEG profile.

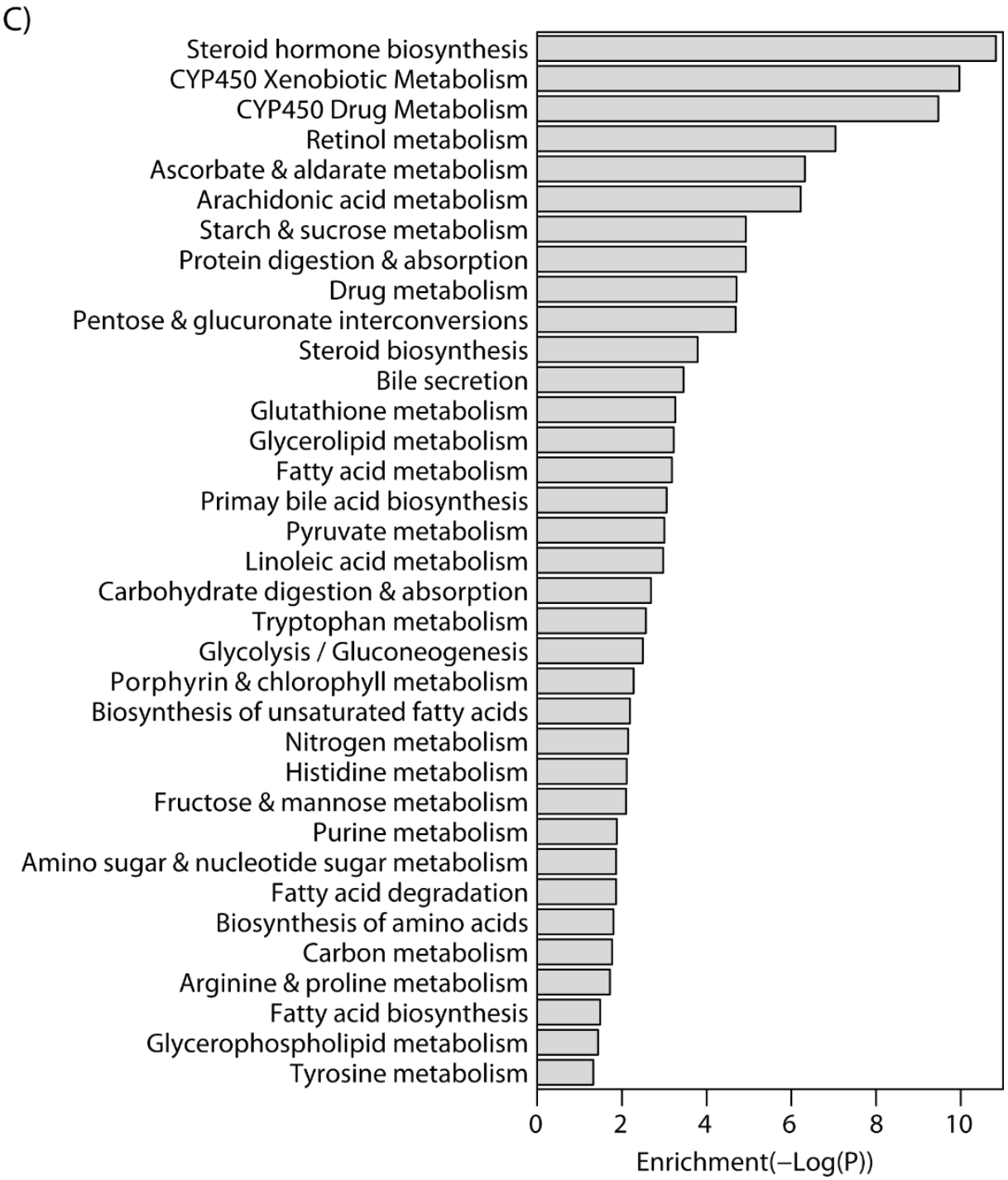


**FIGURE 11. KEGG PATHWAY ENRICHMENT OF DIFFERENTIALLY EXPRESSED GENES**

**FIGURE 11 (cont'd)**

Significantly enriched ($P \leq 0.05$) KEGG pathways for the 3,406 differentially expressed genes (DEGs; |fold-change| ≥ 1.5, P1($t$) ≥ 0.8).

To further evaluate AhR-mediated effects, ChIP-Seq was performed 2 hr post first dose of 30 µg/kg TCDD. Approximately 13,936 enrichment peaks were identified, of which 5,766 satisfied the FDR ≤ 0.05 criteria, with 2,711 located within the coding region or 10kb upstream region. Comparative analysis of 3,406 DEGs with 2,711 AhR enriched regions and 23,054 putative DREs (pDREs) identified 685 genes at the intersection. Only 475 had a pDRE within an AhR enriched region (Figure 12) suggesting AhR-mediated DRE-dependent regulation, while 210 genes with AhR enrichment lacked an overlapping pDRE.

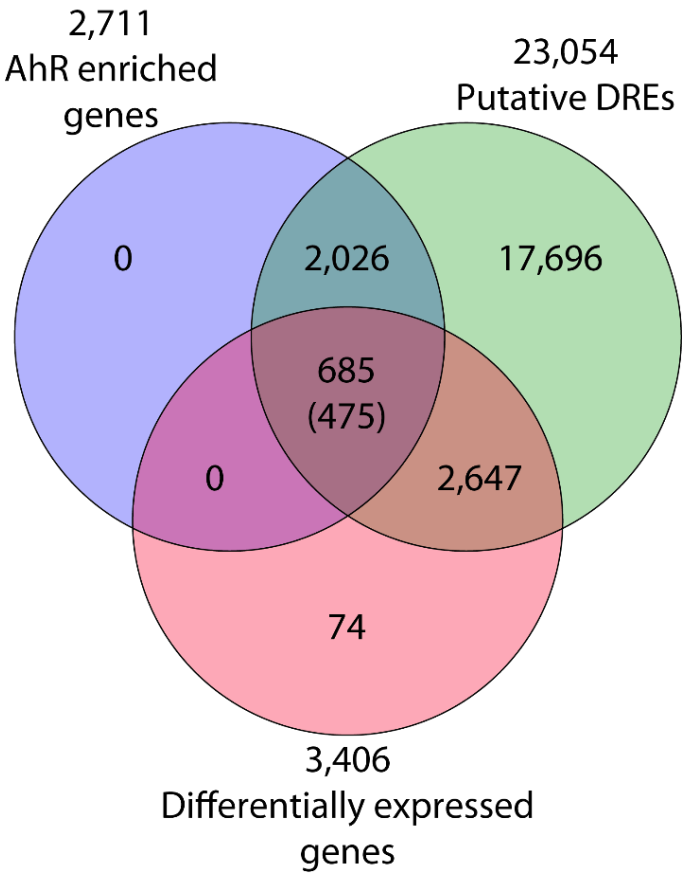


**FIGURE 12. OVERLAP OF DIFFERENTIALLY EXPRESSED GENES, PDRES, AND AHR ENRICHMENT**

**FIGURE 12 (cont'd)**

Venn diagram of genes with AhR enrichment within its genomic region and 10 Kb upstream of the TSS determined by ChIP-Seq (FDR ≤ 0.05), putative dioxin response elements (pDREs), and DEGs. Genes possessing AhR enrichment, pDREs, and differential expression are shown, and the number of genes meeting these criteria where the AhR enrichment peaks overlaps a putative DRE is shown in parentheses.

## INCREASED HEPATIC LIPID UPTAKE BUT INHIBITED FATTY ACID SYNTHESIS AND OXIDATION

KEGG enrichment analysis identified DEGs associated with lipid transport, processing, and metabolism (Figure 13). This included the down-regulation of apolipoproteins (i.e., 3.3-fold

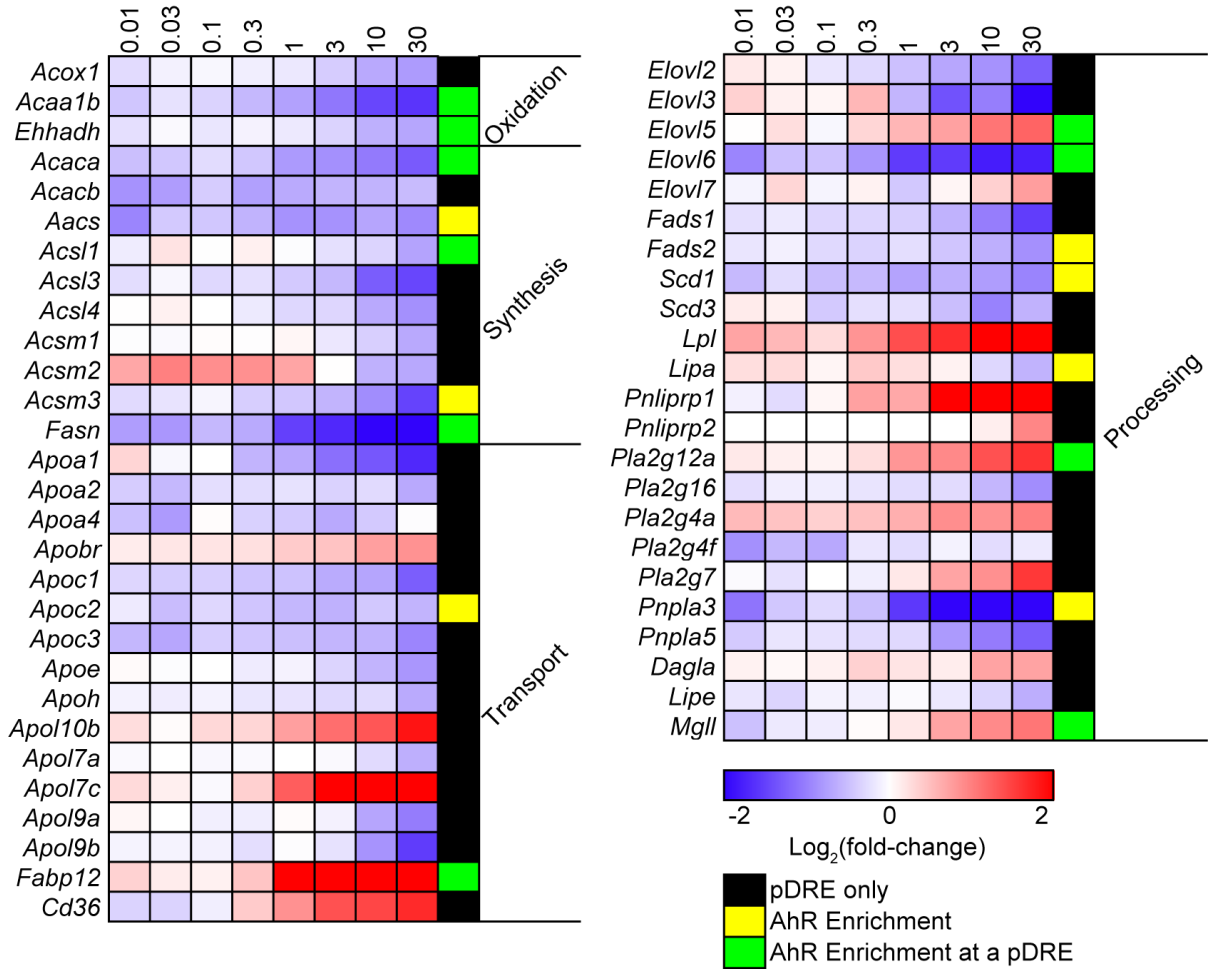


**FIGURE 13. DIFFERENTIALLY EXPRESSED LIPID METABOLISM GENES**

**FIGURE 13 (cont'd)**

Heat map of DEGs associated with lipid transport, processing and metabolism. The presence of AhR enrichment at 2 hr post treatment and/or pDREs is indicated in last column on the right.

*Apoa1*) involved in lipid packaging and transport. Conversely, *Apol7c*, *Apol10d*, and *Fabp12* were induced 3.6-, 14-, and 46-fold, respectively. *Cd36* involved in lipid uptake was also induced 3.2-fold as previously reported [8]. However, AhR enrichment with a pDRE was only observed for *Fabp12*. Similarly, lipid processing genes such as elongases (*Elovl2*, *3*, and *6*) and desaturases (*Fads*, *Scd*) were largely repressed >2-fold. Lipases *Lpl*, *Mgll*, *Pnliprp1*, and *Pnliprp2* were induced 4.8-, 2.1-, 48-, and 1.9-fold, respectively, while *Lipa*, *Pnpla3*, and *Pnpla5* were repressed 1.5-, 8.0-, and 2.4-fold, respectively. Overall, *de novo* fatty acid (FA) synthesis and β-oxidation genes were repressed (Figure 13) including a 5.3-fold repression of fatty acid synthase (*Fasn*) with AhR enrichment including a pDRE. β-Oxidation was marked by repression of acetyl-CoA acyltransferase (*Acaa1b* 3.1-fold), carboxylase (*Acaca* 2.5-fold and *Acacb* 1.5-fold), and enoyl-CoA hydratase (*Ehhadh* 1.6-fold). *Acsl1*, *Acsm3*, *Acaa1b*, *Acaca*, and *Ehhadh* exhibited AhR enrichment with a pDRE (except for *Acsm3*). The inhibition of β-oxidation is consistent with short acyl-CoA reductions, particularly decreases in butanoyl-CoA (2.9-fold).

## INDUCTION OF OXIDATIVE STRESS AND ANTIOXIDANT DEFENSES

CytoKEGG analysis with manual curation also identified the enrichment of oxidative stress (e.g. P450 induction, glutathione metabolism), central carbon metabolism, and amino acid metabolism pathways. These pathways were found to converge on $NADP^+$/NADPH, indicating altered production and/or consumption.

The 1,250-, 807- and 16-fold induction of classical AhR battery genes *Cyp1a1*, *Cyp1b1*, and *Cyp1a2* as well as the 1.6- and 1.9-fold increase in NADPH oxidase (*Nox4*) and nitric oxide synthase (*Nos2*) represent major NADPH consumers as well as producers of reactive oxygen

species (ROS; Figure 14A). In response, glutathione peroxidase (*Gpx2*) was induced 11-fold, an important defense mechanism that uses glutathione (GSH) to reduce lipid peroxide and hydrogen peroxide oxidative stress products to alcohols and water, respectively (Figure 14B). The resulting oxidized glutathione (GSSG) is then reduced to GSH (increased 1.4-fold) using NADPH by glutathione reductase (*Gsr*), which was induced 1.4-fold, to preserve cellular anti-oxidant capacity. TCDD also induced a 1.7-fold increase in glutathione synthetase (*Gss*), which catalyzes the condensation of glycine (Gly) and γ-glutamylcysteine to produce more GSH (Figure 14B). Accordingly, these processes increased total glutathione levels 1.3-fold (Figure 15). The absence of AhR enrichment within *Gpx2*, *Gsr* and *Gss* loci indicate these responses were mediated by oxidative stress as opposed to direct AhR regulation.

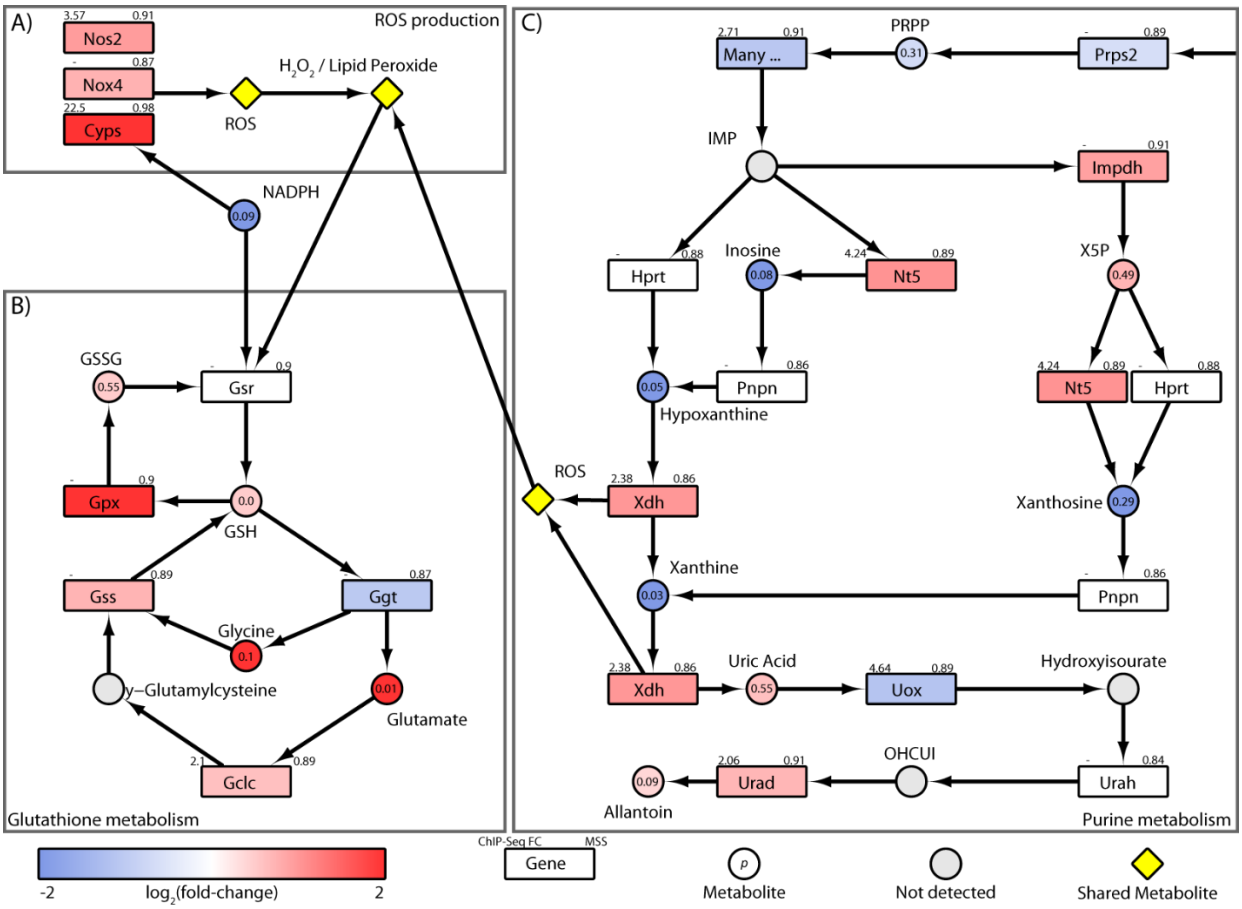


**FIGURE 14. INTEGRATIVE ANALYSIS OF ROS ASSOCIATED PATHWAYS**

**FIGURE 14 (cont'd)**

Induction of oxidative stress and defense pathways. Integration of transcriptomic, metabolomic, and KEGG pathway data for (A) ROS producing xenobiotic metabolizing enzymes, (B) glutathione metabolism, and (C) purine metabolism. Color scale represents the $\log_2$(fold-change) for genes and metabolites. Yellow symbols indicate converging metabolites. Gray symbols indicate metabolites not measured or detected. Genes are identified as rectangles and metabolites as circles. The upper left corner indicates maximum AhR enrichment fold-change and upper right corner indicates the highest scoring pDRE MSS. Circles contain the *p*-value for metabolite changes. An expandable and interactive version of this figure with further information is available at http://dbzach.fst.msu.edu/index.php/supplementarydata.html.

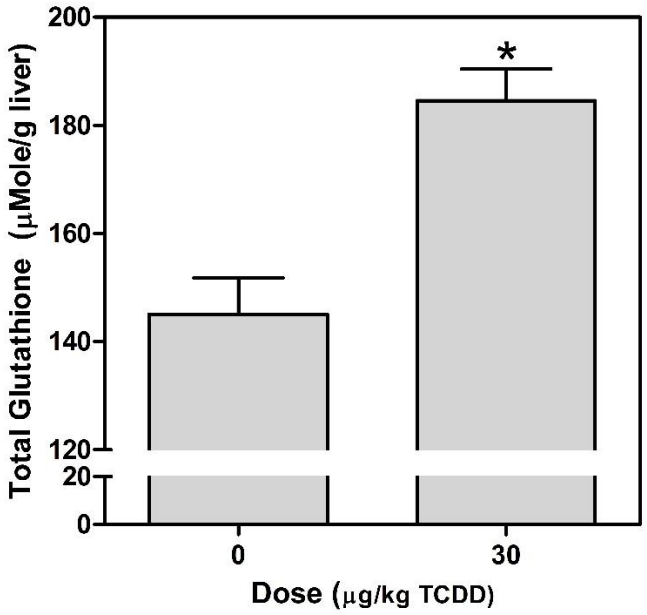


**FIGURE 15. HEPATIC GLUTATHIONE LEVELS**

Total hepatic glutathione levels in livers of mice gavaged with sesame oil vehicle or 30 µg/kg TCDD every 4 days for 28 days. Bars represent mean ± SEM for n=4-5. Asterisks (*) indicates a significant difference ($p \leq 0.05$) determined by student's t-test.

Integrative analysis also highlighted increased purine metabolism that would produce the anti-oxidant, uric acid, which was increased 1.5-fold (Figure 14). Inosine monophosphate (IMP) is converted to inosine by 5' nucleotidase (*Nt5e*), and then to hypoxanthine by purine nucleoside

phosphorylase (*Pnp*) and subsequently to xanthine and uric acid by xanthine dehydrogenase (*Xdh*). Decreases in serum inosine (33-fold), hypoxanthine (170-fold), and xanthine (>1,000-fold), are consistent with the 2.1- and 1.9-fold AhR-mediated induction of *Nt5e* and *Xdh* (Figure 14C). Interestingly, the oxidase form (*XO*) of *Xdh* irreversibly produced under low energy conditions is also a significant ROS contributor.

**INTERACTION OF GLUCOSE, AMINO ACID, AND GLUTATHIONE METABOLISM**

Enrichment analyses also revealed alterations in the catabolic oxidation of glucose (Figure 16A-B). Although hexose transporters with different kinetic properties and substrate preferences were differentially expressed (*Slc2a3*, *2a6*, *2a10* and *2a3* were induced 1.6-, 2.0-, 1.7-, and 1.6-fold, respectively while *Slc2a2, 2a4 and 2a5* were repressed 2.1-, 3.0- and 1.8-fold, respectively), only *Slc2a2* was associated with AhR enrichment. Hexokinases (*Hk*) 1, 2 and 3 were induced 2.3-, 2.5- and 2.2-fold, respectively, while glucokinase (*Gck*) was repressed 4.2-fold. Glucose-6-phosphate (G6P) levels in liver extracts were reduced 1.9-fold, consistent with a ~30% decrease at 168 hrs after a single bolus TCDD dose [12]. There was a negligible decrease in glucose-6-phosphate isomerase (*Gpi*) mRNA with a 1.9-fold decrease in fructose-6-phosphate levels (F6P). Liver phosphofructokinase (*Pfkl*), which catalyzes the production of fructose 1,6-bisphophate (F1,6BP) was also repressed 1.5-fold while fructose 1,6 bisphosphatase (*Fbp1*) catalyzing the reverse reaction was induced 1.7-fold. Phosphofructokinase-2/fructose-2,6-bisphosphatase (*Pfkfb3*) was also induced 1.8 fold, which could decrease fructose-2,6-bisphosphate (F2,6BP) levels, a potent phosphofructokinase allosteric activator [34]. Fructose bisphosphate aldolase B (*Aldob*) expression was also repressed 2.1-fold. Although cytosolic glyceraldehyde-3-phosphate dehydrogenase (*Gpd1*) which converts DHAP to glycerol-3-phosphate to support triglyceride synthesis was unaffected, mitochondrial *Gpd2* was repressed 2.8-fold which may compromise glycerol-3-phosphate re-oxidation to DHAP and $FADH_2$ production, limiting cytosolic NADH while modestly inducing phosphoglycerate kinase (*Pgk1*, 1.3-fold), and repressing enolase

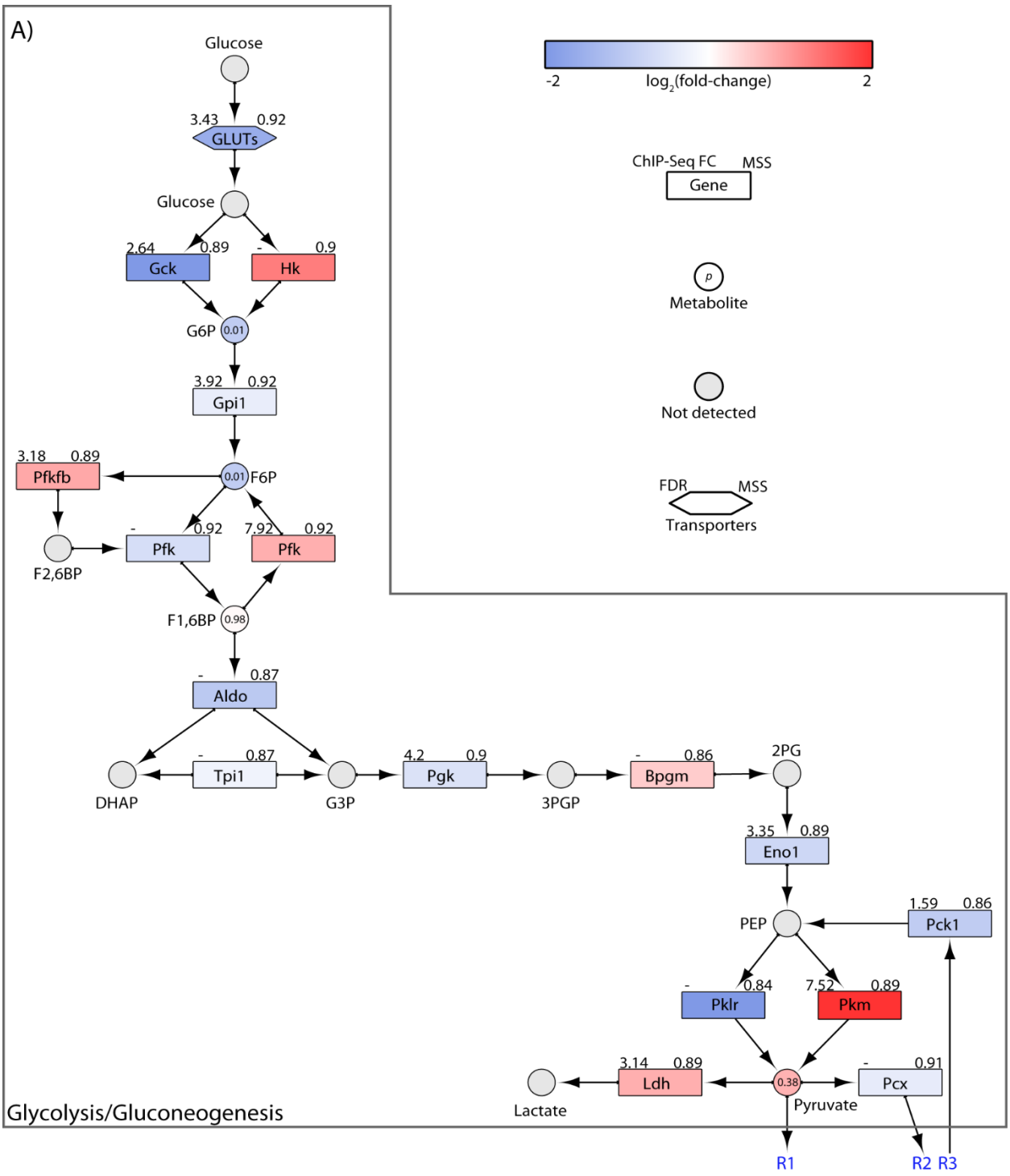


**FIGURE 16. INTEGRATION OF OMICS DATA FOR CARBOHYDRATE METABOLISM**

**FIGURE 16 (cont'd)**

Reprogramming of central carbon and amino acid metabolism. Integration of transcriptomic, metabolomic, and KEGG pathway data for (A) glycolysis/gluconeogenesis, (B) the TCA cycle, (C) glutaminolysis, and (D) malate-aspartate shuttle. QRTPCR confirmation of hepatic *Gls1* (E) GAC and (F) KGA isoforms, as well as (G) the GAC:KGA protein ratio are shown as barplots. In integrative pathways the color scale represents the $\log_2$(fold-change) for genes and metabolites. Gray indicates metabolites not measured or detected. Genes are identified as rectangles, metabolites as circles, and transporters as hexagons. The upper left corner provides the maximum AhR enrichment fold-change and upper right corner indicates the highest pDRE MSS. Circles contain the *p*-value for detected metabolites. Text in blue indicates a reaction extending into a separate panel. An expandable and interactive version of this figure which provides additional information can be viewed at http://dbzach.fst.msu.edu/index.php/supplementarydata.html. Bars in barplots represent mean + SEM. Asterisks (*) indicate $P \leq 0.05$ compared to vehicle determined by one-way ANOVA followed by Dunnett's *post-hoc* test.

**FIGURE 16 (cont'd)**

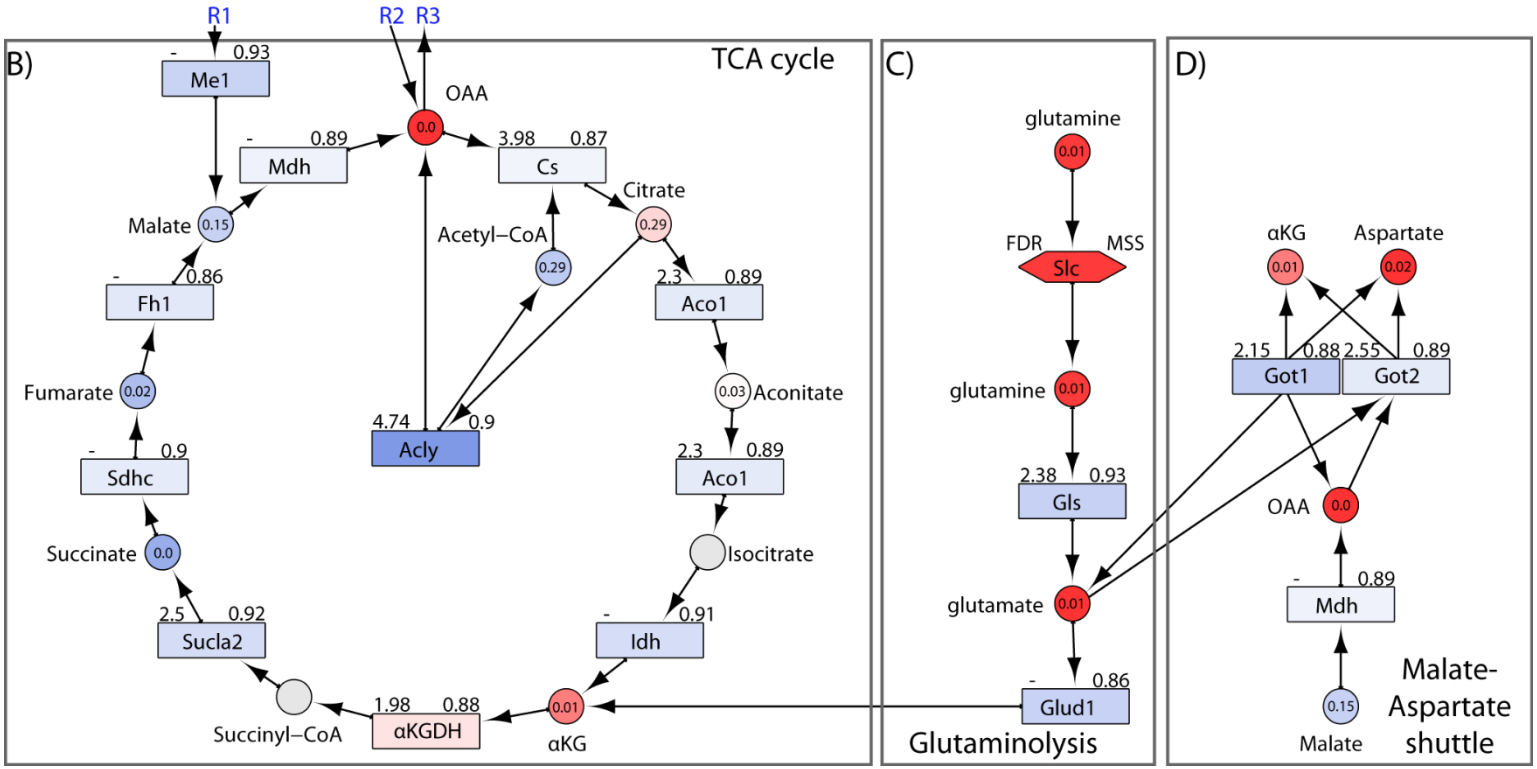

**FIGURE 16 (cont'd)**

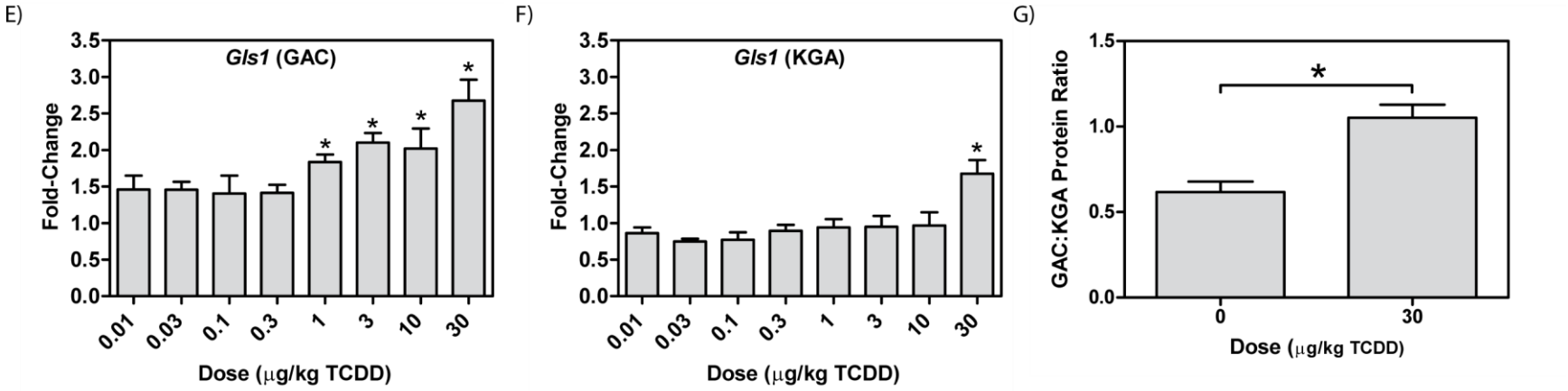

(*Eno1*, 1.6-fold) which catalyzes the transformation of 2-phosphoglycerate (2PG) to phosphoenolpyruvate (PEP). Both *Pgam1* and *Eno1* showed AhR enrichment.

Phosphoenolpyruvate (PEP) conversion to pyruvate by pyruvate kinase is a rate limiting step in glycolysis. Liver/red blood cell pyruvate kinase (*Pklr*) was repressed 6.7-fold, consistent with reported 3.2-fold fold decrease [12] while muscle pyruvate kinase (*Pkm*) was induced 4.6-fold with AhR enrichment, as previously reported [12]. Further analysis of *Pkm* mapped RNA-Seq reads to exon 10 as opposed to exon 9 indicating isoform switching from *Pkm1* to *Pkm2* (Figure 17A). *Pkm2* is typically expressed in cancer cells and is associated with the Warburg effect, with a lower catalytic rate in the dimeric or monomeric form, leading to upstream accumulation of glycolytic intermediates. QRTPCR confirmed a 9.0-fold induction of *Pkm1* compared to 40.0-fold for *Pkm2* (Figure 17B-C). Protein measurements confirmed a 13.4-fold increase in total PKM, with a 1.6-fold increase in PKM1, and a 3.0-fold increase in PKM2 (Figure 17D-F). While *Pkm2* was only induced 2.4-fold compared to 1.7-fold for *Pkm1* at 72 hrs, *Pkm2* was induced 13.8-fold with 1.6-fold induction of *Pkm1* after treatment every 4d for 92d (Figure 18A-B). Other AhR agonists, including 3,3',4,4',5-pentachlorobiphenyl (PCB126), 2,3,7,8-tetrachlorodibenzofuran (TCDF), and β-naphthoflavone (βNF) also induced *Pkm2*, while 2,2',4,4',5,5'-Hexachlorobiphenyl (PCB153), which does not bind to the AhR, had no effect (Figure 18C-D). ChIP-Seq analysis completed after 2 h TCDD treatment identified a 7.5-fold increase in AhR enrichment within the coding region of *Pkm* that contained a pDRE suggesting DRE-dependent AhR-mediated regulation (Figure 17A). This same peak was previously identified by ChIP-chip and confirmed by ChIP-PCR [3].

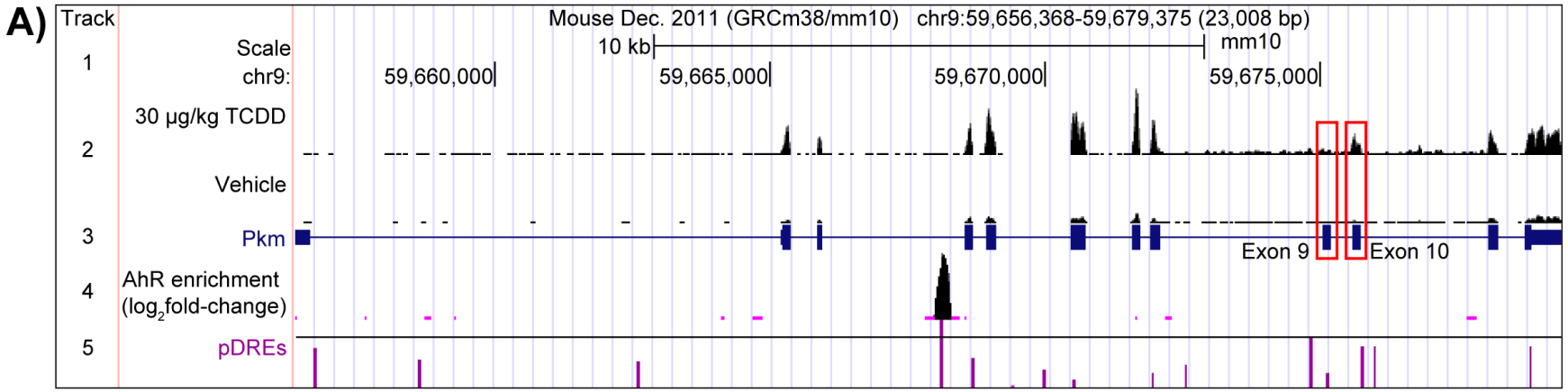


**FIGURE 17. TCDD-ELICITED PKM ISOFORM SWITCHING**

(A) *Pkm* UCSC genome tracks representing (1) the scale, (2) raw number of aligned RNA-Seq reads (scaled to a maximum of 403 for both treatments - red boxes highlight location of exon 9 (*Pkm1*) and exon 10 (*Pkm2*)), (3) *Pkm* exons and introns, (4) AhR enrichment sites, and (5) pDREs with horizontal line indicating matrix similarity score of 0.874. QRTPCR verification of hepatic (B) *Pkm1* and (C) *Pkm2* mRNA expression, and confirmation of changes in hepatic protein levels of (D) PKM1/2, (E) PKM1, and (F) PKM2. Bars represent mean + SEM (N=4-5). Asterisks (*) indicate $P \leq 0.05$ compared to vehicle determined by one-way ANOVA followed by Dunnett's *post-hoc* test or Student's t-test.

**FIGURE 17 (cont'd)**

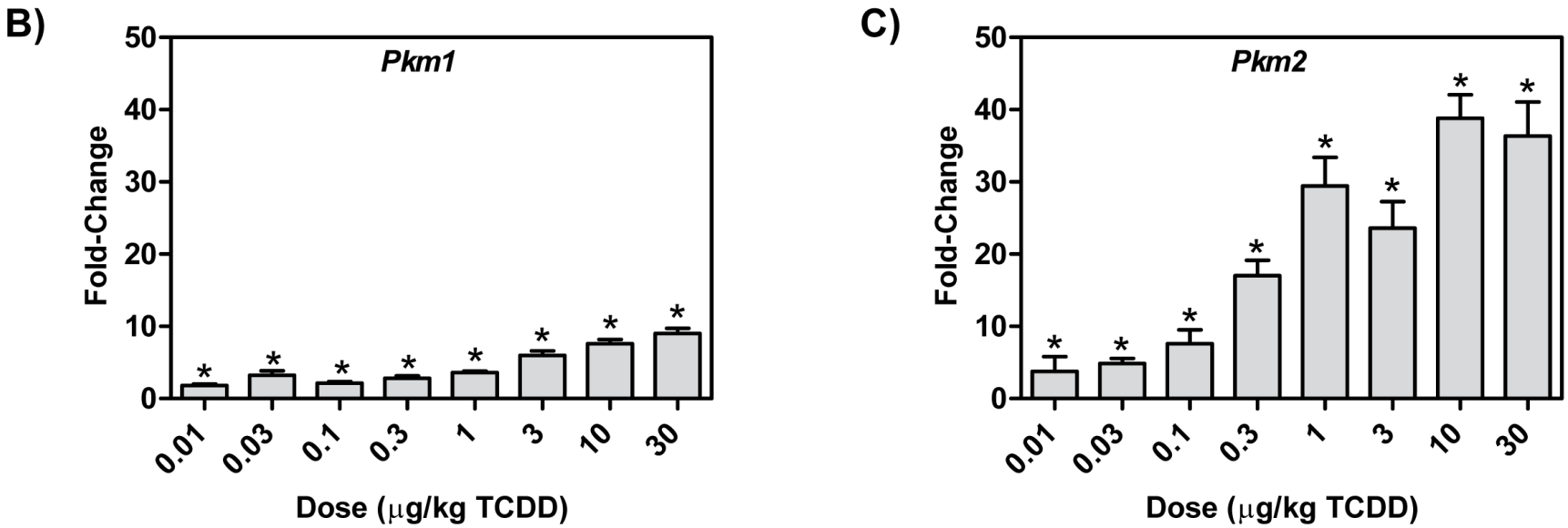

**FIGURE 17 (cont'd)**

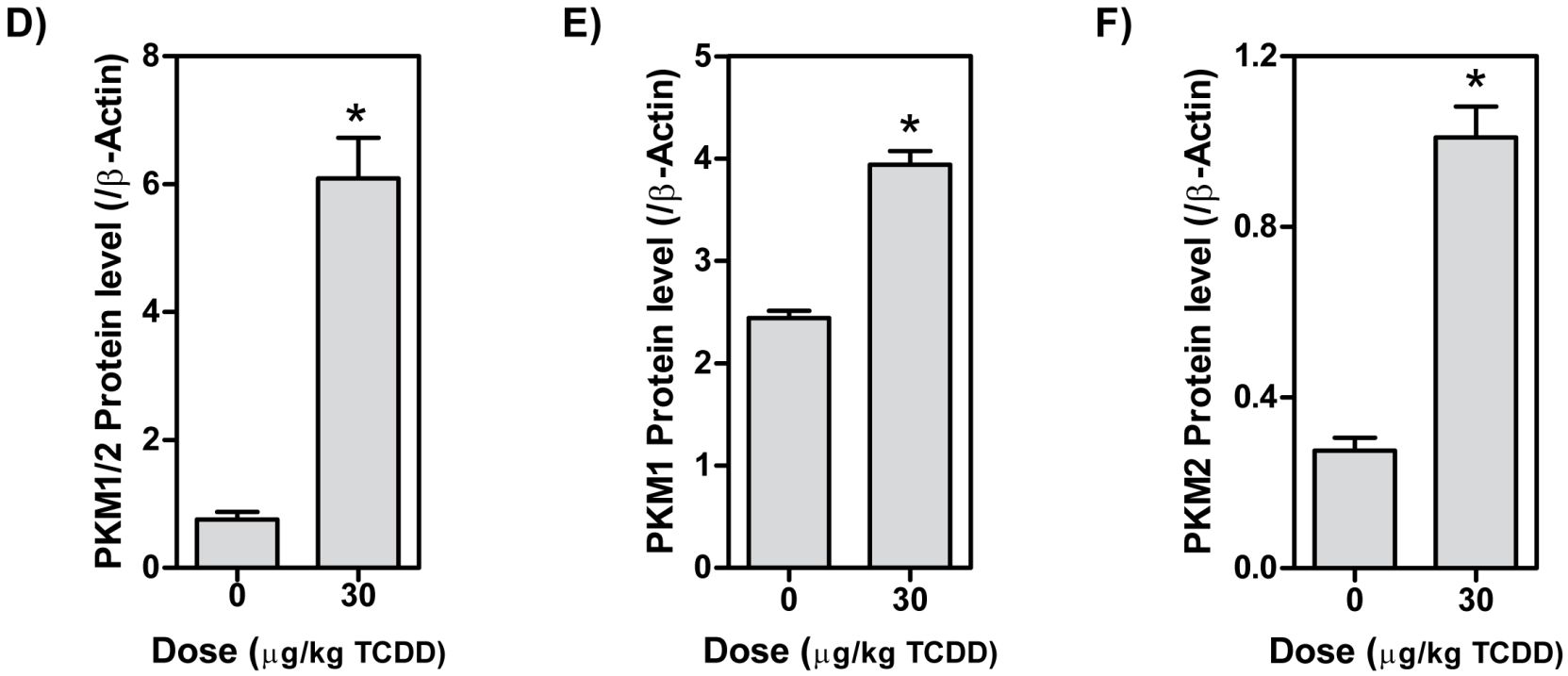

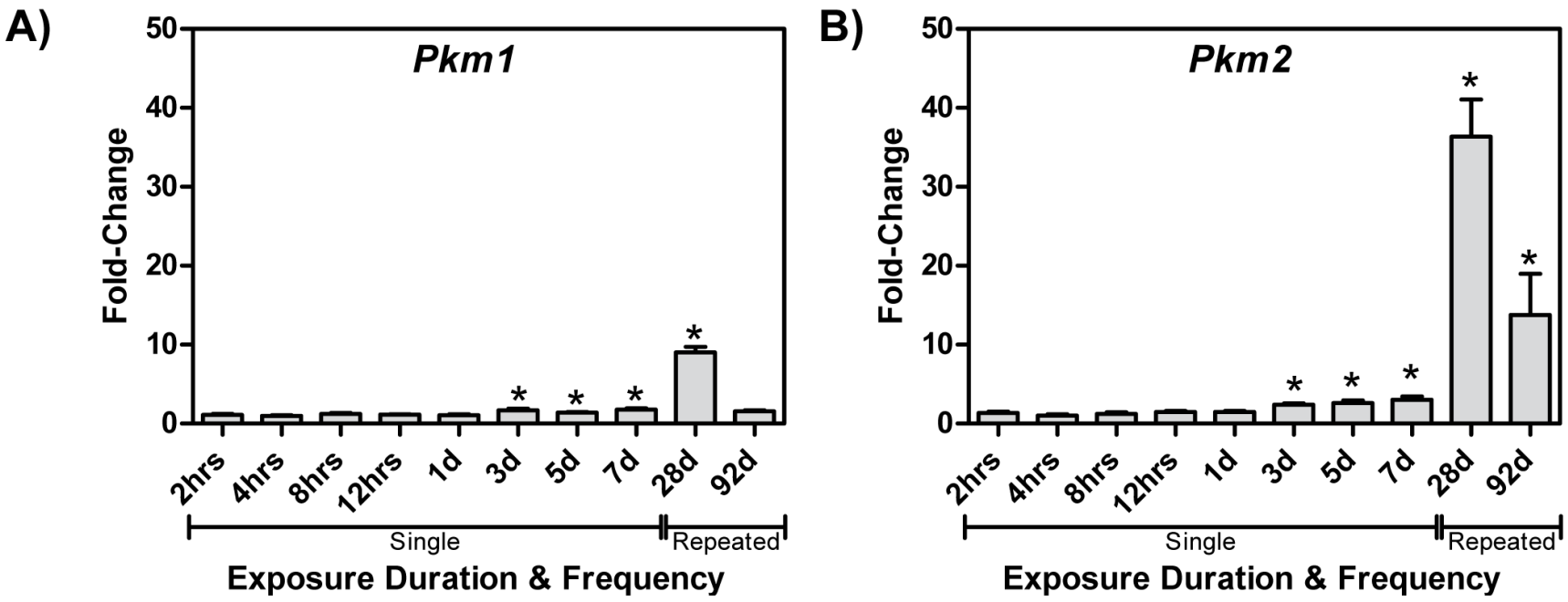


**FIGURE 18. TEMPORAL AND LIGAND DEPENDENT INDUCTION OF PKM ISOFORMS**

Time-dependent expression of (A) *Pkm1* and (B) *Pkm2* mRNA induced by 30 µg/kg TCDD at 2 hrs to 7 d following a single bolus dose, or dosing every 4d for 28d or 92d and ligand dependent expression of (C) *Pkm1* and (D) *Pkm2* following treatment with either AhR ligands PCB126, TCDF, or βNF, or the non-dioxin like PCB153. Bars represent mean + SEM (n=4-5). Asterisks (*) indicate $P \leq 0.05$ compared to vehicle determined by two-way ANOVA followed by Tukey's *post-hoc* test or Student's t-test.

**FIGURE 18 (cont'd)**

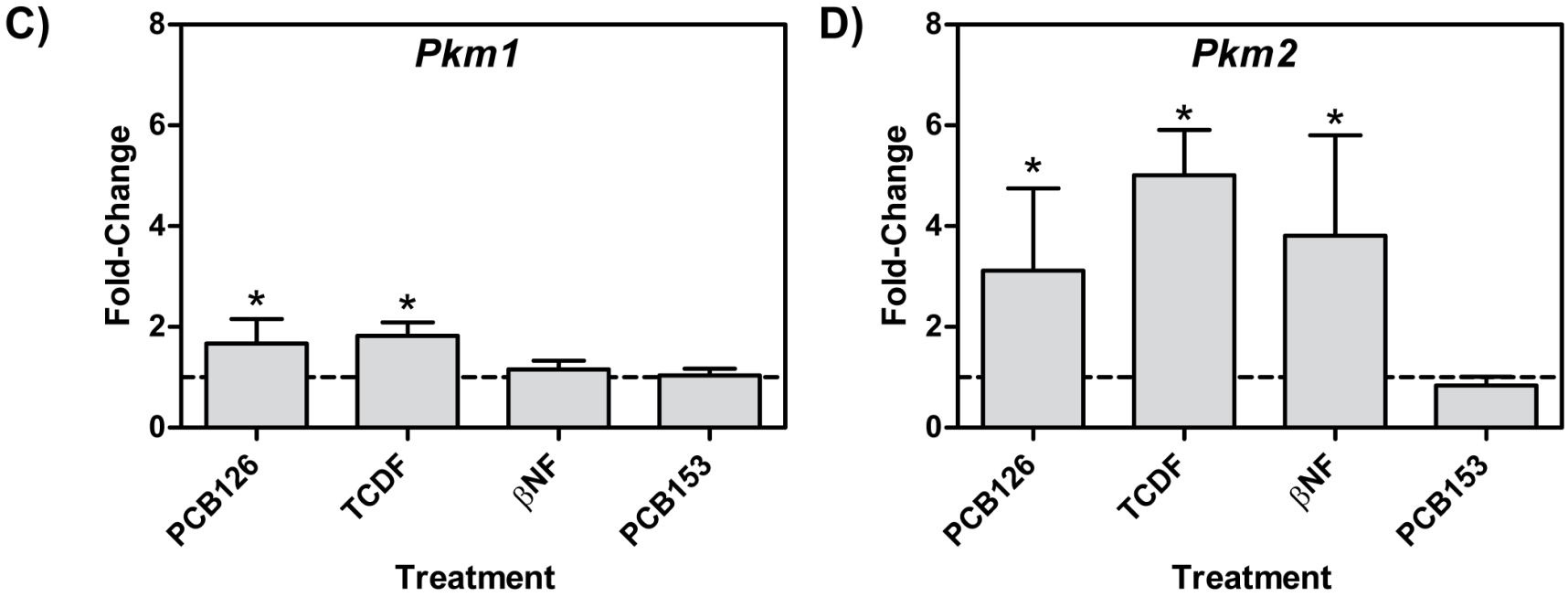

Reduction of glycolytic flux and the inhibition of β-oxidation not only reduce hepatic acetyl-CoA levels, but also impact the TCA cycle and reducing equivalent production. Less pyruvate from glycolysis, inhibition of pyruvate dehydrogenase by pyruvate dehydrogenase kinase (*Pdk3* and *4* induced 1.9 and 1.7-fold, respectively), and β-oxidation inhibition reduces acetyl-CoA availability for condensation with OAA. In cancer cells, central carbon metabolism reprogramming also involves changes in glutamine metabolism (Gln) [35]. TCDD increased Glu levels, altered its metabolism (Figure 10) and induced *Slc1a5* (5.1-fold), *Slc6a19* (3.6-fold), and *Slc38a1* (1.5-fold) transporters while repressing the expression of antiporters *Slc38a3*, *4* and *7* (repressed 1.8-, 1.7- and 1.3-fold respectively; Figure 16). A concomitant 1.4-fold increase in glutaminase (*Gls1*), which catalyzes the transformation of Gln to glutamate (Glu) and ammonia, and a 1.9-fold decrease in glutaminase 2 (*Gls2*) are consistent with increased glutaminolysis, as found in some cancer cell lines [36]. Glutaminolysis may also provide Glu to support GSH biosynthesis.

Coincidentally, mRNA for the cystine (Cyss) transporters, xCT (Slc7a11 induced 1.8-fold), *Slc3a2* (induced 1.9-fold), and *Slc7a6* (induced 1.8-fold) are increased. *Slc7a11* is regulated by *Hfe2l2* (aka *Nrf2*) [37] which was also induced 2.4-fold by TCDD. Once inside the cell, Cyss is reduced to Cys, the rate limiting precursor for *de novo* GSH biosynthesis [38]. Although Cys may be synthesized from Met by the transsulfuration pathway, the primary source of intracellular Cys is likely transport as hepatic Met levels were decreased 5.9-fold in the liver.

Two splice variants associated with tumor environments exist for *Gls1*; kidney-type glutaminase (KGA) consisting of exons 1-14 and 16-19, and the GAC isoform with an alternate carboxy-terminus consisting of exon 15. The GAC:KGA mRNA and protein ratio increases in tumors [35], and was changed by TCDD, with GAC and KGA mRNA induced 2.3- and 1.6-fold, respectively. (Figure 16F-G). Accordingly, the GAC:KGA protein ratio was increased 1.7-fold (Figure 16H).

Higher hepatic Glu levels (2.5-fold) would be expected to be converted to α-ketoglutarate (αKG) by glutamate dehydrogenase (*Glud1*) to replenish the TCA cycle (Figure 16C), and may

explain the 11.0-fold increase in OAA in TCDD treated liver (Figure 16C). The 2.0-fold repression of phosphoenolpyruvate carboxykinase (*Pck1*), the rate-limiting step of gluconeogenesis, is also consistent with gluconeogenesis inhibition [39-41], further contributing to OAA accumulation. However, *Glud1* is repressed 1.8-fold as are succinyl-CoA synthetase (1.6- and 1.5-fold repression of *Sucla2* and *Suclg2* 1.5-fold), succinate dehydrogenase (1.3-fold repression of *Sdhd*), and fumarase (1.4-fold repression of *Fh1*) which may reduce glutaminolysis flux towards OAA.

Alternatively, Glu could be used in the malate-aspartate shuttle to produce pyruvate, which is reported not to contribute to lactate production [42]. In this scenario, mitochondrial OAA and Glu are converted to αKG and aspartate (Asp) by glutamate oxaloacetate transaminase (*Got2*) which is modestly repressed 1.3-fold (Figure 16D). The 1.9-fold repression of cytosolic *Got1* would limit the reconversion of cytosolic Asp, and is consistent with the 4.1-fold increase in hepatic Asp levels.

**REDIRECTING CENTRAL CARBON AND AMINO ACID METABOLISM TO NADPH PRODUCTION**

Increased ROS production and lipid peroxidation create an oxidative environment requiring NADPH-dependent counter-measures for cell survival. In cancer cells, NADPH demands are satisfied by the pentose phosphate pathway (PPP) with smaller contributions from $NADP^+$-dependent malic enzyme (*Me1*) and $NADP^+$-dependent isocitrate dehydrogenase (*Idh*) [43]. With the increase in PKM2 expression, G6P is redirected to the PPP (Figure 19A) consistent with decreases in G6P (1.9-fold), F6P (1.9-fold), 6-phospho-D-gluconate (6PG; 4.5-fold), erythrose-4-phosphate (E4P; 2.1-fold), and 5-phosphoribose 1-diphosphate (PRPP, 1.6-fold). There are also increases in ribulose 5-phosphate (Ru5P; 1.5-fold), and ribose 5-phosphate (R5P; 2.0-fold). In mammalian cells, oxidative stress induces glucose-6-phosphate dehydrogenase

(*G6pdh*) activity so that this enzyme is not rate limiting [44, 45]. Phosphoglucomutase (*Pgm1*), involved in the catalysis of R5P to ribose 1-phosphate (R1P) was also induced 1.6-fold.

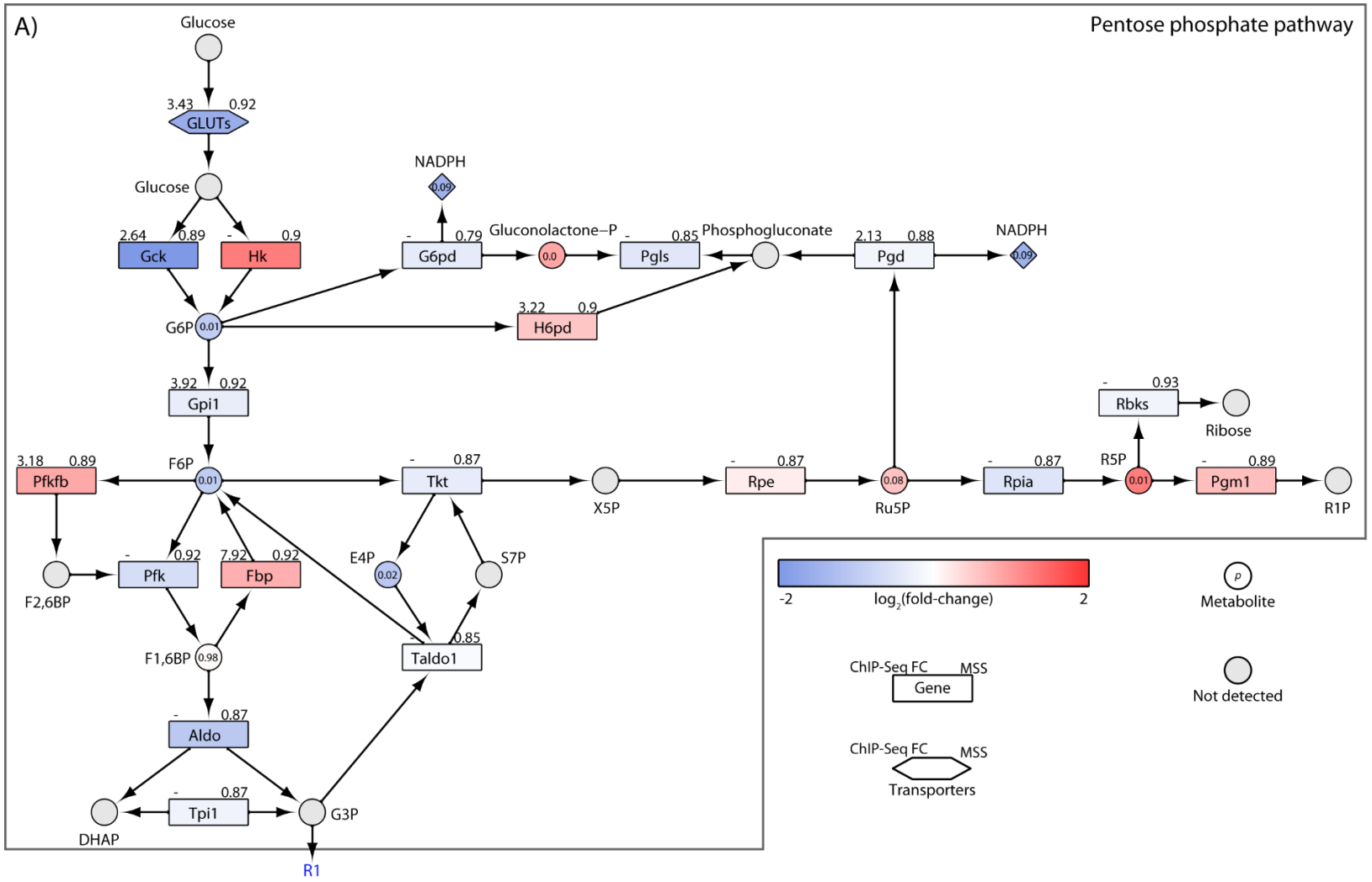


**FIGURE 19. INTEGRATION OF OMICS DATA FOR THE PENTOSE PHOSPHATE PATHWAY AND SERINE METABOLISM**

**FIGURE 19 (cont'd)**

Metabolic reprogramming for NADPH production. Integration of transcriptomic, metabolomic, and KEGG pathway data for (A) the pentose phosphate pathway, and (B) serine and folate metabolism. The color scale represents the $\log_2$(fold-change) for genes and metabolites. Yellow identifies converging metabolites and gray indicates metabolites not measured or detected. Genes are identified as rectangles and metabolites as circles. The upper left corner provides the maximum AhR enrichment fold-change and upper right corner indicates the highest pDRE MSS. Circles contain the *p*-value for detected metabolites. Text in blue indicates a reaction extending into a separate panel. An expandable and interactive version that provides additional complementary information can be viewed at http://dbzach.fst.msu.edu/index.php/supplementarydata.html. (C) Expression of hepatic *Phgdh* was confirmed by QRTPCR. Bars represent mean + SEM (n=5). Asterisks (*) indicates $P \leq 0.05$ compared to vehicle determined by one-way ANOVA followed by Dunnett's *post-hoc* test.

**FIGURE 19 (cont'd)**

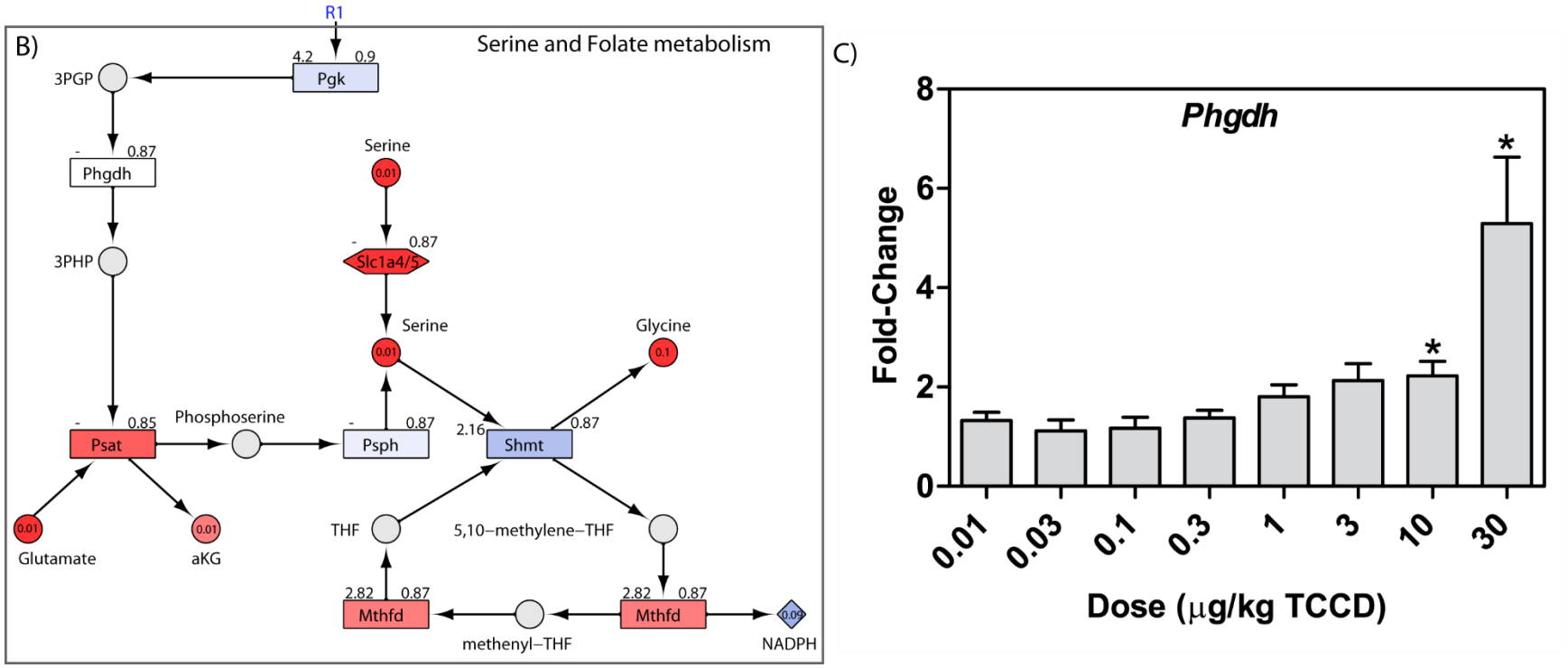

Folate-dependent reactions have been estimated to account for 10-40% of NADPH production, compared to ~30% from the PPP [46]. PKM2 reduced glycolytic flux is consistent with the shunting of 3-phosphoglycerate (3PG) towards Ser biosynthesis and folate-dependent NADPH production (Figure 19B). 3PG is transformed to 3-phosphohydroxypyruvate by phosphoglycerate dehydrogenase (*Phgdh*, 5.8-fold) and subsequently to Ser by phosphoserine aminotransferase (*Psat1*, 3.0-fold), which simultaneously converts Glu to αKG, another potential source of OAA (Figure 16C). Ser and tetrahydrofolate (THF) can then be converted to Gly and 5,10-methylene-tetrahydrofolate (5,10-$CH_2$-THF) by cytosolic and mitochondrial serine hydroxymethyl transferase 1 and 2 (*Shmt1*/*2*). TCDD did not affect *Shmt2* expression but repressed *Shmt1* 2.3-fold. 5,10-$CH_2$-THF is then used by methylenetetrahydrofolate dehydrogenase (*Mthfd1/2*) to produce NADPH. Mitochondrial *Mthfd2* was induced 2.4-fold while cytosolic *Mthfd1* was modestly repressed suggesting greater NADPH production to support mitochondrial oxidative defenses. Besides *de novo* synthesis, Ser is available from protein and Ser-containing phospholipid catabolism, as well as transporter-mediated uptake. The 4.2-fold increase in serum Ser may be made available via the 3.4- and 5.1-fold induction of *Slc1a4* and *1a5*, respectively, two high affinity transporters. In addition to producing NADPH, this pathway also provides Gly to support GSH biosynthesis, thus serving dual anti-oxidant roles.

**CELL CYCLE ARREST BY TCDD**

PKM2 lies at the intersection of cell proliferation and cell survival [47-49]. The AhR has also been linked to anti-oxidant defenses and cell cycle regulation [50, 51]. Jackson *et al.* [51] report that p21 (*Cdkn1a*) is critical to TCDD-induced $G_1$ cell cycle arrest. Similarly, we confirm *Cdkn1a* was induced 7.6-fold with three AhR enriched regions at 28d, but was repressed 1.2-fold following treatment with TCDD every 4d for 92d (Figure 20), while *Pkm2* was induced 13.8-fold.

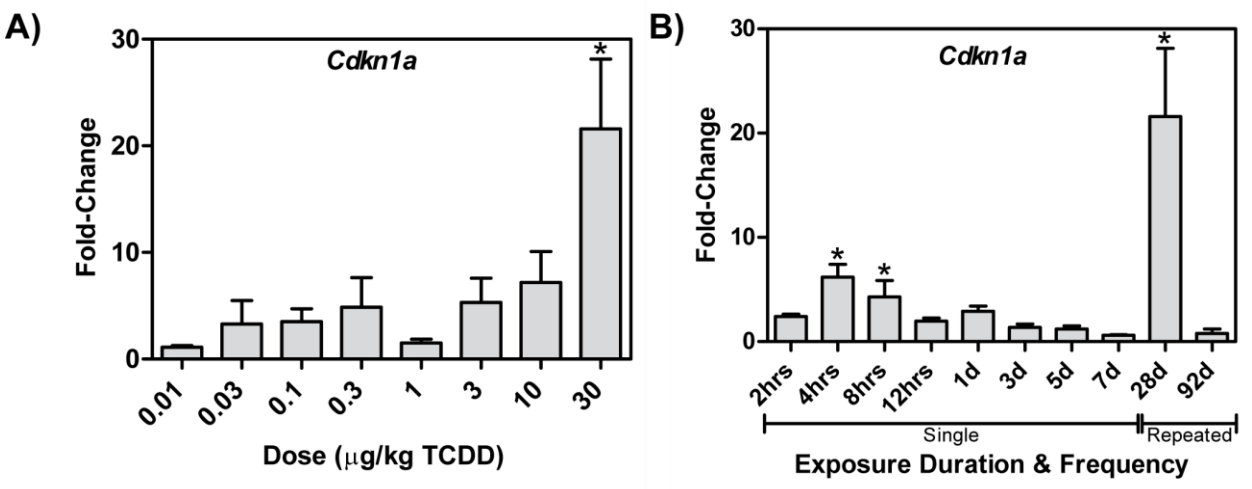


**FIGURE 20. DOSE AND TIME-DEPENDENT CDKN1A EXPRESSION CHANGES**

(A) Dose-dependent hepatic *Cdkn1a* mRNA expression following gavage every 4d for 28d, and (B) time-dependent expression following a single bolus dose of 30 µg/kg TCDD. Bars represent mean + SEM (n=4-5). Asterisks (*) indicate $P \leq 0.05$ compared to vehicle determined by one-way ANOVA followed by Dunnett's *post-hoc* test or two-way ANOVA following by Tukey's *post-hoc* test.

## DISCUSSION

Previous studies have examined TCDD-elicited 'omic' responses in various *in vivo* and *in vitro* models using different designs, doses, treatment protocols, and models, limiting extrapolations between species, and confounding integration and interpretation. Consequently, we examined the metabolomic and transcriptomic effects of TCDD in the same animals, and used KEGG pathways to integrate and manually curate the data while incorporating complementary pDRE and AhR binding (ChIP-Seq) data to further investigate metabolic reprogramming in the mouse liver. Gavaging every 4d for 28d simulated continuous exposure that increased the severity of the hepatic effects but was well tolerated [9]. Our results demonstrate that TCDD elicits a dose-dependent reorganization of hepatic metabolism characterized by the reprogramming of central carbon and amino acid metabolism, reminiscent of the Warburg effect, which supports NADPH production required for antioxidant defenses.

TCDD induced hepatic lipid accumulation by altering gene expression consistent with lipid accumulation, including the inhibition of *de novo* fatty acid synthesis and β-oxidation [7, 8, 33, 52, 53]. The induction of xenobiotic (e.g., cytochrome P450 activity) and purine metabolism (i.e., *Xdh*/XO) would not only increase ROS levels but also lipid peroxidation [54, 55], creating a sustained oxidative burden requiring counter-measures. Redirection of glycolytic flux and the inhibition of β-oxidation would also compromise NADH and ATP production further compounding cell damage [56].

Notably, TCDD repressed *Pklr* expression while inducing *Pkm2,* the isoform typically associated with the Warburg effect and cell proliferation [26]. This is the first report of PKM isoform switching elicited by an exogenous chemical in normal tissue, although switching has been shown in fatty liver of *PTEN*-null mice [57]. PKM2 sits at the intersection of cell growth and cell survival [47-49], and its induction with subsequent metabolic changes illustrates PKM2's putative role in TCDD toxicity. Moreover, under oxidative stress conditions, Cys358 of PKM2 is oxidized further reducing its activity and supporting diversion of upstream intermediates [58]. Interestingly, AhR enrichment has been repeatedly demonstrated within the *Pkm* loci indicating direct regulation. Furthermore, PCB126, TCDF, and βNF also induced *Pkm2* while PCB153, which does not bind to the AhR, had no effect on its expression. Collectively, these results indicate AhR-mediated regulation of PKM2 expression.

In cancer cells, PKM2 redirects accumulating upstream intermediates to other pathways in support of cell growth or survival, and is tightly regulated, both transcriptionally and post-translationally [47-49]. In response to TCDD, our data is consistent with the shunting of accumulated intermediates towards antioxidant pathways as opposed to cell proliferation, especially given the induction of the cell cycle inhibitor p21 [51]. More specifically, G6P and 3PG are redirected to the PPP and Ser biosynthesis, respectively, to satisfy NADPH demand and maintain redox balance in support of antioxidant responses that include GSH biosynthesis and

GSSG reduction, similar to reprogramming reported in cancer cells [36, 47, 48, 59], lipopolysaccharide-activated macrophages [60], and normal cells under oxidative stress [61].

Metabolic reprogramming, including increased intermediate transport, also explains increased hepatic Gly, Cys, OAA and Asp levels. 3PG accumulation due to PKM2 expression is shunted to Ser biosynthesis indicated by *Phgdh* and *Psat1* induction. Ser is then converted to Gly to produce 5,10-$CH_2$-THF and oxidized, producing NADPH. Ser metabolism is estimated to account for 10-40% of NADPH production, compared to ~30% from the PPP [46]. Moreover, Ser biosynthesis involves the conversion of Glu to αKG, another source of OAA, in addition to glutaminolysis and the malate-aspartate shuttle. Decreases in acetyl-CoA, and the inhibition of β-oxidation and gluconeogenesis further contribute to OAA accumulation. *Pck1* repression also inhibits OAA utilization in gluconeogenesis and its metabolism to lactate. Increased OAA levels likely drive Asp biosynthesis despite *Got* repression. Despite our complementary gene expression, protein and targeted metabolomic analyses, more precise tracer studies are required to further characterize TCDD elicited metabolic reprogramming since the regulation of metabolism is mostly regulated by post-translational mechanisms.

In summary, compromised energy production, lipid peroxidation and the resulting oxidative environment cause cell damage that triggers not only immune cell infiltration but also the reprogramming of central carbon and amino acid metabolism towards defensive responses (Figure 21). Induction of p21 further supports cell survival by ensuring accumulating intermediates are shunted towards oxidative stress counter-measures and cell survival, as opposed to biomass production and cell proliferation. Resistance to cell death, energy metabolism reprogramming, and the initiation of inflammation are important cancer hallmarks [62]. TCDD is a known carcinogen in rodents, but its human carcinogenicity is debated [63]. The continued induction of PKM2, and later return to basal expression of *Cdkn1a* at 92d may support proliferation of surviving cells with DNA damage leading to tumor development. This balance between survival and proliferation regulated by metabolic reprogramming could be implicated in AhR-mediated species-

and sex-specific sensitivity and ligand toxicity differences. Moreover, regulating metabolic reprogramming in normal tissue, reminiscent of the Warburg effect, may be a defensive strategy used by normal cells to promote survival in response to other toxicities.

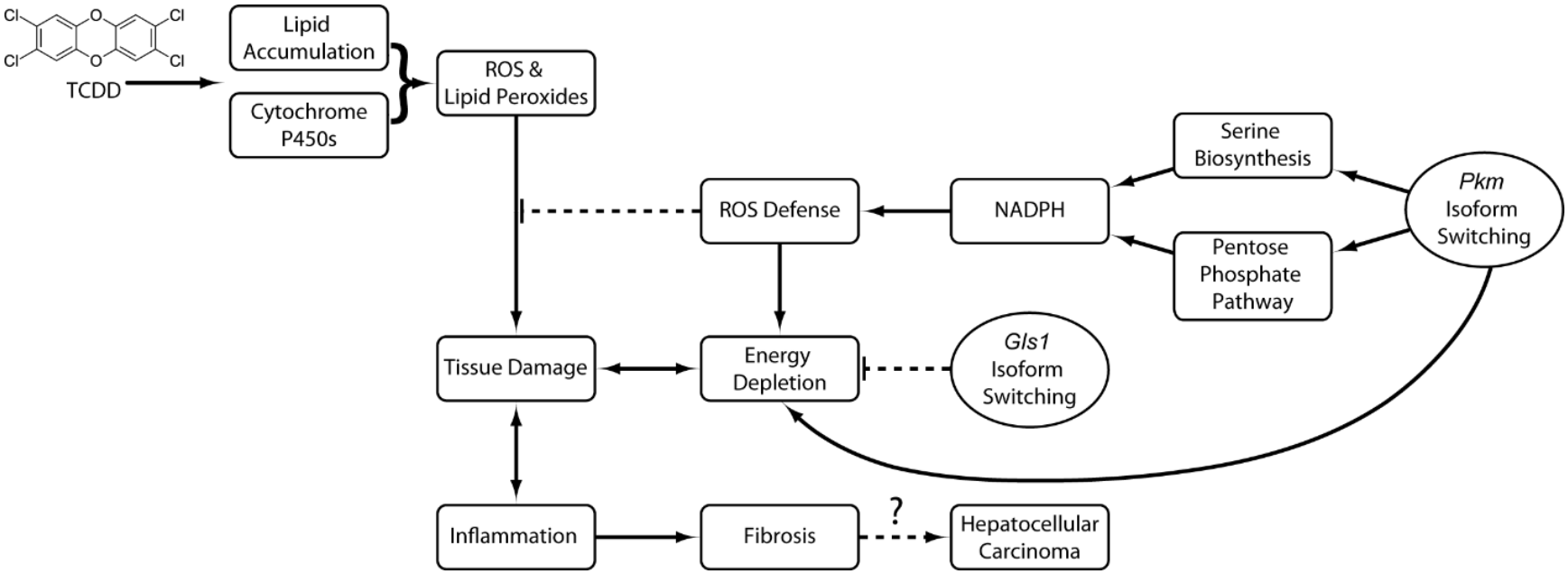


**FIGURE 21. SUMMARY OF HEPATIC METABOLISM REPROGRAMMING IN SUPPORT OF NADPH DEPENDEND PROCESSES**

# APPENDIX

**TABLE 6. MULTIPLE REACTION MONITORING PARENT-DAUGHTER MASS PAIRS**

| Metabolite | Parent Mass | Daughter Mass |
|---|---|---|
| Glycolate | 75 | 45 |
| Pyruvic acid | 87 | 43 |
| Lactate | 89 | 43 |
| Acetoacetate | 101 | 57 |
| Glycerate | 105 | 75 |
| Uracil | 111 | 42 |
| Fumarate | 115 | 71 |
| Fumarate \| ketoisovalerate \| maleic acid | 115 | 71 |
| Ketovaline (3-methyl-2-oxobutyrate) | 115 | 71 |
| Succinate | 117 | 73 |
| Betaine | 118 | 59 |
| Taurine | 124 | 80 |
| Thymine | 125 | 42 |
| Pyroglutamic acid | 128 | 82 |
| Citraconic acid | 129 | 85 |
| Itaconic acid | 129 | 85 |
| N-Acetyl-L-alanine | 130 | 88 |
| Hydroxyisocaproic acid | 131 | 85 |
| Glutaric Acid | 131 | 87 |
| Oxaloacetate | 131 | 87 |
| Glutaric acid | 131 | 113 |
| Aspartate | 132 | 88 |
| Malate | 133 | 71 |
| Malate | 133 | 115 |
| Adenine | 134 | 107 |
| Hypoxanthine | 135 | 92 |
| p-Aminobenzoate \| anthranilate | 136 | 92 |
| p-Hydroxybenzoate | 137 | 93 |
| Acetylphosphate | 139 | 79 |
| N-acetyl-glucosamine-1-phosphate | 139 | 79 |
| Trehalose-6-Phosphate | 139 | 79 |
| Oxoglutaric acid | 145 | 101 |
| Phenylpropiolic acid | 145 | 101 |
| Glutamine | 145 | 109 |
| Glutamine | 145 | 127 |
| Oxoglutaric acid | 146 | 102 |
| Glutamate | 146 | 128 |
| Mevalonic acid | 147 | 59 |
| 2-Hydroxy-2-methylbutanedioic acid | 147 | 85 |
| 2-oxo-4-methylthiobutanoate | 147 | 99 |
| 3-phenylpropionic acid \| 3-methylphenylacetic acid | 149 | 105 |
| Guanine | 150 | 133 |

**TABLE 6 (cont'd)**

| | | |
|---|---|---|
| 3-hydroxyphenylacetic acid | 151 | 107 |
| Xanthine | 151 | 108 |
| 2,3-dihydroxybenzoic acid | 153 | 109 |
| Orotate | 155 | 111 |
| Dihydroorotate | 157 | 113 |
| Allantoin | 157 | 114 |
| Aminoadipic acid | 160 | 116 |
| Indole-3-carboxylic acid | 160 | 116 |
| Phenylpyruvate | 163 | 91 |
| p-Coumaric acid | 163 | 119 |
| Phenylalanine | 164 | 147 |
| Phenyllactic acid | 165 | 103 |
| Tropic acid \| phenyllactic acid | 165 | 103 |
| Atrolactic acid | 165 | 119 |
| 3-methylxanthine | 165 | 122 |
| Quinolinate | 166 | 122 |
| Uric acid | 167 | 124 |
| Dihydroxy-acetone-phosphate | 169 | 79 |
| Glyceraldehyde 3-phosphate | 171 | 79 |
| Aconitate | 173 | 85 |
| Shikimate | 173 | 111 |
| Citrulline | 174 | 131 |
| Ascorbic acid | 175 | 87 |
| Isopropyl malic acid | 175 | 113 |
| Allantoate \| carbamoyl aspartate | 175 | 132 |
| Glucono-lactone | 177 | 129 |
| Pyrophosphate | 177 | 159 |
| Hydroxyphenylpyruvate | 179 | 107 |
| Myo-inositol | 179 | 161 |
| Tyrosine | 180 | 163 |
| Homocysteic acid | 182 | 80 |
| 4-Pyridoxic acid | 182 | 138 |
| phosphoserine | 184 | 97 |
| 2-phosphoglycerate \| 3-phoshoglycerate | 185 | 97 |
| Indoleacrylic acid | 186 | 142 |
| Kynurenic acid | 188 | 144 |
| Diaminopimelic acid | 189 | 128 |
| Citric acid \| isocitric acid | 191 | 111 |
| 2-dehydro-D-gluconate | 193 | 103 |
| Glucuronic acid | 193 | 113 |
| D-gluconate | 195 | 129 |
| Erythrose-4-phosphate | 199 | 97 |
| Tryptophan | 203 | 116 |

**TABLE 6 (cont'd)**

| | | |
|---|---|---|
| Xanthurenic acid | 204 | 160 |
| Methylcitrate | 205 | 125 |
| Glycine-CBZ | 208 | 100 |
| D-glucarate | 209 | 85 |
| Deoxyribose-phosphate | 213 | 79 |
| Pantothenate | 218 | 146 |
| Alanine-CBZ | 222 | 114 |
| Deoxyuridine | 227 | 184 |
| Ribose 5-phosphate | 229 | 79 |
| Ribulose-5-phosphate | 229 | 79 |
| Serine-CBZ | 238 | 130 |
| Uridine | 243 | 200 |
| Proline-CBZ | 248 | 140 |
| Valine-CBZ | 250 | 142 |
| Deoxyinosine | 251 | 135 |
| Threonine-CBZ | 252 | 144 |
| Cysteine-CBZ | 254 | 146 |
| Hexose-phosphate | 259 | 79 |
| Mannose 6-phosphate \| mannose-1-phosphate | 259 | 79 |
| Hexose-phosphate | 259 | 97 |
| Fructose-6-phosphate | 259 | 169 |
| Glucose-6-phosphate | 259 | 199 |
| Galactose-1-phosphate | 259 | 241 |
| Isoleucine \| Leucine-CBZ | 264 | 156 |
| Asparagine-CBZ | 265 | 113 |
| S-Adenosyl-L-homocysteine | 266 | 134 |
| Aspartate-CBZ | 266 | 158 |
| Inosine | 267 | 135 |
| 6-Phosphogluconic acid | 275 | 97 |
| Glutamine-CBZ | 279 | 127 |
| Glutamate-CBZ | 280 | 128 |
| Methionine-CBZ | 282 | 174 |
| Xanthosine | 283 | 151 |
| Histidine-CBZ | 288 | 180 |
| D-Seduheptulose-1/7-phosphate | 289 | 97 |
| Phenylalanine-CBZ | 298 | 147 |
| N-Acetyl-glucosamine-1-phosphate | 300 | 79 |
| dCMP | 306 | 79 |
| Glutathione reduced | 306 | 143 |
| Arginine-CBZ | 307 | 199 |
| Geranyl-pyrophosphate | 313 | 79 |
| Tyrosine-CBZ | 314 | 206 |
| Octulose-1/8-P | 319 | 97 |

**TABLE 6 (cont'd)**

| | | |
|---|---|---|
| dTMP | 321 | 195 |
| Oxalic acid | 322 | 77 |
| CMP | 322 | 79 |
| UMP | 323 | 79 |
| cAMP | 328 | 134 |
| dAMP | 330 | 134 |
| dAMP | 330 | 195 |
| Tryptophan-CBZ | 337 | 229 |
| Fructose 1,6-bisphosphate | 339 | 97 |
| Sucrose | 341 | 179 |
| Cellobiose | 341 | 263 |
| dGMP | 346 | 133 |
| AMP | 346 | 134 |
| GMP | 362 | 79 |
| XMP | 363 | 211 |
| SBP | 369 | 97 |
| S-Adenosyl-L-homocysteine | 383 | 134 |
| dCDP | 386 | 159 |
| 5-Phosphoribosyl-1-pyrophosphate | 389 | 291 |
| Deoxycholic acid | 391 | 345 |
| OBP | 399 | 97 |
| Ornithine-CBZ | 399 | 183 |
| dTDP | 401 | 159 |
| CDP | 402 | 159 |
| UDP | 403 | 159 |
| Cholic acid | 407 | 345 |
| dADP \| dGDP | 410 | 159 |
| Lysine-CBZ | 413 | 197 |
| ADP | 426 | 159 |
| dGDP | 426 | 159 |
| adenosine 5'-phosphosulfate | 426 | 346 |
| IDP | 427 | 159 |
| GDP | 442 | 159 |
| CDP-ethanolamine | 445 | 273 |
| FMN | 455 | 213 |
| Cholesteryl sulfate | 465 | 97 |
| dCTP | 466 | 159 |
| CTP | 482 | 384 |
| UTP | 483 | 159 |
| CDP-choline | 487 | 428 |
| dATP | 490 | 159 |
| Taurodeoxycholic acid | 498 | 124 |
| ATP | 506 | 159 |

**TABLE 6 (cont'd)**

| | | |
|---|---|---|
| GTP | 522 | 424 |
| UDP-D-glucose | 565 | 323 |
| UDP-D-glucuronate | 579 | 403 |
| ADP-D-glucose | 588 | 346 |
| UDP-N-acetyl-glucosamine | 606 | 385 |
| Oxidized glutathione | 611 | 306 |
| NAD | 662 | 540 |
| NADH | 664 | 408 |
| dephospho-CoA | 686 | 339 |
| NADP | 742 | 620 |
| NADPH | 744 | 408 |
| CoA | 766 | 408 |
| FAD | 784 | 437 |
| Acetyl-CoA | 808 | 408 |
| Propionyl-CoA | 822 | 408 |
| Butyryl-CoA | 836 | 408 |
| Acetoacetyl-CoA | 850 | 766 |
| 3-Hydroxybutyryl-CoA | 852 | 408 |
| Malonyl-CoA | 852 | 808 |
| Succinyl-CoA \| methylmalonyl-CoA | 866 | 822 |
| 3-Hydroxy-3-methylglutaryl-CoA | 910 | 408 |

# REFERENCES

## REFERENCES


1. Denison, M.S., A.A. Soshilov, G. He, D.E. DeGroot, and B. Zhao, *Exactly the same but different: promiscuity and diversity in the molecular mechanisms of action of the aryl hydrocarbon (dioxin) receptor.* Toxicol Sci, 2011. 124(1): p. 1-22.

2. Beischlag, T.V., J. Luis Morales, B.D. Hollingshead, and G.H. Perdew, *The aryl hydrocarbon receptor complex and the control of gene expression.* Crit Rev Eukaryot Gene Expr, 2008. 18(3): p. 207-50.

3. Dere, E., R. Lo, T. Celius, J. Matthews, and T.R. Zacharewski, *Integration of genome-wide computation DRE search, AhR ChIP-chip and gene expression analyses of TCDD-elicited responses in the mouse liver.* BMC Genomics, 2011. 12: p. 365.

4. Huang, G. and C.J. Elferink, *A novel nonconsensus xenobiotic response element capable of mediating aryl hydrocarbon receptor-dependent gene expression.* Mol Pharmacol, 2012. 81(3): p. 338-47.

5. Pohjanvirta, R. and J. Tuomisto, *Short-term toxicity of 2,3,7,8-tetrachlorodibenzo-p-dioxin in laboratory animals: effects, mechanisms, and animal models.* Pharmacol Rev, 1994. 46(4): p. 483-549.

6. Taylor, K.W., R.F. Novak, H.A. Anderson, L.S. Birnbaum, C. Blystone, M. Devito, D. Jacobs, J. Kohrle, D.H. Lee, L. Rylander, A. Rignell-Hydbom, R. Tornero-Velez, M.E. Turyk, A.L. Boyles, K.A. Thayer, and L. Lind, *Evaluation of the association between persistent organic pollutants (POPs) and diabetes in epidemiological studies: a national toxicology program workshop review.* Environ Health Perspect, 2013. 121(7): p. 774-83.

7. Boverhof, D.R., L.D. Burgoon, C. Tashiro, B. Chittim, J.R. Harkema, D.B. Jump, and T.R. Zacharewski, *Temporal and dose-dependent hepatic gene expression patterns in mice provide new insights into TCDD-Mediated hepatotoxicity.* Toxicol Sci, 2005. 85(2): p. 1048-63.

8. Lee, J.H., T. Wada, M. Febbraio, J. He, T. Matsubara, M.J. Lee, F.J. Gonzalez, and W. Xie, *A novel role for the dioxin receptor in fatty acid metabolism and hepatic steatosis.* Gastroenterology, 2010. 139(2): p. 653-63.

9. Nault, R., D. Colbry, C. Brandenberger, J.R. Harkema, and T.R. Zacharewski, *Development of a computational high-throughput tool for the quantitative examination of dose-dependent histological features.* Toxicol Pathol, 2015. 43(3): p. 366-75.

10. Pierre, S., A. Chevallier, F. Teixeira-Clerc, A. Ambolet-Camoit, L.C. Bui, A.S. Bats, J.C. Fournet, P. Fernandez-Salguero, M. Aggerbeck, S. Lotersztajn, R. Barouki, and X. Coumoul, *Aryl hydrocarbon receptor-dependent induction of liver fibrosis by dioxin.* Toxicol Sci, 2014. 137(1): p. 114-24.

11. Lin, S., Z. Yang, H. Liu, and Z. Cai, *Metabolomic analysis of liver and skeletal muscle tissues in C57BL/6J and DBA/2J mice exposed to 2,3,7,8-tetrachlorodibenzo-p-dioxin.* Mol Biosyst, 2011. 7(6): p. 1956-65.

12. Forgacs, A.L., M.N. Kent, M.K. Makley, B. Mets, N. DelRaso, G.L. Jahns, L.D. Burgoon, T.R. Zacharewski, and N.V. Reo, *Comparative metabolomic and genomic analyses of TCDD-elicited metabolic disruption in mouse and rat liver.* Toxicol Sci, 2012. 125(1): p. 41-55.

13. Matsubara, T., N. Tanaka, K.W. Krausz, S.K. Manna, D.W. Kang, E.R. Anderson, H. Luecke, A.D. Patterson, Y.M. Shah, and F.J. Gonzalez, *Metabolomics identifies an inflammatory cascade involved in dioxin- and diet-induced steatohepatitis.* Cell Metab, 2012. 16(5): p. 634-44.

14. Christofk, H.R., M.G. Vander Heiden, M.H. Harris, A. Ramanathan, R.E. Gerszten, R. Wei, M.D. Fleming, S.L. Schreiber, and L.C. Cantley, *The M2 splice isoform of pyruvate kinase is important for cancer metabolism and tumour growth.* Nature, 2008. 452(7184): p. 230-3.

15. DeBerardinis, R.J., A. Mancuso, E. Daikhin, I. Nissim, M. Yudkoff, S. Wehrli, and C.B. Thompson, *Beyond aerobic glycolysis: transformed cells can engage in glutamine metabolism that exceeds the requirement for protein and nucleotide synthesis.* Proc Natl Acad Sci U S A, 2007. 104(49): p. 19345-50.

16. Locasale, J.W., *Serine, glycine and one-carbon units: cancer metabolism in full circle.* Nat Rev Cancer, 2013. 13(8): p. 572-83.

17. Maddocks, O.D., C.R. Berkers, S.M. Mason, L. Zheng, K. Blyth, E. Gottlieb, and K.H. Vousden, *Serine starvation induces stress and p53-dependent metabolic remodelling in cancer cells.* Nature, 2013. 493(7433): p. 542-6.

18. Kopec, A.K., L.D. Burgoon, D. Ibrahim-Aibo, A.R. Burg, A.W. Lee, C. Tashiro, D. Potter, B. Sharratt, J.R. Harkema, J.C. Rowlands, R.A. Budinsky, and T.R. Zacharewski, *Automated dose-response analysis and comparative toxicogenomic evaluation of the hepatic effects elicited by TCDD, TCDF, and PCB126 in C57BL/6 mice.* Toxicol Sci, 2010. 118(1): p. 286-97.

19. Kopec, A.K., L.D. Burgoon, D. Ibrahim-Aibo, B.D. Mets, C. Tashiro, D. Potter, B. Sharratt, J.R. Harkema, and T.R. Zacharewski, *PCB153-elicited hepatic responses in the immature, ovariectomized C57BL/6 mice: comparative toxicogenomic effects of dioxin and non-dioxin-like ligands.* Toxicol Appl Pharmacol, 2010. 243(3): p. 359-71.

20. Dere, E., A.L. Forgacs, T.R. Zacharewski, and L.D. Burgoon, *Genome-wide computational analysis of dioxin response element location and distribution in the human, mouse, and rat genomes.* Chem Res Toxicol, 2011. 24(4): p. 494-504.

21. Sun, Y.V., D.R. Boverhof, L.D. Burgoon, M.R. Fielden, and T.R. Zacharewski, *Comparative analysis of dioxin response elements in human, mouse and rat genomic sequences.* Nucleic Acids Res, 2004. 32(15): p. 4512-23.

22. De Abrew, K.N., A.S. Phadnis, R.B. Crawford, N.E. Kaminski, and R.S. Thomas, *Regulation of Bach2 by the aryl hydrocarbon receptor as a mechanism for suppression of B-cell differentiation by 2,3,7,8-tetrachlorodibenzo-p-dioxin.* Toxicol Appl Pharmacol, 2011. 252(2): p. 150-8.

23. Shehin, S.E., R.O. Stephenson, and W.F. Greenlee, *Transcriptional regulation of the human CYP1B1 gene. Evidence for involvement of an aryl hydrocarbon receptor response element in constitutive expression.* J Biol Chem, 2000. 275(10): p. 6770-6.

24. Lo, R. and J. Matthews, *High-resolution genome-wide mapping of AHR and ARNT binding sites by ChIP-Seq.* Toxicol Sci, 2012. 130(2): p. 349-61.

25. Ji, H., H. Jiang, W. Ma, and W.H. Wong, *Using CisGenome to Analyze ChIP-chip and ChIP-seq Data*, in *Curr Protoc Bioinformatics*. 2008, John Wiley & Sons, Inc.

26. Lunt, S.Y., V. Muralidhar, A.M. Hosios, W.J. Israelsen, D.Y. Gui, L. Newhouse, M. Ogrodzinski, V. Hecht, K. Xu, P.N. Acevedo, D.P. Hollern, G. Bellinger, T.L. Dayton, S. Christen, I. Elia, A.T. Dinh, G. Stephanopoulos, S.R. Manalis, M.B. Yaffe, E.R. Andrechek, S.M. Fendt, and M.G. Vander Heiden, *Pyruvate kinase isoform expression alters nucleotide synthesis to impact cell proliferation.* Mol Cell, 2015. 57(1): p. 95-107.

27. Clasquin, M.F., E. Melamud, and J.D. Rabinowitz, *LC-MS data processing with MAVEN: a metabolomic analysis and visualization engine.* Curr Protoc Bioinformatics, 2012. Chapter 14: p. Unit14 11.

28. Melamud, E., L. Vastag, and J.D. Rabinowitz, *Metabolomic analysis and visualization engine for LC-MS data.* Anal Chem, 2010. 82(23): p. 9818-26.

29. Kessner, D., M. Chambers, R. Burke, D. Agus, and P. Mallick, *ProteoWizard: open source software for rapid proteomics tools development.* Bioinformatics, 2008. 24(21): p. 2534-6.

30. Nault, R., K.A. Fader, and T. Zacharewski, *RNA-Seq versus oligonucleotide array assessment of dose-dependent TCDD-elicited hepatic gene expression in mice.* BMC Genomics, 2015. 16(1): p. 373.

31. Xia, J. and D.S. Wishart, *MetPA: a web-based metabolomics tool for pathway analysis and visualization.* Bioinformatics, 2010. 26(18): p. 2342-4.

32. Yu, G., L.G. Wang, Y. Han, and Q.Y. He, *clusterProfiler: an R package for comparing biological themes among gene clusters.* Omics, 2012. 16(5): p. 284-7.

33. Fernandez-Salguero, P.M., D.M. Hilbert, S. Rudikoff, J.M. Ward, and F.J. Gonzalez, *Aryl-hydrocarbon receptor-deficient mice are resistant to 2,3,7,8-tetrachlorodibenzo-p-dioxin-induced toxicity.* Toxicol Appl Pharmacol, 1996. 140(1): p. 173-9.

34. Chesney, J., *6-phosphofructo-2-kinase/fructose-2,6-bisphosphatase and tumor cell glycolysis.* Curr Opin Clin Nutr Metab Care, 2006. 9(5): p. 535-9.

35. van den Heuvel, A.P., J. Jing, R.F. Wooster, and K.E. Bachman, *Analysis of glutamine dependency in non-small cell lung cancer: GLS1 splice variant GAC is essential for cancer cell growth.* Cancer Biol Ther, 2012. 13(12): p. 1185-94.

36. Wise, D.R., R.J. DeBerardinis, A. Mancuso, N. Sayed, X.Y. Zhang, H.K. Pfeiffer, I. Nissim, E. Daikhin, M. Yudkoff, S.B. McMahon, and C.B. Thompson, *Myc regulates a*

*transcriptional program that stimulates mitochondrial glutaminolysis and leads to glutamine addiction.* Proc Natl Acad Sci U S A, 2008. 105(48): p. 18782-7.

37. Conrad, M. and H. Sato, *The oxidative stress-inducible cystine/glutamate antiporter, system x (c) (-) : cystine supplier and beyond.* Amino Acids, 2012. 42(1): p. 231-46.

38. Yin, J., W. Ren, G. Yang, J. Duan, X. Huang, R. Fang, C. Li, T. Li, Y. Yin, Y. Hou, S.W. Kim, and G. Wu, *l-Cysteine metabolism and its nutritional implications.* Mol Nutr Food Res, 2015.

39. Weber, L.W., M. Lebofsky, B.U. Stahl, S. Smith, and K.K. Rozman, *Correlation between toxicity and effects on intermediary metabolism in 2,3,7,8-tetrachlorodibenzo-p-dioxin-treated male C57BL/6J and DBA/2J mice.* Toxicol Appl Pharmacol, 1995. 131(1): p. 155-62.

40. Diani-Moore, S., P. Ram, X. Li, P. Mondal, D.Y. Youn, A.A. Sauve, and A.B. Rifkind, *Identification of the aryl hydrocarbon receptor target gene TiPARP as a mediator of suppression of hepatic gluconeogenesis by 2,3,7,8-tetrachlorodibenzo-p-dioxin and of nicotinamide as a corrective agent for this effect.* J Biol Chem, 2010. 285(50): p. 38801-10.

41. Ahmed, S., D. Bott, A. Gomez, L. Tamblyn, A. Rasheed, T. Cho, L. MacPherson, K.S. Sugamori, Y. Yang, D.M. Grant, C.L. Cummins, and J. Matthews, *Loss of the Mono-ADP-ribosyltransferase, Tiparp, Increases Sensitivity to Dioxin-induced Steatohepatitis and Lethality.* J Biol Chem, 2015. 290(27): p. 16824-40.

42. Son, J., C.A. Lyssiotis, H. Ying, X. Wang, S. Hua, M. Ligorio, R.M. Perera, C.R. Ferrone, E. Mullarky, N. Shyh-Chang, Y. Kang, J.B. Fleming, N. Bardeesy, J.M. Asara, M.C. Haigis, R.A. DePinho, L.C. Cantley, and A.C. Kimmelman, *Glutamine supports pancreatic cancer growth through a KRAS-regulated metabolic pathway.* Nature, 2013. 496(7443): p. 101-5.

43. Jiang, P., W. Du, and M. Wu, *Regulation of the pentose phosphate pathway in cancer.* Protein Cell, 2014. 5(8): p. 592-602.

44. Wang, Y.P., L.S. Zhou, Y.Z. Zhao, S.W. Wang, L.L. Chen, L.X. Liu, Z.Q. Ling, F.J. Hu, Y.P. Sun, J.Y. Zhang, C. Yang, Y. Yang, Y. Xiong, K.L. Guan, and D. Ye, *Regulation of G6PD acetylation by SIRT2 and KAT9 modulates NADPH homeostasis and cell survival during oxidative stress.* Embo J, 2014. 33(12): p. 1304-20.

45. Cosentino, C., D. Grieco, and V. Costanzo, *ATM activates the pentose phosphate pathway promoting anti-oxidant defence and DNA repair.* Embo J, 2011. 30(3): p. 546-55.

46. Fan, J., J. Ye, J.J. Kamphorst, T. Shlomi, C.B. Thompson, and J.D. Rabinowitz, *Quantitative flux analysis reveals folate-dependent NADPH production.* Nature, 2014. 510(7504): p. 298-302.

47. Gorrini, C., I.S. Harris, and T.W. Mak, *Modulation of oxidative stress as an anticancer strategy.* Nat Rev Drug Discov, 2013. 12(12): p. 931-47.

48. Cairns, R.A., I.S. Harris, and T.W. Mak, *Regulation of cancer cell metabolism.* Nat Rev Cancer, 2011. 11(2): p. 85-95.

49. Harris, I., S. McCracken, and T.W. Mak, *PKM2: a gatekeeper between growth and survival.* Cell Res, 2012. 22(3): p. 447-9.

50. Puga, A., Y. Xia, and C. Elferink, *Role of the aryl hydrocarbon receptor in cell cycle regulation.* Chem Biol Interact, 2002. 141(1-2): p. 117-30.

51. Jackson, D.P., H. Li, K.A. Mitchell, A.D. Joshi, and C.J. Elferink, *Ah receptor-mediated suppression of liver regeneration through NC-XRE-driven p21Cip1 expression.* Mol Pharmacol, 2014. 85(4): p. 533-41.

52. Tanos, R., I.A. Murray, P.B. Smith, A. Patterson, and G.H. Perdew, *Role of the Ah receptor in homeostatic control of fatty acid synthesis in the liver.* Toxicol Sci, 2012. 129(2): p. 372-9.

53. Sato, S., H. Shirakawa, S. Tomita, Y. Ohsaki, K. Haketa, O. Tooi, N. Santo, M. Tohkin, Y. Furukawa, F.J. Gonzalez, and M. Komai, *Low-dose dioxins alter gene expression related to cholesterol biosynthesis, lipogenesis, and glucose metabolism through the aryl hydrocarbon receptor-mediated pathway in mouse liver.* Toxicol Appl Pharmacol, 2008. 229(1): p. 10-9.

54. Bansal, S., A.N. Leu, F.J. Gonzalez, F.P. Guengerich, A.R. Chowdhury, H.K. Anandatheerthavarada, and N.G. Avadhani, *Mitochondrial targeting of cytochrome P450 (CYP) 1B1 and its role in polycyclic aromatic hydrocarbon-induced mitochondrial dysfunction.* J Biol Chem, 2014. 289(14): p. 9936-51.

55. Sugihara, K., S. Kitamura, T. Yamada, S. Ohta, K. Yamashita, M. Yasuda, and Y. Fujii-Kuriyama, *Aryl hydrocarbon receptor (AhR)-mediated induction of xanthine oxidase/xanthine dehydrogenase activity by 2,3,7,8-tetrachlorodibenzo-p-dioxin.* Biochem Biophys Res Commun, 2001. 281(5): p. 1093-9.

56. Lu, H., W. Cui, and C.D. Klaassen, *Nrf2 protects against 2,3,7,8-tetrachlorodibenzo-p-dioxin (TCDD)-induced oxidative injury and steatohepatitis.* Toxicol Appl Pharmacol, 2011. 256(2): p. 122-35.

57. Panasyuk, G., C. Espeillac, C. Chauvin, L.A. Pradelli, Y. Horie, A. Suzuki, J.S. Annicotte, L. Fajas, M. Foretz, F. Verdeguer, M. Pontoglio, P. Ferre, J.Y. Scoazec, M.J. Birnbaum, J.E. Ricci, and M. Pende, *PPARgamma contributes to PKM2 and HK2 expression in fatty liver.* Nat Commun, 2012. 3: p. 672.

58. Anastasiou, D., G. Poulogiannis, J.M. Asara, M.B. Boxer, J.K. Jiang, M. Shen, G. Bellinger, A.T. Sasaki, J.W. Locasale, D.S. Auld, C.J. Thomas, M.G. Vander Heiden, and L.C. Cantley, *Inhibition of pyruvate kinase M2 by reactive oxygen species contributes to cellular antioxidant responses.* Science, 2011. 334(6060): p. 1278-83.

59. Amelio, I., F. Cutruzzola, A. Antonov, M. Agostini, and G. Melino, *Serine and glycine metabolism in cancer.* Trends Biochem Sci, 2014. 39(4): p. 191-8.

60. Palsson-McDermott, E.M., A.M. Curtis, G. Goel, M.A. Lauterbach, F.J. Sheedy, L.E. Gleeson, M.W. van den Bosch, S.R. Quinn, R. Domingo-Fernandez, D.G. Johnston, J.K. Jiang, W.J. Israelsen, J. Keane, C. Thomas, C. Clish, M. Vanden Heiden, R.J. Xavier, and L.A. O'Neill, *Pyruvate kinase M2 regulates Hif-1alpha activity and IL-1beta induction and is a critical determinant of the warburg effect in LPS-activated macrophages*. Cell Metab, 2015. 21(1): p. 65-80.

60. Kuehne, A., H. Emmert, J. Soehle, M. Winnefeld, F. Fischer, H. Wenck, S. Gallinat, L. Terstegen, R. Lucius, J. Hildebrand, and N. Zamboni, *Acute Activation of Oxidative Pentose Phosphate Pathway as First-Line Response to Oxidative Stress in Human Skin Cells.* Mol Cell, 2015. 59(3): p. 359-71.

61. Hanahan, D. and R.A. Weinberg, *Hallmarks of cancer: the next generation.* Cell, 2011. 144(5): p. 646-74.

62. Boffetta, P., K.A. Mundt, H.O. Adami, P. Cole, and J.S. Mandel, *TCDD and cancer: a critical review of epidemiologic studies.* Crit Rev Toxicol, 2011. 41(7): p. 622-36.

# CHAPTER 5. DOSE-DEPENDENT METABOLIC REPROGRAMMING AND DIFFERENTIAL GENE EXPRESSION IN MOUSE TCDD-ELICITED HEPATIC FIBROSIS.

**ABSTRACT**

We have previously shown that in response to 2,3,7,8-tetrachlorodibenzo-*p*-dioxin (TCDD)-elicited NAFLD progression, central carbon, glutaminolysis and serine/folate metabolism are reprogrammed to support NADPH production and ROS defenses. To further investigate underlying dose-dependent responses associated with TCDD-induced fibrosis, female C57BL/6 mice were gavaged with TCDD every 4 days (d) for 28 d or 92 d. RNA-Seq, ChIP-Seq (2hr), and 28d metabolomic (urine, serum, and hepatic extract) analyses were conducted with complementary serum marker assessments at 92 d. Additional vehicle and 30 µg/kg treatment groups were allowed to recover for 36 d following the 9 2d treatment regimen to examine recovery from TCDD-elicited fibrosis. Histopathology revealed dose-dependent increases in hepatic fat accumulation, inflammation, and periportal collagen deposition at 9 2d with increased fibrotic severity in the recovery group. Serum proinflammatory and profibrotic interleukins-1β, -2, -4, -6, and -10, as well as TNFα and IFNγ, exhibited dose-dependent induction. An increase in glucose tolerance was observed with a concomitant 3.0-fold decrease in hepatic glycogen linked to increased ascorbic acid biosynthesis and proline metabolism, consistent with increased fibrosis. RNA-Seq identified differential expression of numerous matrisome genes including an 8.8-fold increase in *Tgfb2* indicating myofibroblast activation. Further analysis suggests reprogramming of glycogen, ascorbic acid, and amino acid metabolism in support of collagen deposition and the use of proline as a substrate for ATP production via the proline cycle. *Conclusion:* In addition to metabolic reprogramming in support of NADPH production for ROS defense, we demonstrate that glycogen, ascorbic acid, and amino acid metabolism are also reorganized to support remodeling of the extracellular matrix, progressing to hepatic fibrosis in response to chronic injury from TCDD.

**INTRODUCTION**

Exposure to the environmental contaminant 2,3,7,8-tetrachlorodibenzo-*p*-dioxin (TCDD) has been associated with the development of reversible hepatic steatosis, and the progression of steatosis to steatohepatitis with hepatic fibrosis [1, 2]. These and the majority of responses to

TCDD and related compounds, if not all, are mediated through the aryl hydrocarbon receptor (AhR) [3]. AhR activation leads to the dissociation of chaperone proteins and subsequent dimerization with the AhR nuclear translocator (ARNT). The liganded heterodimer then binds to dioxin response elements (DRE; also known as AHRE or XRE) initiating changes in gene expression, although DRE independent mechanisms have also been reported [4, 5]. Not surprisingly, AhR activation plays an important role in TCDD-elicited fibrosis [2] although the mechanisms involved in AhR-mediated fibrogenesis remain poorly understood.

Fibrosis is a wound-healing, protective response to repeated and chronic injury leading to the accumulation of extracellular matrix (ECM) due to the unbalancing of deposition and turnover of the matrisome [6]. Although the etiology of fibrosis in different organs is poorly defined, the process is believed to involve shared common mechanisms at the onset and during fibrotic progression. Following injury, cytokines and growth factors released by damaged tissue initiate a provisional ECM response allowing resident and infiltrating immune cells to adhere and initiate repair [7]. Further development is mediated by prolonged or persistent inflammation that triggers profibrotic signaling such as the overproduction/activation of cytokines and TGFβ, immune cell migration to damaged areas, and epithelial to mesenchymal transition (EMT) of hepatic stellate cells (HSC) and fibroblasts to myofibroblasts which synthesize excessive amounts of ECM proteins [7-9]. The accumulation of hepatocyte and cholangiocyte damage, increased ROS production, secretion of proinflammatory mediators, and the exhaustion of antioxidant defenses releases endogenous damage-associated molecular patterns (DAMPS) that further promote fibrogenesis. The deposition of ECM is continuously remodeled altering tissue tensile and compression strength and elasticity which ultimately impairs function and increases cell leakiness and death, promoting further inflammation.

We have recently shown that TCDD dosing over 28 d elicits a Warburg-like response well before hepatic ECM remodeling and myofibroblast activation [10]. Interestingly, myofibroblast activation has also been linked to a Warburg-like response wherein cells increase glycolytic flux

and lactate production [11]. However, few studies have examined the metabolic reprogramming underlying the development of hepatic fibrosis. To further investigate the relationships between metabolic reprogramming and fibrosis, we evaluated systemic metabolic changes, serum cytokine and adipo/hepatokine levels, and differential gene expression in mice treated with TCDD every 4 d for 92 d. Furthermore, published metabolomic and transcriptomic data from mice exposed for 28 d [10] were used to investigate the temporal progression of these pathologies, supplemented with urinary metabolomic data. We show that, in addition to supporting antioxidant responses, hepatic metabolic reprogramming also supports collagen deposition through the redirection of glycogen, ascorbic acid, and proline metabolism.

## MATERIALS AND METHODS

### ANIMAL HANDLING AND TISSUE PROCESSING

Female C57BL/6 mice (Charles River Laboratories, Portage, MI) on postnatal day 25 (PND 25) were housed in polycarbonate cages with cellulose fiber chips (Aspen Chip Laboratory Bedding, Warrensberg, NY) at 30-40% humidity and a 12 h light/dark cycle. Animals were fed ad libitum (Harlan Teklad 22/5 Rodent Diet 8940, Madison, WI) and had free access to deionized water. Following 4 d acclimation (PND 28), animals (n = 10) were orally gavaged with 0.1 mL sesame oil or 0.01, 0.03, 0.1, 0.3, 1, 3, 10, or 30 µg/kg TCDD (Dow Chemical Company, Midland, MI) every $4^{th}$ day for 92 d for a total of 23 exposures. Two additional groups (vehicle and 30 µg/kg) were allowed to recover for 36d following the 92 d treatment regimen. Body weight and food intake were monitored every 4 days. Urine was collected from individual mice over 2 hrs on day 26 in absence of food or water and stored immediately at -80°C**.** Oral glucose tolerance tests (OGTT) were performed at 31 d, 63 d, and 96 d in sesame oil and 30 µg/kg TCDD groups only. Briefly, at time 0 min animals were orally gavaged with 2g/kg glucose in a 25% solution and tail blood glucose was measured after 0, 15, 30, 60, and 120 min using a FreeStyle Lite handheld glucose meter (Abbott Laboratories, IL).

Prior to termination animals were fasted for 6 hours. Blood was collected by submandibular vein puncture prior to cervical dislocation, centrifuged and stored at -80°C. Liver and gonadal white adipose tissue (gWAT) were excised, weighed, and frozen at -80°C. Liver sections were stored in 10% neutral buffered formalin (Sigma-Aldrich, MO) or frozen in Tissue-Tek O.C.T compound (Sakura, CA) for Haematoxylin & Eosin (H&E), Oil Red O staining (ORO), and PicroSirius Red (PSR) staining as previously described [12]. Hepatic TCDD levels were determined as previously described [1]. All animal procedures were approved by the Michigan State University Institutional Animal Care and Use Committee.

**CLINICAL CHEMISTRY, GLYCOGEN ASSAY, AND PROTEIN MEASUREMENTS**

Serum cholesterol, triglycerides, and glucose were determined using commercially available reagents (Pointe Scientific, Canton, MI). Adiponectin (R&D systems), FGF21 (R&D systems), insulin (Crystal Chem, Inc.), and leptin (Crystal Chem, Inc.) were determined using commercially available ELISAs. Hepatic glucose and glycogen levels were determined as previously described by Keppler *et al.* [13]. Briefly, liver samples (~50 mg) or glycogen standards (Sigma-Aldrich) were homogenized in 6% PCA (250 µL) using a Polytron PT2100 homogenizer (Kinematica AG, Luzern, CH). 25 µL of 1 M $NaHCO_3$ was added to 50 µL of the homogenate. 125 µL of 2 mg/mL amyloglucosidase (Sigma-Aldrich) was added to each sample to hydrolyze glycogen. Samples were incubated and shaken for 2 h at 37°C and then centrifuged to remove debris. Glycogen and glucose was assayed using the glucose assay kit (Pointe Scientific, Canton, MI) a M200 plate reader (Tecan, Durham, NC). Total hepatic levels were corrected using hepatic glucose levels, and expressed as glycosyl units. Serum cytokine levels were assayed using the Meso Scale V-PLEX Proinflammatory panel kit and Sector S 600 (Meso Scale Discovery, Rockville, MD). Protein determinations are described in supplementary methods.

Protein determinations were performed using the Wes system (ProteinSimple, San Jose, CA) as previously described [10]. Total protein was quantitated by bicinchinonic acid assay

(Sigma-Aldrich). Antibodies for PKM1 (Sigma-Aldrich; 1:400), PKM2 (Cell Signaling, Danvers, MA; 1:65), PKM1/2 (Cell Signaling; 1:65), GLS1 (ProteinTech, Chicago, IL; 1:30), PEPCK-C (Santa Cruz Biotechnology, Dallas, TX; 1:20), and PYGL (Novus Biologicals, Littleton, CO; 1:30) were duplexed when possible with β-actin (Cell Signaling; 1:65) or SDHA (Novus; 1:100) as a loading control. Chemiluminescence signals from the Compass software (ProteinSimple) were used to calculate fold-change.

**RNA EXTRACTION AND RNA-SEQUENCING**

Total RNA extraction and RNA-Seq analysis was performed as previously described [14] for 3 animals (N=3). Reads were mapped to the GRCm38 release 74 mouse reference genome. RNA-Seq data has been deposited in the Gene Expression Omnibus (GSE81990) and published 28d RNA-Seq data [14] used to complement the 92 d gene expression profiles are available on GEO (GSE62902).

**TARGETED URINARY METABOLOMICS**

Urine samples, collected at 26 d (PND 54, 7 TCDD doses), were sent onto a trapping column (C18, 4 mm×2 mm, Phenomenex) and desalted for 30 s with HPLC grade water containing 10 mM tributylamine and 15 mM acetic acid (pH 4.95). Samples were examined by liquid chromatography (LC) and tandem mass spectrometry (MS/MS) using a Paradigm MS4 HPLC (Michrom Bioresources, Auburn, CA), and a Synergi Hydro column (4 µm particle size, 80 Å, 150 mm×2 mm, from Phenomenex) [15]. HPLC was coupled with negative-mode electrospray ionization (ESI) to a TSQ Vantage Triple Stage Quadrupole Mass Spectrometer (Thermo Scientific) operating in multiple reaction monitoring (MRM) mode. The LC parameters were as follows: autosampler temperature, 10 ºC; injection volume, 10 µl; column temperature, room temperature; and flow rate, 200 µl·min-1. The LC solvents were Solvent A: 10 mM tributylamine and 15 mM acetic acid in 97:3 water:methanol (pH 4.95); and Solvent B: methanol. Elution from

the column was performed over 50 min with the following gradient: t = 0, 0% B; t = 5, 0% B; t = 10, 20% B; t = 20, 20% B; t = 35, 65% B; t = 38, 95% B; t = 42, 95% B, t = 43, 0% B; t = 50, 0% B. ESI spray voltage was 3,000 V. Nitrogen was used as the sheath gas at 30 psi and as the auxiliary gas at 10 psi, and argon as the collision gas at 1.5 mTorr, with the capillary temperature at 325 ºC. Dwell time for each MRM transition was 0.1 s with a scan width of 1 m/z. The LC runs were divided into time segments, with the MRM scans within each time segment containing compounds eluting during that time interval. For compounds eluting near boundaries between time segments, the MRM scan corresponding to the compound was conducted in both time segments. Instrument control, chromatographic control, and data acquisition were performed by the Xcalibar software (Thermo Scientific). Raw data and MRM parameters are deposited in www.ebi.ac.uk/metabolights (MTBLS225). Data analysis, including peak integration was performed using MAVEN [16]. One-way ANOVA was performed in SAS 9.3. Urinary metabolomic data was supplemented with previously published serum and hepatic extract metabolomic assessments [10].

**PATHWAY ENRICHMENT ANALYSIS AND INTEGRATION OF DATASETS**

Over-representation of metabolites within a pathway, as well as impact scores reflecting the connectivity of altered metabolites was determined using the Metabolic Pathway Enrichment Analysis tool (MetPA)[17]. CytoKegg 0.0.5 plugin (Cytoscape 3.2.0) was used to generate pathway templates which were also manually curated. Reactions catalyzed by several enzymes were streamlined by combining in a single node. Previously identified putative dioxin response elements (pDREs) and AhR enrichment peaks [10], as well as the largest change in gene expression at 92d, and/or altered metabolite level for liver, serum [10], and urine, are represented for each node (e.g. largest AhR enrichment fold-change, highest matrix similarity score of pDREs, or largest |fold-change| of gene expression) regardless of the dose.

## RESULTS

### TCDD TISSUE LEVELS AND GROSS PATHOLOGY

In this study, animals were gavaged every 4 d for a total of 92 d in order to examine the progression of fibrosis. The higher doses used compensate for TCDD half-life differences in humans (1-11 years) compared to mice (8-12 d[18]), the short duration of our study considering the bioaccumulative nature of halogenated AhR ligands, and the potential cumulative lifetime exposure from diverse AhR ligands, acknowledging the potential for non-additive interactions for some responses. Importantly, the hepatic TCDD levels achieved in mice using this dose range (0 – 30 µg/kg) and treatment regimen (oral gavage every 4 days for 28 d or 92 d) were comparable to levels reported in some human exposures (Figure 22). Therefore, although the doses are not environmentally relevant, the TCDD levels achieved in mouse hepatic tissue approximate levels reported in humans.

Although our previous 28 d studies did not elicit overt toxicity [12], there were losses in this 92 d study (Figure 23). Individual losses within a dose group prior to 28 d were sudden, did not exhibit weight loss or decreased food intake, and did not appear to be treatment related. In contrast, later deaths were treatment related, and predicted based on sudden body weight decreases (~15%), and therefore terminated. Survivors did not exhibit a difference in terminal body weight (Table 5). At 0.3 and 3 µg/kg TCDD, body weights increased as of day 43 and 27, respectively, with a corresponding increase in gonadal white adipose tissue (gWAT) at 0.3 µg/kg (Table 5). We have previously observed body weight gain at 3 µg/kg [1] suggesting TCDD may increase body weight gain within certain dose ranges using this treatment regimen, although additional studies are required to further evaluate this response. Food intake measurements do not indicate increased consumption at 0.3, or 3 µg/kg TCDD, although consumption was greater at 30 µg/kg TCDD. There was a dose-dependent increase in relative liver weight with a dose-dependent decrease in gWAT that was not statistically significant (Table 5). Visual examination

found pale colored livers with a mottled surface and evidence of dimpling, consistent with Pierre *et al.* [2].

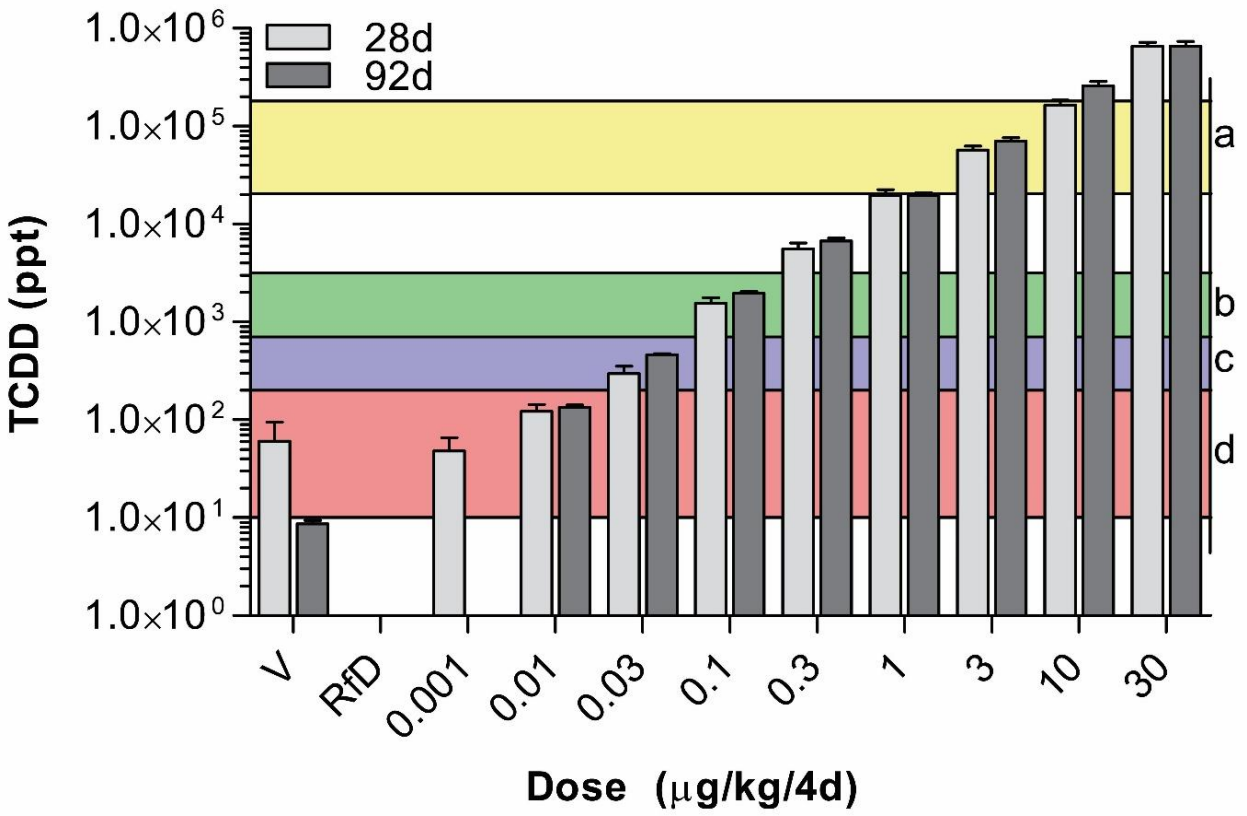


**FIGURE 22. COMPARISON OF MOUSE HEPATIC TCDD LEVELS TO HUMAN**

Hepatic TCDD levels in female mice gavaged every 4 days for 28 or 92 days compared to lipid adjusted TEQs for TCDD and dioxin-like compounds reported in (a) V. Yuschenko 4-39 mo. following TCDD poisoning [19], (b-c) Seveso Health Study women with or without chloracne, respectively, following 1976 accidental chemical release [20], and (d) background TCDD and dioxin-like compound levels in US, German, Spain, and UK populations [21-27]. The USEPA reference dose (RfD; $1x10^{-6}$ ng/kg/day) for TCDD is shown for context.

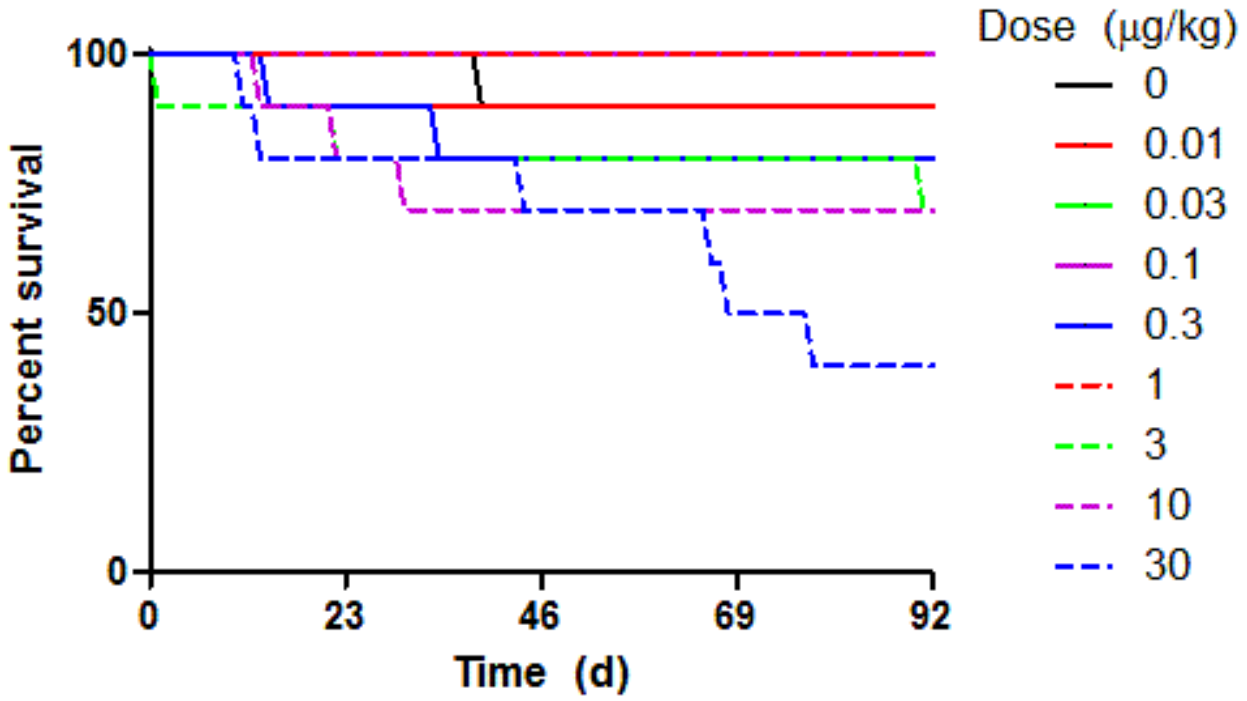


**FIGURE 23. SURVIVAL CURVES OF TCDD TREATED MICE**

Survival curves for female C57BL/6 mice gavaged every 4 days for 92 days with sesame oil vehicle or TCDD. Losses prior to 28d were sudden and unexpected as animals did not exhibit weight loss or decreased food intake. This and our prior studies [1, 10] suggest these deaths were not treatment related. In contrast, later losses were predicted based on a sudden decrease in body weight (~15%), and were subsequently terminated and considered treatment related.

**TABLE 5. TERMINAL BODY AND TISSUE WEIGHTS**

| Dose (µg/kg) | Terminal Body Weight (g) | Food Intake | RLW[#] | gWAT*(g) | Serum Cholesterol (mg/dL) | Serum Glucose (mg/dL) | Serum Triglycerides (mg/dL) |
|---|---|---|---|---|---|---|---|
| *Treated for 92 d* | | | | | | | |
| 0 | 21.86 ± 0.31 | | 5.76 ± 0.35 | 0.27 ± 0.02 | 108.3 ± 15.1 | 112.3 ± 32.3 | 66.8 ± 15.2 |
| 0.01 | 21.82 ± 0.58 | | 5.42 ± 0.21 | 0.23 ± 0.03 | 102.4 ± 12.9 | 120.0 ± 45.4 | 62.8 ± 6.0 |
| 0.03 | 21.91 ± 0.32 | | 5.39 ± 0.11 | 0.24 ± 0.02 | 95.3 ± 10.8 | 159.0 ± 18.7 | 62.6 ± 20.8 |
| 0.1 | 22.1 ± 0.31 | | 5.66 ± 0.11 | 0.25 ± 0.02 | 121.1 ± 8.0 | 149.2 ± 26.7 | 66.9 ± 9.8 |
| 0.3 | 23.24 ± 0.31[a] | | 6.73 ± 0.54[a] | 0.41 ± 0.05[a] | 108.6 ± 22.3 | 149.1 ± 21.0 | 55.2 ± 13.1 |
| 1 | 22.25 ± 0.28 | | 6.44 ± 0.28 [a] | 0.24 ± 0.03 | 94.1 ± 17.6 | 141.5 ± 15.9 | 54.0 ± 8.4 |
| 3 | 23.62 ± 0.3[a] | | 6.79 ± 0.61 [a] | 0.33 ± 0.03 | 68.7 ± 13.1[a] | 139.0 ± 18.2 | 58.0 ± 5.4 |
| 10 | 23.14 ± 0.41 | | 6.89 ± 0.25 [a] | 0.28 ± 0.02 | 59.2 ± 11.3[a] | 142.2 ± 28.2 | 57.9 ± 4.2 |
| 30 | 21.27 ± 1.33 | | 8.71 ± 0.39 [a] | 0.18 ± 0.05 | 59.0 ± 21.3[a] | 125.5 ± 26.5 | 69.7 ± 11.4 |
| *Allowed to recover for 36 d* | | | | | | | |
| 0 | 23.19 ± 0.48 | | 4.61 ± 0.12 | 0.28 ± 0.02 | NM | NM | NM |
| 30 | 24.08 ± 0.89 | | 7.46 ± 0.62 [a] | 0.2 ± 0.01 | NM | NM | NM |

[a]Significant difference compared to vehicle control determined by one-way ANOVA followed by Dunnett's post-hoc test.

[#]Relative liver weight (%)

*Gonadal white adipose tissue

NM indicates that the endpoint was not measured

**HISTOLOGY OF HEPATIC NAFLD FEATURES**

Similarly to dosing every 4 days for 28 d [10], 92 d of treatment elicited dose-dependent increases in centrilobular hepatocyte vacuolation, inflammation, and fibrosis (Figure 24A). However, quantitative assessment revealed hepatic lipid accumulation at lower doses (0.3 µg/kg vs. 1 µg/kg; Figure 24B). Similarly, inflammatory foci were present at 1 µg/kg, with portal fibrosis at 10 µg/kg TCDD. In contrast, inflammation and fibrosis at 28 d were only observed at 10 and 30 µg/kg, respectively. Collagen deposition along portal tracts is in agreement with Pierre *et al.* [2]. Quantitative assessment of collagen deposition by PSR staining showed a ~1.7-fold increase at 28 d and 92 d (Figure 24C). Fibrotic portal regions extended outward with the deposited ECM, appearing to pull the visceral surface internally creating a regular dimpled pattern (Figure 25). There were also instances of minimal bile duct proliferation and extramedullary hematopoiesis at 30 µg/kg TCDD. Although reduced hepatocyte vacuolation was observed in the 36 d recovery group, inflammation, collagen deposition, and bile duct proliferation occurred at a similar or increased frequency and severity.

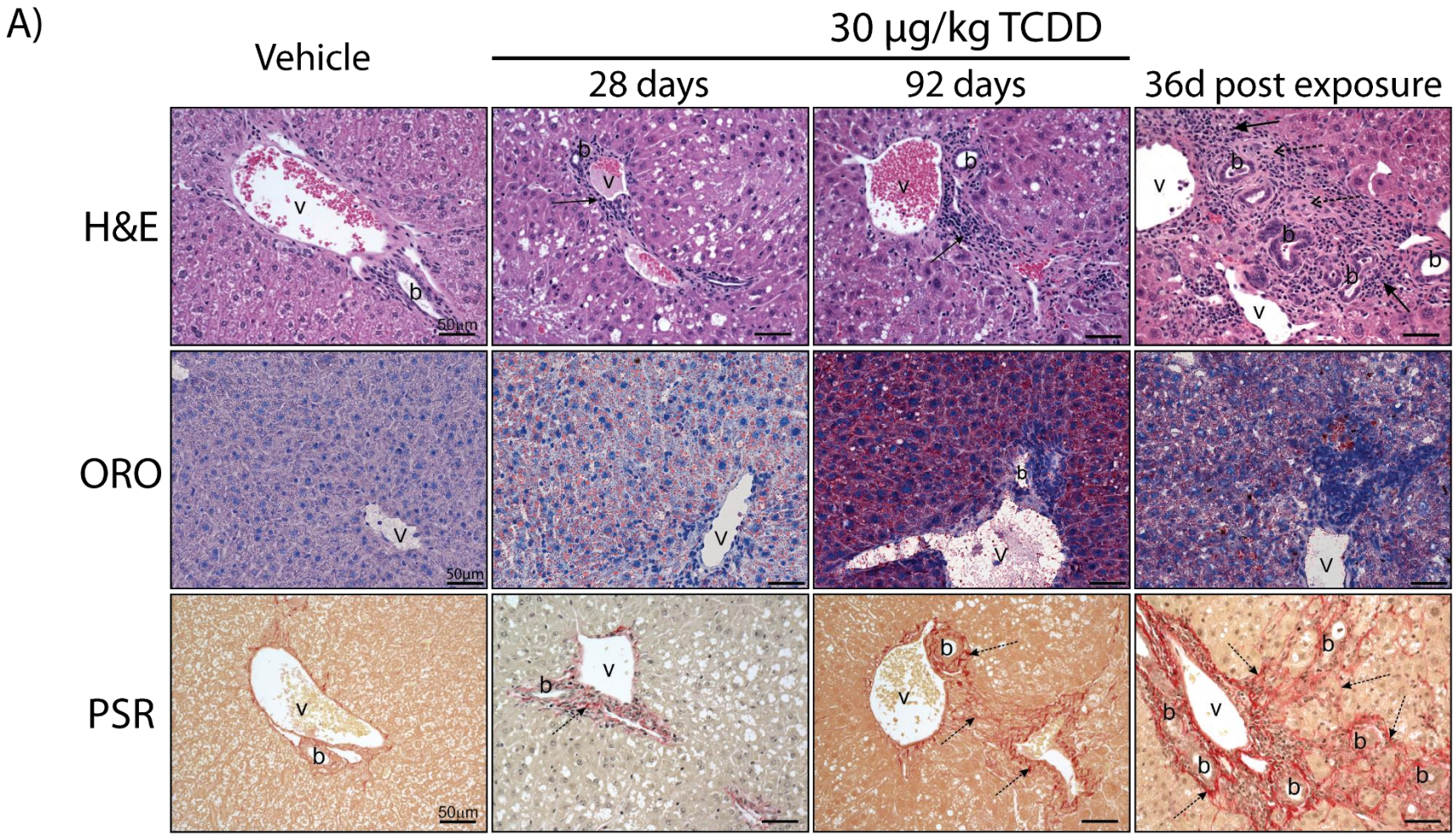


**FIGURE 24. HISTOLOGICAL EVALUATION OF LIVERS FROM TCDD TREATED MICE**

**FIGURE 24 (cont'd)**

Histological evaluation of livers from mice gavaged with sesame oil vehicle or 30 µg/kg TCDD every 4 days for 28 and 92d, as well as following a 36d recovery period (i.e., no treatment) following the final dose at 88d. (A) Representative micrographs of sections stained with hematoxylin and eosin staining (H&E) was used to survey hepatic lesions. Oil Red O (ORO) was used to determine neutral lipid accumulation. PicroSirius Red (PSR) was used to verify collagen deposition. Scale bar represents 50 µm. Portal veins are labeled with the letter v and bile ducts with the letter b while inflammation is denoted by a solid arrow and collagen deposition by a dashed arrow. Quantitation of (B) Oil Red O (ORO) and (C) PicroSirius Red (PSR) staining performed using the Quantitative Histological Analysis Tool [12]. Bars represent mean + SEM for at least 3 animals (n=3-5). Asterisks (*) indicate a significant difference ($P \leq 0.05$) between TCDD and vehicle treatment groups determined by two-way ANOVA and Dunnett's *post-hoc* test for ORO and Students t-test for PSR

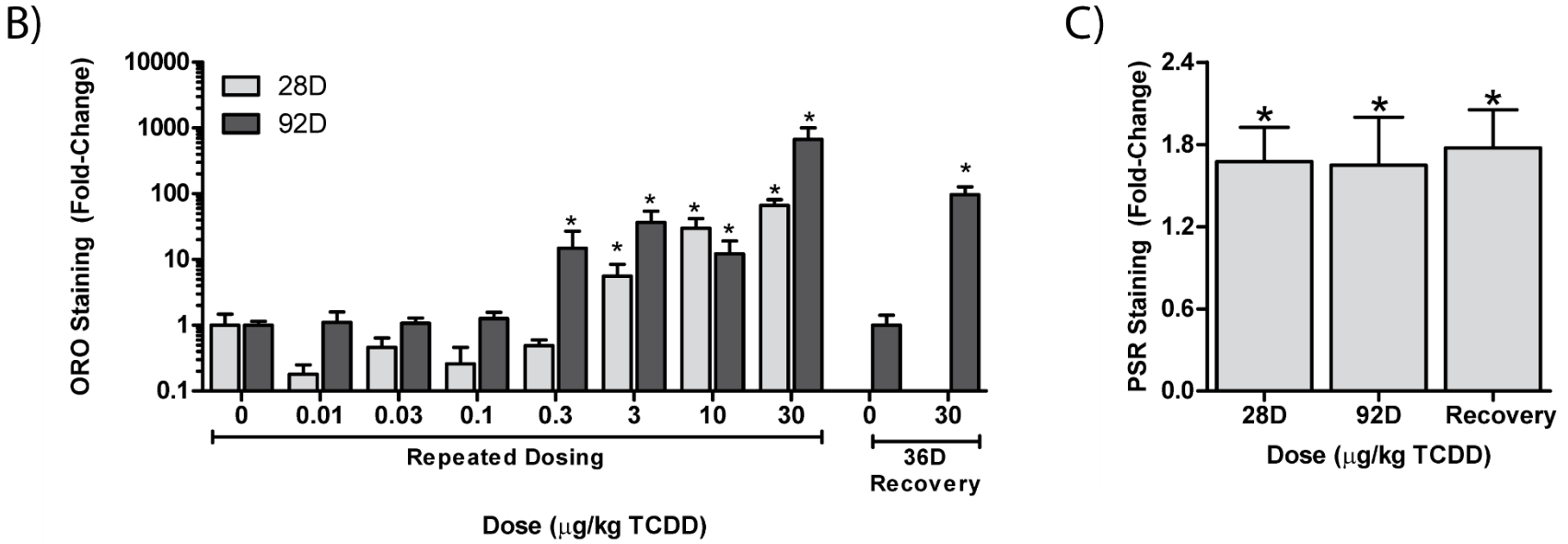

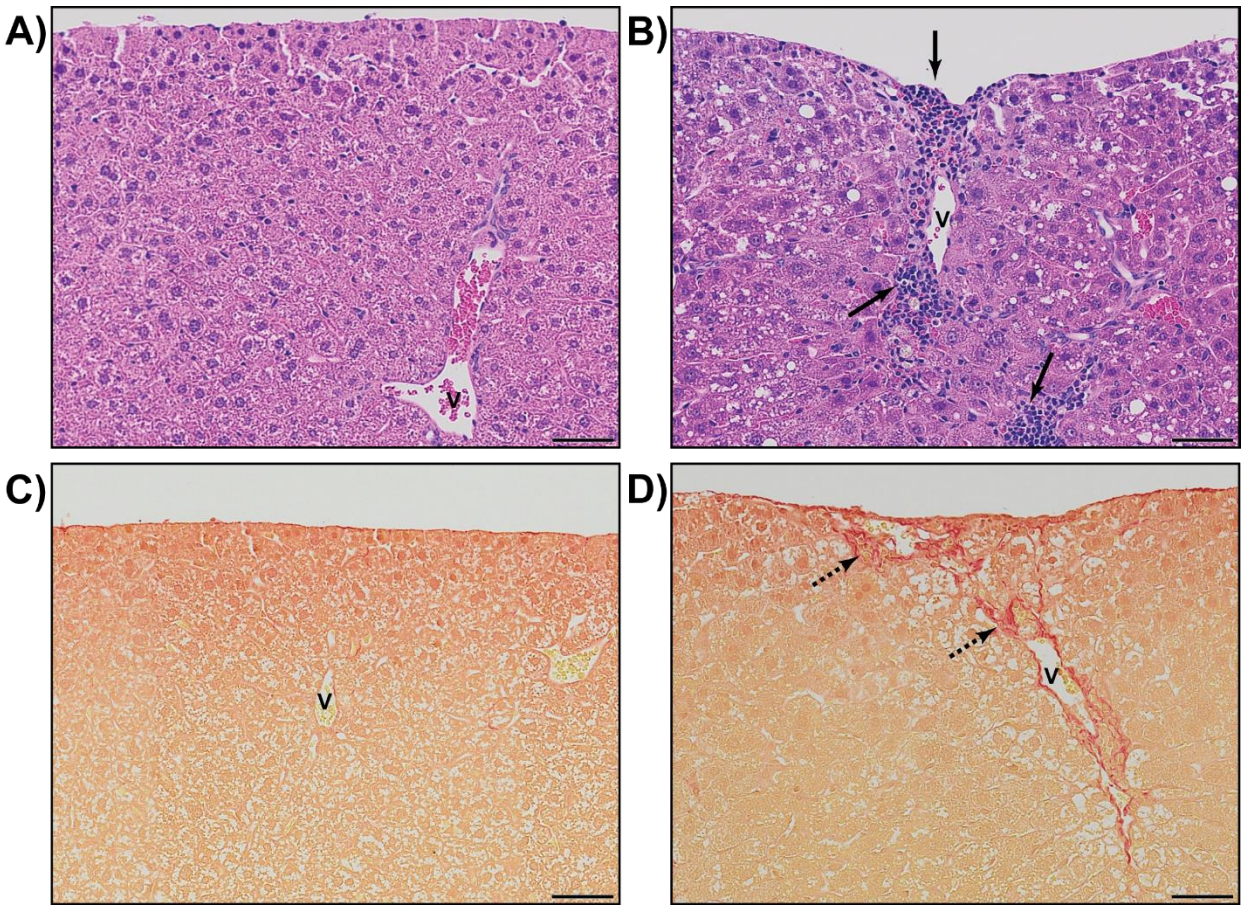


**FIGURE 25. REPRESENTATIVE MICROGRAPHS OF HEPATIC DIMPLING**

Representative histological micrographs of liver sections from mice gavaged with (A,C) sesame oil vehicle or (B,D) 30 µg/kg TCDD every 4 days for 92d demonstrating dimpled regions of the visceral surface. Hematoxylin and eosin staining (H&E; A,B) illustrates inflammatory infiltration while PicroSirius Red (PSR; C,D) demonstrates collagen deposition. Scale bar represents 50 µm. Portal veins are labeled with the letter v while inflammation is denoted by a solid arrow and collagen deposition by a dashed arrow.

**DIFFERENTIAL GENE EXPRESSION IN THE LIVER**

In our published 28 d dataset (GSE62902), 17,464 unique Ensembl annotated genes were detected, 3,406 of which were differentially expressed while at 92 d 19,935 unique genes were expressed (min count ≥ 5) with 4,575 differentially expressed using |fold-change| ≥ 1.5 and P1(*t*) ≥ 0.8 criteria. The larger number of detected genes may be due to differing sequencing depths

which confounds direct read count comparisons, but still allows for fold-change comparisons. 2,233 DEGs were conserved in both datasets with those unique to a single time-point largely representing lower fold changes. Overall, the same genes exhibited the greatest induction or repression at both time-points. Comparative analysis found >90% of the 2,233 common DEGs were positively correlated (similar responses) for both fold-change and P1(*t*) values (Figure 26; quadrant I). 98% of the expression patterns were positively correlated illustrating the similarity between these datasets (Figure 26; quadrants I and IV). In many cases, 92d DEGs exhibited

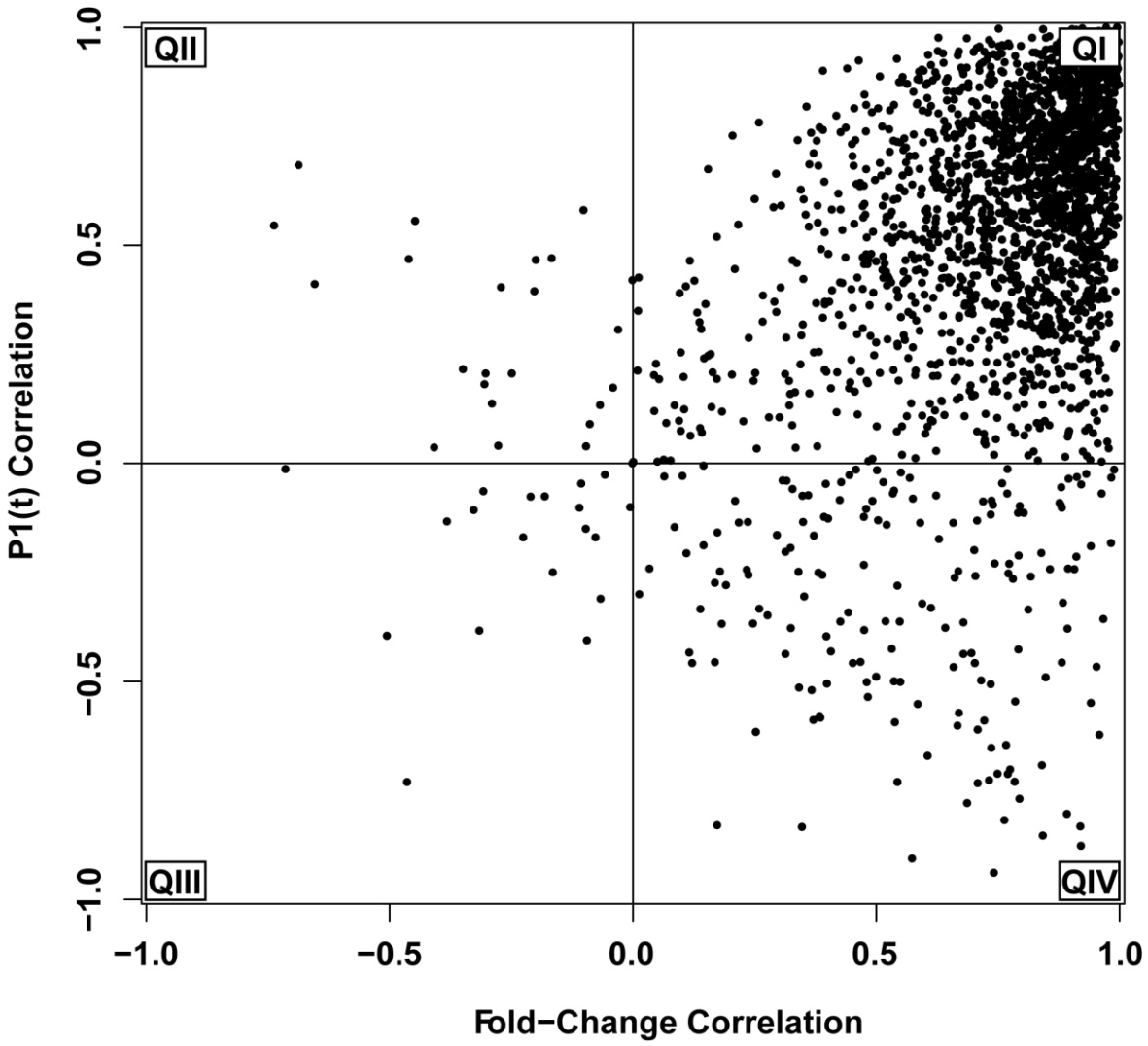


**FIGURE 26. CORRELATION OF TCDD-ELICITES GENE EXPRESSION CHANGES AT 28 AND 92D**

**FIGURE 26 (cont'd)**

Correlation analysis of differentially expressed genes (|fold-change| ≥ 1.5 and P1(*t*) ≥ 0.8) at both 28 and 92d. Quadrant I represents highly correlated genes in both expression and P1(*t*) values, II in P1(*t*) values only, III in neither P1(*t*) or gene expression values, or IV in gene expression changes only.

differential expression at lower doses (~36% or 80% at lower or equal dose, respectively) and larger fold changes (~60%) compared to 28 d DEGs. For example, *Cd36*, a lipid transporter integral to TCDD-induced hepatic steatosis [28] was induced at 0.03 µg/kg at 92 d compared to 1 µg/kg at 28 d with 9.2-fold and 3.2-fold increases, respectively. Not surprisingly, *Cyp1a1* and *Cyp1b1* exhibited the highest induction at 28 d (1,250- and 807-fold, respectively) and 92 d (1,228- and 578-fold, respectively).

**INCREASED ASCORBIC ACID BIOSYNTHESIS SUPPORTS FIBROSIS**

LC-MS/MS analysis detected 132 urinary metabolites, of which 39 were altered by treatment. MetPA analysis identified phenylalanine and tryptophan metabolism as the most enriched pathways (over-represented altered metabolites within a pathway) while most impacted pathways (high connectivity among altered metabolites) included the TCA cycle, alanine, aspartate and glutamate metabolism, glycolysis and gluconeogenesis, and ascorbate and aldarate metabolism (Figure 27).

Urinary metabolomic analysis was marked with a 124-fold increase in ascorbic acid, the largest measured metabolite change in TCDD treated animals. Similarly, hepatic levels of ascorbic acid were also increased 1.3-fold. Interestingly, glycogen is used as substrate for ascorbic acid biosynthesis which serves important roles in anti-oxidant response, iron homeostasis, and collagen synthesis [29]. Unlike humans and other vertebrates, mice synthesize ascorbic acid due to the expression of *Gulo* (21). Downstream from glycogenolysis, R*gn*, a gene involved in ascorbic acid synthesis was repressed 2.8-fold with AhR enrichment (Figure 28B).

However, *Gulo*, the rate-limiting step in ascorbic acid synthesis was induced 2.0-fold, consistent with increased urinary levels. Ascorbic acid is a required cofactor for prolyl 4-hydroxylase (*P4h*), a 2-oxoglutarate dioxygenase that catalyzes the hydroxylation of free proline and the post-translational hydroxylation of proline in collagen. Consequently, changes in ascorbic acid metabolism are consistent with TCDD-elicited fibrosis.

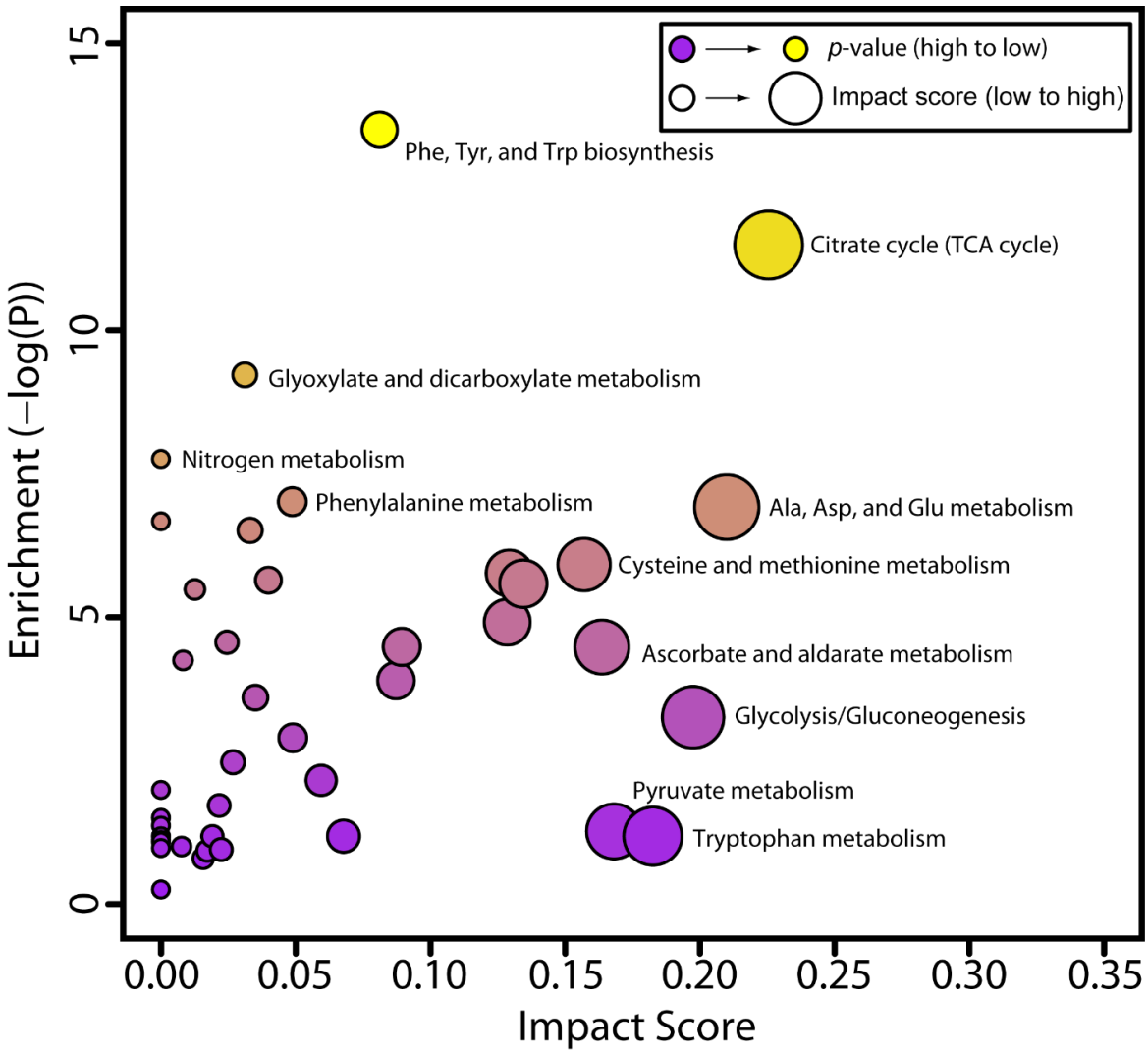


**FIGURE 27. METABOLIC PATHWAY ENRICHMENT ANALYSIS OF ALTERED URINARY METABOLITES**

Metabolic pathway enrichment analysis (MetPA) of urinary metabolites altered by TCDD ($P \leq 0.05$). Pathway alterations were considered significant when enrichment values (pathway over-representation) ≥ 4.0. Impact scores (connectedness of altered metabolites) were used to rank pathways most affected by TCDD treatment

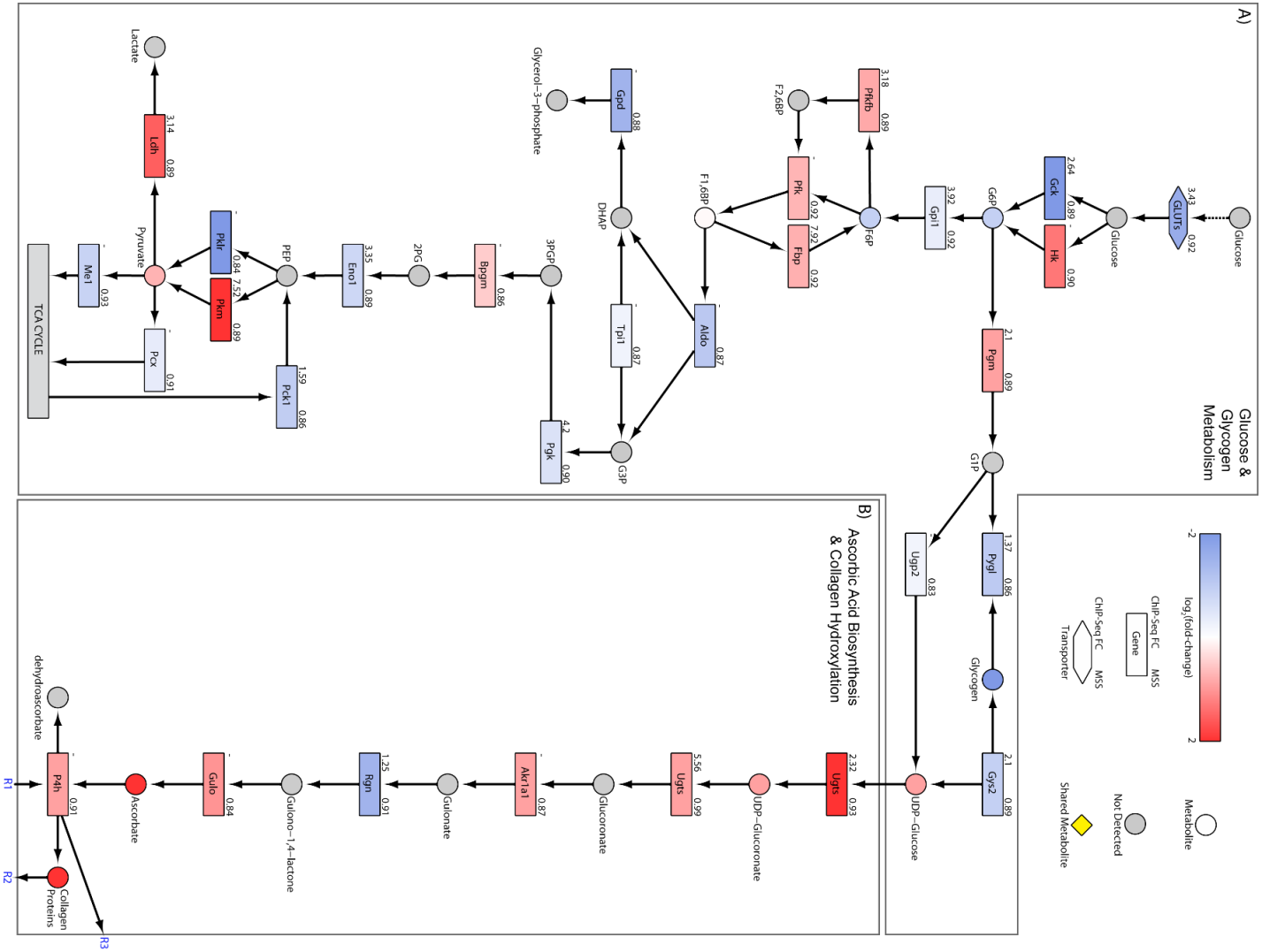


**FIGURE 28. INTEGRATION OF OMICS DATA FOR CARBOHYDRATE, ASCORBIC ACID, AND PROLINE METABOLISM PATHWAYS**

**FIGURE 28 (cont'd)**

Integrative analysis of (A) glucose and glycogen, (B) ascorbic acid, and (C) hydroxyproline metabolism (D) proline metabolism, and (E) glutamine uptake. The color scale represents the $\log_2$(fold-change) for genes and metabolites. Gray indicates metabolites not measured or detected. Genes are identified as rectangles, metabolites as circles, and transporters as hexagons. Values in the upper left corner of genes provides the maximum AhR enrichment fold-change while upper right corner indicates the highest pDRE MSS. Text in blue indicates a reaction extending into a separate panel. An expandable and interactive version that provides additional information can be viewed at http://dbzach.fst.msu.edu/index.php/supplementarydata.html.

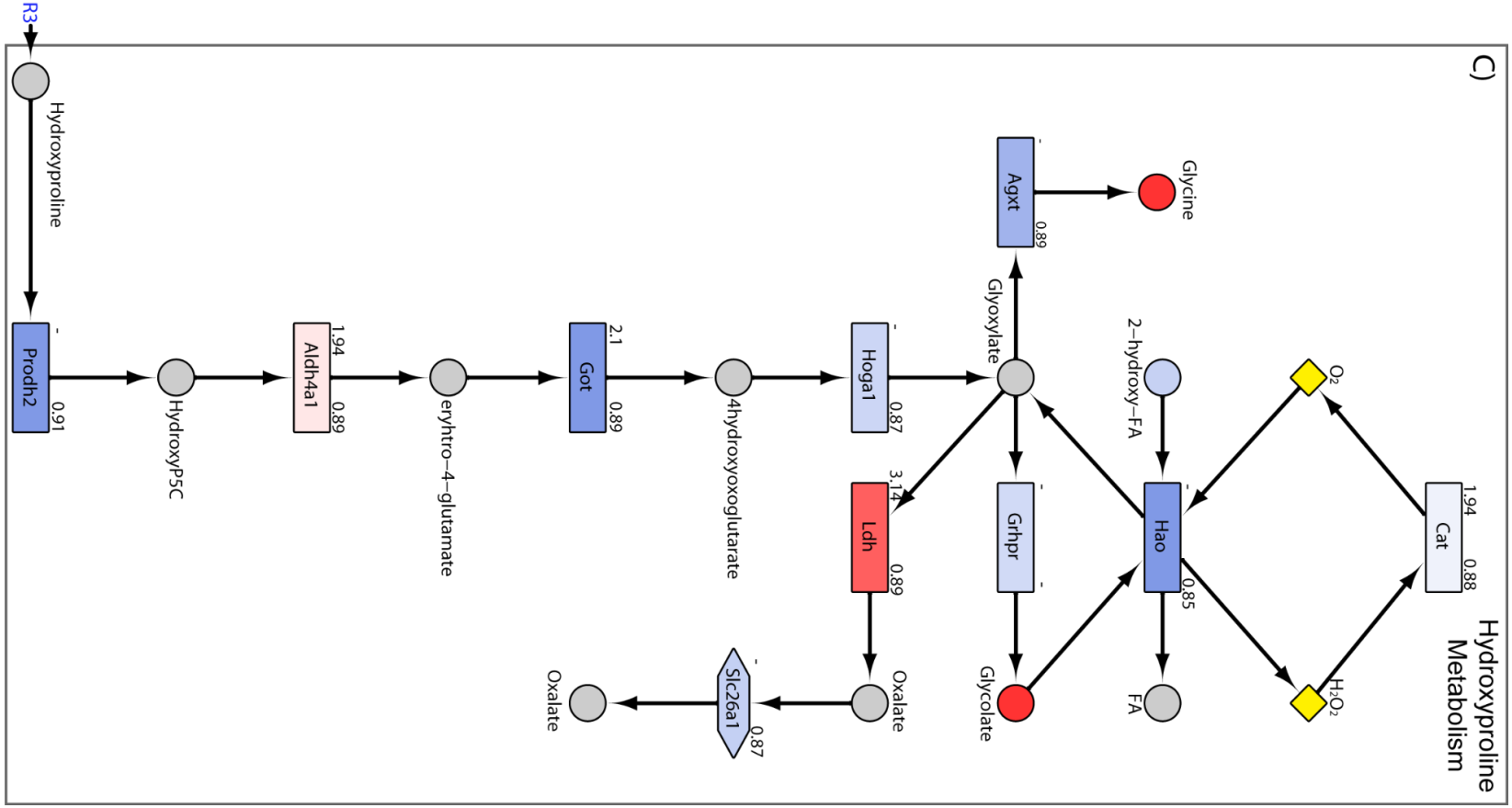

**FIGURE 28 (cont'd)**

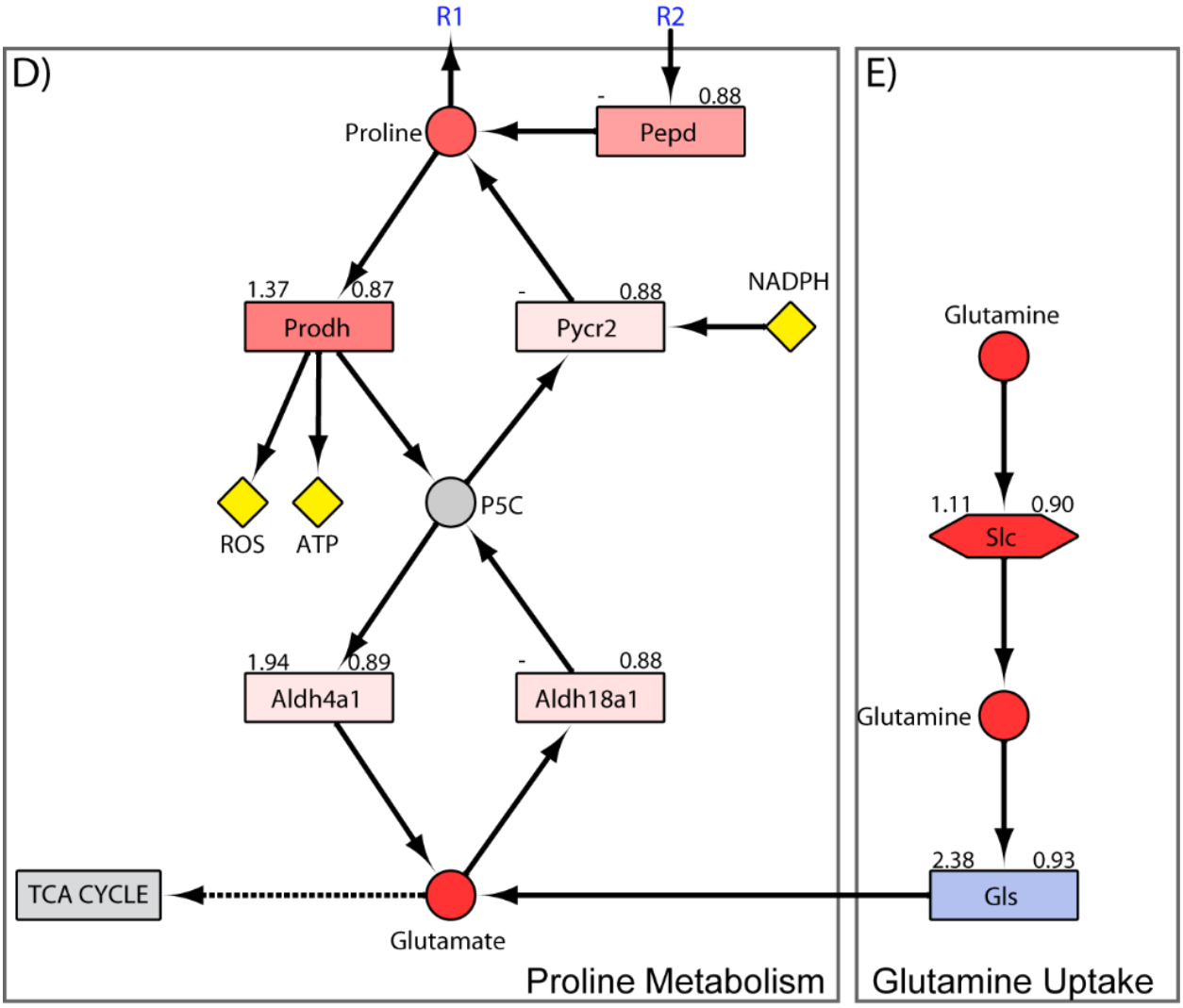

## ALTERED GLUCOSE AND GLYCOGEN METABOLISM

Insulin, which plays an important role in glucose homeostasis, was within the normal range (~0.5 ng/mL) in all groups (Figure 29A). However, adiponectin which is secreted by adipocytes

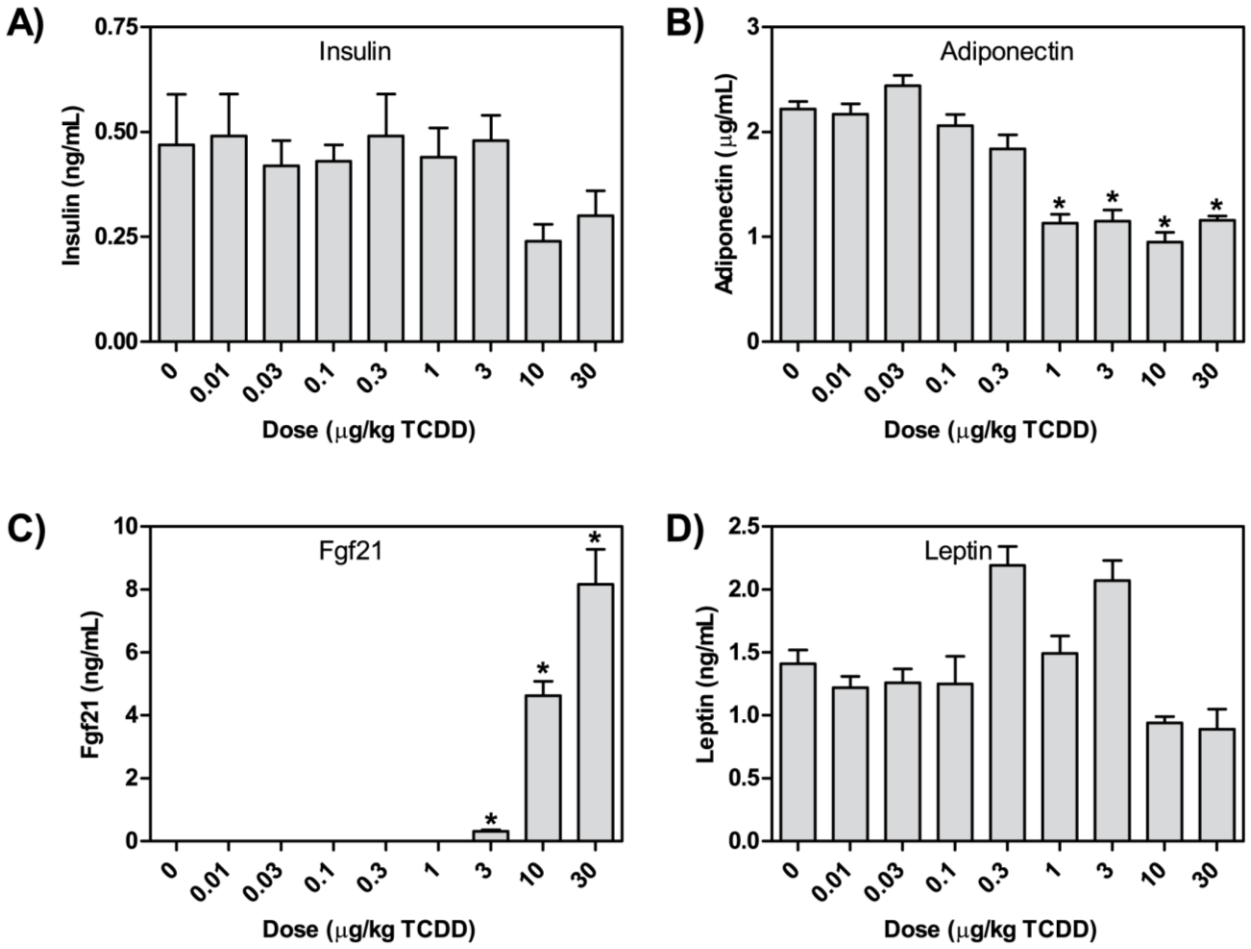


**FIGURE 29. SERUM ADIPO/HEPATOKINE LEVELS**

Serum levels of (A) insulin, (B) adiponectin, (C) FGF21, and (D) leptin were determined in mice orally gavaged with TCDD every 4 days for 92 days. Cytokines were determined using Meso Scale Discovery V-Plex assay kits. Adiponectin and FGF21 were determined by ELISA. Bars represent mean + SEM (n = 4-5). Asterisks (*) indicate a significant difference ($P \leq 0.05$) compared to vehicle control determined by one-way ANOVA and Dunnett's post-hoc test.

to regulate glucose and lipid metabolism, and improve insulin sensitivity [30], decreased from 2.2 µg/mL in controls to 1.2 µg/mL at 30 µg/kg TCDD (Figure 29B). Conversely, hepatic FGF21 which also regulates glucose and lipid metabolism by increasing sensitivity to insulin [30], was induced

from undetectable levels to 8.2 ng/mL at 30 µg/kg TCDD (Figure 29C). *Fgf21* mRNA was induced 17.2- and 6.2-fold at 28 and 92 d, respectively. No AhR enrichment as observed, unlike previous reports [31, 32] which could be accounted for by differences in treatment duration and model.

OGTTs were performed at days 31, 63, and 96 on vehicle and 30 µg/kg TCDD treated groups to further examine hepatic glucose metabolism reprogramming (Figure 30A-C). Although basal fasted blood glucose levels did not differ (Table 5), consistent with unaltered insulin levels, TCDD-elicited a dose-dependent decrease in hepatic glucose and glycogen levels (Figure 30D-E), and improved glucose tolerance suggesting increased glucose uptake and metabolism. This is consistent with the 1.7- and 2.0-fold induction of rate-limiting hexokinases *Hk2* and *Hk3*, although the glucose transporter *Glut2* (*Slc2a2*) and glucokinase (*Gck*) were repressed 3.4- and 8.0-fold, respectively (Figure 28). TCDD-elicited metabolic reprogramming is marked by pyruvate kinase (PKM) and glutaminase (GLS1) isoform switching [10] that may partially account for the increase in hepatic glucose metabolism. At 92d, total PKM protein levels increased 2.7-fold, matched by a 2.7-fold increase in PKM2 and no change PKM1 (Figure 31). A concomitant decrease in pyruvate carboxykinase (PEPCK-C; *Pck1*) mRNA (2.0-fold at 28 and 92d) and protein (1.4-fold; *P*-value=0.06) with a 4.0-fold increase in AhR enrichment is in line with TCDD-elicited repression of gluconeogenesis (Figure 31) [33].

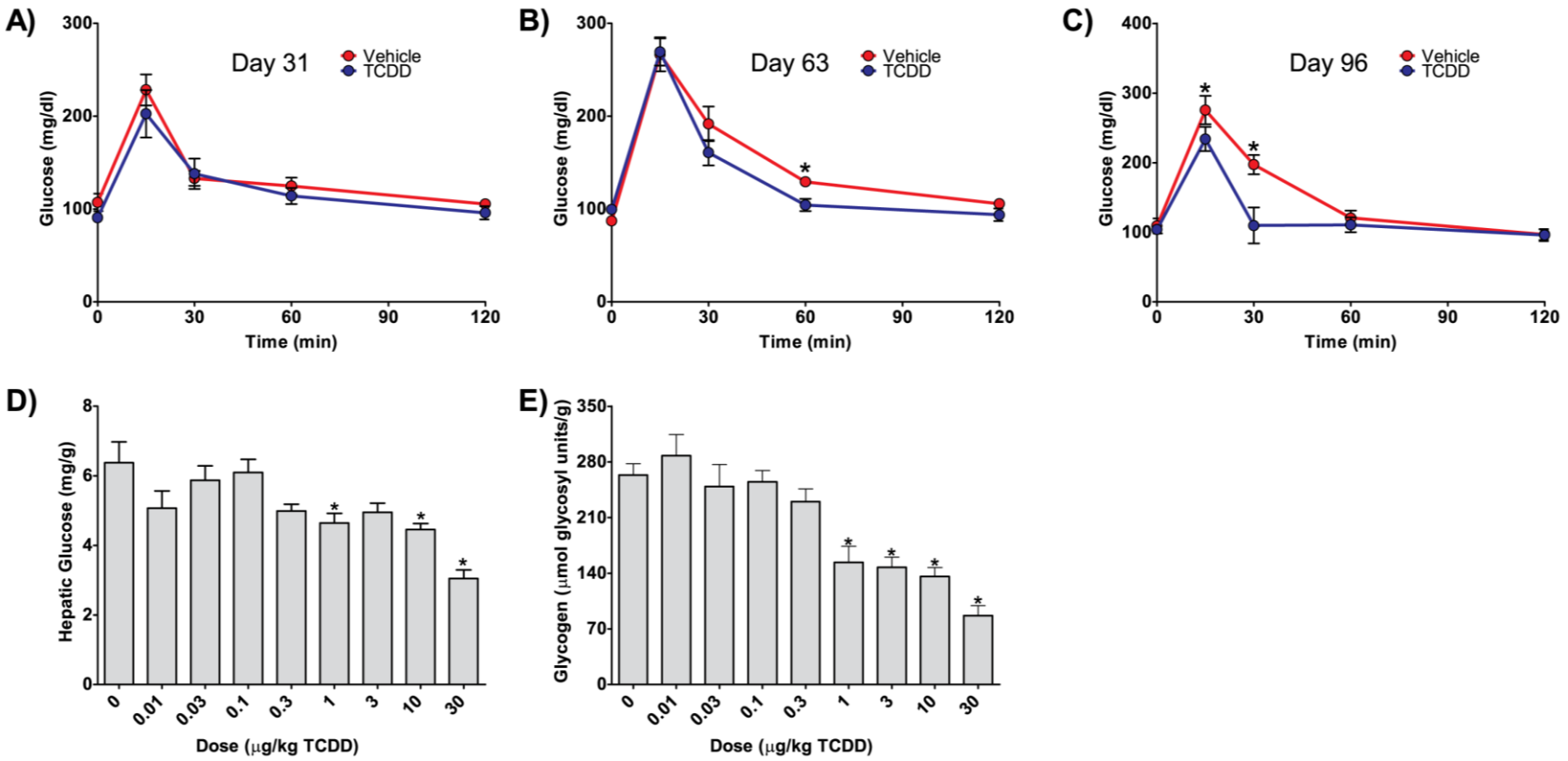


**FIGURE 30. ORAL GLUCOSE TOLERANCE TESTS AND HEPATIC GLUCOSE AND GLYCOGEN CONTENT**

Glucose and glycogen homeostasis. Oral glucose tolerance tests (OGTT) at (A) 31 d, (B) 63 d, and (C) 96 d following oral gavage with sesame oil (red) or 30 µg/kg TCDD (blue) every 4 days in female C57BL/6 mice. Values represent mean ± SEM for 5 animals (n = 5). Dose-dependent changes in hepatic (D) glucose or (E) glycogen levels at 92 d. Values represent mean + SEM for 5 animals (n=5). Asterisks (*) indicate a significant difference ($P \leq 0.05$) determined by repeated measures two-way ANOVA for the OGTT and one-way ANOVA followed by Dunnett's *post-hoc* test for hepatic glucose and glycogen levels.

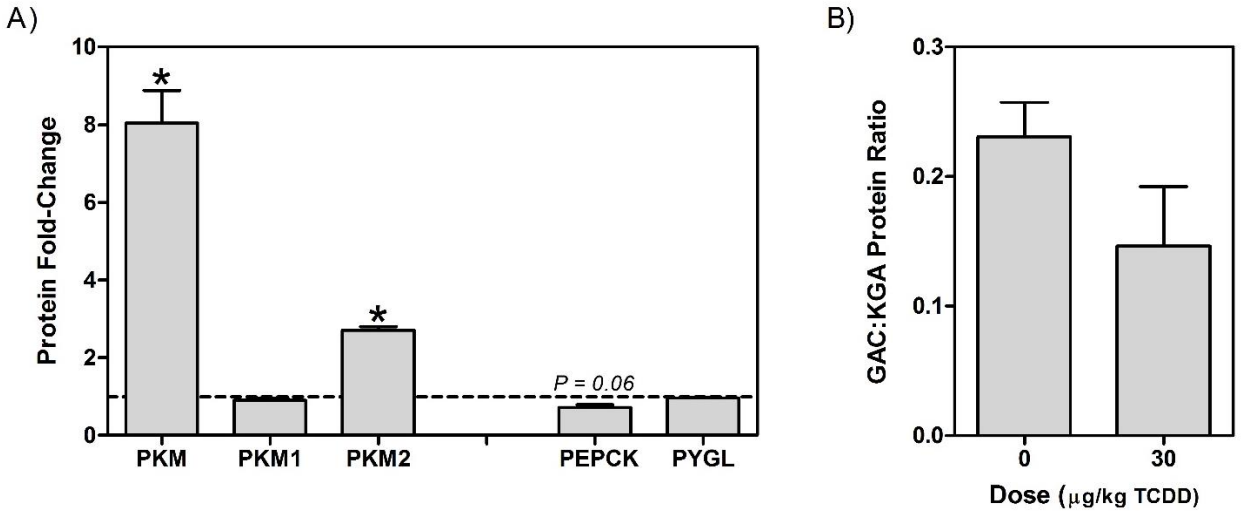


**FIGURE 31. HEPATIC PROTEIN LEVEL MEASURES IN TCDD TREATED MICE**

Hepatic protein level of (A) *PKM* isoforms, *PEPCK*, and *PYGL*, and (B) ratio of *GLS1* isoforms *GAC* and *KGA* following gavage of sesame oil vehicle or 30 µg/kg TCDD every 4d for 92d. Values represent mean + SEM for at least 4 animals (N=4-5). **P* ≤ 0.05 compared to vehicle control, Students t-test.

Moreover, genes associated with glycogen catabolism including *Pgm*, *Ugdh*, and *Ugt1a6a* were induced 1.7-, 7.5-, and 2.1-fold, respectively. However, expression of glycogen phosphorylase (*Pygl*) which catalyzes the rate-limiting step in glycogen breakdown was repressed 2.1-fold. The repression was not reflected at the protein level (Figure 31). ChIP-Seq analysis identified enrichment within *Pygl*, *Pgd*, *Ugdh*, *Ugt1a6a* genomic regions (Figure 28A-B) implicating AhR regulation. Glycogen synthase (*Gys2*) which is involved in the biosynthesis of glycogen was downregulated 1.9-fold and showed a 2.7-fold increase in AhR genomic binding. Taken together, these results suggest glucose is not being stored as glycogen, and is likely being catabolized in TCDD treated animals.

**EFFECTS OF TCDD ON THE MATRISOME**

Fibrosis is an initial form of tissue repair that progressively impairs function following chronic disease or persistent damage. It is defined by the excessive deposition of ECM, the non-cellular component of all tissues and organs that provides not only scaffolding, but also initiates signaling required for morphogenesis, differentiation, homeostasis and function. In addition, it acts as a growth factor reservoir and selective filter to control the flow of materials between cells. Qualitative and quantitative changes in ECM composition not only affect tissue function, elasticity, tension, and compression strength, but also cell integrity and viability. While characterized by collagen deposition, fibrosis involves interactions between the ~1100 ECM structural and associated proteins that constitute the matrisome, including a core set ~300 human and mouse collagens, proteoglycans and glycoproteins [6]. This includes: (i) fibrous proteins such as collagens, elastins, fibronectins, and lamins, and (ii) interstitial proteoglycans that provide unique tissue buffering, hydration, binding, lubrication, and force-resistance properties [34]. In addition to PSR staining along hepatic portal tracts (Figure 24), 344 matrisomal genes exhibited differential expression with 55 possessing AhR enrichment (Figure 33).

Several collagen genes exhibited differential expression including *Col4a3*, *Col4a4* and *9a2* which were upregulated 5.7-, 2.1-, and 206-fold at 92d, respectively (Figure 33A), with AhR enrichment, although only *Col4a3* contained a pDRE. Biosynthesis of collagen triple helixes is a complex multistep process beginning with post-translational proline hydroxylation and crosslinking by prolyl 4-hydroxylases (*P4h*) *a2* (induced 1.8-fold) and *b* subunits requiring oxygen, $Fe^{2+}$, ascorbic acid, and α-ketoglutarate (Figure 28D). Hydroxylated proline is essential for the stabilization of the collagen triple helix. Similarly, lysyl oxidase (*Lox*) and lysyl oxidase-like (*Loxl*) 1, 2 and 3 which were induced 3.0-, 1.4-, 1.5- and 2.1-fold, respectively, and *Loxl4* repressed 7.7-fold also participate in the crosslinking of collagen. In the endoplasmic reticulum (ER), the procollagen triple helix peptide is then folded with the assistance of chaperone proteins such as *Hsp47* (*Serpinh1*) which was induced 1.7-fold. Procollagen is transported through the Golgi stacks

and secretory vesicles followed by cleavage of N- and C- terminal propeptides producing tropocollagen which spontaneously self-assemble into fibrils, and undergoes further LOX and LOXL crosslinking to produce mature collagen fibrils. Elastin which was induced 2.1-fold also associates with collagen while Transglutaminase (*Tgm*) *1*, *2* and *3* which add more cross-links that stiffen and decrease the solubility of the ECM, were induced 1.9-, 1.8-, and 11.5-fold, respectively.

Despite the prolonged induction of ECM structural genes, there is a lack of additional fibrotic accumulation between 28d and 92d (Figure 24). ECM is continuously turned over by enzymes associated with synthesis and degradation that allow the fine tuning of ECM remodeling. This includes the induction of various MMP, Adam, Adamt, heparanase proteases, and their inhibitors (e.g., *Timp*, *Serpin*, *A2m*) (Figure 33B). For example, MMPs degrade ECM to open up avenues for migration, and activate pro-factors stored within the ECM such as TGFβ. Among the 115 differentially expressed ECM regulators, only 19 showed AhR enrichment including *Adamts14* which was induced 2.4-fold with a 2.6-fold increase in AhR genome binding. Although typically associated with converting plasminogen to plasmin, urokinase/tissue type plasminogen activators (*Plau*/*Plat*) which were induced 1.9- and 2.3-fold, respectively, also activate latent forms of TGFβ and pro-MMPs, and aid in the migration of collagen producing cells to damaged tissue [35]. *Serpine1* (commonly known as PAI-1), the predominant inhibitor of PLAU/PLAT, was induced 54.3-fold by TCDD. Therefore, SERPINE1 interaction with PLAU/PLAT could attenuate these responses. Conversely, *Lrp1* which clears proteases, protease inhibitors, and other fibrogenic factors following endocytosis, was repressed 1.6-fold [36]. In contrast to *Serpine1*, *Serpin a1*, *a3*, *b*, *c1*, *f2*, *g* and *i1* clades and isoforms, which inhibit trypsin, chymotrypsin, urokinase/tissue plasminogen activator, and fibrinolysis activity, were largely repressed with some exceptions (Figure 33B).

**EFFECTS OF TCDD ON PROLINE AND HYDROXYPROLINE METABOLISM**

Proline/hydroxyproline represents ~23% of the amino acids in collagen with glycine (~30%) and alanine (~20%) the other major residues [37]. Although hepatic extract levels of free glycine increased 20.3-fold, alanine and proline were reduced 2.0- and 2.4-fold, respectively (Figure 28). Proline serves multiple roles in metabolism including protein synthesis, cell signaling, and as a precursor for other amino acids. Moreover, during periods of cell stress, proline released during ECM remodeling can be used as substrate for ATP production [38]. ECM fragments from remodeling can serve as a substrate for prolidase (*Pepd*), a peptidase that hydrolyzes di- and tri-peptides to release C-terminal proline or hydroxyproline residues. Subsequently, proline dehydrogenase (*Prodh*) oxidizes proline to pyrroline-5-carboxylate (P5C) producing mitochondrial ATP and ROS, and the cytosolic P5C reductase 2 (*Pycr2*) then reduces P5C to proline at the expense of NADPH. TCDD induced *Pepd*, *Prodh* and *Pycr2* 1.9-, 2.1-, and 1.3-fold, respectively (Figure 28). Although hepatic proline levels are lower in treated animals, a 4.6-fold increase was observed in the serum. However, there was no evidence of altered expression of the proline transporters *Slc6a7* or *Sit1* suggesting intracellular hepatic proline is sequestered in collagen and that proline released by extrahepatic protein catabolism and *Pepd* activity may be elevating serum levels. Proline can also be synthesized from glutamine and *Slc1a5*, a glutamine transporter which is induced 10.7-fold by TCDD with a 2.9-fold increase in AhR enrichment. Glutamine is then deaminated to glutamate by glutaminase (*Gls*) which was induced 1.9-fold. Glutamate is a substrate for P5C synthetase (*Aldh18a1*) producing glutamic-γ-semialdehyde that spontaneously converts to P5C which can cycle back to proline producing ATP. Consequently, glutaminolysis may support proline cycling in addition to GSH biosynthesis in response to TCDD. However, the relevance of proline cycling to cellular bioenergetics in combating TCDD-elicited energy depletion and hepatotoxicity remains to be determined.

Hydroxyproline released during collagen turnover is not re-incorporated into protein [38] and is directed to glyoxylate synthesis to produce oxalate, glycolate, or glycine [39]. Paradoxically,

*Prodh2*, *Got1*, *Got2, and Hoga1* involved in the metabolism of hydroxyproline to glyoxylate are down-regulated 5.0-, 4.3-. 1.8-, and 1.7-fold, respectively (Figure 28C), suggesting pathway repression. Although glyoxylate, a highly reactive aldehyde, can be metabolized to glycine which was increased 20.3-fold in liver extracts, *Agxt* was repressed 2.6-fold. Similarly, glyoxylate reductase/hydroxypyruvate reductase (*Grhpr*) which uses NADPH to reduce glyoxylate to glycolate was also repressed 1.6-fold despite 2.3- and 4.0-fold increases in hepatic extracts and urine. Notably, *Hao1* which uses NADPH to convert glycolate to glyoxylate while generating ROS, was the most repressed gene with a 137.0- and 71.4-fold, at 28 and 92d, respectively. Therefore, HAO1 repression likely lowers oxidative stress, NADPH consumption, and the production of a reactive aldehyde. Lastly, glyoxylate metabolism by lactate dehydrogenase (*Ldh*) produces oxalate, a poorly metabolized dicarboxylic acid that can form tissue-damaging calcium oxalate crystals in the kidney. However, *Slc26a1* which exports oxalate from the liver into the blood was repressed 1.9-fold. Hydroxyproline tracer studies are required to determine the fate of hydroxyproline derived from collagen remodeling.

**PRO-INFLAMMATORY SIGNALING AND FIBROSIS**

As fibrosis progresses, the ECM is enriched with hyaluronan and versican (*Vcan*) which bind and trap inflammatory cells infiltrating the damaged tissue. Hyaluronan is a non-sulfated glycosaminoglycan polymer that increases in length with the addition of glucuronic acid and N-acetylglucosamine. It forms a pericellular coat through interaction with CD44 (induced 3.2-fold) that maintains the myofibroblast phenotype. TGFβ also increases hyaluronan retention in the ECM, thus creating an autostimulatory cycle since myofibroblasts secrete TGFβ [40]. Glucuronic acid, which is increased 2.7- and 2.6-fold in hepatic extracts and urine, respectively, is a metabolite in the TCDD-induced ascorbic acid biosynthesis pathway. N-acetylglucosamine is a product of the hexosamine biosynthesis pathway. *Gfpt1* and *2*, the rate limiting steps in the hexosamine biosynthesis, were induced 1.4- and 3.1-fold, respectively. In addition, *Uap1l1*, a

paralog of *Uap1*, which catalyzes the last step in N-acetylglucosamine synthesis, was also induced 4.4-fold. Furthermore, *Vcan*, an ECM proteoglycan, was induced 3.9-fold. High molecular weight hyaluronan also promotes the induction of IL-10, which was induced 3.0-fold (Figure 32A).

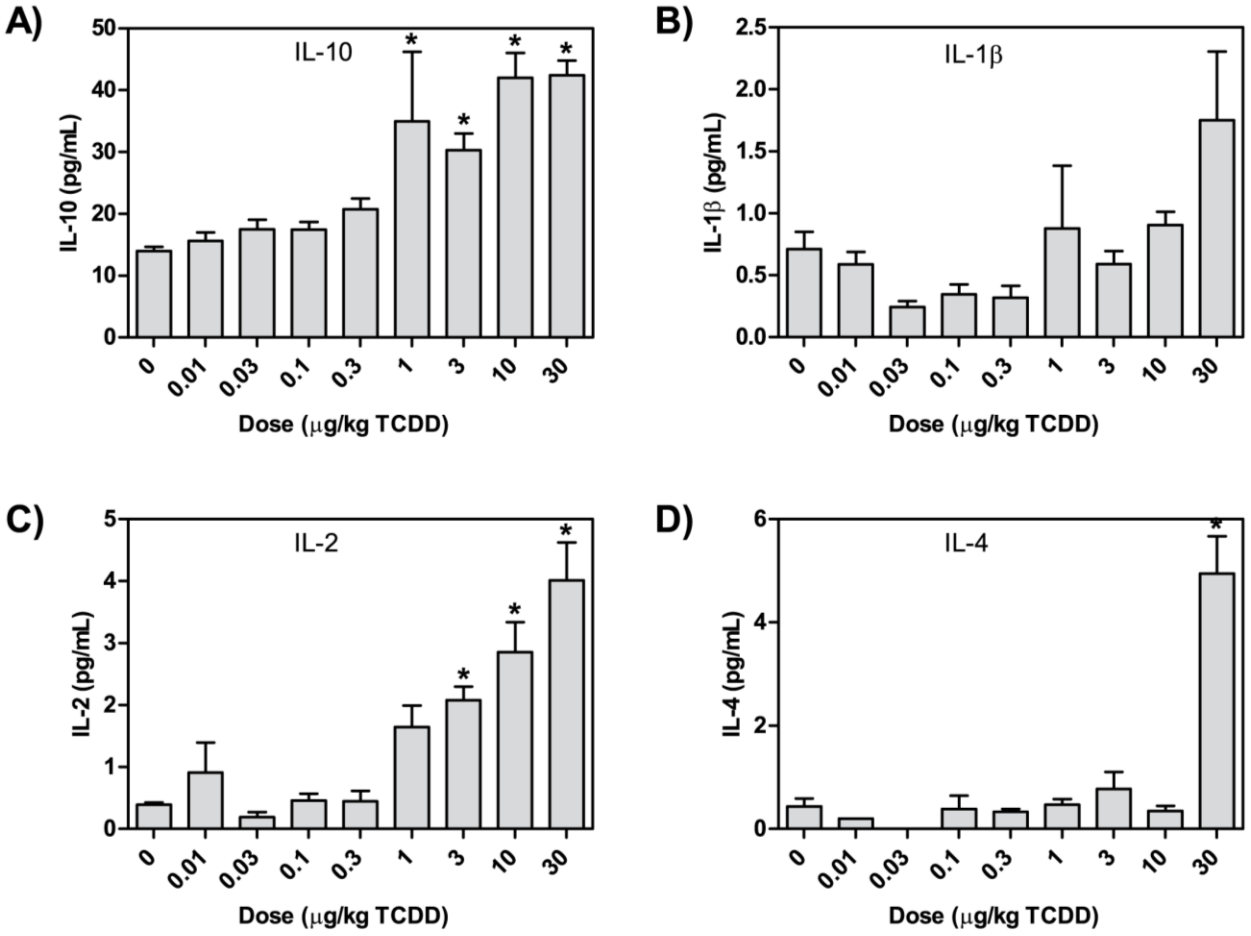


**FIGURE 32. SERUM CYTOKINE LEVELS IN TCDD TREATED ANIMALS**

Serum levels of cytokines (A) IL-10, (B) IL-1β, (C) IL-2, (D) IL-4, (E) IL-6, (F) TNFα, (G) IFNγ, (H) IL-12p70, (I) KC/GRO, and (J) IL-5 were determined in mice orally gavaged with TCDD every 4 days for 92 days. Cytokines were determined using Meso Scale Discovery V-Plex assay kits. Bars represent mean + SEM (n = 4-5). Asterisks (*) indicate a significant difference ($P \leq 0.05$) compared to vehicle control determined by one-way ANOVA and Dunnett's post-hoc test.

**FIGURE 32 (cont'd)**

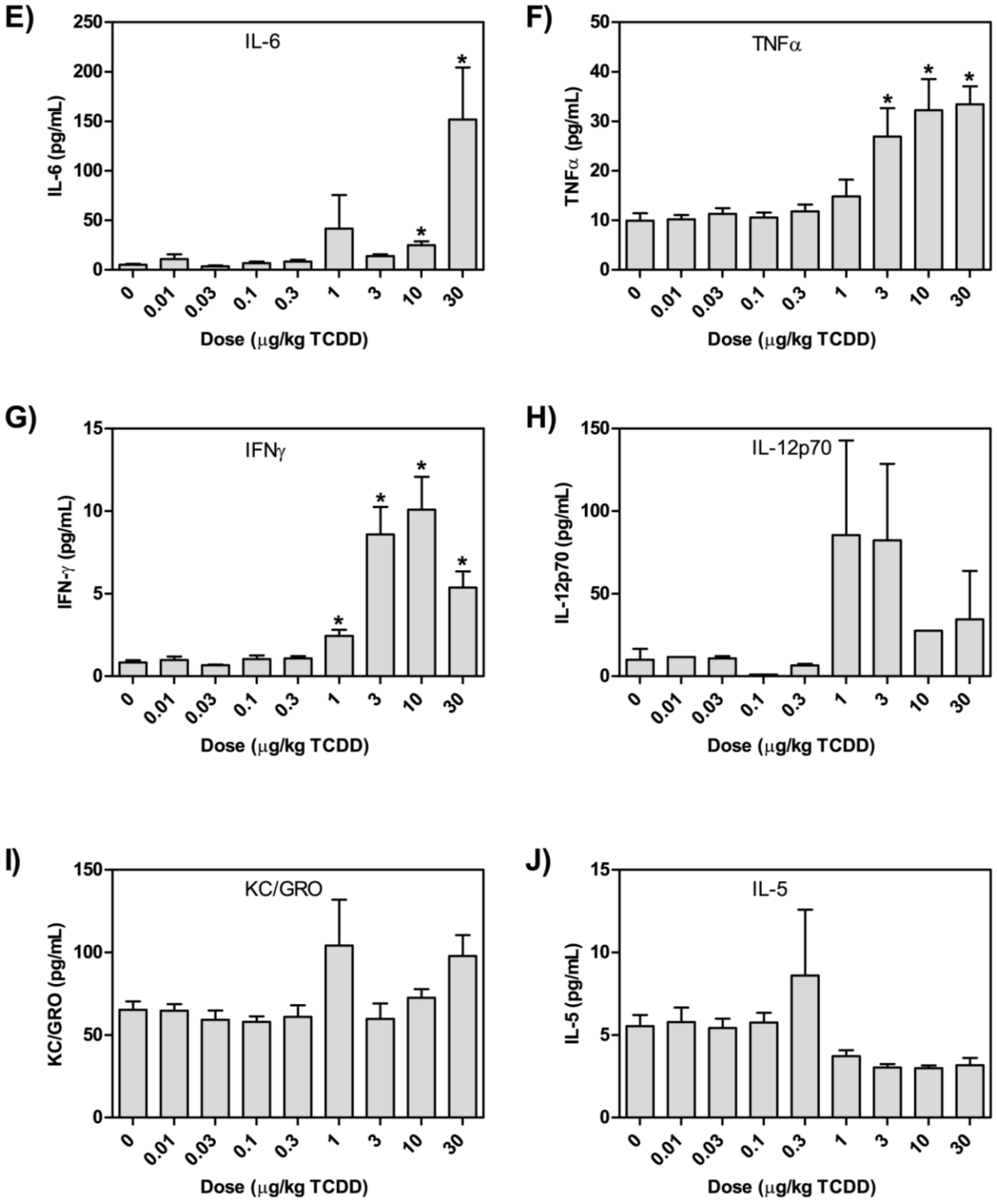

Injury to cholangiocytes, activated myofibroblasts, and hepatic macrophages also recruit immune cells such as circulating monocytes, T cells, and neutrophils due to proinflammatory mediator secretion. In accordance with hepatic inflammation (Figure 24), serum levels of IL-1β, IL-2, IL-4, IL-6, IL-10, TNFα, and IFNγ exhibited dose-dependent induction (Figure 32). The 2.4- and 28.7-fold increases of proinflammatory factors IL-1β and IL-6, respectively, and myofibroblast activation are consistent with an inflammatory–profibrogenic cycle resulting in ECM deposition along portal tracts. Myofibroblasts also release soluble hedgehog ligands which stimulate cholangiocytes to produce *Cxcl16* (induced 2.1-fold) and recruit NKT cells [8] that produce IL-2, IL-4, TNFα, and IFNy which were induced 13.3-, 20.3-, 3.3-, and 12.5-fold, respectively. Osteopontin (*Spp1*), a target of hedgehog transcription factors commonly induced in fibrotic liver disease, was induced 4.3-fold at 92d in the absence of AhR enrichment (Figure 33A). Other TCDD-elicited proinflammatory and immunogenic activities include the hepatic induction of *Il1a*, *Ccl2*, *Ccl3*, and *Ccl4* mRNA levels 1.9-, 1.7-, 1.7-, and 1.7-fold, respectively (Figure 33C). Countering these pro-inflammatory signals was the 28.7- and 58.1-fold induction of glycoprotein nonmetastatic melanoma B (*Gpnmb*), a macrophage expressed transmembrane glycoprotein that negatively regulates inflammation [41].

## TCDD-ELICITED EPITHELIAL TO MESENCHYMAL TRANSITION (EMT) AND ALTERED CELL ADHESION

Epithelial to mesenchymal transition (EMT) is commonly associated with fibrosis [42]. Collagen producing myofibroblasts are not detected in normal liver, but appear during the course of chronic liver disease, leading to fibrosis. HSCs, portal fibroblasts, bone marrow cells, epithelial cells, and endothelial cell have been identified as possible ECM sources [42]. These cells transition from an epithelial to a mesenchymal phenotype allowing them to polarize, migrate, invade, resist apoptosis, and produce ECM [9]. EMT is induced in response to DAMPS, immune

cell derived cytokines such as TGFβ, and the mechanical tension produced by infiltrating cells. Although *Tgfβ1* was only induced ~1.5-fold, *Tgfβ2* was induced 7.7-fold and 8.8-fold at 28 and

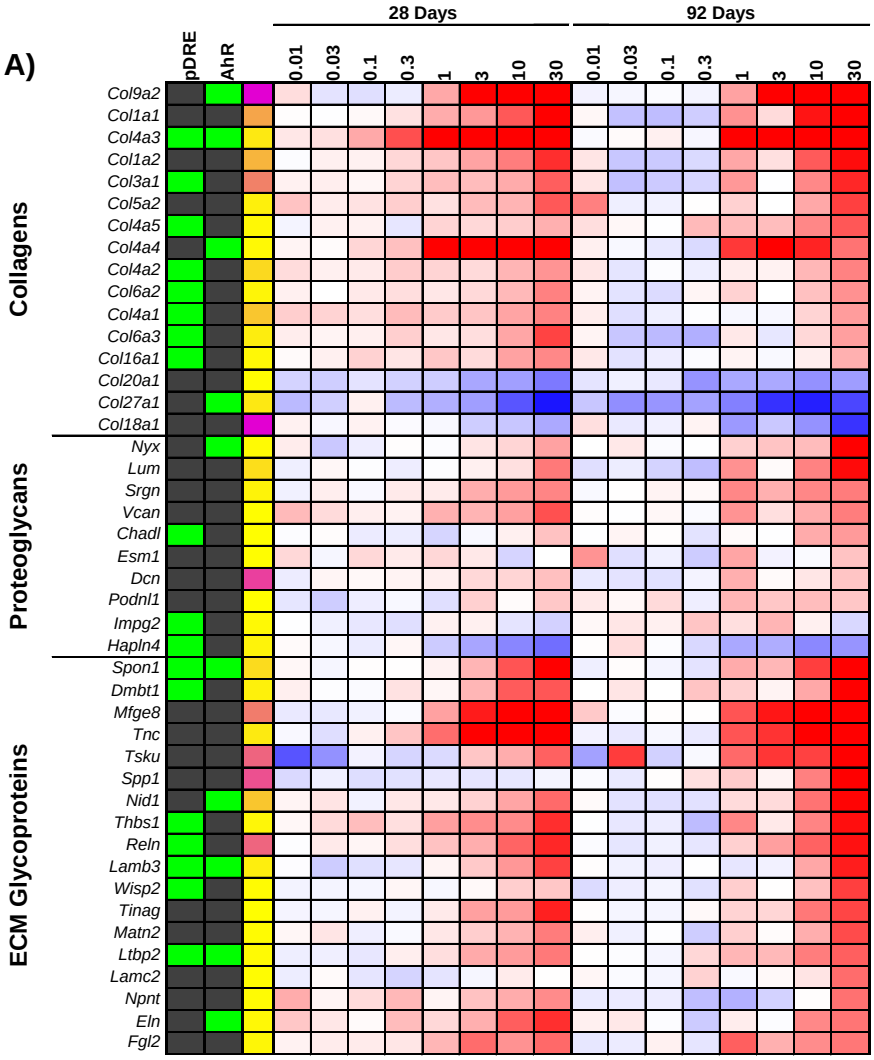


**FIGURE 33. CHANGES IN GENE EXPRESSION FOR GENES RELATED TO THE MATRISOME AND EXTRACELLULAR REMODELING**

Hepatic gene expression changes of the matrisome (http://matrisomeproject.mit.edu/) in mice gavaged every 4d for 28 or 92d categorized by (A) structural genes, (B) secreted factors, or (C) inflammatory chemokines and interleukins, (D) anchoring genes of the cadherin, integrin, and selectin families, and (E) epithelial and mesenchymal markers. The presence of pDREs (DRE; MSS ≥ 0.89) and AhR enrichment peaks (FDR ≤ 0.05) determined by ChIP-Seq [10] are shown as green boxes. Relative transcript representation describing the raw number of aligned reads to each transcript is shown to indicate potential importance of the genes function in the liver.

**FIGURE 33 (cont'd)**

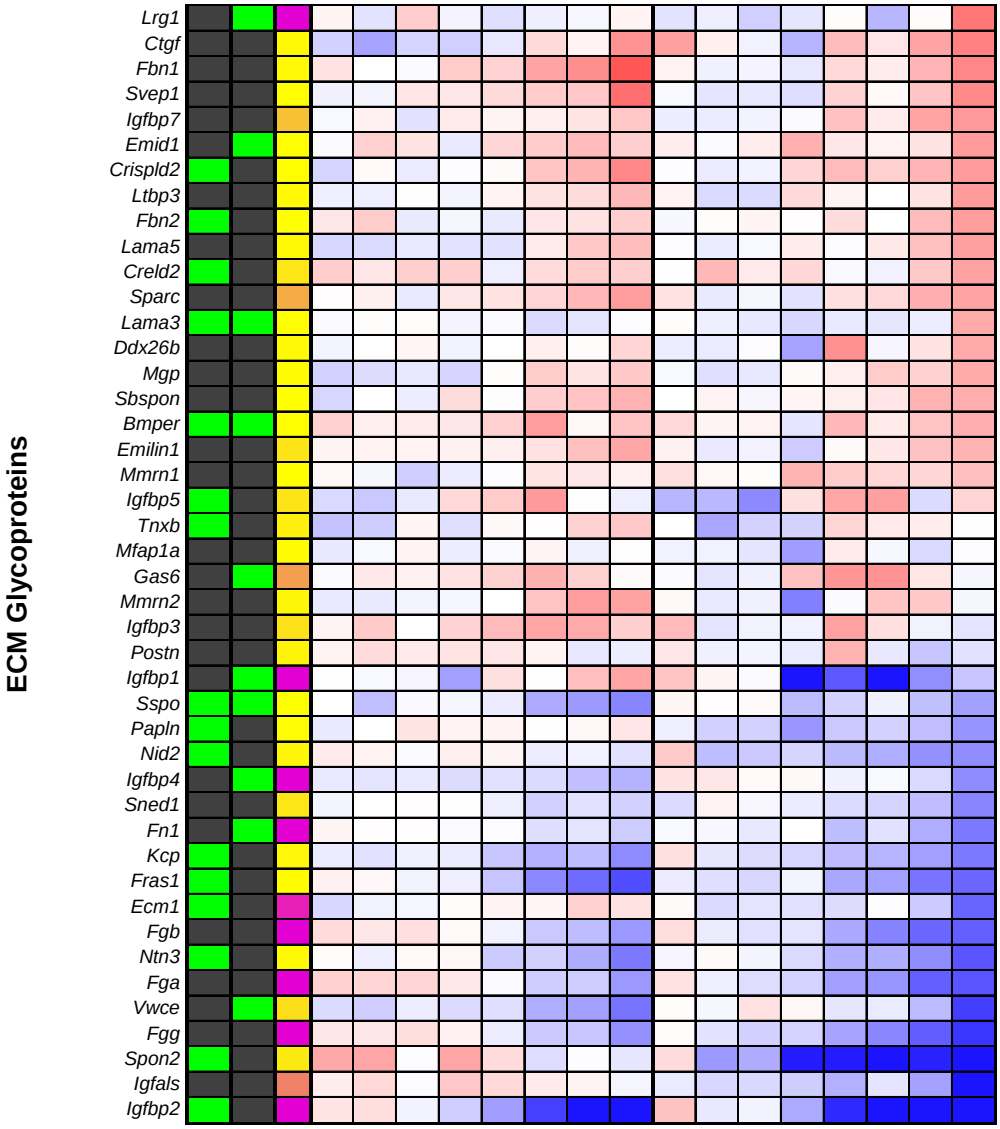

**FIGURE 33 (cont'd)**

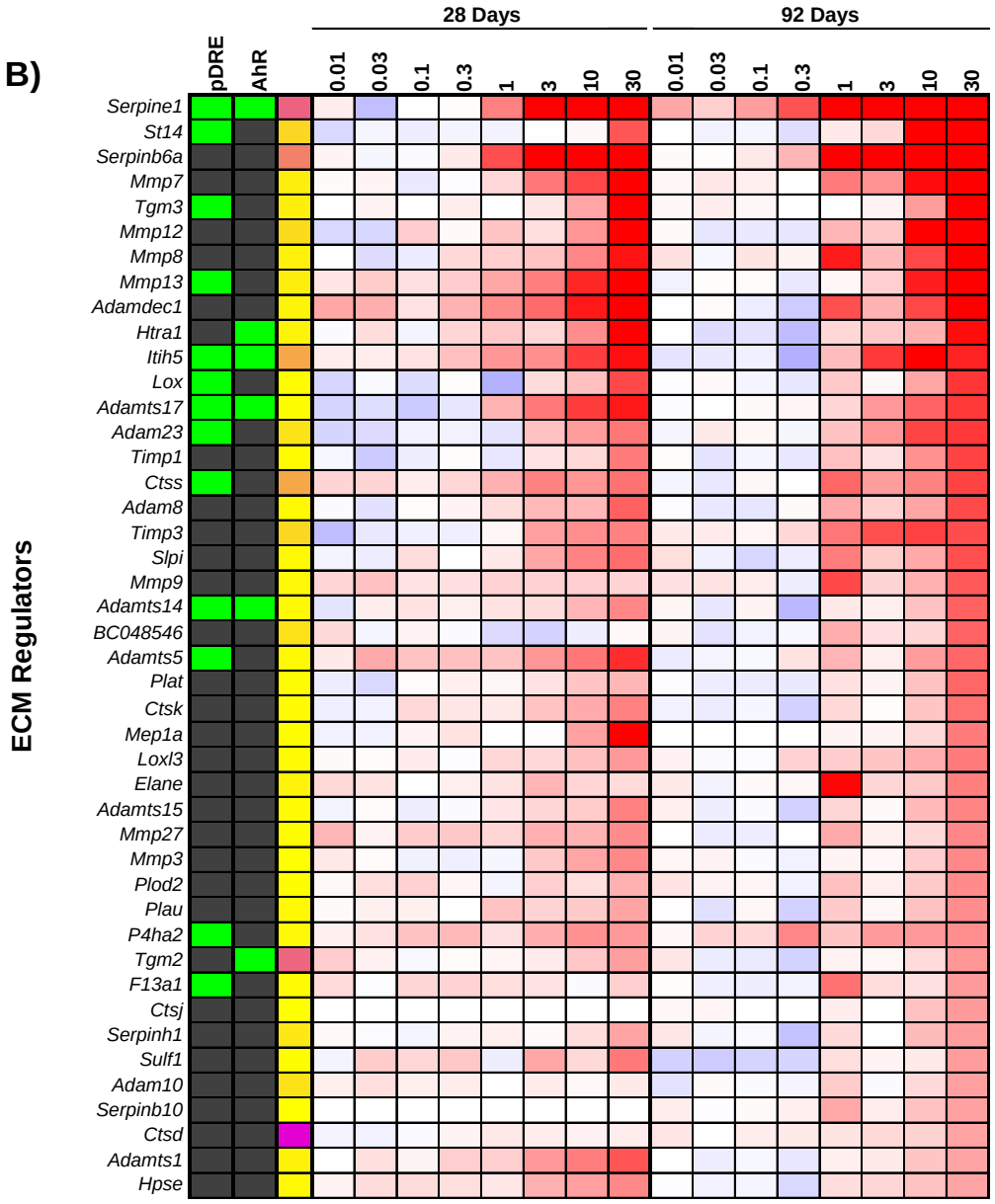

**FIGURE 33 (cont'd)**

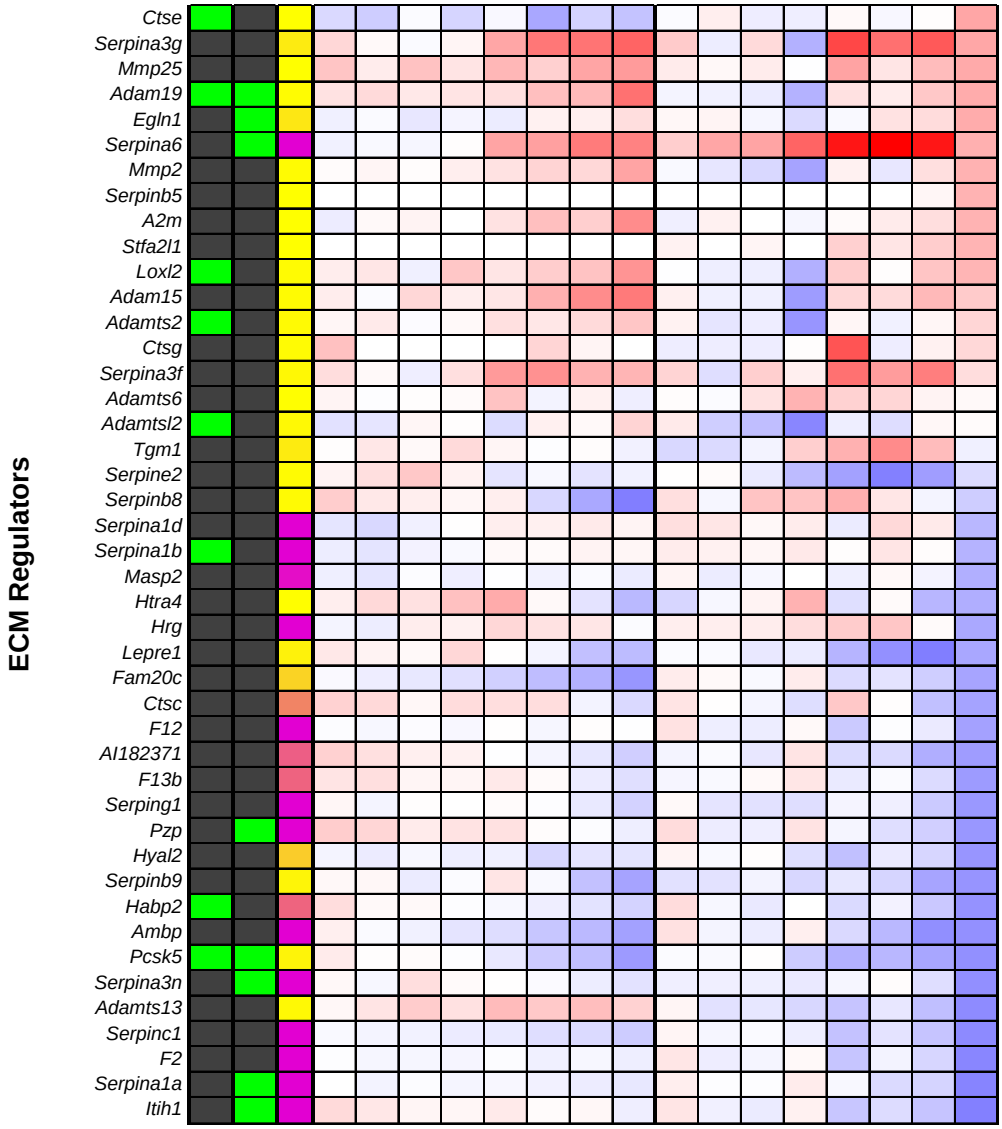

**FIGURE 33 (cont'd)**

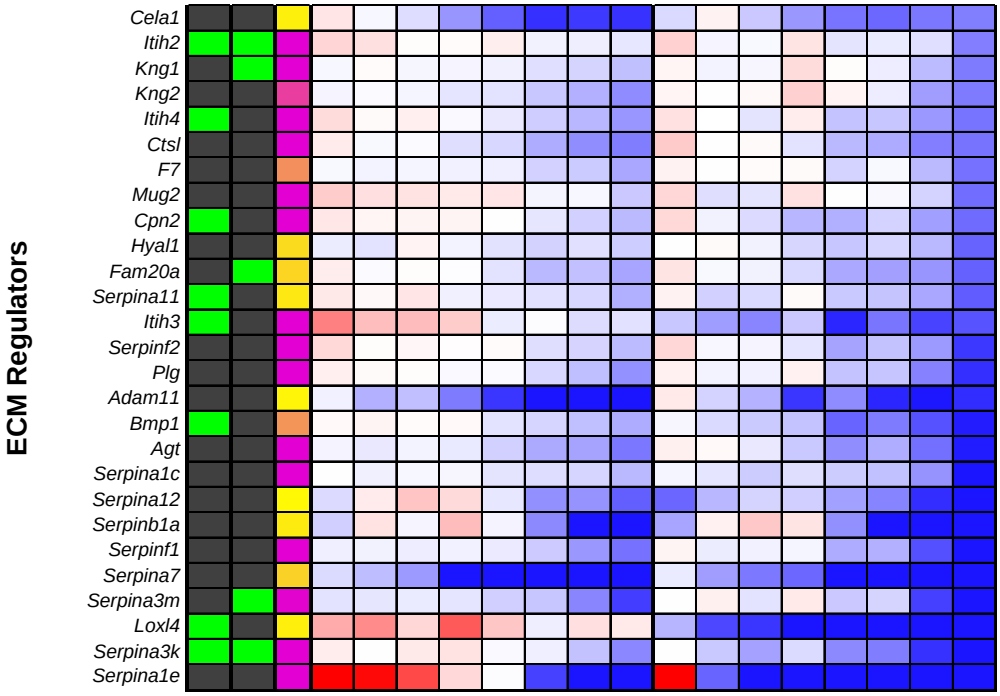

**FIGURE 33 (cont'd)**

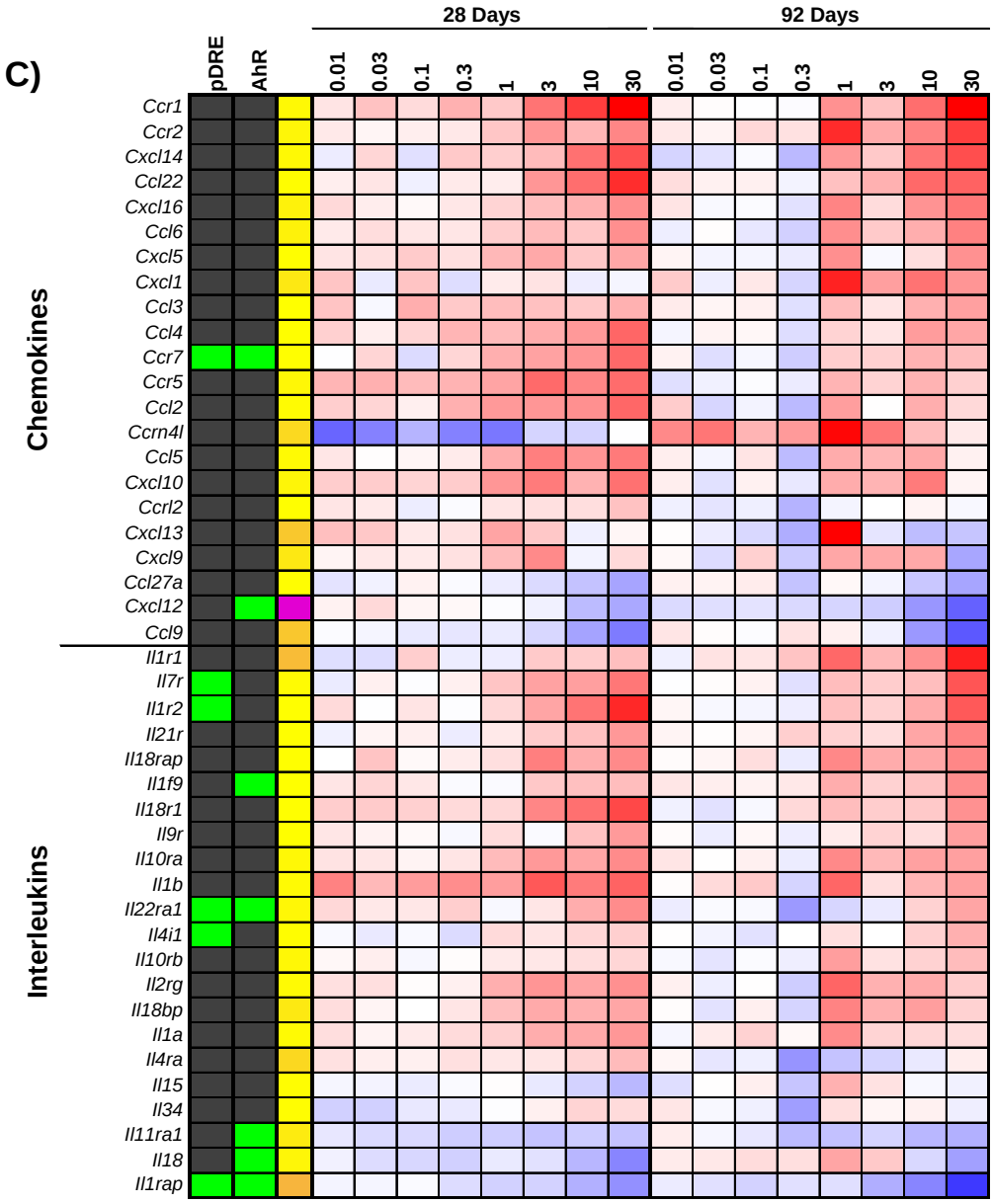

**FIGURE 33 (cont'd)**

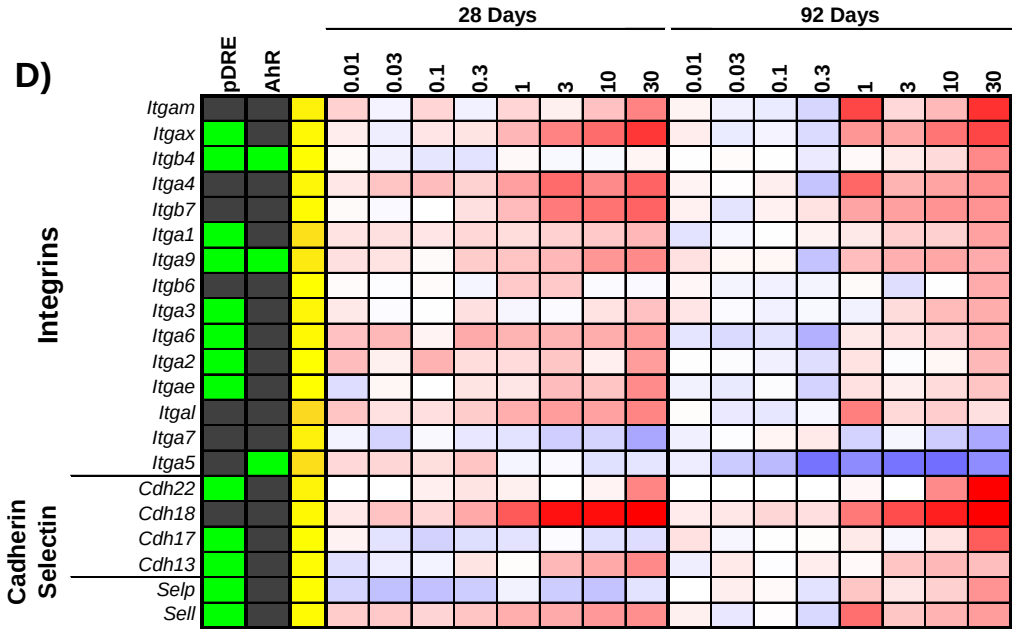

**FIGURE 33 (cont'd)**

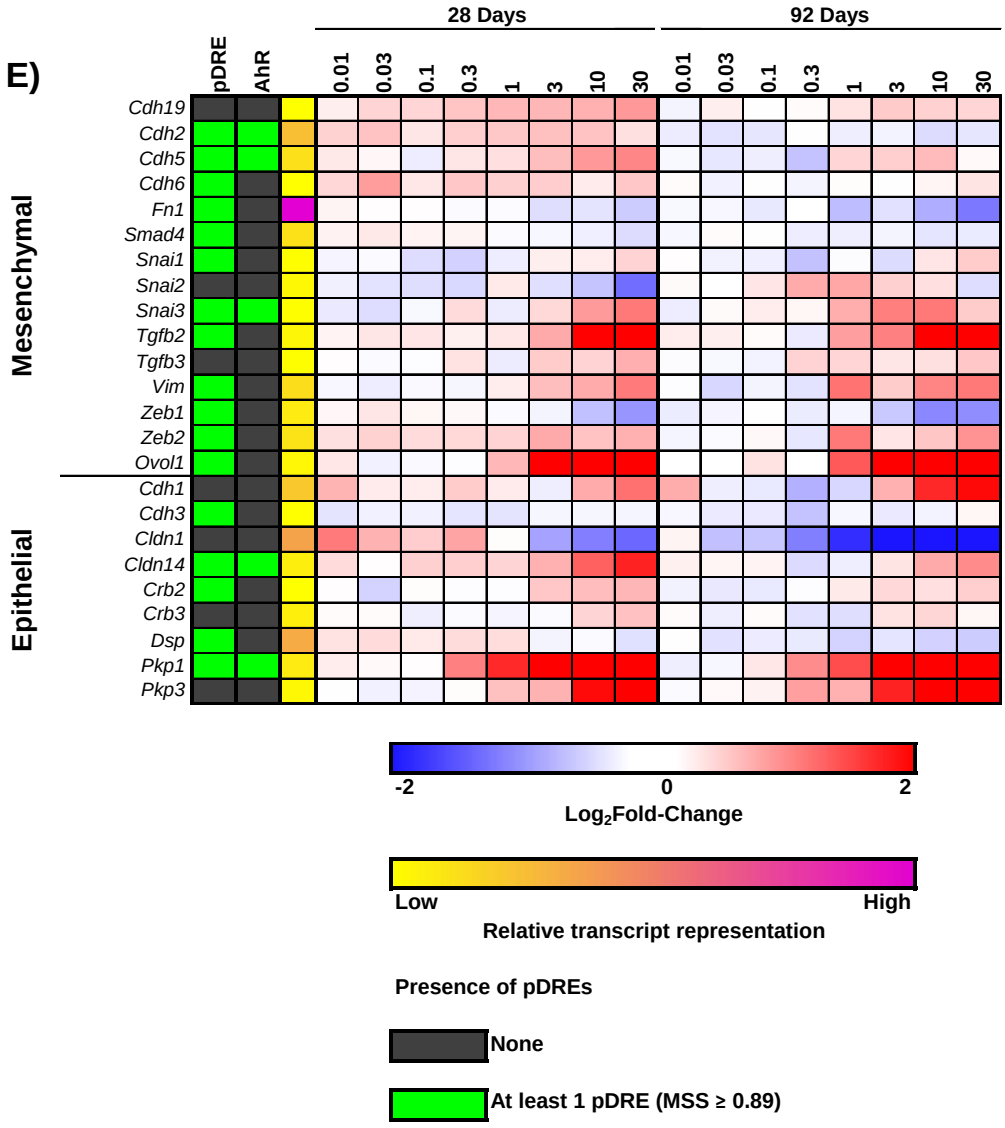

92d, respectively. These isoforms are reported to possess interchangeable activities [43]. TGFβ induced EMT is mediated by the activation of SMADs (SMAD2, 3, 4, and 7; unchanged), *Zeb1* (repressed 2.0-fold), *Zeb2* (induced 1.8-fold), and *Hmga2* (induced 2.2-fold) [44]. TCDD induced both epithelial (e.g. E-cadherin (*Cdh1*), cadherin3, plakophilin 1 (*Pkp1*)) and mesenchymal (e.g. N-cadherin (*Cdh2*), vimentin (*Vim*), snail 1/2/3) markers. More specifically, *Cdh1* was induced 3.8-fold at 92 days while *Cdh2* and *Vim* were unchanged (Figure 33E). Conversely, the 2.0-fold repression of *Zeb1* is consistent with a mesenchymal phenotype as well as the 43.9- and 13.4-fold increase of *Pkp1* at 28 and 92 days, respectively. Conversely, *Ovol1*, a transcription factor that induces mesenchymal to epithelial transition (MET), was induced 33.2- and 6.4-fold, respectively, at 28 and 92 days possibly indicating EMT reversion [45].

While cadherins play an integral role in defining epithelial and mesenchymal phenotypes, integrins, selectins, and other matrisome proteins (e.g. laminins, proteoglycans, nidogens, fibulins, and fibronectin) are implicated in cell adhesion and interactions with the ECM. The majority of integrins were induced with *Itg4* and *9* demonstrating a 1.9- and 1.5-fold induction, respectively, with concomitant AhR enrichment. Selectins *Selp* and *Sell* were also induced 1.8- and 1.7-fold, respectively. Tenascin C (*Tnc*) which inhibits interactions between syndecans and fibronectin was induced 7.8-fold 92d while syndecans (*Sdc1* and *2*) and fibronectin (*Fn1*) were repressed 2.4-, 2.6-, and 2.2-fold, respectively (Figure 33B).

## DISCUSSION

TCDD and related compounds have been linked to the development of metabolic disorders. In rodents, TCDD induces dose-dependent increases in hepatic steatosis, and steatohepatitis with underlying AhR-mediated differential gene expression driving metabolic reprogramming [2, 10, 12]. In this study we examined the metabolic changes associated with TCDD-elicited fibrogenesis. Hepatic fibrosis is an important risk factor in hepatocellular carcinoma and other liver disease related deaths [46]. Our studies revealed further AhR-mediated metabolic

reprogramming that affected glycogen and proline metabolism, as well as the expression of matrisomal genes associated with TCDD-elicited hepatotoxicity and fibrosis.

The cumulative burden of TCDD on hepatic lipid accumulation and differential gene expression change was more evident at lower doses after 92 d of treatment compared to that at 28 d. In humans TCDD has a longer half-life which sustains AhR activation and partially explains potential links between metabolic disease and environmental contaminant exposure [47]. However, as exposure duration increased glucose tolerance improved, contrary to expectations [47]. No changes in insulin levels were observed, consistent with a previous report [48], suggesting insulin signaling is not responsible for improved tolerance. Both adiponectin (ADIPOQ) and FGF21 regulate insulin sensitivity and glucose uptake, with increased ADIPOQ enhancing FGF21-mediated insulin sensitivity [30]. However, ADIPOQ was reduced by ~50% in treated mice, suggesting improved glucose tolerance is more likely due to gluconeogenesis inhibition and the TCDD-elicited hepatic Warburg-like response representing a putative sink for glucose [10].

Integrating 28 d and 92 d transcriptomic datasets with published hepatic and serum metabolomic data [10], as well as complementary urinary metabolomic data, identified changes in glycogen, ascorbic acid, and proline metabolism, in addition to the reprogramming of glycolysis, gluconeogenesis and the TCA cycle. In murine hepatocytes, glycogen metabolism and ascorbic acid biosynthesis are associated with anti-oxidant responses as well as proline hydroxylation in ECM remodeling [49]. Notably, glycogenolysis is required for ascorbic acid synthesis in mouse hepatocytes [49]. Moreover, xenobiotics including AhR ligands, increase urinary excretion of ascorbic acid and induce UDP glucuronosyltransferase (*UGTs*) which participates in glycogenolysis [50]. Coincidentally, *UGTs* are also members of the AhR “gene battery” including *Ugt1a6* suggesting a direct regulatory role of the AhR in glycogenolysis [51]. Moreover, glutathione and oxidative stress regulate ascorbate synthesis [49]. These data suggest that hepatic metabolism is reprogrammed to use glycogen in support of ECM remodeling and antioxidant responses.

The ECM is constantly remodeled by fine tuning the balance between the deposition of structural proteins, expression and/or activity of ECM degradation enzymes, and interactions with other matrisome associated proteins [6]. TCDD affected the expression of >30% of the matrisome, resulting in the deposition of ECM along hepatic portal tracts. This pattern is similar to the fibrosis seen in chronic viral hepatitis and cholestatic disorders, suggesting deposition is largely mediated by myofibroblasts resulting from the EMT of portal fibroblasts and migrating HSCs [42]. Portal fibroblasts, cholangiocytes, and IL-6 are also interact to promote bile duct proliferation in biliary fibrosis [52] which may explain the bile duct proliferation in some TCDD treated mice. Furthermore, the forces exerted by ECM deposition along portal ducts may cause the dimpled appearance of the visceral surface of TCDD-treated livers. Despite conflicting epithelial and mesenchymal marker expression, it is clear that HSCs and portal fibroblasts undergo EMT to generate ECM producing myofibroblasts [9]. However, *Ovol1* induction suggests possible EMT reversal to replace dead and damaged cells [53]. Reductions in adiponectin were contrary to improved glucose tolerance, but consistent with increased fibrosis since adiponectin inhibits myofibroblast proliferation and mobility [54]. TIMP-1 which was induced by TCDD cooperates with adiponectin to reduce fibrogenic activity [54], although other studies suggest pro-fibrogenic interactions [55]. IFNγ blocks fibrogenesis by inhibiting TGFβ/Smad signaling [56]. Additionally, AhR-mediated changes in the gut microbiome [57] and intestinal permeability may increase endotoxin levels resulting in hepatic injury via activation of TLR4, promoting collagen deposition [58]. Collectively, the differential expression of the matrisome suggests TCDD-elicits qualitative and quantitative changes in ECM composition and structure that could influence cell function, organization, migration, differentiation, proliferation, apoptosis, and adhesion.

In addition to providing tensile strength, regulating cell adhesion, supporting chemotaxis and migration, and directing tissue development, collagen can serve as reservoir for proline/hydroxyproline, an important anaplerotic substrate for the TCA cycle and ATP source from proline cycling at the expense of NADPH [38]. Consequently, collagen can be considered as

proline storage, similar to glycogen serving as glucose storage or triglycerides as storage for fatty acids [38]. Continuous ECM remodeling by TCDD-induced metalloproteinases (e.g., *MMPs*, *Adams* and *Adamts*) can mobilize collagen stored proline/hydroxyproline, making it available for ATP production in response to AhR-mediated *PKM* isoform switching [10]. Excess hydroxyproline can also be diverted towards glycolate, oxalate, and glycine synthesis [39] although this pathway is repressed by TCDD with the fate of released hydroxyproline being unclear. In addition, proline can also be converted to arginine and subsequently used for creatinine, urea, and polyamine synthesis [59]. Limited proline availability is likely associated with reduced polyamine production [60], but little is known about effects on the urea cycle or proline-glutamine-arginine interconversion. The relevance of proline cycling on ATP production and overall cellular bioenergetics in combating TCDD-elicited energy depletion and hepatotoxicity remains to be determined.

In summary, TCDD-elicited metabolic reprogramming extends to ascorbic acid synthesis, glycogen metabolism and ECM remodeling/proline cycling (Figure 34). As TCDD exposure duration increased, the doses necessary for NAFLD pathology progression decreased suggesting a putative role for anthropogenic, dietary, and endogenous AhR ligands in NAFLD, particularly for compounds with long half-lives. However, ascorbic acid synthesis is not conserved and therefore the relevance of these results in human disease remains to be determined. Nevertheless, TCDD-elicited fibrosis involves complex interactions between diverse cell types and signaling pathways involving metabolic reprogramming to support fibrogenesis. The energetic costs of metabolic reprogramming and mechanism for sustaining ATP levels in response to TCDD exposure warrants further investigation, particularly the use of collagen as a proline source and the consumption of glycogen for ascorbic acid synthesis. Further elucidation of the roles of these pathways in pathology progression may identify novel targets for the treatment of fibrotic diseases.

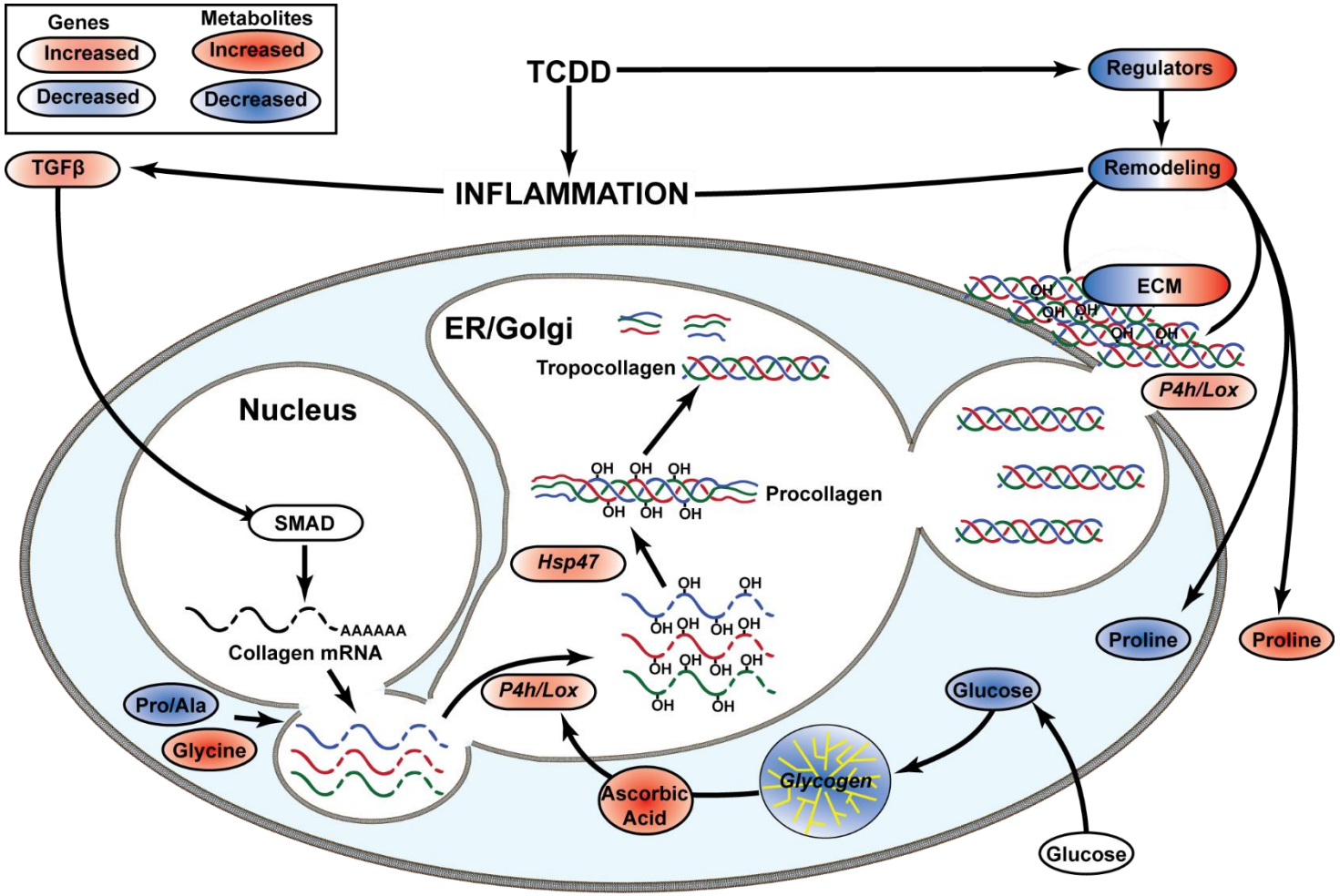


**FIGURE 34. OVERVIEW OF ALTERED HEPATIC METABOLISM TO SUPPORT EXTRACELLULAR MATRIX REMODELING**

# REFERENCES

## REFERENCES


1. Fader, K.A., R. Nault, D.A. Ammendolia, J.R. Harkema, K.J. Williams, R.B. Crawford, N.E. Kaminski, D. Potter, B. Sharratt, and T.R. Zacharewski, *2,3,7,8-Tetrachlorodibenzo-p-Dioxin Alters Lipid Metabolism and Depletes Immune Cell Populations in the Jejunum of C57BL/6 Mice.* Toxicol Sci, 2015. 148(2): p. 567-80.

2. Pierre, S., A. Chevallier, F. Teixeira-Clerc, A. Ambolet-Camoit, L.C. Bui, A.S. Bats, J.C. Fournet, P. Fernandez-Salguero, M. Aggerbeck, S. Lotersztajn, R. Barouki, and X. Coumoul, *Aryl hydrocarbon receptor-dependent induction of liver fibrosis by dioxin.* Toxicol Sci, 2014. 137(1): p. 114-24.

3. Fernandez-Salguero, P.M., D.M. Hilbert, S. Rudikoff, J.M. Ward, and F.J. Gonzalez, *Aryl-hydrocarbon receptor-deficient mice are resistant to 2,3,7,8-tetrachlorodibenzo-p-dioxin-induced toxicity.* Toxicol Appl Pharmacol, 1996. 140(1): p. 173-9.

4. Dere, E., R. Lo, T. Celius, J. Matthews, and T.R. Zacharewski, *Integration of genome-wide computation DRE search, AhR ChIP-chip and gene expression analyses of TCDD-elicited responses in the mouse liver.* BMC Genomics, 2011. 12: p. 365.

5. Huang, G. and C.J. Elferink, *A novel nonconsensus xenobiotic response element capable of mediating aryl hydrocarbon receptor-dependent gene expression.* Mol Pharmacol, 2012. 81(3): p. 338-47.

6. Naba, A., K.R. Clauser, H. Ding, C.A. Whittaker, S.A. Carr, and R.O. Hynes, *The extracellular matrix: Tools and insights for the "omics" era.* Matrix Biol, 2016. 49: p. 10-24.

7. Glaser, S.S., E. Gaudio, T. Miller, D. Alvaro, and G. Alpini, *Cholangiocyte proliferation and liver fibrosis.* Expert Rev Mol Med, 2009. 11: p. e7.

8. Omenetti, A., W.K. Syn, Y. Jung, H. Francis, A. Porrello, R.P. Witek, S.S. Choi, L. Yang, M.J. Mayo, M.E. Gershwin, G. Alpini, and A.M. Diehl, *Repair-related activation of hedgehog signaling promotes cholangiocyte chemokine production.* Hepatology, 2009. 50(2): p. 518-27.

9. Kalluri, R. and R.A. Weinberg, *The basics of epithelial-mesenchymal transition.* J Clin Invest, 2009. 119(6): p. 1420-8.

10. Nault, R., K.A. Fader, M.P. Kirby, S. Ahmed, J. Matthews, A.D. Jones, S.Y. Lunt, and T.R. Zacharewski, *Pyruvate Kinase Isoform Switching and Hepatic Metabolic Reprogramming by the Environmental Contaminant 2,3,7,8-Tetrachlorodibenzo-p-Dioxin.* Toxicol Sci, 2016. 149(2): p. 358-71.

11. Chen, Y., S.S. Choi, G.A. Michelotti, I.S. Chan, M. Swiderska-Syn, G.F. Karaca, G. Xie, C.A. Moylan, F. Garibaldi, R. Premont, H.B. Suliman, C.A. Piantadosi, and A.M. Diehl, *Hedgehog controls hepatic stellate cell fate by regulating metabolism.* Gastroenterology, 2012. 143(5): p. 1319-29 e1-11.

12. Nault, R., D. Colbry, C. Brandenberger, J.R. Harkema, and T.R. Zacharewski, *Development of a computational high-throughput tool for the quantitative examination of dose-dependent histological features.* Toxicol Pathol, 2015. 43(3): p. 366-75.

13. Keppler, D. and K. Decker, *Glycogen determination with amyloglucosidase*, in *Methods of enzymatic analysis*, H.U. Bergmeyer, Editor. 1974, Academic Press: New York. p. 1127-1131.

14. Nault, R., K.A. Fader, and T. Zacharewski, *RNA-Seq versus oligonucleotide array assessment of dose-dependent TCDD-elicited hepatic gene expression in mice.* BMC Genomics, 2015. 16(1): p. 373.

15. Lunt, S.Y., V. Muralidhar, A.M. Hosios, W.J. Israelsen, D.Y. Gui, L. Newhouse, M. Ogrodzinski, V. Hecht, K. Xu, P.N. Acevedo, D.P. Hollern, G. Bellinger, T.L. Dayton, S. Christen, I. Elia, A.T. Dinh, G. Stephanopoulos, S.R. Manalis, M.B. Yaffe, E.R. Andrechek, S.M. Fendt, and M.G. Vander Heiden, *Pyruvate kinase isoform expression alters nucleotide synthesis to impact cell proliferation.* Mol Cell, 2015. 57(1): p. 95-107.

16. Clasquin, M.F., E. Melamud, and J.D. Rabinowitz, *LC-MS data processing with MAVEN: a metabolomic analysis and visualization engine.* Curr Protoc Bioinformatics, 2012. Chapter 14: p. Unit14 11.

17. Xia, J. and D.S. Wishart, *MetPA: a web-based metabolomics tool for pathway analysis and visualization.* Bioinformatics, 2010. 26(18): p. 2342-4.

18. Kopec, A.K., D.R. Boverhof, R. Nault, J.R. Harkema, C. Tashiro, D. Potter, B. Sharratt, B. Chittim, and T.R. Zacharewski, *Toxicogenomic Evaluation of Long-term Hepatic Effects of TCDD in Immature, Ovariectomized C57BL/6 Mice.* Toxicol Sci, 2013. 135(2): p. 465-75.

19. Sorg, O., M. Zennegg, P. Schmid, R. Fedosyuk, R. Valikhnovskyi, O. Gaide, V. Kniazevych, and J.H. Saurat, *2,3,7,8-tetrachlorodibenzo-p-dioxin (TCDD) poisoning in Victor Yushchenko: identification and measurement of TCDD metabolites.* Lancet, 2009. 374(9696): p. 1179-85.

20. Eskenazi, B., P. Mocarelli, M. Warner, S. Samuels, P. Vercellini, D. Olive, L.L. Needham, D.G. Patterson, Jr., P. Brambilla, N. Gavoni, S. Casalini, S. Panazza, W. Turner, and P.M. Gerthoux, *Serum dioxin concentrations and endometriosis: a cohort study in Seveso, Italy.* Environ Health Perspect, 2002. 110(7): p. 629-34.

21. Zober, A. and O. Päpke, *Concentrations of PCDDs and PCDFs in human tissue 36 years after accidental dioxin exposure.* Chemosphere, 1993. 27(1–3): p. 413-418.

22. Masuda, Y., A. Schecter, and O. Papke, *Concentrations of PCBs, PCDFs and PCDDs in the blood of Yusho patients and their toxic equivalent contribution.* Chemosphere, 1998. 37(9-12): p. 1773-80.

23. Shen, H., J. Han, X. Tie, W. Xu, Y. Ren, and C. Ye, *Polychlorinated dibenzo-p-dioxins/furans and polychlorinated biphenyls in human adipose tissue from Zhejiang Province, China.* Chemosphere, 2009. 74(3): p. 384-8.

24. Choi, J.W., Y. Miyabara, S. Hashimoto, and M. Morita, *Comparison of PCDD/F and coplanar PCB concentrations in Japanese human adipose tissue collected in 1970-1971, 1994-1996 and 2000.* Chemosphere, 2002. 47(6): p. 591-7.

25. Papke, O., *PCDD/PCDF: human background data for Germany, a 10-year experience.* Environ Health Perspect, 1998. 106 Suppl 2: p. 723-31.

26. Alcock, R.E., P.A. Behnisch, K.C. Jones, and H. Hagenmaier, *Dioxin-like PCBs in the environment-human exposure and the significance of sources.* Chemosphere, 1998. 37(8): p. 1457-72.

27. Aylward, L.L. and S.M. Hays, *Temporal trends in human TCDD body burden: decreases over three decades and implications for exposure levels.* J Expo Anal Environ Epidemiol, 2002. 12(5): p. 319-28.

28. Lee, J.H., T. Wada, M. Febbraio, J. He, T. Matsubara, M.J. Lee, F.J. Gonzalez, and W. Xie, *A novel role for the dioxin receptor in fatty acid metabolism and hepatic steatosis.* Gastroenterology, 2010. 139(2): p. 653-63.

29. De Tullio, M.C., *Beyond the antioxidant: the double life of vitamin C.* Subcell Biochem, 2012. 56: p. 49-65.

30. Lin, Z., H. Tian, K.S. Lam, S. Lin, R.C. Hoo, M. Konishi, N. Itoh, Y. Wang, S.R. Bornstein, A. Xu, and X. Li, *Adiponectin mediates the metabolic effects of FGF21 on glucose homeostasis and insulin sensitivity in mice.* Cell Metab, 2013. 17(5): p. 779-89.

31. Cheng, X., S.G. Vispute, J. Liu, C. Cheng, A. Kharitonenkov, and C.D. Klaassen, *Fibroblast growth factor (Fgf) 21 is a novel target gene of the aryl hydrocarbon receptor (AhR).* Toxicol Appl Pharmacol, 2014.

32. Girer, N.G., I.A. Murray, C.J. Omiecinski, and G.H. Perdew, *Hepatic Aryl Hydrocarbon Receptor Attenuates Fibroblast Growth Factor 21 Expression.* J Biol Chem, 2016.

33. Ahmed, S., D. Bott, A. Gomez, L. Tamblyn, A. Rasheed, T. Cho, L. MacPherson, K.S. Sugamori, Y. Yang, D.M. Grant, C.L. Cummins, and J. Matthews, *Loss of the Mono-ADP-ribosyltransferase, Tiparp, Increases Sensitivity to Dioxin-induced Steatohepatitis and Lethality.* J Biol Chem, 2015. 290(27): p. 16824-40.

34. Frantz, C., K.M. Stewart, and V.M. Weaver, *The extracellular matrix at a glance.* J Cell Sci, 2010. 123(Pt 24): p. 4195-200.

35. Loskutoff, D.J. and J.P. Quigley, *PAI-1, fibrosis, and the elusive provisional fibrin matrix.* J Clin Invest, 2000. 106(12): p. 1441-3.

36. Van Gool, B., S. Dedieu, H. Emonard, and A.J. Roebroek, *The Matricellular Receptor LRP1 Forms an Interface for Signaling and Endocytosis in Modulation of the Extracellular Tumor Environment.* Front Pharmacol, 2015. 6: p. 271.

37. Barbul, A., *Proline precursors to sustain Mammalian collagen synthesis.* J Nutr, 2008. 138(10): p. 2021S-2024S.

38. Phang, J.M., W. Liu, C.N. Hancock, and J.W. Fischer, *Proline metabolism and cancer: emerging links to glutamine and collagen.* Curr Opin Clin Nutr Metab Care, 2015. 18(1): p. 71-7.

39. Jiang, J., L.C. Johnson, J. Knight, M.F. Callahan, T.J. Riedel, R.P. Holmes, and W.T. Lowther, *Metabolism of [13C5]hydroxyproline in vitro and in vivo: implications for primary hyperoxaluria.* Am J Physiol Gastrointest Liver Physiol, 2012. 302(6): p. G637-43.

40. Wight, T.N. and S. Potter-Perigo, *The extracellular matrix: an active or passive player in fibrosis?* Am J Physiol Gastrointest Liver Physiol, 2011. 301(6): p. G950-5.

41. Katayama, A., A. Nakatsuka, J. Eguchi, K. Murakami, S. Teshigawara, M. Kanzaki, T. Nunoue, K. Hida, N. Wada, T. Yasunaka, F. Ikeda, A. Takaki, K. Yamamoto, H. Kiyonari, H. Makino, and J. Wada, *Beneficial impact of Gpnmb and its significance as a biomarker in nonalcoholic steatohepatitis.* Sci Rep, 2015. 5: p. 16920.

42. Brenner, D.A., T. Kisseleva, D. Scholten, Y.H. Paik, K. Iwaisako, S. Inokuchi, B. Schnabl, E. Seki, S. De Minicis, C. Oesterreicher, and K. Taura, *Origin of myofibroblasts in liver fibrosis.* Fibrogenesis Tissue Repair, 2012. 5(Suppl 1): p. S17.

43. Roberts, A.B., S.J. Kim, T. Noma, A.B. Glick, R. Lafyatis, R. Lechleider, S.B. Jakowlew, A. Geiser, M.A. O'Reilly, D. Danielpour, and et al., *Multiple forms of TGF-beta: distinct promoters and differential expression.* Ciba Found Symp, 1991. 157: p. 7-15; discussion 15-28.

44. Lamouille, S., J. Xu, and R. Derynck, *Molecular mechanisms of epithelial-mesenchymal transition.* Nat Rev Mol Cell Biol, 2014. 15(3): p. 178-96.

45. Roca, H., J. Hernandez, S. Weidner, R.C. McEachin, D. Fuller, S. Sud, T. Schumann, J.E. Wilkinson, A. Zaslavsky, H. Li, C.A. Maher, S. Daignault-Newton, P.N. Healy, and K.J. Pienta, *Transcription factors OVOL1 and OVOL2 induce the mesenchymal to epithelial transition in human cancer.* PLoS One, 2013. 8(10): p. e76773.

46. Baffy, G., E.M. Brunt, and S.H. Caldwell, *Hepatocellular carcinoma in non-alcoholic fatty liver disease: an emerging menace.* J Hepatol, 2012. 56(6): p. 1384-91.

47. Taylor, K.W., R.F. Novak, H.A. Anderson, L.S. Birnbaum, C. Blystone, M. Devito, D. Jacobs, J. Kohrle, D.H. Lee, L. Rylander, A. Rignell-Hydbom, R. Tornero-Velez, M.E. Turyk, A.L. Boyles, K.A. Thayer, and L. Lind, *Evaluation of the association between persistent organic pollutants (POPs) and diabetes in epidemiological studies: a national toxicology program workshop review.* Environ Health Perspect, 2013. 121(7): p. 774-83.

48. Takuma, M., K. Ushijima, M. Kumazaki, H. Ando, and A. Fujimura, *Influence of dioxin on the daily variation of insulin sensitivity in mice.* Environ Toxicol Pharmacol, 2015. 40(2): p. 349-351.

49. Braun, L., M. Csala, A. Poussu, T. Garzo, J. Mandl, and G. Banhegyi, *Glutathione depletion induces glycogenolysis dependent ascorbate synthesis in isolated murine hepatocytes.* FEBS Lett, 1996. 388(2-3): p. 173-6.

50. Hassan, M.Q., H. Mohammadpour, S.J. Hermansky, W.J. Murray, and S.J. Stohs, *Comparative effects of BHA and ascorbic acid on the toxicity of 2,3,7,8-tetrachlorodibenzo-p-dioxin (TCDD) in rats.* Gen Pharmacol, 1987. 18(5): p. 547-50.

51. Yeager, R.L., S.A. Reisman, L.M. Aleksunes, and C.D. Klaassen, *Introducing the "TCDD-inducible AhR-Nrf2 gene battery".* Toxicol Sci, 2009. 111(2): p. 238-46.

52. Dranoff, J.A. and R.G. Wells, *Portal fibroblasts: Underappreciated mediators of biliary fibrosis.* Hepatology, 2010. 51(4): p. 1438-44.

53. Syn, W.K., Y. Jung, A. Omenetti, M. Abdelmalek, C.D. Guy, L. Yang, J. Wang, R.P. Witek, C.M. Fearing, T.A. Pereira, V. Teaberry, S.S. Choi, J. Conde-Vancells, G.F. Karaca, and A.M. Diehl, *Hedgehog-mediated epithelial-to-mesenchymal transition and fibrogenic repair in nonalcoholic fatty liver disease.* Gastroenterology, 2009. 137(4): p. 1478-1488 e8.

54. Ramezani-Moghadam, M., J. Wang, V. Ho, T.J. Iseli, B. Alzahrani, A. Xu, D. Van der Poorten, L. Qiao, J. George, and L. Hebbard, *Adiponectin Reduces Hepatic Stellate Cell Migration by Promoting Tissue Inhibitor of Metalloproteinase-1 (TIMP-1) Secretion.* J Biol Chem, 2015. 290(9): p. 5533-42.

55. Yoshiji, H., S. Kuriyama, Y. Miyamoto, U.P. Thorgeirsson, D.E. Gomez, M. Kawata, J. Yoshii, Y. Ikenaka, R. Noguchi, H. Tsujinoue, T. Nakatani, S.S. Thorgeirsson, and H. Fukui, *Tissue inhibitor of metalloproteinases-1 promotes liver fibrosis development in a transgenic mouse model.* Hepatology, 2000. 32(6): p. 1248-54.

56. Weng, H., P.R. Mertens, A.M. Gressner, and S. Dooley, *IFN-gamma abrogates profibrogenic TGF-beta signaling in liver by targeting expression of inhibitory and receptor Smads.* J Hepatol, 2007. 46(2): p. 295-303.

57. Zhang, L., R.G. Nichols, J. Correll, I.A. Murray, N. Tanaka, P.B. Smith, T.D. Hubbard, A. Sebastian, I. Albert, E. Hatzakis, F.J. Gonzalez, G.H. Perdew, and A.D. Patterson, *Persistent Organic Pollutants Modify Gut Microbiota-Host Metabolic Homeostasis in Mice Through Aryl Hydrocarbon Receptor Activation.* Environ Health Perspect, 2015. 123(7): p. 679-88.

58. Brenner, D.A., Y.H. Paik, and B. Schnabl, *Role of Gut Microbiota in Liver Disease.* J Clin Gastroenterol, 2015. 49 Suppl 1: p. S25-7.

59. Morris, S.M., Jr., *Recent advances in arginine metabolism: roles and regulation of the arginases.* Br J Pharmacol, 2009. 157(6): p. 922-30.

60. Thomas, T., S.A. MacKenzie, and M.A. Gallo, *Regulation of polyamine biosynthesis by 2,3,7,8-tetrachlorodibenzo-p-dioxin (TCDD).* Toxicol Lett, 1990. 53(3): p. 315-25.

# CHAPTER 6. CONCLUSIONS AND FUTURE RESEARCH

The studies presented in this report describe the development and progression of NAFLD pathologies following continuous activation of the AhR by its prototypical ligand TCDD. Leveraging technological advances, these studies quantitatively describe the dose- and time-dependent progression of simple hepatic steatosis to steatohepatitis and fibrosis, and the underlying hepatic and systemic metabolic changes associated with the progression of disease. They reveal novel mechanisms used by the liver to prevent or minimize damage, by supporting anti-oxidant defenses and pro-fibrotic processes, leading to NAFLD development and progression. For example, AhR-mediated switching of pyruvate kinase isoforms from the highly active PKLR and PKM1 to PKM2 which reduces glycolytic flux, commonly associated with proliferating cancer cells, redirects intermediates to the pentose phosphate pathway and NADPH production in support of antioxidant defenses [1-4]. Through the integration of metabolomics, transcriptomics, AhR ChIP-Seq, and computationally identified DREs within the context of metabolic pathways it is evident that TCDD-elicited NAFLD progression involves direct and indirect AhR-mediated hepatic metabolism reprogramming, consistent with previous reports [5-10]. The presented work further elucidates the metabolic changes associated with AhR activation and NAFLD disease progression, and provides further evidence that TCDD and related compounds may be contributing to NAFLD development and progression.

**ACTIVATION OF THE AHR BY TCDD PROMOTES PROGRESSION OF NAFLD**

TCDD has been linked to NAFLD pathologies in epidemiological studies [11-13], and demonstrated to cause hepatic steatosis, steatohepatitis, and fibrosis in rodent studies [5, 6, 11, 14-16]. However, they do not address the role of AhR activation in the sequential progression of NAFLD pathologies as duration of exposure persists, a scenario more likely to reflect human exposure to anthropogenic AhR agonists. The ability of TCDD to facilitate the progression of simple steatosis to more severe pathologies suggests that AhR ligands are a contributing factor to the development of many NAFLD pathologies. NAFLD progression nevertheless remains a

complex process and elucidating the role of the AhR in disease progression offers valuable insight for understanding NAFLD development as well as identifies potential targets for therapeutic intervention. While the presented studies offers some information, describing how direct targets of the AhR are implicated in NAFLD development requires further investigation. Future studies examining the ability of AhR ligands to promote NAFLD pathology progression should examine alternate models of steatosis/steatohepatitis such as Western or methionine-choline deficient diet fed mice and ob/ob obese mice to determine if AhR activation plays an additive or even synergistic role.

**TCDD EXPOSURE REPROGRAMS HEPATIC AND SYSTEMIC METABOLISM**

Hepatic and systemic changes in metabolism likely play an important role in reducing the hepatotoxic effects of AhR activation. Changes in *Pkm* isoform expression, typical of proliferating cancer cells, was found to occur in TCDD treated mice representing a novel AhR-mediated response which attempts to minimize hepatotoxicity. Consequently, we can hypothesize that the improved glucose tolerance in TCDD treated animals supports metabolic reprogramming to the pentose phosphate pathway. Examination of glucose tolerance and hepatotoxicity in a hepatocyte specific *Pkm2* knock-out model will demonstrate the importance of this response in TCDD treated animals while using labeled metabolites (i.e., tracer studies) would provide invaluable information on altered metabolic fluxes [17]. Furthermore, evaluating the incidence of hepatocellular carcinoma in *Pkm2* knock-out mice would be of interest, although could require longer (2 years) exposures [18]. The presented studies also implicate an intragenic DRE found within the PKM gene as putative regulator of PKM isoform switching. Abolishing AhR binding at this DRE through genetic manipulation such as the CRISPR/CAS9 system could help elucidate the importance of this genomic region in PKM isoform switching.

In support of previous studies in mouse hepatocytes [19, 20], integration of omics datasets demonstrated the role of glycogenolysis on ascorbic acid synthesis in TCDD treated animals, and

links this metabolic pathway to support of pro-fibrotic and energy production. Rodents, however, possess a functional *Gulo* gene while humans, Guinea pigs, and some bat species lack the functional enzyme and therefore diet is their only source of vitamin C [21]. Guinea pigs are among the most sensitive species to TCDD toxicity [22], suggesting a possible role for endogenous ascorbic acid biosynthesis in species sensitivity differences. To further evaluate the importance of vitamin C metabolism in human health, future studies should examine TCDD-elicited hepatic fibrosis in *Gulo* null mice [23] as well as Guinea pigs. Collectively, understanding changes in metabolism associated with TCDD elicited NAFLD development are of value in the elucidation of mechanisms involved in disease progression. These pathways present potential therapeutic targets and may also reveal further similarities with cancer metabolism which is currently being targeted by a variety of drugs either approved or in clinical trials.

# REFERENCES

## REFERENCES


1. Gorrini, C., I.S. Harris, and T.W. Mak, *Modulation of oxidative stress as an anticancer strategy.* Nat Rev Drug Discov, 2013. 12(12): p. 931-47.

2. Cairns, R.A., I.S. Harris, and T.W. Mak, *Regulation of cancer cell metabolism.* Nat Rev Cancer, 2011. 11(2): p. 85-95.

3. Harris, I., S. McCracken, and T.W. Mak, *PKM2: a gatekeeper between growth and survival.* Cell Res, 2012. 22(3): p. 447-9.

4. Yang, W., *Structural basis of PKM2 regulation.* Protein Cell, 2015. 6(4): p. 238-40.

5. Lee, J.H., T. Wada, M. Febbraio, J. He, T. Matsubara, M.J. Lee, F.J. Gonzalez, and W. Xie, *A novel role for the dioxin receptor in fatty acid metabolism and hepatic steatosis.* Gastroenterology, 2010. 139(2): p. 653-63.

6. Pierre, S., A. Chevallier, F. Teixeira-Clerc, A. Ambolet-Camoit, L.C. Bui, A.S. Bats, J.C. Fournet, P. Fernandez-Salguero, M. Aggerbeck, S. Lotersztajn, R. Barouki, and X. Coumoul, *Aryl hydrocarbon receptor-dependent induction of liver fibrosis by dioxin.* Toxicol Sci, 2014. 137(1): p. 114-24.

7. Ruiz-Aracama, A., A. Peijnenburg, J. Kleinjans, D. Jennen, J. van Delft, C. Hellfrisch, and A. Lommen, *An untargeted multi-technique metabolomics approach to studying intracellular metabolites of HepG2 cells exposed to 2,3,7,8-tetrachlorodibenzo-p-dioxin.* BMC Genomics, 2011. 12: p. 251.

8. Lin, S., Z. Yang, H. Liu, and Z. Cai, *Metabolomic analysis of liver and skeletal muscle tissues in C57BL/6J and DBA/2J mice exposed to 2,3,7,8-tetrachlorodibenzo-p-dioxin.* Mol Biosyst, 2011. 7(6): p. 1956-65.

9. Forgacs, A.L., M.N. Kent, M.K. Makley, B. Mets, N. DelRaso, G.L. Jahns, L.D. Burgoon, T.R. Zacharewski, and N.V. Reo, *Comparative metabolomic and genomic analyses of TCDD-elicited metabolic disruption in mouse and rat liver.* Toxicol Sci, 2012. 125(1): p. 41-55.

10. Shi, X., B. Wahlang, X. Wei, X. Yin, K.C. Falkner, R.A. Prough, S.H. Kim, E.G. Mueller, C.J. McClain, M. Cave, and X. Zhang, *Metabolomic analysis of the effects of polychlorinated biphenyls in nonalcoholic Fatty liver disease.* J Proteome Res, 2012. 11(7): p. 3805-15.

11. Neel, B.A. and R.M. Sargis, *The paradox of progress: environmental disruption of metabolism and the diabetes epidemic.* Diabetes, 2011. 60(7): p. 1838-48.

12. Taylor, K.W., R.F. Novak, H.A. Anderson, L.S. Birnbaum, C. Blystone, M. Devito, D. Jacobs, J. Kohrle, D.H. Lee, L. Rylander, A. Rignell-Hydbom, R. Tornero-Velez, M.E. Turyk, A.L. Boyles, K.A. Thayer, and L. Lind, *Evaluation of the association between persistent organic pollutants (POPs) and diabetes in epidemiological studies: a national toxicology program workshop review.* Environ Health Perspect, 2013. 121(7): p. 774-83.

13. Lee, D.H., I.K. Lee, M. Porta, M. Steffes, and D.R. Jacobs, Jr., *Relationship between serum concentrations of persistent organic pollutants and the prevalence of metabolic syndrome among non-diabetic adults: results from the National Health and Nutrition Examination Survey 1999-2002.* Diabetologia, 2007. 50(9): p. 1841-51.

14. Kopec, A.K., D.R. Boverhof, R. Nault, J.R. Harkema, C. Tashiro, D. Potter, B. Sharratt, B. Chittim, and T.R. Zacharewski, *Toxicogenomic Evaluation of Long-term Hepatic Effects of TCDD in Immature, Ovariectomized C57BL/6 Mice.* Toxicol Sci, 2013. 135(2): p. 465-75.

15. Fernandez-Salguero, P.M., D.M. Hilbert, S. Rudikoff, J.M. Ward, and F.J. Gonzalez, *Aryl-hydrocarbon receptor-deficient mice are resistant to 2,3,7,8-tetrachlorodibenzo-p-dioxin-induced toxicity.* Toxicol Appl Pharmacol, 1996. 140(1): p. 173-9.

16. Boverhof, D.R., L.D. Burgoon, C. Tashiro, B. Chittim, J.R. Harkema, D.B. Jump, and T.R. Zacharewski, *Temporal and dose-dependent hepatic gene expression patterns in mice provide new insights into TCDD-Mediated hepatotoxicity.* Toxicol Sci, 2005. 85(2): p. 1048-63.

17. Lunt, S.Y., V. Muralidhar, A.M. Hosios, W.J. Israelsen, D.Y. Gui, L. Newhouse, M. Ogrodzinski, V. Hecht, K. Xu, P.N. Acevedo, D.P. Hollern, G. Bellinger, T.L. Dayton, S. Christen, I. Elia, A.T. Dinh, G. Stephanopoulos, S.R. Manalis, M.B. Yaffe, E.R. Andrechek, S.M. Fendt, and M.G. Vander Heiden, *Pyruvate kinase isoform expression alters nucleotide synthesis to impact cell proliferation.* Mol Cell, 2015. 57(1): p. 95-107.

18. Huff, J.E., A.G. Salmon, N.K. Hooper, and L. Zeise, *Long-term carcinogenesis studies on 2,3,7,8-tetrachlorodibenzo-p-dioxin and hexachlorodibenzo-p-dioxins.* Cell Biol Toxicol, 1991. 7(1): p. 67-94.

19. Braun, L., M. Csala, A. Poussu, T. Garzo, J. Mandl, and G. Banhegyi, *Glutathione depletion induces glycogenolysis dependent ascorbate synthesis in isolated murine hepatocytes.* FEBS Lett, 1996. 388(2-3): p. 173-6.

20. Braun, L., T. Garzo, J. Mandl, and G. Banhegyi, *Ascorbic acid synthesis is stimulated by enhanced glycogenolysis in murine liver.* FEBS Lett, 1994. 352(1): p. 4-6.

21. Drouin, G., J.R. Godin, and B. Page, *The genetics of vitamin C loss in vertebrates.* Curr Genomics, 2011. 12(5): p. 371-8.

22. Korkalainen, M., J. Tuomisto, and R. Pohjanvirta, *The AH receptor of the most dioxin-sensitive species, guinea pig, is highly homologous to the human AH receptor.* Biochem Biophys Res Commun, 2001. 285(5): p. 1121-9.

23. Harrison, F.E., M.E. Meredith, S.M. Dawes, J.L. Saskowski, and J.M. May, *Low ascorbic acid and increased oxidative stress in gulo(-/-) mice during development.* Brain Res, 2010. 1349: p. 143-52.